

Synthesis and Applications of Linear and
Cross-linked pH- Responsive Polycarbo-,
Polyphospho- and PolySulfobetaines

BY

Othman Charles S. O. Al Hamouz

A Dissertation Presented to the
DEANSHIP OF GRADUATE STUDIES

KING FAHD UNIVERSITY OF PETROLEUM & MINERALS

DHAHRAN, SAUDI ARABIA

In Partial Fulfillment of the
Requirements for the Degree of

DOCTOR OF PHILOSOPHY

In

CHEMISTRY

April 2013

KING FAHD UNIVERSITY OF PETROLEUM & MINERALS

DHAHRAN- 31261, SAUDI ARABIA

DEANSHIP OF GRADUATE STUDIES

This thesis, written by **OTHMAN CHARLES SADEQ OTHMAN AL HAMOUZ** under the direction his thesis advisor and approved by his thesis committee, has been presented and accepted by the Dean of Graduate Studies, in partial fulfillment of the requirements for the degree of **DOCTOR OF PHILOSOPHY IN CHEMISTRY**.



Dr. Abdullah Jafar Al-Hamdan
Department Chairman



Dr. Salam A. Zummo
Dean of Graduate Studies

20/4/13

Date

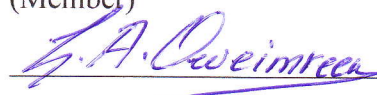




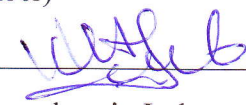
Dr. Shaikh Asrof Ali
(Advisor)



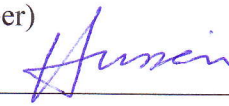
Dr. Bassam El Ali
(Member)



Dr. Ghassan Oweimreen
(Member)



Dr. Anverhusein Isab
(Member)



Dr. Ibnelwaleed Hussein
(Member)

© OTHMAN CHARLES SADEQ OTHMAN AL HAMOUZ

2013

ACKNOWLEDGMENTS

First and foremost I Thank ALLAH for his blessings and guidance, and I hope that this science earned will be of great benefit to all world.

I would like to express my deepest gratitude for my Wife and children for their patience, devotion and encouragement during my Ph. D. Without their support I would never had the ability to complete it.

I would also like to express my greatest gratitude to my Father Prof. Sadeq Al-Hamouz and my mother for their continuous support, du`aa, and prayers. Also, to my brother's and sister's for their support.

I would like to express my profound appreciation to my advisor Professor Shaikh Asrof Ali. It has been an honor for me to be one of his Ph. D. students. He taught me to be aggressive in perusing my Ph. D. research and how to think, design experimental procedures and write scientific papers that opened my eyes to the real world of organic and polymer chemistry. The perseverance and devotion that I saw from him in science makes him the best idol for being a future scientist.

I would like to express my deepest gratitude for my committee members, Prof. Bassam El Ali is a committee member and also a graduate coordinator, who has facilitated the progress of my PhD degree, Prof. Ghassan Oweimreen, Prof. Anverhusein Isab and Prof. Ibnelwaleed Hussein are also appreciated for their valuable comments and corrections.

I would like to thank Dr. Abdullah al Hamdan, chairman of the chemistry department who has never hesitated to help and guide me through my PhD work.

I would like to thank KFUPM for its exceptional care of its graduate students where all success is highly appreciated. I would like to thank Dr. Mohammed al-Daous, for his helpful discussions about BET analysis and help in TGA analysis, Dr. Nouri M. Hassan for his help in AAS and ICP analysis and Dr. Abbas Hakeem for his help in SEM and EDX analysis. A part of the thesis work was financially supported by King Abdulaziz City for Science and Technology (KACST) through the Science & Technology Unit at King Fahd University of Petroleum & Minerals (KFUPM) through project No. 11-ADV2132-04 as part of the National Science, Technology and Innovation Plan.

I finally, would like to thank Mr. Mohammed Arab for his help with NMR, Mr. Ayman Al-Majid, Mr. Amjad El-Khodiry for their assistant in AAS and ICP analysis, Mr. Bahauddin for his kindness and help in conducting organic labs.

Finally, I would like to thank my friends Dr. Amer El-Batta, Dr. Musa El-Musa, Dr. Rami Samarah, Dr. Abdulaziz Amro and Mr. Shamsuddeen Haladu for their support during this work.

TABLE OF CONTENTS

ACKNOWLEDGMENTS	IV
TABLE OF CONTENTS	VI
LIST OF TABLES	XIII
LIST OF FIGURES	XVI
ABSTRACT	XX
CHAPTER 1: INTRODUCTION	1
1.1 Cationic, anionic, zwitterionic and ampholytic polymers	1
1.2 Resins for waste water treatment	5
1.3 Objectives	6
1.4 Present state of the problem	12
CHAPTER 2: PH-RESPONSIVE POLYPHOSPHONATES USING BUTLER'S CYCLOPOLYMERIZATION	13
Abstract	13
2.1 Introduction	14
2.2 Experimental	19
2.2.1 Physical methods.....	19
2.2.2 Materials	19
2.2.3 Synthesis of Bromo(diethylphosphonato)methane (2).....	19
2.2.4 Synthesis of N,N-Diallyl-(diethylphosphonato) methylamine (4).....	20
2.2.5 Synthesis of N,N-Diallyl-(diethylphosphonato) methylammonium Chloride (5).....	21
2.2.6 Synthesis of Ethyl 3-(N,N-diallylammonio) methanephosphonate (7).....	21
2.2.7 Synthesis of Sodium Ethyl-3-(N,N-diallylammonio) methanephosphonate (6)	22
2.2.8 General Procedure for the Polymerization of Cationic Monomer (5).....	23
2.2.9. Acidic Hydrolysis of CPE (8) to PZA (9)	23
2.2.10. Basification of PZA (9) to DAPE (11)	23
2.2.11. General Procedure for the Polymerization of Zwitterionic Monomer (7).....	24
2.2.12. Acidic Hydrolysis of PZE (13) to PZA (9).....	24
2.2.13. Basification of PZA (9) to DAPE (11)	25

2.2.14.	Potentiometric Titrations	25
2.2.15.	Phase Compositions and Phase Diagram of PEG-DAPE 11 (0.4 N NaCl) System	26
2.3	Results and Discussion	27
2.3.1.	Synthesis of Monomers.....	27
2.3.2.	Synthesis and Physical Characterization of Cationic Polyelectrolyte (8).....	27
2.3.3.	Synthesis and Physical Characterization of Polyzwitterions Ester (13).....	32
2.3.4.	Viscosity Measurements	34
2.3.5.	Basicity Constants	36
2.3.6.	Phase Diagram.....	40
2.4	Conclusions	41
CHAPTER 3: COMPARATIVE SOLUTION PROPERTIES OF CYCLOCOPOLYMERS HAVING CATIONIC, ANIONIC, ZWITTERIONIC AND ZWITTERIONIC/ANIONIC BACKBONES OF SIMILAR DEGREE OF POLYMERIZATION.....		43
Abstract.....		43
3.1	Introduction	44
3.2	Experimental	47
3.2.1	Physical methods.....	47
3.2.2	Materials	49
3.2.3	General procedure for the copolymerization of the cationic monomer (1) with SO ₂	49
3.2.4	Acidic hydrolysis of CPE (2) to polyzwitterionic acid (PZA 3)	53
3.2.5	Basification of PZA (3) to dianionic polyelectrolyte (DAPE 6)	54
3.2.6	Acidification of DAPE (6) to zwitterionic-anionic polyelectrolyte (ZAPE 5).....	54
3.2.7	General procedure for the copolymerization of monomer (7) with SO ₂	54
3.2.8	Acidic hydrolysis of PZE (8) to PZA (3).....	56
3.2.9	Basification of PZA (3) (derived from entry 5, Table 3.2) to DAPE (6).....	56
3.2.10	Basification of PZE (8) to anionic polyelectrolyte (APE 9).....	56
3.2.11	Potentiometric titrations.....	56
3.2.12	Phase compositions and phase diagram of PEG-DAPE 6 (0.4 N NaCl) system.....	58
3.3	Results and discussion	60
3.3.1	Synthesis of the copolymers	60
3.3.2	Infrared and NMR spectra.....	60
3.3.3	Solubility and critical salt concentrations (CSC)	61
3.3.4	Viscosity measurements	64
3.3.5	Basicity constants.....	71
3.3.6	Phase diagram	72
3.3.7	Polymer structure versus solubility and basicity constant.....	73

3.4	Conclusions	74
------------	--------------------------	-----------

**CHAPTER 4: AQUEOUS TWO-PHASE SYSTEMS OF PH-RESPONSIVE
DIALLYLAMMONIOMETHANEPHOSPHONATE-*ALT*-SULFUR DIOXIDE
CYCLOPOLYMER WITH POLYETHYLENE GLYCOL 76**

4.1	Introduction	77
------------	---------------------------	-----------

4.2	Experimental	78
------------	---------------------------	-----------

4.2.1	Materials	78
-------	-----------------	----

4.2.2	Phase compositions and phase diagram of PEG –DAPE systems	80
-------	-----------------------------------------------------------------	----

4.3	Results and Discussion	91
------------	-------------------------------------	-----------

4.3.1	Solution properties.....	91
-------	--------------------------	----

4.3.2	Effect of NaCl and HCl on the binodal of DAPE 4-PEG ATPS.....	93
-------	---------------------------------------------------------------	----

4.3.3	The Correlation of the Phase Diagrams Using the Method of Diamond and Hsu.....	98
-------	--------------------------------------------------------------------------------	----

4.4	Conclusions	100
------------	--------------------------	------------

**CHAPTER 5: SYNTHESIS AND CYCLOPOLYMERIZATION OF
DIALLYLAMMONIOMETHANESULFONATE..... 101**

Abstract	101
-----------------------	------------

5.1	Introduction	102
------------	---------------------------	------------

5.2	Experimental	106
------------	---------------------------	------------

5.2.1	Physical Methods	106
-------	------------------------	-----

5.2.2	Materials	107
-------	-----------------	-----

5.2.3	Sodium diallylaminomethanesulfonate (6)	107
-------	--------------------------------------------------------	-----

5.2.4	Diallylammoniomethanesulfonate (7)	109
-------	---------------------------------------------------	-----

5.2.5	General Procedure for the Homopolymerization of a mixture of (7) and (8)	110
-------	--------------------------------------------------------------------------------------------------	-----

5.2.6	General Procedure for the Copolymerization of 1:1 mixture of monomers (7/8) with SO ₂	113
-------	----------------------------------------------------------------------------------------------------------------	-----

5.2.7	Conversion of PSB (16) to Anionic Polyelectrolyte (APE 17)	117
-------	-----------------------------------------------------------------------------------	-----

5.2.8	Reconversion of APE (17) to PSB (16).....	117
-------	-------------------------------------------------------------	-----

5.2.9	Solubility Measurements and Cloud Point Titrations in Aqueous Salt Solutions	117
-------	------------------------------------------------------------------------------------	-----

5.3	Results and discussion	118
------------	-------------------------------------	------------

5.3.1	Monomer Synthesis	118
-------	-------------------------	-----

5.3.2	Homocyclopolymerization	119
-------	-------------------------------	-----

5.3.4	Cocyclopolymerization with SO ₂	120
-------	--------------------------------------------------	-----

5.3.5	Solubility behaviors of the homo-and copolymers	122
-------	-------------------------------------------------------	-----

5.3.6	Estimated pKa Values of the PSBs.....	125
-------	---------------------------------------	-----

5.3.7	Comparative Stability of Homopolymer (11) versus Copolymer (16)	126
-------	-----------------------------------------------------------------------------------------	-----

5.4	Conclusions	127
------------	--------------------------	------------

CHAPTER 6: REMOVAL OF HEAVY METAL IONS USING A NOVEL CROSS-LINKED POLYZWITTERIONIC PHOSPHONATE 129

6.1 Introduction130

6.2 Experimental131

6.2.1 Physical Methods131

6.2.2 Materials131

6.2.3 Synthesis of monomers.....131

6.2.4 General procedure for the copolymerization of (2) and (3).....132

6.2.5 Basification of CPZA (4) to cross-linked anionic polyelectrolyte (CAPE 5)133

6.2.6 Sample characterizations134

6.2.7 Adsorption experiments.....134

6.3 Results and discussion135

6.3.1 Synthesis of cross-linked polymer (4) and (5)135

6.3.2 Ion-exchange properties of CAPE (5)138

6.3.3 Adsorption kinetics.....139

6.3.4 Effect of initial concentration on the adsorption of Cu²⁺ and Pb²⁺ ions.....142

6.3.5 Effect of pH and temperature on adsorption.....147

6.3.6 Scanning electron microscopy (SEM)152

6.3.7 Desorption experiment154

6.4 Conclusion.....154

CHAPTER 7: REMOVAL OF ZINC AND CADMIUM IONS USING A CROSS-LINKED POLYAMINOPHOSPHONATE..... 156

ABSTRACT156

7.1 Introduction157

7.2 Experimental158

7.2.1 Physical Methods158

7.2.2 Materials160

7.2.3 Synthesis of Monomers and Polymers.....160

7.2.4 Sample Characterization160

7.2.5 Adsorption Experiments.....161

7.3 Results and Discussion162

7.3.1 Ion Exchange Properties and Thermal Stability of CAPE (5).....162

7.3.2 Adsorption Kinetics164

7.3.3 Effect of Initial Concentration on the Adsorption of Copper and Lead Ions168

7.3.4 Effect of pH on Adsorption.....172

7.3.5 Effect of Temperature on Adsorption173

7.3.6 Scanning Electron Microscopy (SEM).....177

7.4 Conclusions	179
------------------------------	------------

CHAPTER 8: A NOVEL CROSS-LINKED POLYPHOSPHONATE FOR THE REMOVAL OF Pb^{2+} AND Cu^{2+} FROM AQUEOUS SOLUTION 180

Abstract.....	180
----------------------	------------

8.1 Introduction	181
-------------------------------	------------

8.2 Experimental	182
-------------------------------	------------

8.2.1 Physical Methods	182
8.2.2 Material	185
8.2.3 Synthesis of monomers.....	185
8.2.4 General procedure for the terpolymerization of (2) and (3) with sulfur dioxide.....	186
8.2.5 Basification of CPZA (4) to cross-linked anionic polyelectrolyte (CAPE 5)	186
8.2.6 Sample characterizations	187
8.2.7 Adsorption experiments.....	188

8.3 Results and discussion	189
-----------------------------------------	------------

8.3.1 Synthesis and characterization of cross-linked polymers (4) and (5).....	189
8.3.2 Adsorption properties of CAPE (5) and IR spectroscopy	190
8.3.3 Adsorption kinetics.....	192
8.3.4 Effect of initial concentration on the adsorption of Cu^{2+} and Pb^{2+} ions.....	196
8.3.5 Effect of pH and temperature on adsorption.....	199
8.3.6 Scanning electron microscopy (SEM)	204
8.3.7 Desorption experiment.	206

8.4 Conclusion.....	206
----------------------------	------------

CHAPTER 9: REMOVAL OF ZINC AND CADMIUM IONS USING A CROSS-LINKED POLYZWITTERIONIC PHOSPHONATE/SULFUR DIOXIDE TERPOLYMERS..... 208

ABSTRACT	208
-----------------------	------------

9.1 Introduction	209
-------------------------------	------------

9.2 Experimental	212
-------------------------------	------------

9.2.1 Physical Methods	212
9.2.2 Materials	212
9.2.3 Synthesis of monomers and cross-linked polymers.....	212
9.2.4 Sample characterization.....	212
9.2.5 Adsorption experiments.....	213

9.3 Results and Discussion	214
-----------------------------------------	------------

9.3.1 Ion exchange properties and FTIR spectroscopy of CAPE (5).....	214
9.3.2 Adsorption kinetics.....	216

9.3.3	Effect of initial concentration on the adsorption of Zinc and Cadmium ions	220
9.3.4	Effect of pH on adsorption	224
9.3.5	Effect of Temperature on adsorption	225
9.3.6	Scanning electron microscopy (SEM)	228
9.4	Conclusion	230

CHAPTER 10:NOVEL CROSS-LINKED POLYMERS HAVING PH-RESPONSIVE AMINO ACID RESIDUES FOR THE REMOVAL OF CU²⁺ FROM AQUEOUS SOLUTION AT LOW CONCENTRATIONS..... 231

ABSTRACT	231
-----------------------	------------

10.1 Introduction	232
--------------------------------	------------

10.2 Experimental.....	233
-------------------------------	------------

10.2.1	Apparatus	233
10.2.2	Materials.....	234
10.2.3	Synthesis of monomers	234
10.2.4	Copolymerization of monomer (3) and (4) to form cross-linked polyzwitterion (CPZA 5) ..	236
10.2.5	Terpolymerization of (4), (7), and sulfur dioxide to cross-linked cationic polyelectrolyte (CCPE 8)	237
10.2.6	Sample characterizations	237
10.2.7	Adsorption experiments.....	238
10.2.8	Desorption experiment	239
10.2.9	QA/QC.....	239

10.3 Results and discussion.....	240
-----------------------------------------	------------

10.3.1	Synthesis of cross-linked polymer (6) and (9).....	240
10.3.2	Adsorption properties of CAPE (6) and CAPE (9).....	243
10.3.3	Effect of pH on the adsorption	245
10.3.4	Effect of contact time on the adsorption	246
10.3.5	Effect of initial concentration on the adsorption of Cu ²⁺ ions.....	250
10.3.6	Effect temperature on adsorption.....	256
10.3.7	Desorption experiment	259

10.4 SEM and EDX images for CAPE (6) and CAPE (9) unloaded and loaded with Copper ions	259
-----------------------------------------------------------------------------------------------------	------------

10.5 Treatment of real wastewater samples.....	262
-------------------------------------------------------	------------

10.6 Conclusion	265
------------------------------	------------

CHAPTER 11: A NOVEL CROSS-LINKED POLYAMINODIPHOSPHONATE FOR THE REMOVAL OF COPPER AND CADMIUM IONS FROM AQUEOUS SOLUTION AT LOW CONCENTRATIONS 266

ABSTRACT	266
11.1 Introduction.....	267
11.2 Experimental.....	270
11.2.1 Apparatus	270
11.2.2 Materials.....	270
11.2.3 Synthesis of monomers	271
11.2.4 General procedure for the copolymerization of the diallylaminomethylphosphonic acid (2) and 1,1,4,4-tetraallylpiperazinium dichloride (3)	271
11.2.5 Basification of CPZA (4) to cross-linked anionic polyelectrolyte (CAPE 5).....	272
11.2.6 Sample characterization	272
11.2.7 Adsorption experiments	272
11.2.8 QA/QC.....	273
11.3 Results and discussion.....	274
11.3.1 Synthesis of cross-linked polyanion (CAPE 5)	274
11.3.2 Adsorption properties of CAPE (5)	276
11.3.3 Adsorption kinetics.....	278
11.3.4 Adsorption isotherms	286
11.3.5 Effect of pH.....	292
11.3.6 Adsorption thermodynamics.....	293
11.3.7 SEM and EDX images for CAPE (5) unloaded and loaded with Copper and Cadmium ions	295
11.4 Treatment of real wastewater samples.....	297
11.5 Conclusion	298
REFERENCES.....	300
VITAE.....	321

LIST OF TABLES

Table 2.1	Cyclopolymerization of Cationic Monomer 5 to CPE 8	31
Table 2.2	Cyclopolymerization of Zwitterionic Monomer 7 to PZE 13	33
Table 2.3	Experimental Details for the Protonation of Polymer PZE 13 (ZH^+) (entry 3, Table 2.2) at 23 °C in Salt-Free Water and in 0.1N NaCl.....	39
Table 3.1	Cyclocopolymerization of the cationic monomer 1 with sulfur dioxide ^a to cationic polyelectrolyte (CPE) 2	50
Table 3.2	Cyclocopolymerization of the zwitterionic monomer 7 with sulfur dioxide ^a to PZE 8	55
Table 3.3	Experimental Details for the potentiometric titration of Polymer PZE 8 (ZH^+) at 23 °C in Salt-Free Water and in 0.1 N NaCl.....	58
Table 3.4	Solubility ^{a,b} of polymer CPE 2 , PZA 3 and PZE 8	62
Table 3.5	Critical salt concentration (CSC) for aqueous solutions of PZA 3 at 23°C...	63
Table 3.6	Effect of added salts on the intrinsic viscosity ($[\eta]^a$ and Huggins constant (K') of PZE 8 (entry 5, Table 2).	70
Table 3.7	Correlation using intrinsic viscosity in 0.1 N NaCl at 30°C of CPE 2 and PZE 8 and their corresponding DAPE 6	71
Table 3.8	Solubility behavior of several PZs and the basicity constants $\log K_i^a$ of their conjugate bases at 23°C in salt-free water.	74
Table 4.1	Viscosity of ZAPE 3 and DAPE 4	80
Table 4.2	Phase Composition of the PEG – DAPE 4 System at 23°C, (0.0 equiv. HCl, 0.1N NaCl) shown in figure 4.2a.....	84
Table 4.3	Phase Composition of the PEG – DAPE 4 System at 23°C, (0.0 equiv. HCl, 0.25N NaCl) shown in figure 4.2b.....	85
Table 4.4	Phase Composition of the PEG – DAPE 4 System at 23°C, (0.0 equiv. HCl, 0.4N NaCl) shown in Figure 4.2c.....	86
Table 4.5	Phase Composition of the PEG – DAPE 4 system at 23°C,(0.5 equiv. HCl, 0.25NaCl) shown in figure 4.3a.....	87
Table 4.6	Phase Composition of the PEG – DAPE 4 system at 23°C (1 equiv. HCl, 0.25 N NaCl) shown in figure 4.3b.....	88
Table 4.7	Phase Composition of the PEG – DAPE 4 system at 23°C (0.5 equiv. HCl, 0.4N NaCl) shown in figure 4.3c.....	89
Table 4.8	Phase Composition of the PEG – DAPE 4 system at 23°C, (1 equiv. HCl, 0.4N NaCl) shown in figure 4.3d.....	90
Table 5.1	Homopolymerization of the monomer 7	111
Table 5.2	Cyclocopolymerization of the monomer 7 with SO ₂	114
Table 5.3	Critical Salt Concentration for Aqueous Solutions of Polysulfobetaines 11 and 16 at 23 °C.....	118
Table 6.1	Copolymerization of monomers 2 and 3	133

Table 6.2	Lagergren second–order kinetic model parameters for Cu ²⁺ and Pb ²⁺ adsorption.....	141
Table 6.3	Langmuir and Freundlich isotherm model constants for Cu ²⁺ and Pb ²⁺ adsorption.....	145
Table 6.4	The R _L values based on the Langmuir isotherm model.....	146
Table 6.5	Thermodynamic data for Pb ²⁺ and Cu ²⁺ adsorption.....	151
Table 6.6	Comparison of CAPE 5 with those of different types of sorbents in References.....	155
Table 7.1	Lagergren second–order kinetic model parameters for Zn ²⁺ and Cd ²⁺ adsorption.....	167
Table 7.2	Ionic radius, effective hydrated ionic radius, hydration energy, electronegativity, and hardness Index of Zn ²⁺ and Cd ²⁺ ions.....	167
Table 7.3	Langmuir and Freundlich isotherm model constants for Zn ²⁺ and Cd ²⁺ adsorption.....	171
Table 7.4	The R _L values based on the Langmuir isotherm model.....	172
Table 7.5	Thermodynamic Data for Zn ²⁺ and Cd ²⁺ adsorption.....	176
Table 7.6	Comparison of CAPE 5 with those of different types of sorbents in References.....	179
Table 8.1	Lagergren Second–Order Kinetic Model Parameters for Pb ²⁺ and Cu ²⁺ Adsorption.....	195
Table 8.2	Langmuir and Freundlich isotherm model constants for Cu ²⁺ and Pb ²⁺ adsorption.....	198
Table 8.3	The R _L values based on the Langmuir isotherm model.....	199
Table 8.4	Thermodynamic Data for Pb ²⁺ and Cu ²⁺ adsorption.....	203
Table 8.5	Comparison of CAPE 5 with those of different types of sorbents in References.....	207
Table 9.1	Lagergren second–order kinetic model parameters for Zn ²⁺ and Cd ²⁺ adsorption.....	218
Table 9.2	Ionic radius, effective hydrated ionic radius, hydration energy, electronegativity, and hardness Index of Zn ²⁺ and Cd ²⁺ ions.....	219
Table 9.3	Langmuir and Freundlich isotherm model constants for Zn ²⁺ and Cd ²⁺ adsorption at 25°C.....	223
Table 9.4	The R _L values based on the Langmuir isotherm model.....	223
Table 9.5	Thermodynamic Data for Zn ²⁺ and Cd ²⁺ adsorption.....	228
Table 9.6	Comparison of CAPE 5 with those of different types of sorbents in References.....	230
Table 10.1	ICP-MS instrumental operating parameters ICP-MS XSERIES-II Thermo Scientific.....	240
Table 10.2	Lagergren second–order kinetic model parameters for CAPE 6 and CAPE 9 adsorption.....	249

Table 10.3	Langmuir, Freundlich and Temkin isotherm model constants for Cu ²⁺ adsorption.....	254
Table 10.4	The R_L values based on the Langmuir isotherm model and %Cu ²⁺ removal at different initial concentration.....	255
Table 10.5	Thermodynamic Data for Cu ²⁺ adsorption.....	259
Table 10.6	Comparison of metals concentration from Water treatment plant sample (Doha, Saudi Arabia) before and after adding the polymer.....	263
Table 10.7	Comparison of metals concentration from Petrochemical plant sample (Dhahran, Saudi Arabia) before and after adding the polymer.....	264
Table 11.1	ICP-MS instrumental operating parameters ICP-MS XSERIES-II Thermo Scientific.	274
Table 11.2	Lagergren First and Second–Order Kinetic Model Parameters for the adsorption of Cu ²⁺ and Cd ²⁺ ions ^a on CAPE 5	282
Table 11.3	Ionic radius, effective hydrated ionic radius, hydration energy, electronegativity, and hardness Index of Cu ²⁺ and Cd ²⁺ ions	282
Table 11.4	Intraparticle Diffusion coefficients and intercept values for the adsorption of Cu ²⁺ and Cd ²⁺ ions on CAPE 5 at different temperatures.....	284
Table 11.5	Langmuir and Freundlich isotherm model constants for Cu ²⁺ and Cd ²⁺ adsorption at different temperatures.	287
Table 11.6	The R_L values based on the Langmuir isotherm model and % Removal at different initial concentration at different temperatures	292
Table 11.7	Thermodynamic Data for Cu ²⁺ and Cd ²⁺ adsorption on CAPE 5	295
Table 11.8	Comparison of metals concentration from Water treatment plant sample (Doha, Saudi Arabia) before and after adding the polymer.....	298
Table 11.9	Comparison of metals concentration from Petrochemical plant sample (Dhahran, Saudi Arabia) before and after adding the polymer.....	298

LIST OF FIGURES

Figure 1.1	ionic polymers having different charges on the polymer backbone..... 2
Figure 2.1	¹ H NMR spectrum of (a) 5 , (b) 8 , (c) 13 and (d) 11 in D ₂ O 29
Figure 2.2	¹³ C NMR spectrum of (a) 5 , (b) 8 , (c) 13 and (d) 11 in D ₂ O 30
Figure 2.3	The viscosity behavior at 30 °C using an Ubbelohde Viscometer of (a) CPE 8 (entry 5, Table 2.1) in salt-free water and 0.1 N NaCl; (b) PZE 13 (entry 3, Table 2.2) in the presence of varying concentrations of added salts; (c) a 1.0 g/dL solution of polymer PZE 13 (entry 3, Table 2.2) in salt-free water versus equivalent of added NaOH. Negative (-) values indicate the equivalent of added HCl. (d) □ (i) DAPE 11 (derived from CPE 8 of entry 5, Table 2.1); ■ (ii) DAPE 11 (derived from PZE 13 entry 3, Table 2.2); ▲ (iii) PZE 13 (entry 3, Table 2.2); and Δ (iv) CPE 8 (entry 5, Table 2.1) 0.1 N NaCl..... 35
Figure 2.4.	Plot for the apparent log K_1 versus degree of protonation (α) for PZE 13 in salt-free water and 0.1 N NaCl..... 38
Figure 2.5	Phase diagram of PEG -DAPE 11 -Water (0.4 N NaCl) in the presence of (a) 0 HCl; (b) 0.5 equiv. HCl and (c) 1 equiv. HCl; and (d) binodals for the systems presented in (a)-(c) at 23 °C..... 41
Figure 3.1	¹ H NMR spectrum of (a) 1 , (b) 2 , (c) 8 and (d) 6 in D ₂ O. 51
Figure 3.2	¹³ C NMR spectrum of (a) 1 , (b) 2 , (c) 8 and (d) 6 in D ₂ O. 52
Figure 3.3	Using an Ubbelohde Viscometer at 30 °C: The viscosity behavior of (a) CPE 2 (entry 4, Table 1) in salt-free water, 0.1 N and 0.5 N NaCl, (b) DAPE 6 (prepared from entry 4, Table 1) in salt-free water, 0.1 N, 0.3 and 0.5 N NaCl, (c) a 1.0 g/dL solution of polymer DAPE 6 (prepared from entry 4, Table 1) in salt-free water in the presence of different equivalent of added HCl and (d) ZAPE 5 (prepared from entry 4, Table 1) in salt-free water, 0.1 N and 0.5 N NaCl..... 65
Figure 3.4	The viscosity behavior of CPE 2 , DAPE 6 and ZAPE 5 (all from or derived from entry 4, Table 1) in salt-free water, and 0.1 N NaCl at 30 °C using an Ubbelohde Viscometer. 67
Figure 3.5	Using an Ubbelohde Viscometer at 30 °C: (a) The viscosity behavior of PZE 8 (entry 5, Table 2) and APE 9 (derived from entry 5, Table 2) in salt-free water and 0.1 N NaCl; (b) The intrinsic viscosity [η] behavior of PZE 8 (entry 5, Table 2) in the presence of varying concentrations of added salts; (c) Reduced viscosity (η_{sp}/C) of a 1.0 g/dL solution of PZE 8 (entry 5, Table 2) in salt-free water versus equivalent of added NaOH. Negative (-) values indicate the equivalent of added HCl. (d) Plot for the apparent log K_1 versus degree of protonation (α) for PZE 8 (entry 5, Table 2) in salt-free water and 0.1 N NaCl..... 69

Figure 3.6	Phase diagram of PEG -DAPE 4 -Water (0.4 N NaCl) at 23 °C.....	73
Figure 4.1	¹ H NMR spectra of (a) DAPE 4 . (b) Bottom phase, system 2: (DAPE 4 , PEG, 0.4N NaCl, 0.0 equiv. HCl). (c) Top Phase, system 3: (DAPE 4 , PEG, 0.4N NaCl, 0.0 equiv. HCl).	81
Figure 4.2	Phase diagram of PEG-DAPE 4 -H ₂ O in the presence of (a) 0.0 equiv. HCl, 0.1 N NaCl; (b) 0.0 equiv. HCl, 0.25 N NaCl; (c) 0.0 equiv. HCl, 0.4 N NaCl; (d)The effect of salt concentration on the binodal curve of PEG-DAPE 4 -H ₂ O system.	94
Figure 4.3	Phase diagram of PEG-DAPE 4 -H ₂ O in the presence of (a) 0.5 equiv. HCl, 0.25 N NaCl; (b) 1.0 equiv. HCl, 0.25 N NaCl; (c) 0.5 equiv. HCl, 0.4 N NaCl; (d) 1.0 equiv. HCl, 0.4N NaCl.(e) Effect of HCl and NaCl concentration on the binodal curves of DAPE 4 / PEG/H ₂ O ATPSs.	95
Figure 4.4	Effect of added salt on the conformation of polyelectrolytes and polyzwitterions.	97
Figure 4.5	Correlation of the phase diagrams of DAPE 4 - PEG-HCl systems using the method of Diamond and Hsu: using the tie line data of :(a) Fig. 4.2b; (b) Fig. 4.2c; (c) Fig. 4.3a;(d) Fig. 4.3c;(e) Fig. 4.3b;(f) Fig. 4.3d.	99
Figure 5.1	¹ H NMR spectra of (a) 6 , (b) 6/7 (60:40), and (c) 7/8 (60:40) in D ₂ O....	108
Figure 5.2	¹³ C NMR spectra of (a) 6 , (b) 6/7 (60:40), and (c) 7/8 (60:40) in D ₂ O. .	109
Figure 5.3	(a) ¹ H and (b) ¹³ C NMR spectra of 11 in (D ₂ O + NaCl).	112
Figure 5.4	¹ H NMR spectra of (a) 16 in (D ₂ O + KCl) and (b) 17 in D ₂ O.	115
Figure 5.5	¹³ C NMR spectra of (a) 16 in (D ₂ O + KCl) and (b) 17 in D ₂ O.	116
Figure 5.6	Depiction of intragroup, intrachain, and interchain attractions in polyzwitterions	125
Figure 6.1	IR spectra of (A) Cross-linked polyanion 5 , (B) Cross-linked polyanion 5 loaded with Cu ²⁺ and (C) Cross-linked polyanion 5 loaded with Pb ²⁺	139
Figure 6.2	Absorption kinetic curves of Cu ²⁺ and Pb ²⁺ in 0.1 M solution at pH 4 at 25°C.....	140
Figure 6.3	Lagergren second-order kinetic model for adsorption of Cu ²⁺ and Pb ²⁺ on CAPE 5	141
Figure 6.4	The effect of initial concentration on the adsorption capacity of CAPE 5 at pH 4 for 24 h at 25°C.	143
Figure 6.5	Langmuir isotherm of the adsorption of Cu ²⁺ and Pb ²⁺ ions on CAPE 5	143
Figure 6.6	Freundlich isotherm of the adsorption of Cu ²⁺ and Pb ²⁺ ions on CAPE 5	144
Figure 6.7	pH dependence of metal uptake by CAPE 5	147
Figure 6.8	Effect of temperature on the adsorption capacity of CAPE 5	148
Figure 6.9	Plots of log q _e versus (1/T)×10 ³	149
Figure 6.10	Plots of log(q _e /C _e) versus (1/T)×10 ³	150

Figure 6.11	SEM images for unloaded and loaded CAPE 5 with Pb ²⁺ and Cu ²⁺	153
Figure 7.1	FT-IR of unloaded and loaded CAPE 5 with Zn ²⁺ and Cd ²⁺	163
Figure 7.2	TGA curve for CAPE 5	164
Figure 7.3	(a) Effect of time on the adsorption capacity; (b) Lagergren second-order kinetic model.(c) intraparticle diffusion model	166
Figure 7.4	(a) Effect of initial concentration on the adsorption capacity; (b) Langmuir isotherm plot; (c) Freundlich isotherm plot.....	170
Figure 7.5	Effect of pH on the adsorption capacity.....	173
Figure 7.6	(a) Effect of temperature on the adsorption capacity; (b) Arrhenius plot; (c) Vant-Hoff plot	175
Figure 7.7	SEM images and EDX analysis for:(a) CAPE 5 ; (b) CAPE 5 loaded with Zinc; (c) CAPE 5 loaded with Cadmium.	178
Figure 8.1	TGA curve of CAPE 5	187
Figure 8.2	IR spectra of (A) Cross-linked polyanion 5 , (B) Cross-linked polyanion 5 loaded with Cu ²⁺ and (C) Cross-linked polyanion 5 loaded with Pb ²⁺ ..	191
Figure 8.3	(a) Absorption kinetic curves of Cu ²⁺ and Pb ²⁺ in 0.1 M solution at pH 4 at 25°C; (b) Lagergren second-order kinetic model for adsorption of Cu ²⁺ and Pb ²⁺ on CAPE 5 ; (c) Intraparticle diffusion model.	193
Figure 8.4	(a) The effect of initial concentration on the adsorption capacity of CAPE 5 at pH 4 for 24 h at 25°C; (b) Langmuir and (c) Freundlich isotherm of the adsorption of Cu ²⁺ and Pb ²⁺ ions on CAPE 5	197
Figure 8.5	pH dependence of metal uptake by CAPE 5	200
Figure 8.6	(a) Effect of temperature on the adsorption capacity of CAPE 5 ; (b) Arrhenius plot; (c) Vant-Hoff plot.	202
Figure 8.7	SEM images for unloaded and loaded CAPE 5 with Pb ²⁺ and Cu ²⁺	205
Figure 9.1	FT-IR of unloaded and loaded CAPE 5 with Zn ²⁺ and Cd ²⁺	215
Figure 9.2	(a) Effect of time on the adsorption capacity; (b) Lagergren second-order kinetic model.(c) Intraparticle diffusion model.....	217
Figure 9.3	(a) Effect of concentration on the adsorption capacity; (b) Langmuir isotherm plot ; (c) Freundlich isotherm plot.....	221
Figure 9.4	Effect of pH on the adsorption capacity.....	225
Figure 9.5	(a) Effect of temperature on the adsorption capacity; (b) Arrhenius plot; (c) Vant-Hoff plot	226
Figure 9.6	SEM images and EDX analysis for:(a) CAPE 5 ; (b) CAPE 5 loaded with Zinc; (c) CAPE 5 loaded with Cadmium.	229
Figure 10.1	TGA analysis for CAPE 6 and CAPE 9	243
Figure 10.2	IR spectra for unloaded and loaded CAPE 6 and CAPE 9 with Copper.	244
Figure 10.3	Effect of pH on the adsorption capacity.....	246
Figure 10.4	(a) Effect of time on the adsorption capacity, (b) Lagergren second order kinetic model; (c) Intraparticle diffusion model	247

Figure 10.5	(a) Effect of metal concentration on the adsorption capacity (b) Langmuir plot, (c) Freundlich plot, (d) Temkin plot.	251
Figure 10.6	(a) Effect of temperature on adsorption capacity,(b) Arrhenius plot, (c) Van't - Hoff plot	257
Figure 10.7	SEM and EDX analysis for unloaded and loaded CAPE 6 with Cu.	260
Figure 10.8	SEM and EDX analysis for unloaded and loaded CAPE 9 with Cu.	261
Figure 10.9	Resins before and after the adsorption of Cu ²⁺ ions.....	262
Figure 11.1	TGA analysis of CAPE 5	276
Figure 11.2	FT-IR for: (a) Unloaded CAPE 5 ; (b) CAPE 5 loaded with Cu ²⁺ ;(c) CAPE 5 loaded with Cd ²⁺	277
Figure 11.3	(a) Effect of time on the adsorption capacity of Copper. (b) Lagergren First- order kinetic model. (c) Lagergren second-order kinetic model (d) Intraparticle diffusion model.....	279
Figure 11.4	(a) Effect of time on the adsorption capacity of Cadmium. (b) Lagergren First- order kinetic model. (c) Lagergren second-order kinetic model (d) Intraparticle diffusion model.....	281
Figure 11.5	Arrhenius plot.....	286
Figure 11.6	(a) Effect of copper initial concentration on the adsorption capacity at different temperatures. (b) Langmuir isotherm model. (c) Freundlich isotherm model.....	289
Figure 11.7	(a) Effect of Cadmium initial concentration on the adsorption capacity at different temperatures. (b) Langmuir isotherm model. (c) Freundlich isotherm model.....	290
Figure 11.8	Effect of pH on the adsorption capacity of CAPE 5	293
Figure 11.9	(a) Effect of temperature on the adsorption capacity of CAPE 5 ; (b) Vant-Hoff plot.	294
Figure 11.10	(a) Unloaded CAPE 5 ; (b) CAPE 5 loaded with Cu ²⁺ ions; (c) CAPE 5 loaded with Cd ²⁺ ions.....	296

ABSTRACT

Full Name : Othman Charles Sadeq Othman Al Hamouz
Thesis Title : Synthesis and Applications of Linear and Cross-linked pH-Responsive Polycarbo-, Polyphospho- and Polysulfobetaines
Major Field : Chemistry
Date of Degree : March 2013

N,N-diallyl-(diethylphosphonato)methylammonium chloride **I** and ethyl 3-(*N,N*-diallylammonio)methanephosphonate **II** underwent cyclopolymerization to give a cationic polyelectrolyte (CPE) **III** and a polyzwitterion (PZ) **IV**, respectively. Both **III** and **IV** upon acidic hydrolysis afforded a pH-responsive polyzwitterionic acid (PZA) **V**: poly[3-(*N,N*-diallylammonio)methanephosphonic acid, which was converted to a zwitterionic/polyelectrolyte (ZAPE) **VI** and dianionic polyelectrolyte (DAPE) **VII** having interesting solution properties. The basicity constants for the protonation of nitrogen in **II** and **IV** have been determined. Monomers **I** and **II** underwent cocyclopolymerization with SO₂ to give their corresponding alternating copolymers **VIII** [i.e., poly(**I**-*alt*-SO₂)] and **IX** [i.e., poly(**II**-*alt*-SO₂)], respectively. The acidic hydrolysis of **VIII** or **IX** led to PZA **X**, ZAPE **XI** and DAPE **XII**.

Phase diagrams of polyethylene glycol-DAPE **VII** and polyethylene glycol-DAPE **XII** aqueous two-phase systems (ATPSs) have been investigated, which may lead to their use in the purification of proteins.

The alternating cocyclopolymer of zwitterionic *N,N*-diallylammoniomethanesulfonate **XIII** with SO₂ gave a polyzwitterion **XIV** [i.e., poly(**XIII**-*alt*-SO₂)] which represents the first example of a polysulfobetaine having a single methylene spacer separating the charge centers and showed very strong zwitterionic interactions.

Novel cross-linked polyzwitterionic acids (CPZAs) were synthesized via cyclocopolymerization of diallylaminomethylphosphonic acid, diallylammonioethanoate and diallylaminomethyldiphosphonic acid in the presence of cross-linker 1,1,4,4-

tetraallylpiperazinium dichloride. CPZAs, upon treatment with NaOH, were converted into cross-linked anionic polyelectrolytes (CAPEs) which were found to be very efficient in the removal of toxic Pb^{2+} , Cu^{2+} , Zn^{2+} , and Cd^{2+} from aqueous solution both at high and low concentrations (200–1000 ppb range). Thermodynamic and kinetic parameters for the adsorption process were determined.

ملخص الرسالة

الاسم الكامل: عثمان شارل صادق عثمان الحموز

عنوان الرسالة:

تخليق مبلمرات خطية و متصلة تتأثر بتعديل الرقم الهيدروجيني و تحتوي على المجموعات الوظيفية التالية:
الكربو-، الفوسفو- والسلفوبيتين وتطبيقاتها في المجالات المختلفة.

التخصص: الكيمياء

تاريخ الدرجة العلمية: 2013

عملية البلمرة الحلقية باستخدام مونومرات موجبة I (N,N-diallyl-) ethyl) II (diethylphosphonato)methylammonium chloride و ثنائية الشحنة III (CPE) و فوق كبريتات (APS) أو ثالثي بيوتيل هيدروبيروكسيد (TBHP) لإنتاج بوليمرات موجبة III (CPE) و بوليمر ثنائي الشحنة IV (PZ). التميؤ الحمضي ل III و IV أنتج مبلمر حمضي ثنائي الشحنة V (PZA)، الذي تحول تحت تعديل درجة الحموضة إلى ثنائي الشحنة سالب VI (ZAPE) و مبلمر ثنائي سالب الشحنة VII (DAPE) ذات خصائص مشيرة للاهتمام. وقد تم تحديد الثوابت القاعدية لبروتوناتيون النيتروجين في IV و II. تمت عملية البلمرة الحلقية للمونومرات I و II مع ثاني أكسيد الكبريت في ثنائي ميشيل سلفوكسايد باستخدام azoisobutyronitrile كبادئ للتفاعل لإعطاء ما يقابلها من بوليمرات VIII ([i.e. poly(I-alt-SO₂)] and IX [i.e., poly(II-alt-SO₂)], عملية التميؤ الحمضي ل VIII و IX أنتج PZA X و ZAPE XI و DAPE XII التي وجد أن لها خصائص مشيرة للاهتمام.

تم بناء محطات جديدة من البولي إيثيلين جلايكول - DAPE XII و البولي إيثيلين جلايكول - DAPE VII باستخدام طريقة الأنظمة ثنائية الطور المائية (ATPSs) و التي يؤدي إلى استخدامها في تنقية الجزئيات الحيوية مثل البروتينات.

عملية البلمرة بين ثاني أكسيد الكبريت و *N,N*-diallylammoniomethanesulfonate XIII أنتجت مبلمر ثنائي الشحنة (PZ) و الذي يمثل أول مثال على وجود مبلمر السلفوييتين يحتوي على مجموعة ميشيل واحدة بين الشحنات المختلفة.

تم تخليق مبلمرات متخصصة لمعالجة أيونات الرصاص والنحاس و الكاديوم و الزنك من المياه عن طريق عملية البلمرة الحلقية لثنائي أليل امينوثنائي حمض الفوسفونيك و ثنائي أليل ميشيل الفوسفونات و ثنائي أليل ميشيل الإيثانوات مع رباعي أليل البيرازينيوم ثنائي الكلوريد. معالجة هذه المبلمرات باستخدام هيدروكسيد الصوديوم أدى إلى تحويلها إلى الشكل الأيوني السالب (CAPes)، و تم تحديد المعايير الحرارية و الحركية لعملية الإمتصاص. النتائج أثبتت قدرة هذه المبلمرات قد يتم إستخدامها في معالجة المياه العادمة.

CHAPTER 1: INTRODUCTION

1.1 Cationic, anionic, zwitterionic and ampholytic polymers

The polymerization of carbo-, phospho- or sulfo-betaines (zwitterions) (M^{\pm}) having positive and negative charges in the same molecular framework lead to polyzwitterions (PZs) (polybetaines)^[1, 2]. The presence of both M^+ and M^- in the same polymer chain constitutes a polyampholyte (PA) with or without charge symmetry (Figure 1). Synthetic PAs and PZs, whose structure and behavior seem to mimic biopolymers (like proteins or DNA) that mediate life processes, have offered many new applications in various fields^[1,2,4-6]. Butler's cyclopolymerization^[3-6] of zwitterionic diallylammonium monomers or their copolymerizations with sulfur dioxide have been an attractive method for the synthesis of PZs. The PAs and PZs, unlike cationic or anionic polyelectrolytes^[7], exhibit anti-polyelectrolyte behavior^[4, 8, 9] i.e. enhancement in viscosity and solubility in the presence of added electrolytes (e.g. NaCl) owing to the neutralization of the ionically cross-linked network in a collapsed coil conformation of the polymers.

Polyphosphobetaines (containing repeating unit of a dialkylphosphate motif: a derivative of phosphoric acid, H_3PO_4), which seem to mimic phospholipid biomembranes, have offered many new applications^[1, 10]. To our knowledge, there are only a few reports^[11-16] that describe the cyclopolymerization of phosphorous acid (H_3PO_3) derivatives like diallylaminoalkyl phosphonic acids to polyphosphonobetaines. Extraordinary chelating properties of aminomethylphosphonic acid groups have been exploited to form polymer-heavy metal ion complexes from waste water^[17-19]. In pursuit

of tailoring pH-responsive polymers, we describe herein the synthesis of new monomers, a cationic phosphonium salt (**5**), and a zwitterionic phosphonobetaine (**7**) (Scheme 1), and their cyclopolymers (Schemes 2 and 3). To the best of our knowledge, cyclopolymers of **5** and **7** represents the first examples of this class of ionic polymers having a single carbon spacer separating the nitrogen and the phosphonate ester motifs.

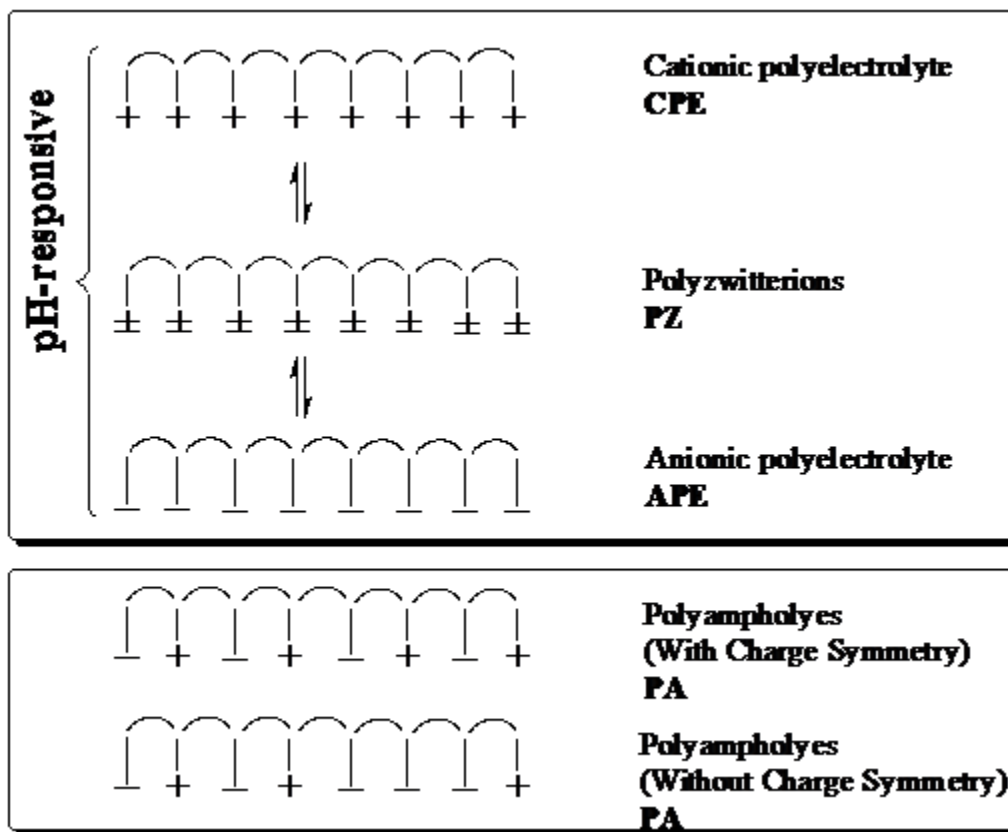
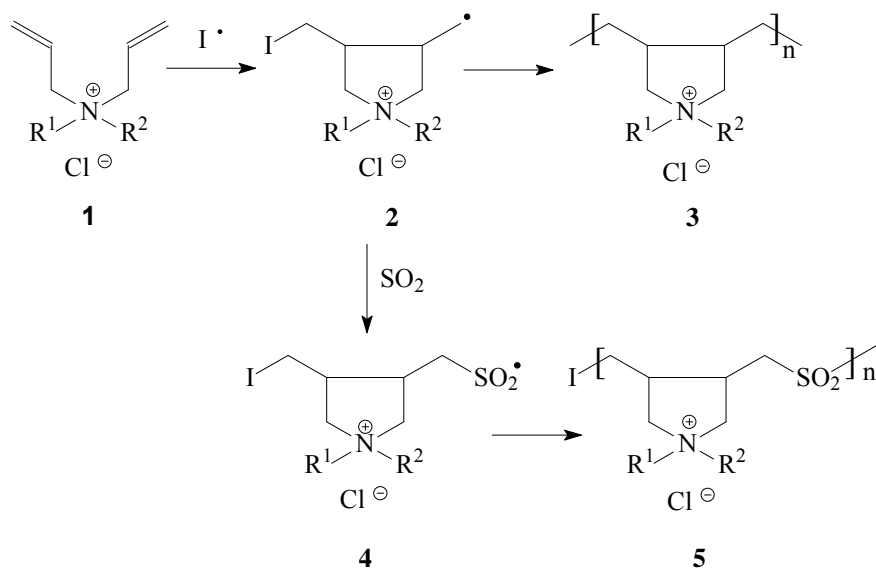


Figure 1.1 ionic polymers having different charges on the polymer backbone.

The synthesis of a series of new pH-responsive polymers would pave the way to study cationic polyelectrolyte – to – polyzwitterionic – to – anionic polyelectrolyte transitions of polymers with identical degree of polymerization.

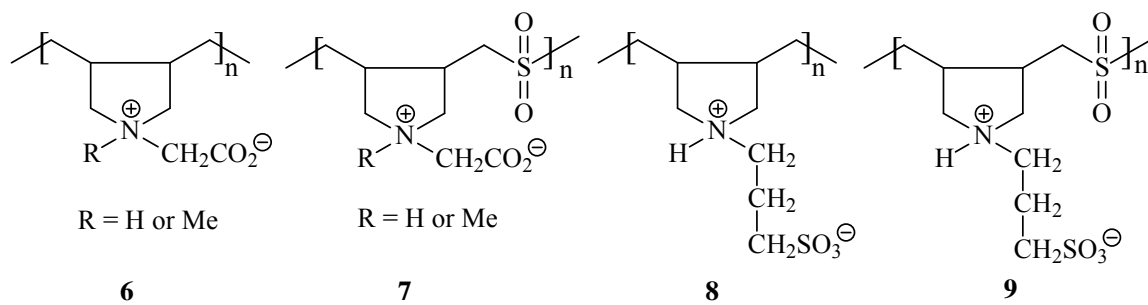
The cyclopolymerization process of *N,N*-diallyl quaternary ammonium salts led to the synthesis of an array of industrially important water-soluble cationic polyelectrolytes (Scheme 1). The polymer-architecture having five-membered cyclic units embedded in the backbone has been recognized as the eighth major structural type of synthetic polymers. Polydiallyldimethylammonium chloride alone accounts for over 1000 patents and publications. Over 33 million pounds of poly(diallyldimethylammonium chloride) alone are sold annually for water treatment and another 2 million pounds are used for personal care formulation^[20].



Scheme 1.

Pioneering work by Butler and co-workers^[21] led to the polymerization of a variety of diallyl quaternary ammonium salts **1** via an intra- and inter-molecular chain propagation (termed cyclopolymerization)^[14, 22-24], through the five-membered cyclic structure **2** to yield linear water-soluble polymers **3** (Scheme 1). Quaternary ammonium salts copolymerized with sulfur dioxide **5** are also manufactured^[25] commercially and are useful as textile furnishes, polymer additives, coagulants and thickeners.

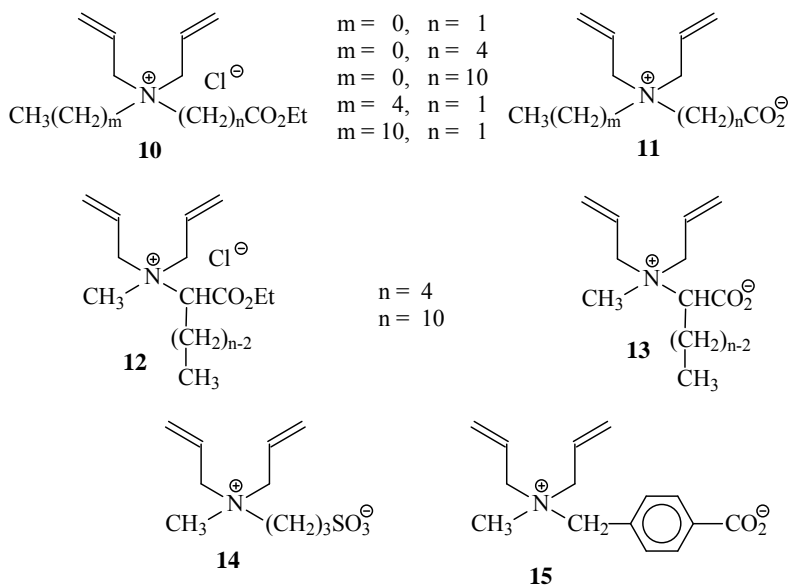
Some of the representative examples of polyzwitterions (**6-9**) are synthesized via the cyclopolymerization reaction are given in Scheme 2^[5, 26-31]. In contrast to normal polyelectrolytes, the viscosity of the ampholytic (zwitterionic) polymers is known to increase with increasing the concentration of added salt (like NaCl). Polyampholytes are extensive chain expansion upon increasing the salt concentration. Solubility in water is promoted by electrolytes, which disrupt the intra- and inter-molecular ionic or dipolar network^[32-34]. The increase in viscosity, which is observed in the presence of brine (anti-polyelectrolyte behavior), makes the polyampholytes ideal candidates for high salinity media and attractive in view of possible applications in enhanced oil recovery^[35]. Water-soluble polymers are extremely important for their relevance to theoretical and applied research^[36] in biotechnology, controlled delivery of active agents and protection of the environment. Cationic polyelectrolytes have been utilized extensively in water treatment, papermaking, reduction of drag in mineral processing, and in petroleum recovery^[37-40].



Scheme 2

A series of new polycarbobetaines from monomers **10-15** has been synthesized with varying lengths and positions of the hydrophobic side chains; together with the cationic analogs^[41]. The polycarbobetaines form homogeneous blends with selected inorganic salts, to provide organic-inorganic hybrid materials (Scheme 3). Catch and release of

DNA in coacervate-dispersed gels has been successfully carried out by the use of polyzwitterions^[42]. Interactions between sulfobetaine-based polyzwitterions and polyelectrolytes have been recently reported^[43]. There are several reviews that deal with the properties and applications of water-soluble and water-swelling integral- and pendant-type polyampholytes^[44], the preparation and properties of water-soluble polymers of various types, including polybetaines, cationic polyelectrolytes and grafted polymers^[45], and synthesis, characterization, and application of polymeric betaines.^[46]



Scheme 3.

1.2 Resins for waste water treatment

The presence of heavy metal ions, such as Pb^{2+} , Cu^{2+} , etc., in natural and waste water systems is a matter of great concern due to their negative effects on the environment and human health. These toxic pollutants are nonbiodegradable and can accumulate in the human body causing a variety of diseases and disorders^[46-51]. Various techniques, like adsorption, precipitation, dialysis, ion exchange, reverse osmosis, and extraction, have been developed in the past for the removal of metal contaminants from water resources.

One of the most attractive among these techniques is the adsorption process due to the availability of different types of low-cost and environment-friendly adsorbents.^[52-54] Inorganic/organic polymer hybrid adsorbents have been widely investigated; their efficacies in metal ion removal attributed to the formation of a stronger chemical bonding between M^{n+} and, for instance, amine motifs in the hybrid materials^[54-58]. Recently, researchers have focused on the syntheses of zwitterionic cross-linked inorganic/organic hybrid materials for the removal of heavy metal ions via electrostatic effects.^[47, 59, 60]

A titania-phosphonate hybrid porous material was found to have a large capacity for selective adsorption of Cd^{2+} ions^[61, 62]. Considerable attention has been given to synthesize chelating agents containing aminomethylphosphonate motif owing to its extraordinary chelating properties in extracting heavy metal ions from waste water.^[10] In this work, a novel class of cross-linked polymers containing aminomethylphosphonate and aminomethylcarboxylate motifs will be synthesized and tested for its efficiency as an adsorbent for the removal of heavy metal ions like Pb^{2+} and Cu^{2+} from aqueous solutions.

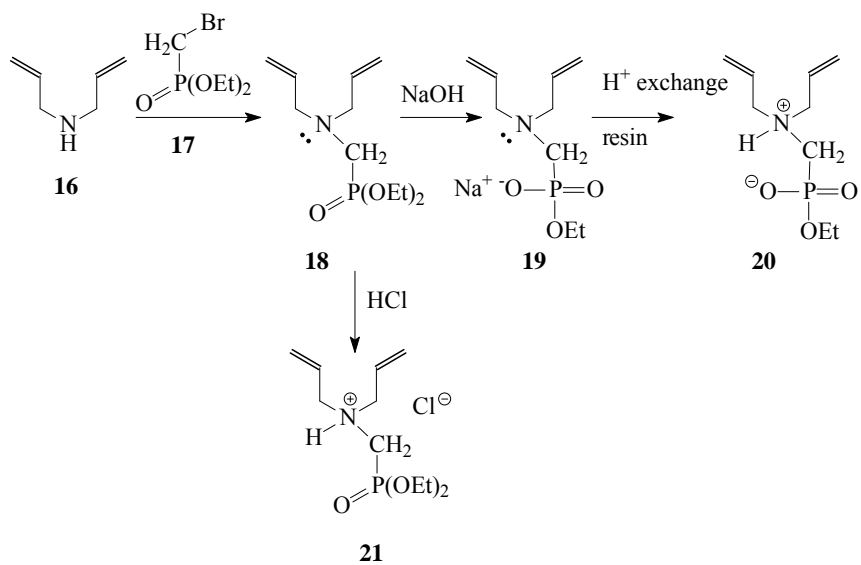
1.3 Objectives

The aim of this proposed research is to synthesize a series of pH-responsive polymers derived via cyclopolymerization of a new class of specialty diallyl ammonium monomers. The pH-responsive polymers containing trivalent nitrogen, phosphonate, carboxylate, diphosphonate, and sulfonate functionalities will be tested as antiscalants in the desalination process. A series of novel cross-linked resins containing metal-chelating carboxyl, phosphonate motifs will be synthesized via cyclopolymerization. The resins will be tested to determine their efficacy in the removal of heavy metal ions using a novel cross-linked polyphosphonate.

To achieve this, the proposed study will have the following objectives:

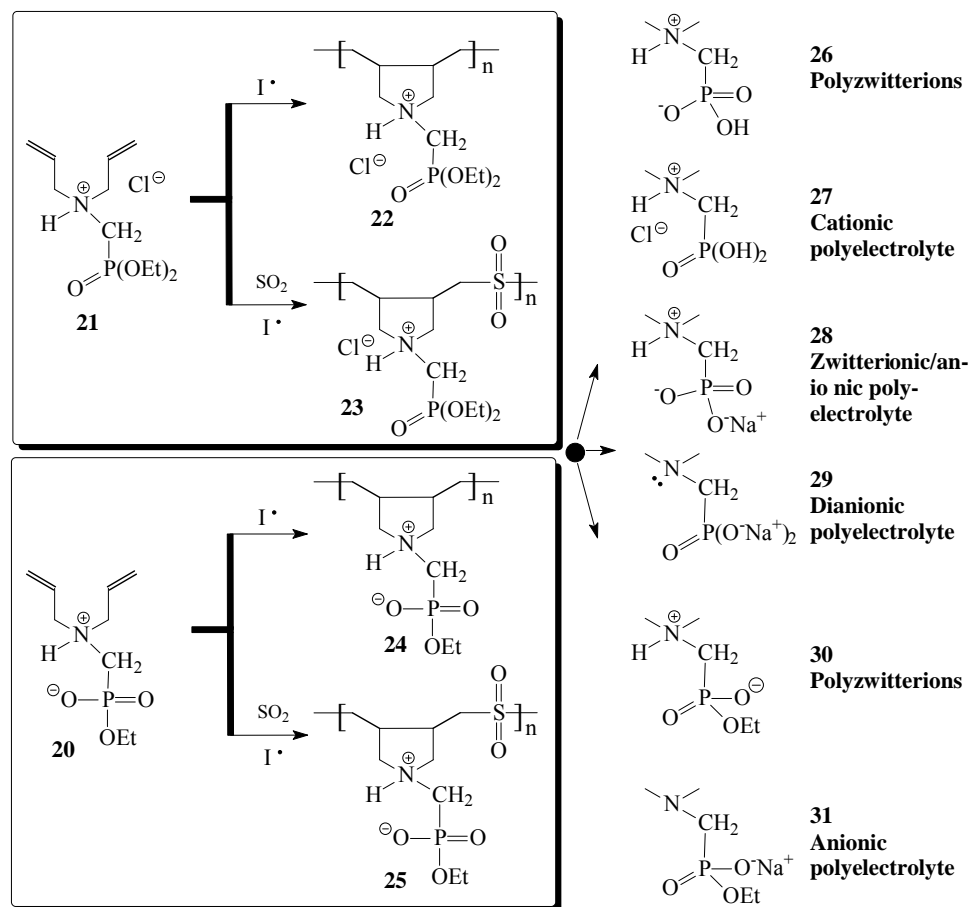
1. To synthesize new diallyl monomer salt containing phosphonate pendants

(Scheme 4).



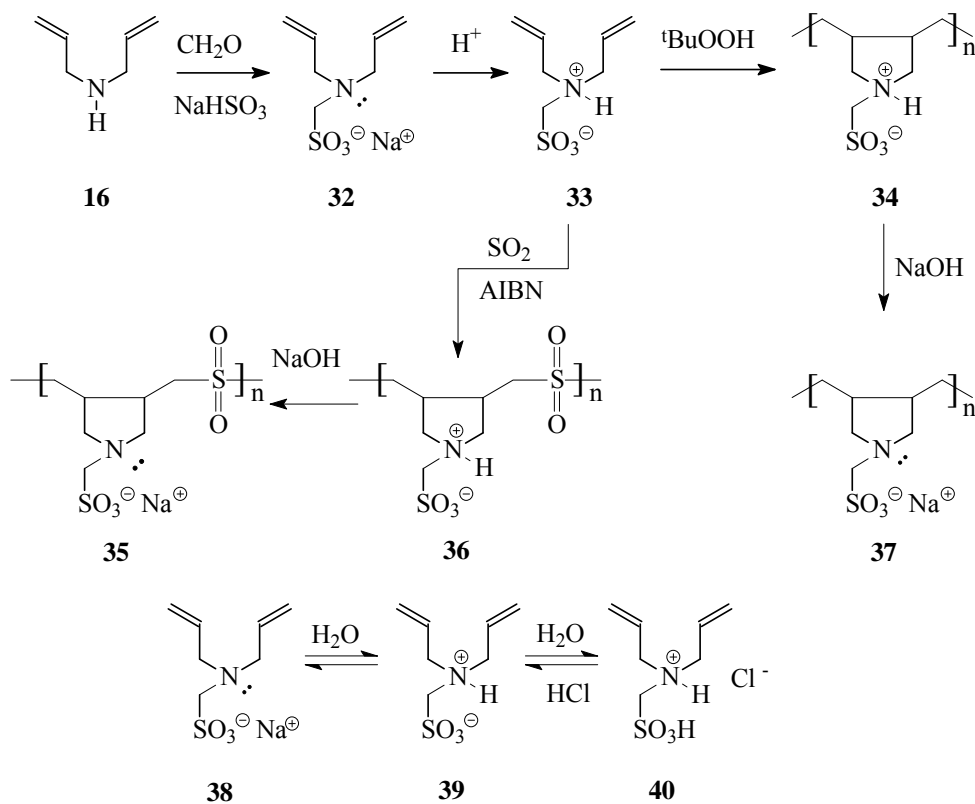
Scheme 4.

2. Homo- and co-cyclopolymerization of the phosphonate monomers (presented in Scheme 5): Homopolymerization and copolymerization with SO₂ to give a series of homo and co-polymers (Scheme 5).



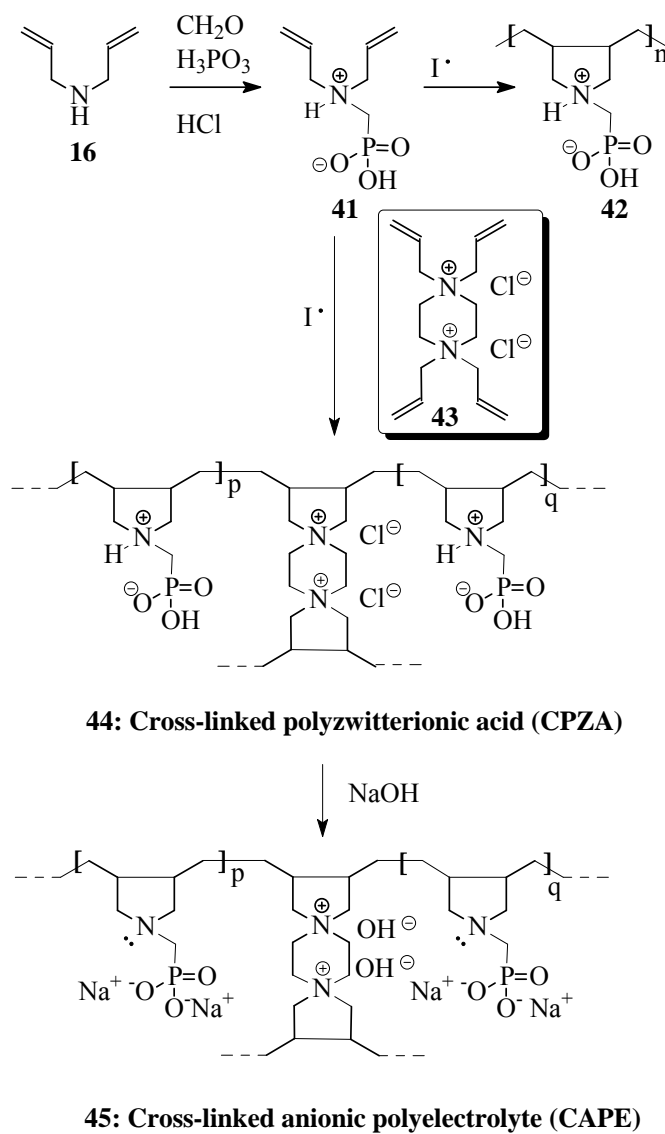
Scheme 5.

3. To synthesize new diallyl monomer salts containing sulfonate pendants and their homo- and cyclopolymerizations (Scheme 6).



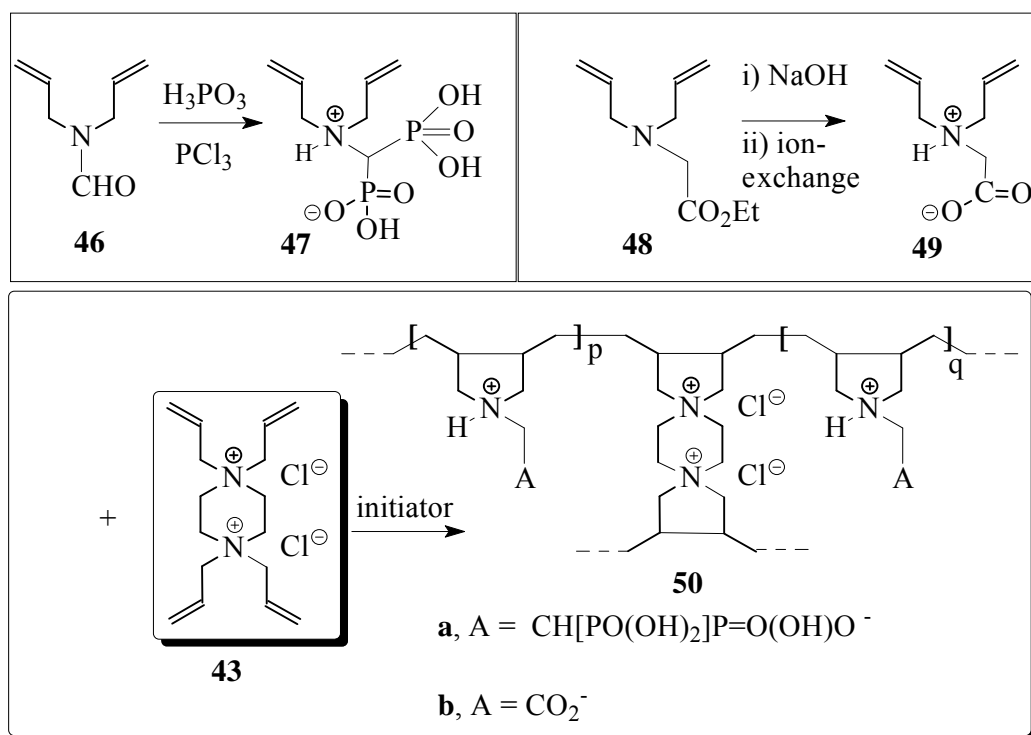
Scheme 6.

4. To synthesize new cross-linked resins containing phosphonate pendants
(Scheme 7).



Scheme 7.

5. To synthesize new cross-linked resins containing diphosphonate and carboxylate pendants (Scheme 8).



Scheme 8.

6. The resulting polymers (Schemes 5 and 6) would be interconverted to polyelectrolytes, zwitterionic/anionic polyelectrolyte, anionic polyelectrolytes and cationic electrolytes. The solution behavior of the resulting polymers will be studied.
7. Evaluation of the cross-linked resins as adsorbents for the removal of heavy metal ions like Pb^{2+} and Cu^{2+} ions from aqueous solutions.

1.4 Present state of the problem

To the best of our knowledge, cyclopolymers of monoethyl phosphonate **20** and diethyl phosphonate **21** would represent the first examples of this class of ionic polymers having a one carbon spacer separating the nitrogen and the phosphonate ester motifs. The synthesis of a series of new pH-responsive polymers would pave the way to study cationic polyelectrolyte – to – polyzwitterionic – to – anionic polyelectrolyte transitions involving polymers having identical degree of polymerization. Polysulfobetaine having a single carbon spacer is not known to this date.

In this work, a series of novel cross-linked polymer containing aminomethyl-phosphonate, -carboxylate, and diphosphonate motifs has been synthesized and tested for its efficiency as an adsorbent for the removal of heavy metal ions like Pb(II) and Cu(II) ions from aqueous solutions.

CHAPTER 2: pH-Responsive Polyphosphonates Using Butler's Cyclopolymerization

Taken from Othman Charles S. Al-Hamouz, Shaikh A. Ali, pH-Responsive Polyphosphonates Using Butler's Cyclopolymerization, *Journal of Polymer Science: Polymer Chemistry*, 50 (2012), 3580–3591

Abstract

The cationic monomer, *N,N*-diallyl-(diethylphosphonato)methylammonium chloride, and zwitterionic monomer, ethyl 3-(*N,N*-diallylammonio)methanephosphonate, were cyclopolymerized in aqueous solutions using ammonium persulfate or *t*-butylhydroperoxide as initiators to afford a cationic polyelectrolyte (CPE) and a polyzwitterion ester (PZE), respectively. The CPE and PZE on acidic hydrolysis of the ester functionalities afforded the same polyzwitterionic acid (PZA): poly[3-(*N,N*-diallylammonio)methanephosphonic acid]. The solution properties of the CPE, pH-responsive PZE, and PZA were studied in detail by potentiometric and viscometric techniques. Basicity constants of the phosphonate ($\text{P}=\text{O}(\text{OEt})\text{O}^-$) and amine groups in the PZE and in the conjugate base of the PZE, respectively, were found to be “apparent” and as such follow the modified Henderson–Hasselbalch equation. In contrast to many polycarbobetaines and sulfobetaines, PZE was found to be soluble in salt-free water as well as salt (including Ca^{2+} , Li^+)-added solutions, and demonstrated “antipolyelectrolyte” solution behavior. The PZA, on the other hand, was found to be insoluble in salt-free water, and on treatment with NaOH gave dianionic polyelectrolyte (DAPE) containing

trivalent nitrogen and $[P=O(O)_2]^{2-}$ groups. For the first time, several new phase diagrams of polyethylene glycol-DAPE aqueous two-phase systems (ATPSs) have been constructed in the presence of varying proportions of HCl. The ATPSs may find application in affinity partitioning of metal ions because DAPE is expected to be an effective chelator.

KEYWORDS: cyclopolymerization; pH-responsive polymers; polyphosphonobetaine; water-soluble polymers; polyzwitterions

2.1 Introduction

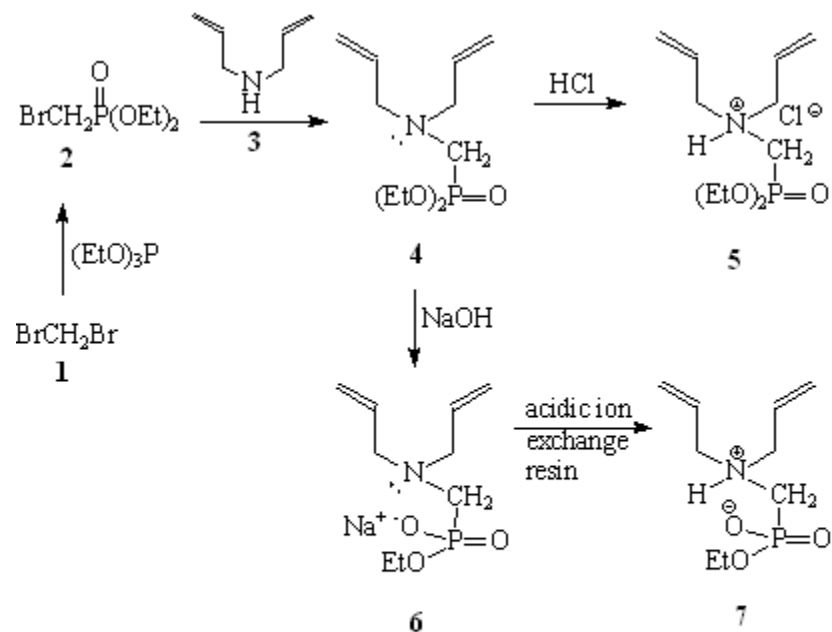
While the polymerization of carbobetaines, phosphobetaines, or sulfobetaines (zwitterions) (M^\pm) having charges of both algebraic signs in the same molecular framework lead to polyzwitterions (PZs) (polybetaines)^[1, 2] the presence of both M^+ and M^- in the same polymer chain constitutes a polyampholyte (PA) with or without charge symmetry. Synthetic polyampholytes (Pas) and PZs, whose structure and behavior seem to mimic biopolymers such as proteins or DNA that mediate life processes, have offered many new applications in various fields. Butler's cyclopolymerization^[3-5] of zwitterionic diallylammonium monomers or their copolymerizations with sulfur dioxide have been an attractive method for the synthesis of PZs. The PAs and PZs, unlike cationic or anionic polyelectrolytes (APE),^[7] exhibit antipolyelectrolyte behavior,^[4, 8, 9] that is, enhancement in viscosity and solubility in the presence of added electrolytes (e.g., NaCl) owing to the

neutralization of the ionically crosslinked network in a collapsed coil conformation of the polymers.

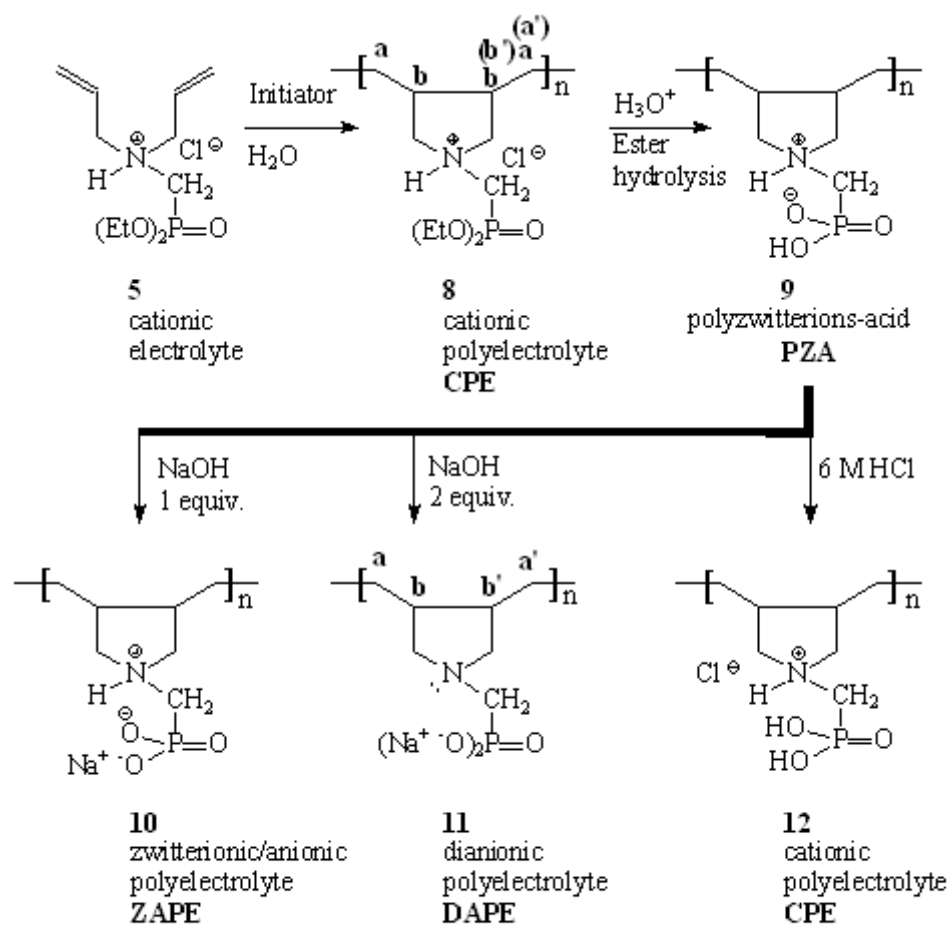
Polyphosphobetaines (containing repeating unit of a dialkylphosphate motif: a derivative of phosphoric acid, H_3PO_4), which seem to mimic phospholipid biomembranes, have offered many new applications.^[1, 10] To our knowledge, there are only a few reports^[11, 13-16, 65] that describe the cyclopolymerization of phosphorous acid (H_3PO_3) derivatives such as diallylaminoalkyl phosphonic acids to polyphosphonobetaines. Extraordinary chelating properties of aminomethylphosphonic acid groups have been exploited to form polymer-heavy metal ion complexes from waste water^[17-19]. In pursuit of tailoring pH-responsive polymers, we describe, herein, the synthesis of new monomers **5**, a cationic phosphonium salt, and **7**, a zwitterionic phosphonobetaine (Scheme 1), and their cyclopolymers (Schemes 2 and 3). To the best of our knowledge, cyclopolymers of **5** and **7** would represent the first examples of this class of ionic polymers having a single carbon spacer separating the nitrogen and the phosphonate ester motifs. The synthesis of a series of new pH-responsive polymers would pave the way to study cationic polyelectrolyte (CPE)-to-polyzwitterionic-to-APE transitions involving polymers having identical degree of polymerization.

Extraction of proteins in aqueous two-phase systems (ATPSs) has received considerable attention owing to the friendly environment they provide for the labile protein products^[69-71]. Recently, there has been considerable interest in the use of polyethylene glycol (PEG)-salt-based ATPSs in the selective separation of toxic metal ions.^[72-75] With the discussion in mind, the newly synthesized polyphosphonates would

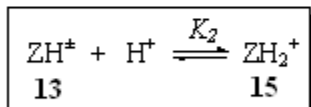
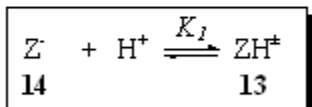
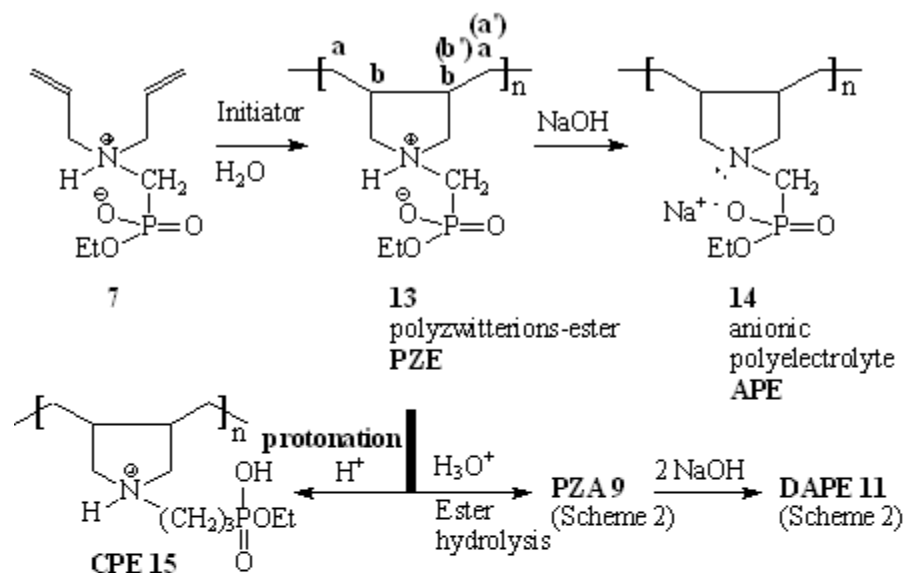
be used for the first time to construct ATPSs that may find applications in bioseparation and separation of toxic metal ions



Scheme 1. Monomer synthesis.



Scheme 2. Synthesis of CPE 8 and its conversion to PZA, ZAPE, and DAPE.



$$\log K_1 = \text{pH} - \log [(1 - \alpha)/\alpha] \quad \text{Eq 1}$$

$$\text{pH} = \log K_1^{\circ} + n \log [(1 - \alpha)/\alpha] \quad \text{Eq 2}$$

$$\log K_1 = \log K_1^{\circ} + (n - 1) \log [(1 - \alpha)/\alpha] \quad \text{Eq 3}$$

Scheme 3. Synthesis of PZE and protonation of APE and PZE.

2.2 Experimental

2.2.1 Physical methods

Elemental analysis has been carried out on a Perkin-Elmer Elemental Analyzer Model EA3000. IR spectra have been recorded on a Perkin-Elmer 16F PC FTIR spectrometer. The ^{31}P , ^{13}C , and ^1H NMR spectra of the polymers have been measured in CDCl_3 (using TMS as internal standard) or D_2O on a JEOL LA 500 MHz spectrometer. ^{31}P was referenced with 85% H_3PO_4 in DMSO. Viscosity measurements were made by Ubbelohde viscometer (having viscometer constant of 0.005718 cSt/s at all temperatures) using CO_2 -free water under N_2 to avoid CO_2 absorption that may affect the viscosity data. For the potentiometric titrations, the pH of the solutions was recorded using a Corning pH Meter 220. Molecular weights of some of the synthesized polymers were determined by the GPC measurement performed on an Agilent 1200 series apparatus equipped with a refractive index (RI) detector and PL aquagel-OH MIXED column using polyethylene oxide/glycol as a standard and water as eluent at a flow rate of 1.0 mL/min at 25 °C.

2.2.2 Materials

PEG of MW of 35,000 was purchased from Merck-Schuchardt. APS, TBHP (70% aqueous solution), dibromomethane, triethyl phosphate, diallyl amine, and Dowex 50 W $\times 8$ resin (ionic form: H^+) from Fluka Chemie AG (Buchs, Switzerland) were used as received. For dialysis, a spectra/Por membrane with a MW cut-off value of 6000–8000 was purchased from Spectrum Laboratories, Inc.

2.2.3 Synthesis of Bromo(diethylphosphonato)methane (2)

The reaction was carried out as described^[63]. A stirred mixture of triethyl phosphite (114 g, 0.686 mol) and dibromomethane (478 g, 2.75 mol) was heated at 110

°C for 48 h, while nitrogen was gently bubbled through the reaction mixture to remove the volatile product bromoethane. The liquid was then fractionally distilled to obtain **2** (66.5 g, 42%)

Bp_{8 mmHg} 125–126 °C. v_{\max} . (neat) 2985, 2943, 1478, 1444, 1392, 1258, 1182, 1164, 1027, 970, 827, 721, 627, and 511 cm^{-1} ; δ_{H} (500 MHz, CDCl_3) 1.37 (6H, 2 CH_3 , t, J 7.0 Hz), 3.29 (2H, BrCH_2 , d, J 9.8 Hz), 4.22 (4H, 2 OCH_2 , apparent quintet, J 7.3 Hz); δ_{P} (202 MHz, CDCl_3) 16.62 (1P, septet, 9.8 Hz); δ_{C} (125 MHz, CDCl_3): 16.20 (2C, Me, $^3J(\text{PC})$ 5.1 Hz), 17.59 (1 C, d, PCH_2 , $^1J(\text{PC})$ 164 Hz), 63.25 (d, 2C, OCH_2CH_3 , $^2J(\text{PC})$ 6.2 Hz).

2.2.4 Synthesis of N,N-Diallyl-(diethylphosphonato) methylamine (**4**)

A solution of diallylamine (**3**) (97 g, 1 mol) and bromo(diethylphosphonato)methane **2** (45 g, 0.195 mol) in toluene (150 cm^3) was heated at 90 °C for 24 h. The mixture was treated with aqueous NaOH (0.2 mol NaOH in 50 cm^3 H_2O) and extracted with ether (3 \times 100 cm^3). The combined organic layers was dried (Na_2SO_4), concentrated, and distilled to obtain **4** as a colorless liquid.

Bp_{0.15 mbarHg}, 94 °C (29 g, 60%). Found: C, 53.2; H, 9.05; N, 5.6. $\text{C}_{11}\text{H}_{22}\text{NO}_3\text{P}$ requires C, 53.43; H, 8.97; N, 5.66%; v_{\max} . (neat) 3076, 2980, 2930, 2908, 2803, 1643, 1445, 1417, 1392, 1367, 1256, 1162, 1095, 1055, 1030, 962, 852, 776, 723, and 549 cm^{-1} ; δ_{H} (500 MHz, CDCl_3) 1.33 (6H, t, J 7.3 Hz), 2.87 (2H, d, J 9.8 Hz), 3.26 (4H, d, J 7.3 Hz), 4.14 (4H, m), 5.18 (4H, m), 5.83 (2H, m); δ_{C} (125 MHz, CDCl_3): 16.39 (d, 2C, Me, $^3J(\text{PC})$ 6.2 Hz), 48.14 (1C, d, PCH_2 , $^1J(\text{PC})$ 161 Hz), 57.97 (2C, d, PCH_2NCH_2 , $^3J(\text{PC})$ 8.2 Hz), 61.80 (d, 2C, OCH_2CH_3 , $^2J(\text{PC})$ 6.2 Hz), 118.05 (2C,

s, $\underline{\text{C}}\text{H}_2=\text{CH}$), 134.94 (2C, s, $\text{C}\text{H}_2=\underline{\text{C}}\text{H}$); δ_{P} (202 MHz, CDCl_3): 32.85 (1P, t, J 7.3 Hz); δ_{P} (202 MHz, CDCl_3) 23.81 (1P, septet, 7.3 Hz).

2.2.5 Synthesis of N,N-Diallyl-(diethylphosphonato) methylammonium Chloride (5)

To a salt-ice cooled stirred solution of **4** (50 g, 0.2 mol) in diethyl ether (300 cm^3) was bubbled moisture-free HCl until the supernatant ether layer became clear, and no further milky solution was observed. The separated chloride salt was washed several times with ether to obtain **5** as a viscous liquid, which was dried under vacuum at 40 °C to a constant weight (52.7 g, 92%).

Found: C, 46.2; H, 8.4; N, 4.8. $\text{C}_{11}\text{H}_{23}\text{ClNO}_3\text{P}$ requires C, 46.56; H, 8.17; N, 4.94%; ν_{max} (neat) 3500 (very broad), 3000–1900 (very broad), 1565, 1430, 1224, 1160, 1013, 952, 837, and 784 cm^{-1} ; δ_{H} (D_2O) 1.22 (6 H, t, J 6.8 Hz), 3.58 (2 H, d, 1J (PC) 14.7 Hz), 3.79 (4 H, d, J 7.3 Hz), 4.14 (4 H, qd, 3J (PC) 7.1, 8.6 Hz), 5.53 (4 H, m), 5.79 (2 H, m); δ_{C} (125 MHz, D_2O): 16.46 (d, 2C, $\underline{\text{M}}\text{e}$, 3J (PC) 4.1 Hz), 46.13 (1C, d, $\text{P}\underline{\text{C}}\text{H}_2$, 1J (PC) 153 Hz), 58.19 (2C, s, $\text{P}\text{C}\text{H}_2\underline{\text{N}}\text{C}\text{H}_2$), 66.06 (d, 2C, $\text{O}\underline{\text{C}}\text{H}_2\text{CH}_3$, 2J (PC) 6.2 Hz), 125.70 (2C, s, $\text{C}\text{H}_2=\underline{\text{C}}\text{H}$), 128.82 (2C, s, $\underline{\text{C}}\text{H}_2=\text{CH}$); δ_{P} (202 MHz, D_2O): 15.00 (1P, septet, J 7.2 Hz). ^{13}C spectral assignments were supported by DEPT 135 NMR analysis.

2.2.6 Synthesis of Ethyl 3-(N,N-diallylammonio) methanephosphonate (7)

A mixture of **4** (25.0 g, 0.101 mol) in 1.0 N NaOH (102 cm^3) under N_2 was heated in a closed flask at 105 °C for 18 h. After cooling to 20 °C, the reaction mixture was washed with ether (3 \times 40 cm^3). The aqueous solution containing sodium salt **6** in water was stirred with Dowex 50 W \times 8 (36 g) at 20 °C for 1 h. The solution was filtered through a cotton bed in a column, and the resin was thoroughly washed by passing deionized water (70 cm^3) through it. The zwitterionic monomer **7** was recovered by

freeze-drying (19.5 g, 88%). An analytical sample was made by washing the white solid with ether.

Mp. 95–97 °C. Found: C, 49.0; H, 8.37; N, 6.2. C₉H₁₈NO₃P requires C, 49.31; H, 8.28; N, 6.39%; ν_{\max} . (neat) 3500, 3089, 2983, 2936, 2887, 2800–2200 (very broad), 1433, 1380, 1327, 1283, 1216, 1087, 1037, 930, 881, 827, 774, and 658 cm⁻¹; δ_{H} (500 MHz, D₂O) 1.10 (3 H, t, *J* 7.0 Hz), 3.13 (2H, d, *J* 12.2 Hz), 3.78 (4H, m), 3.82 (2H, m), 5.49 (4H, m), 5.79 (2H, m); δ_{C} (125 MHz, D₂O): 16.83 (d, 2C, Me, ³*J* (PC) 5.2 Hz), 48.01 (d, PCH₂, ¹*J* (PC) 139 Hz), 57.62 (d, NCH₂CH=, ³*J* (PC) 4.1 Hz), 62.43 (d, 1C, OCH₂CH₃, ²*J* (PC) 6.2 Hz), 126.29 (2C, s, CH₂=CH), 128.07 (2C, s, CH₂=CH); δ_{P} (202 MHz, D₂O): 7.74. ¹³C spectral assignments were supported by DEPT 135 NMR analysis.

2.2.7 Synthesis of Sodium Ethyl-3-(N,N-diallylammonio) methanephosphonate (6)

In a separate experiment, sodium salt **6** was prepared as described above and isolated as a white solid by freeze-drying its aqueous solution (97%). Mp 250 °C (dec.); Found: C, 44.6; H, 7.2; N, 5.7%. C₉H₁₇NNaO₃P requires C, 44.82; H, 7.10; N, 5.81%; ν_{\max} . (KBr) 3076, 2980, 2925, 2888, 2806, 1564, 1426, 1356, 1206, 1048, 921, 848, 779, and 551 cm⁻¹; δ_{H} (500 MHz, D₂O) 1.58 (3 H, t, *J* 7.3 Hz), 2.62 (2H, d, *J* 11.0 Hz), 3.15 (4H, *J* 7.3 Hz), 3.79 (2H, q, *J* 7.3 Hz), 5.15 (4H, m), 5.77 (2H, m); δ_{C} (125 MHz, D₂O): 16.92 (s, 2C, Me), 49.19 (d, PCH₂, ¹*J* (PC) 149 Hz), 58.10 (2C, =CH—CH₂, s), 61.46 (s, C, OCH₂CH₃), 120.38 (2C, s, CH₂=CH), 134.76 (2C, s, CH₂=CH); δ_{P} (202 MHz, D₂O): 18.83.

2.2.8 General Procedure for the Polymerization of Cationic Monomer 5

A solution of monomer **5** in deionized water in a 10-cm³ round bottomed flask was purged with N₂, and after adding the required amount of the initiator (as listed in Table 2.1), the mixture was stirred in the closed flask at the specified temperature for a specified time. The viscous and transparent reaction mixture was dialyzed against deionized water for 24 h. The polymer solution of CPE **8** was then freeze-dried.

The onset of thermal decomposition (closed capillary): 300–310 °C (decomposed, turned black); Found: C, 46.3; H, 8.3; N, 4.7%. C₁₁H₂₃ClNO₃P requires C, 46.56; H, 8.17; N, 4.94%; ν_{\max} (KBr) 3416, 2978, 2937, 1652, 1456, 1393, 1218, 1079, 1044, 948, 784, 668, and 544 cm⁻¹; δ_p (202 MHz, D₂O): 9.74.

2.2.9. Acidic Hydrolysis of CPE 8 to PZA 9

A solution of polymer **8** (5.7 g, 20 mmol) (entry 5, Table 2.1) in HCl (60 cm³) and water (40 cm³) was hydrolyzed in a closed vessel at 90 °C for 24 h. The homogeneous mixture was cooled to room temperature and polymer **9** was precipitated in a large excess of acetone. The white polymer was dried under vacuum at 55 °C to a constant weight (3.7 g, 97%).

The onset of thermal decomposition (Closed capillary): 310–320 °C (dec, turned light brown). (Found: C, 43.8; H, 7.5; N, 7.1%. C₇H₁₄CNO₃P requires C, 43.98; H, 7.38; N, 7.33%); ν_{\max} (KBr) 3511, 3430, 3034, 2938, 1638, 1463, 1196, 1022, 949, 818, 761, and 527 cm⁻¹.

2.2.10. Basification of PZA 9 to DAPE 11

A mixture of **9** (derived from hydrolysis of CPE **8** from entry 5, Table 2.1) (2.87 g, 15 mmol) and 1.0 N NaOH (40 cm³, 40 mmol) was stirred until the mixture became

homogeneous. The resultant DAPE **11** was precipitated in methanol and dried under vacuum at 55 °C to a constant weight (3.26 g, 92%).

The onset of thermal decomposition (closed capillary) 310–320 °C (decomposed, light brown); Found: C, 35.5; H, 5.1; N, 5.8%. $C_7H_{12}NNa_2O_3P$ requires C, 35.76; H, 5.14; N, 5.96%. ν_{\max} (KBr) 3396, 2937, 2791, 1655, 1465, 1265, 1089, 978, 764, and 556 cm^{-1} . δ_P (202 MHz, D_2O): 6.89.

2.2.11. General Procedure for the Polymerization of Zwitterionic Monomer 7

The polymerization was carried out in a closed flask under N_2 as described in Table 2.2. The reaction mixture was dialyzed against deionized water for 48 h. The polymer solution of PZE **13** was then freeze-dried. The onset of thermal decomposition (closed capillary): 310–320 °C (decomposed, turned black); Found: C, 49.12; H, 8.10; N, 6.20%. $C_9H_{18}NO_3P$ requires C, 49.31; H, 8.28; N, 6.39%; ν_{\max} (KBr) 3457, 3408, 2984, 2940, 1654, 1465, 1395, 1220, 1080, 1043, 950, 785, 693, 649, and 539 cm^{-1} . δ_P (202 MHz, D_2O): 9.74 ppm as a broad singlet. The 1H NMR and ^{13}C NMR spectra are displayed in Figures 2.1 and 2.2. A 2% (w/w) solution of PZE **13** was made after heating the mixture at 70 °C for 1 h and then cooling to 23 °C. The solvent used, with the dielectric constant, ϵ , and solubility (+) or insolubility (–) written in parentheses, were as follows: formamide (111.0), (+); water (78.4), (+); formic acid (58.5), (+); DMSO (47), (–); ethylene glycol (37.3), (+); DMF (37), (–); methanol (32.7), (–); diethyleneglycol (31.7), (–); ethanol (24.5), (–); acetone (21), (–).

2.2.12. Acidic Hydrolysis of PZE 13 to PZA 9

A solution of **13** (1.0 g, 4.56 mmol, entry 3, Table 2.2) in 6M HCl (20 cm^3) was heated in a closed vessel at 90 °C for 24 h. The homogeneous mixture was cooled to room temperature, and polymer **9** was precipitated in a large excess of acetone. After

filtration, the white polymer was dried under vacuum at 55 °C to a constant weight (0.84 g, 96%).

2.2.13. Basification of PZA 9 to DAPE 11

A sample of **9** (derived from hydrolysis of PZE **13** from entry 3, Table 2.2) was basified as described (vide supra) to obtain DAPE **11**.

2.2.14. Potentiometric Titrations

The potentiometric titrations were carried out as described elsewhere.^[13, 14] The $\text{Log } K_1$ of the amine nitrogen is calculated at each pH value by the Henderson–Hasselbalch eq 1 (Scheme 3) where α is the ratio $[\text{ZH}^\pm]_{\text{eq}}/[\text{Z}]_0$. For the titration with NaOH, the $[\text{Z}]_0$ is the initial concentration of repeating units in PZE **13** or monomer **7**, and $[\text{ZH}^\pm]_{\text{eq}}$ is the concentration of the protonated species at the equilibrium given by $[\text{ZH}^\pm]_{\text{eq}} = [\text{Z}]_0 - C_{\text{OH}^-} - [\text{H}^+] + [\text{OH}^-]$, where C_{OH^-} is the concentration of the added NaOH; $[\text{H}^+]$ and $[\text{OH}^-]$ at equilibrium were calculated from the pH value^[63, 76]. The polyelectrolytes having apparent basicity constants could be described by the eq 2 (Scheme 3) where $\log K^\circ = \text{pH}$ at $\alpha = 0.5$ and $n = 1$ in the case of sharp basicity constants. The linear regression fit of pH versus $\log [(1 - \alpha)/\alpha]$ gave $\log K^\circ$ and “ n ” as the intercept and slope, respectively. The second step protonation constant ($\log K_2$) involving the $\text{PO}(\text{OEt})\text{O}^-$ is calculated by titration of the PZE **13** or of monomer **7** with HCl. In this case, α represents the ratio $[\text{ZH}_2^+]_{\text{eq}}/[\text{Z}]_0$ whereby $[\text{ZH}_2^+]_{\text{eq}}$ equals $C_{\text{H}^+} - [\text{H}^+] + [\text{OH}^-]$ and C_{H^+} is the concentration of the added HCl. For titration of the monomeric sodium salt **6** with HCl, $\text{Log } K_1$, is calculated using $[\text{ZH}^\pm]_{\text{eq}} = C_{\text{H}^+} - [\text{H}^+] + [\text{OH}^-]$, while $\log K_2$ involving the $\text{P}(=\text{O})(\text{OEt})\text{O}^-$ is calculated by subtracting the equivalent volume from the total volume of the titrant, and using $[\text{ZH}_2^+]_{\text{eq}} = C_{\text{H}^+} - [\text{H}^+] + [\text{OH}^-]$.

2.2.15. Phase Compositions and Phase Diagram of PEG-DAPE 11 (0.4 N NaCl) System

2.2.15.1. The NMR Method

Four systems of known compositions (A_{total}) of PEG and DAPE 11 were made in 0.4 N NaCl. The mixtures were centrifuged briefly and kept at 23 °C for 24 h. The ^1H NMR spectra of the top and bottom layers were measured after exchanging H_2O by D_2O . The above procedure was repeated using in the presence of 0.5 and 1 equiv of HCl (equivalent to concentration of the repeating units). The calculation for NaCl concentration took into account the equivalent amount of NaCl generated by the addition of HCl to DAPE 11. The mole ratios ($[\text{PEG}]/[\text{APE}]$) of the repeating units of the polymers in both layers were calculated using the integration of the four-proton singlet at δ 3.60 for PEG and the 12-proton complex signals in the range δ 0.5–3.4 for the DAPE. Weight percent of each polymer is determined by using the eqs 4 and 5 as described in our earlier work: [26, 77]

$$[\text{DAPE}_b] = \frac{\text{PEG}_0 / 44.03 - (\text{DAPE}_0 / 235.13)([\text{PEG}]/[\text{DAPE}]_t)}{V_b \{([\text{PEG}]/[\text{DAPE}]_b - ([\text{PEG}]/[\text{DAPE}]_t)\}} \quad (4)$$

$$\text{DAPE}_b = [\text{DAPE}_b] V_b \times 235.13 \text{ mg} \quad (5)$$

Where, subscript t and b represent top and bottom phase, respectively. DAPE_0 and PEG_0 represent the total mass (mg) of the polymers. Molar masses of the repeat units of the DAPE and PEG were taken as 235.13 and 44.03, respectively.

2.2.15.2. The Turbidity Method

The binodal curve was constructed using procedure as described elsewhere.^[26] About 1.5 g of a concentrated solution ($\sim 10\%$ w/w) of DAPE 11 in 0.4 N NaCl was titrated with a concentrated solution ($\sim 20\%$ w/w) of the PEG in 0.4 N NaCl.

Points obtained by turbidity method are joined together in the phase diagrams (*vide infra*). The experiments were carried out at 23 °C.

2.3 Results and Discussion

2.3.1. Synthesis of Monomers

Cationic phosphonate monomer **5** and its phosphobetaine counterpart **7** were prepared for the first time as outlined in Scheme 1. One of the ester groups of **4** was selectively hydrolyzed with 1 equiv of sodium hydroxide to give the sodium salt of monoester **6** (97%), which upon cation exchange with Dowex 50 W ×8 (in H⁺ form) led to zwitterionic monomer **7** in excellent yield (88%).

2.3.2. Synthesis and Physical Characterization of Cationic Polyelectrolyte **8**

The results of the cyclopolymerization of monomer **5** to give CPE **8** (Scheme 2) under various conditions are given in Table 2.1. The low molecular weight as indicated by lower intrinsic viscosity values could be the result of chain transfer between the polymer and monomer via the abstraction of allylic or OCH₂ proton of the ethoxy group.^[72, 78] CPE **8** was stable up to 320 °C. It was water-soluble and hydrolyzed in 6 M HCl to give polyzwitterionic acid (PZA) **9**, which on treatment with NaOH-afforded dianionic polyelectrolyte (DAPE) **11**. PZA **9** was found to be water-insoluble but soluble in 6 M HCl owing to its conversion to CPE **12**. As expected, DAPE **11** was found to be water-soluble. ¹H and ¹³C NMR spectra of monomer **5**, CPE **8** and DAPE **11** are displayed in Figures 2.1 and 2.2. The absence of any residual alkene proton or carbon signal in the polymer spectra suggested the chain transfer process^[79] for the termination reaction. Note that PZA **9** has been synthesized earlier; however, its yield has not been reported.^[65] The ¹H NMR spectrum of CPE **8** [Fig. 2.1(b)] revealed the presence of two

triplets at δ 1.12 and 1.21 ppm in a respective ratio of 72:28, attributed to the OCH_2CH_3 protons of the symmetrical major *cis* (*b,b*) and unsymmetrical minor *trans* (*b,b'*) disposed substituents in the five-membered ring structure [Fig. 2.1(b) and Scheme 2].^[14] The integration of the relevant ^{13}C peaks yielded the *cis/trans* ratio of the ring substituents to be 75/25 which is similar to that observed for the related cyclopolymers^[5, 14, 77] Note that the ^{13}C NMR spectrum [Fig. 2.2(d)] for DAPE **11** is much more simpler as a result of fast nitrogen inversion that makes the substituents at C-*b* and C-*b'* identical (Scheme 2) in both the *cis* and *trans* isomers. ^{31}P NMR signal for **5**, CPE**8**, and DAPE **11** appeared at δ 15, 9.7, and 6.9 ppm, respectively; the upfield shift in DAPE **11** is attributed to the higher electron density around P in the dianion.

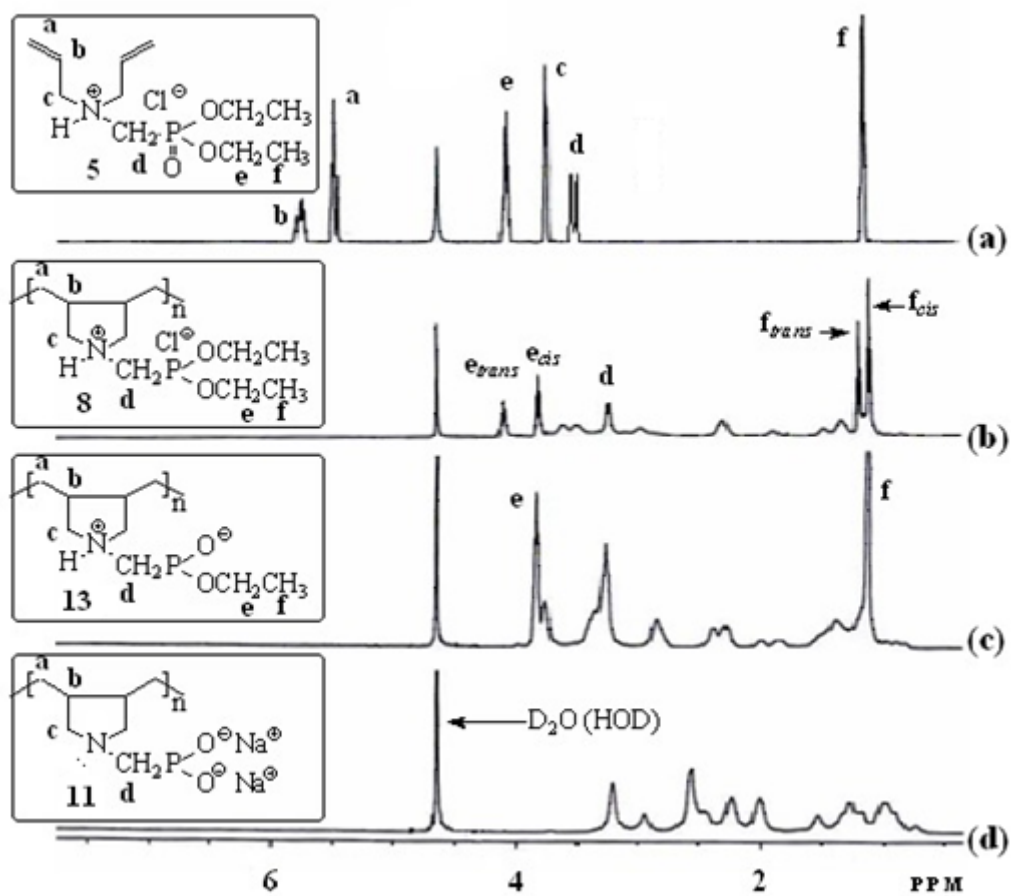


Figure 2.1. ^1H NMR spectrum of (a) 5, (b) 8, (c) 13 and (d) 11 in D_2O

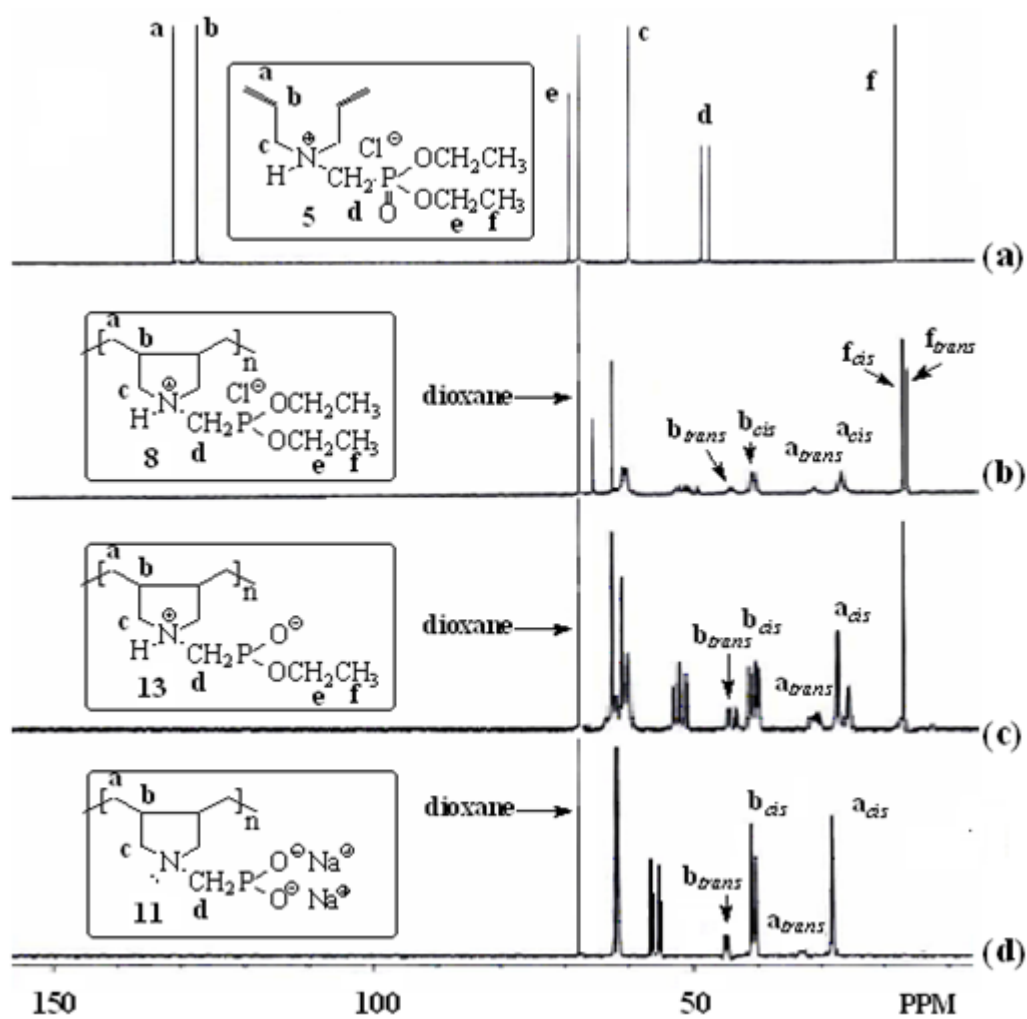


Figure 2.2. ^{13}C NMR spectrum of (a) 5, (b) 8, (c) 13 and (d) 11 in D_2O

Table 2.1 Cyclopolymerization of Cationic Monomer 5^a to CPE 8

Entry	Initiator (mg)	Temp (°C)	Time (h)	Yield (%)	Intrinsic Viscosity ^b (dl g ⁻¹)	\overline{M}_w	(PDI) ^c
1	APS (180)	95	4	37	0.128	–	–
2	TBHP (15)	85	24	16	0.131	–	–
3	TBHP (37)	85	24	17	0.138	81,700	2.7
4	TBHP (57)	85	24	27	0.141	–	–
5 ^d	TBHP (100)	85	24	61	0.126 ^d	79,800	2.9

^aPolymerization reactions were carried out in aqueous solution of monomer **5** (10 mmol) (70 w/w% monomer) in the presence of ammonium persulfate (APS) or tertiary butylhydroperoxide (TBHP).

^bViscosity of 1-0.25 % polymer solution in 0.1 N NaCl at 30 °C was measured with a Ubbelohde Viscometer (K=0.005718).

^cPolydispersity index.

^dEntry 5 was repeated on a large scale using 60 mmol of monomer and 600 mg of TBHP.

2.3.3. Synthesis and Physical Characterization of Polyzwitterions Ester 13

Zwitterionic monomer **7** underwent cyclopolymerization in aqueous solution in the presence of *t*-butylhydroperoxide (TBHP) or ammonium persulfate (APS) to give polyzwitterion ester (PZE) **13** (Scheme 3, Table 2.2). As evident from the table, changing the initiator from APS to TBHP improved the polymer yield considerably. PZE **13** was readily soluble in water as well as in protic solvents having higher dielectric constants (ϵ) because of H-bonding (See Experimental section). However, it remained insoluble in nonprotic solvents like DMF and DMSO even though they have very high ϵ . The solubility of PZs in salt-free water is not unusual; a considerable number of water-soluble polycarbobetaines and sulfobetaines are reported^[4] The negative charges on the carbobetaines having higher carboxyl pK_a values (>2) are expected to be less dispersed, thus more hydrated^[24, 26, 27], and as such tend to exhibit weaker Coulombic interactions with the cationic charges on nitrogens^[80], thereby imparting solubility in salt-free water. Steric factor plays a dominant part in the solubility behavior of the PZs **9** and **13**; sterically crowded charge centers in the later owing to the presence of an ethoxy group are unable to manifest effective intramolecular or intermolecular zwitterionic interactions, thereby leading to its solubility in salt-free water^[81]. PZE**13** was expected^[24, 26, 27] to be soluble in salt-free water as its phosphonate pK_a was determined to be >2 (*vide infra*). Note that the phosphonate pK_a in PZA **9** could not be determined owing to its insolubility in water.

Table 2.2 Cyclopolymerization of Zwitterionic Monomer 7 to PZE 13^a

Entry	Initiator (mg)	Temp (°C)	Time (h)	Yield (%)	Intrinsic Viscosity ^b (dl g ⁻¹)	\overline{M}_w	(PDI) ^c
1	APS (270)	95	3	25	0.109	–	–
2	APS (270)	95	3	51	0.0892	65,800	3.0
3	TBHP (115)	85	48	75	0.120	71,200	2.8

^aPolymerization reactions were carried out in solution of monomer **7** (15 mmol) in 0.5 N NaCl (75 w/w% monomer) in the presence of ammonium persulfate (APS) or tertiary butylhydroperoxide (TBHP).

^bViscosity of 1-0.25 % polymer solution in salt-free water at 30 °C was measured with a Ubbelohde Viscometer (K=0.005718).

^cPolydispersity index.

The strong absorptions at 1220 and 1043 cm⁻¹ in the IR spectrum of PZE 13 were attributed to the stretching frequency of P=O and P—O—C, respectively. ¹H and ¹³C NMR spectra are displayed in Figures 2.1 (c) and 2.2 (c). Integration of the relevant peaks in the ¹³C spectrum yields the cis/trans ratio of the ring substituents to be 75/25, which is similar to that observed for the related polymers derived from cyclopolymerizations (Scheme 3).^[21, 23, 81]

2.3.4. Viscosity Measurements

Figure 2.3(a) displays the viscosity behavior of CPE 8 (entry 5, Table 2.1) in salt-free water and 0.1 N NaCl. In the absence and presence of NaCl, the viscosity plot became concave upward and linear, respectively, as expected. According to Munk,^[82] the addition of a small electrolyte (NaCl, etc.) to solution of polyelectrolytes leads to Debye–Hückel shielding effect that permits the polymer to adopt a more entropically favored compact conformation (polyelectrolyte effect). The viscosity plots for PZE 13, as evaluated by the Huggins equation: $\eta_{sp}/C = [\eta] + k[\eta^2]C$, remain linear in both the absence and presence of added salt (Table 2.2). Increase in the intrinsic viscosity $[\eta]$ values in the presence of added salts LiCl, NaCl, and NaI demonstrates the “anti-polyelectrolyte” behavior of PZE 13 [Fig. 2.3(b)]. Note that for a common Na^+ cation, $[\eta]$ increases as the anion is changed from Cl^- to more polarizable (soft) I^- , which can neutralize the cationic charges on the polymer backbone more efficiently than Cl^- . As a result, the increased repulsions among the more exposed phosphonate anions in the presence of NaI leads to a greater expansion of the polymer coil. Note that a much harder Na^+ with its large hydration shell cannot shield the negative phosphonates effectively.^[14] The Li^+ is harder and has larger hydration shell than Na^+ , thus less efficient in shielding the phosphonates thereby leading to higher $[\eta]$ values in its presence [Fig. 2.3(b)]. In all cases of the added salts, the viscosity values levels off at 0.5 N concentration as a result of near completion of the site and atmospheric binding around the charges. The divalent cation Ca^{2+} , which is usually known to precipitate APE from aqueous solution, did not precipitate PZE 13. The $[\eta]$ s of PZE 13 (entry 3, Table 2.2) in 0.1 N NaCl, 0.1 N CaCl_2 , and 0.1 N HCl at 30 °C were determined to be 0.120, 0.163, and 0.143 dL/g, respectively. The Huggins constant k in salt-free water, 0.1 N solutions

of NaCl, NaI, LiCl, CaCl₂, and HCl were calculated to be 3.22, 1.44, 0.146, 0.0633, 0.192, and 0.630, respectively. A decrease in the value for Huggins constant k in the presence of added salts demonstrates an increased polymer-solvent interaction.

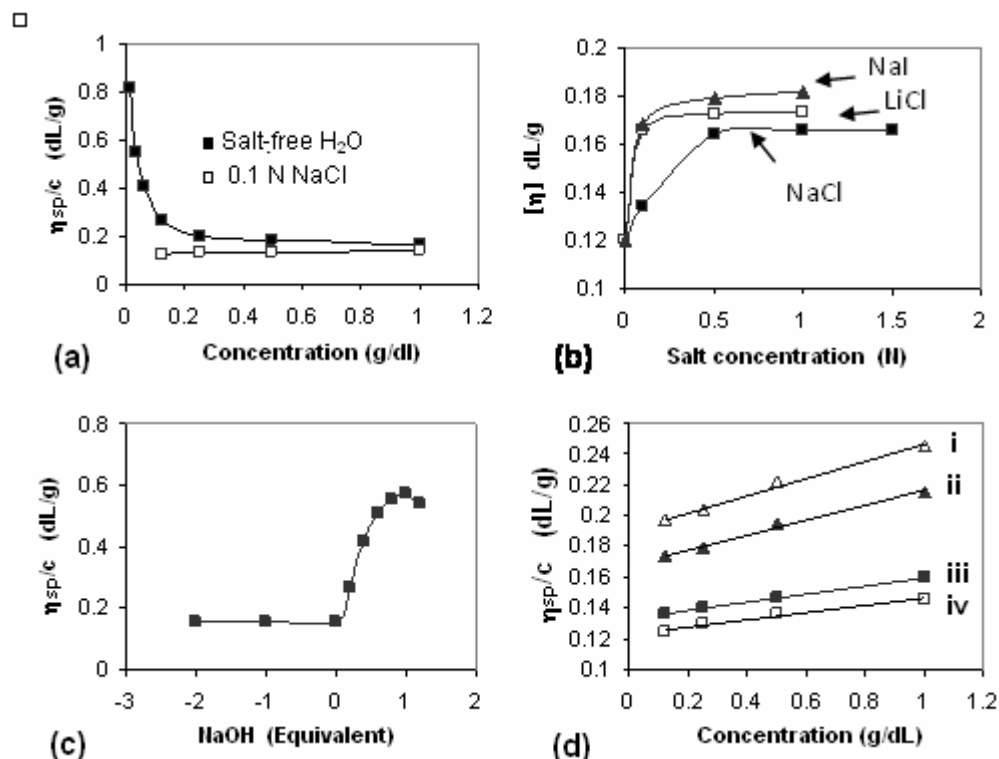


Figure 2.3. The viscosity behavior at 30 °C using an Ubbelohde Viscometer of (a) CPE 8 (entry 5, Table 2.1) in salt-free water and 0.1 N NaCl; (b) PZE 13 (entry 3, Table 2.2) in the presence of varying concentrations of added salts; (c) a 1.0 g/dL solution of polymer PZE 13 (entry 3, Table 2.2) in salt-free water versus equivalent of added NaOH. Negative (-) values indicate the equivalent of added HCl. (d) □ (i) DAFE 11 (derived from CPE 8 of entry 5, Table 2.1); ■ (ii) DAFE 11 (derived from PZE 13 entry 3, Table 2.2); ▲ (iii) PZE 13 (entry 3, Table 2.2); and Δ (iv) CPE 8 (entry 5, Table 2.1) 0.1 N NaCl

The pH-responsiveness of PZE 13 was demonstrated by the change in the reduced viscosities of a 1.0 g/dL solution of the polymer (entry 3, Table 2.2) in salt-free water [Fig. 2.3(c)]. The addition of HCl and NaOH shifts the equilibria toward CPE 15 and

APE **14**, respectively (Scheme 3). A steep increase in the viscosity values on the addition of NaOH is attributed to a change in the zwitterionic motifs in **13** to anionic motifs in **14**, thereby provoking an extension of the polymer backbone as a result of increased repulsion among negative charges. However, the reduced viscosity increases slightly with the addition of HCl because it is not able to protonate PZ **13** to CPE **15** to a great extent because of the relatively higher acidity of the $-\text{P}(=\text{O})(\text{OEt})\text{OH}$ ($\text{p}K_{\text{a}}$: 2.2).

CPE **8** (Table 2.1, entry 5) and PZE **13** (Table 2.2, entry 3) have been correlated by their conversions to DAPE **11** via PZA **9**. The viscosity data for CPE **8**, PZE **13**, and their corresponding DAPE **11** are shown in Figure 2.3(d). In 0.1 N NaCl, PZE **13** has a slightly higher $[\eta]$ than CPE **8** [*cf.* Fig. 2.3(d-iii,d-iv)]. However, the corresponding DAPE **11** derived from CPE **8** demonstrated higher viscosities than that derived from PZE**13** [*cf.* Fig. 2.3(d-i,d-ii)]. The viscosity data thus support the higher M_{w} for CPE **8** (Table 2.1, entry 5) than that for PZE **13** (Table 2.2, entry 3).

2.3.5. Basicity Constants

To gain further information on the conformational transitions, we have determined the basicity constants, K_i° , and the corresponding n_i values relative to the protonation of the tertiary amine ($i = 1$) in APE **14** (and **6**) and phosphonate ($i = 2$) in PZE **13** (and **7**) by potentiometric titrations details of which are summarized in Table 2.3. Inserting the value of pH from eq 2 into Henderson–Hasselbalch eq 1 leads to modified Henderson–Hasselbalch equation (eq. 3)^[83] (Scheme 3) where $(n - 1)$ gives a measure of the deviation of the studied polymers (**13**, **14**) from the behavior of small molecules (**6**, **7**) showing sharp basicity constants when n becomes 1. The n_1 values of 2.10 and 1.79 in salt free and 0.1 N NaCl, respectively, demonstrate the “apparent”^[83, 84] nature of the

$\log K_1$. The n_1 values of >1 indicates the decrease in the basicity of nitrogen with the increase in the degree of protonation (α), which leads to a decrease in the overall negative charge density and electrostatic field force that encourages protonation (Fig. 2.4). The basicity constant $\log K_1^\circ$ (at the α value of 0.5) of the amine group was found to be 9.49 and 8.77 salt-free water and 0.1 N NaCl, respectively (Table 2.3). A polyelectrolyte is more expanded, thus more hydrated in salt-free water than in 0.1 N NaCl. As a result of each protonation in APE **14**, the greater number of water molecules are released in salt-free water than in 0.1 N NaCl, thereby leading to the entropy-driven higher $\log K_1^\circ$ in the former medium.^[83] Note that the $\log K_1^\circ$ for the protonation of monomeric **6** was determined to be 7.94 and 7.81 in salt-free and 0.1 N NaCl, respectively; an n value of almost 1 certifies the “real” nature of the basicity constant as expected for a small molecule (Table 2.3).

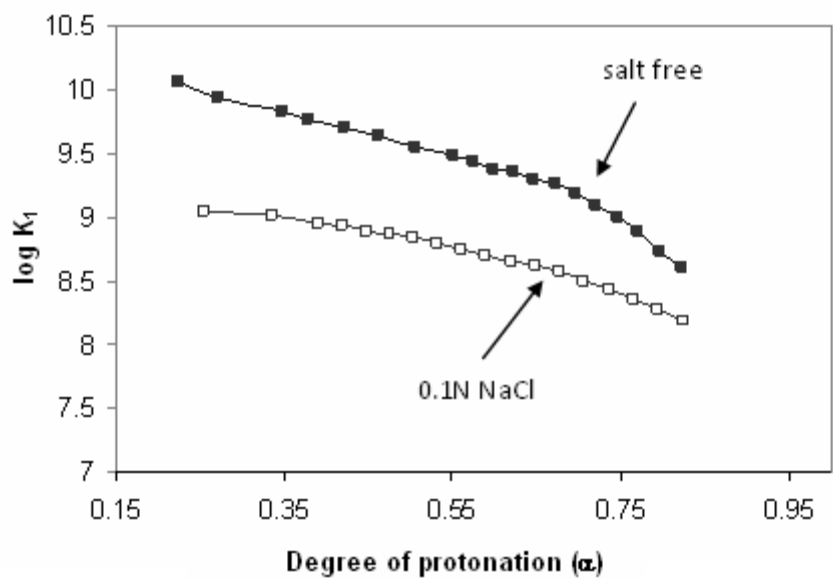


Figure 2.4. Plot for the apparent $\log K_1$ versus degree of protonation (α) for PZE 13 in salt-free water and 0.1 N NaCl.

Table 2.3. Experimental Details for the Protonation of Polymer PZE 13 (ZH[±]) (entry 3, Table 2.2) at 23 °C in Salt-Free Water and in 0.1N NaCl.

Run	ZH [±] (mmol)	C _T ^a (mol dm ⁻³)	α-range	pH-range	Points ^b	Log K _i ^{o,c}	n _i ^c	R ^{2, d}
<i>Polymers PZE 13 (ZH[±]) in salt-free water</i>								
1	0.2850 (ZH [±])	-0.1059	0.81–0.26	7.90–10.38	14	9.46	2.17	0.9867
2	0.3201 (ZH [±])	-0.1059	0.80–0.22	8.15–10.59	14	9.49	2.02	0.9843
3	0.4137 (ZH [±])	-0.1059	0.82–0.22	7.95–10.60	19	9.53	2.10	0.9977
Average						9.49 (4)	2.10 (7)	
Log K _i ^e = 9.49 + 1.10 log [(1-α)/α]; For the reaction: Z ⁻ + H ⁺ ⇌ ZH [±]								
<i>Monomer Anion 6 (Z⁻) in salt-free water</i>								
1	0.3273 (Z ⁻)	+0.0993	0.13–0.84	8.82–7.20	17	7.96	1.04	0.9992
2	0.3909 (Z ⁻)	+0.0993	0.15–0.86	8.68–7.10	17	7.93	1.04	0.9987
3	0.4537 (Z ⁻)	+0.0993	0.18–0.82	8.57–7.02	20	7.92	1.05	0.9991
Average						7.94 (2)	1.04 (1)	
Log K _i ^e = 7.94; For the reaction: Z ⁻ + H ⁺ ⇌ ZH [±]								
Polymers PZE 13 (ZH[±]) in 0.1 N NaCl								
1	0.2505 (ZH [±])	-0.1059	0.83–0.19	7.40–9.63	16	8.74	1.80	0.9802
2	0.2965 (ZH [±])	-0.1059	0.86–0.24	7.26–9.60	18	8.76	1.76	0.9925
3	0.3599 (ZH [±])	-0.1059	0.82–0.25	7.52–9.52	18	8.80	1.80	0.9920
Average						8.77 (3)	1.79 (2)	
Log K _i ^e = 8.77 + 0.79 log [(1-α)/α] For the reaction: ZH [±] + H ⁺ ⇌ ZH ₂ ⁺								
<i>Monomer Anion 6 (Z⁻) in 0.1 N NaCl</i>								
1	0.3394 (ZH [±])	+0.0993	0.12–0.76	8.64–7.22	15	7.77	1.05	0.9985
2	0.3799 (ZH [±])	+0.0993	0.13–0.80	8.63–7.19	18	7.80	1.04	0.9920
3	0.4282 (ZH [±])	+0.0993	0.14–0.83	8.64–7.15	20	7.85	1.06	0.9978
Average						7.81 (4)	1.04 (1)	
Log K _i ^e = 7.81; For the reaction: Z ⁻ + H ⁺ ⇌ ZH [±]								

^aTitrant concentration (negative and positive values indicate titrations with NaOH and HCl, respectively).

^bNumber of data points from titration curve.

^cValues in the parentheses are standard deviations in the last digit.

^dR = Correlation coefficient. ^elog K_i = log K_i^o + (n - 1) log [(1 - α)/α].

The log K₂^o and n₂ values for the protonation of the P(=O)OEtO⁻ group in PZE 13 (Scheme 3) are found to be similar in the salt-free and 0.1 N NaCl solution (in salt-free water: log K₂^o = 2.29 (±0.07), n₂ = 0.55 (±0.10); in 0.1 N NaCl: log K₂^o = 2.15

(± 0.08), $n_2 = 0.82$ (± 0.06). The corresponding values for monomer **7** were determined as $\log K_2^\circ = 2.11$ (± 0.07), $n_2 = 1.02$ (± 0.06) in salt-free water; $\log K_2^\circ = 2.20$ (± 0.05), $n_2 = 1.01$ (± 0.04) in 0.1 N NaCl. For the polymer, the n_2 values of < 1 is considered as diagnostic of a compact conformation of a PZs. With the increase in the α , a progressive conversion of the zwitterionic motifs in the compact coil of PZE **13** to cationic motifs in the expanded backbone of CPE **15** exposes the remaining P(=O)OEtO⁻ groups for easier access to protonation (Scheme 3). The $\log K_2$ thus increases progressively. This behavior seems to be general in all cases in which the anionic motif is separated from the nitrogen by a single methylene spacer.^[83]

2.3.6. Phase Diagram

Phase compositions of several PEG-DAPE **11**-H₂O (0.4 N NaCl) systems in the presence of 0, 0.5, and 1 equivalent HCl are shown in Figure 2.5 (a–c), respectively. The top and bottom layers were found to be rich in PEG and DAPE **11**, respectively. The polymers displayed segregative phase separation behavior. The binodal was found to be symmetrical, and thus the two polymers may have very similar hydrodynamic volumes.^[70] Phase separation happened at relatively low total polymer concentrations of much below than 10%, which could be useful from an industrial point of view. The tie lines are helpful in constructing two-phases with suitable volume ratio of the top and bottom phases. For instance, the total system represented by the point A_{total} will have the top and bottom phase compositions represented by A_{top} and A_{bottom} , respectively, but the volume or the mass ratio of the top and bottom phases will be determined by the respective ratio of the tie line lengths of $A-A_{\text{bottom}}$ and $A-A_{\text{top}}$.

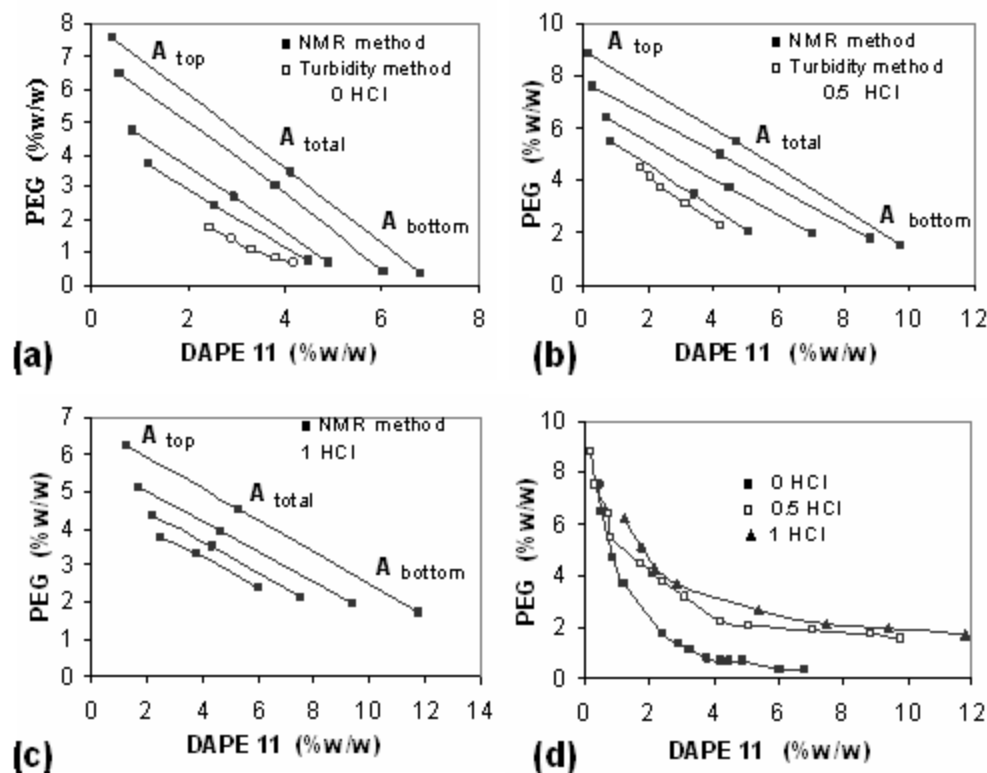


Figure 2.5. Phase diagram of PEG -DAPE 11-Water (0.4 N NaCl) in the presence of (a) 0 HCl; (b) 0.5 equiv. HCl and (c) 1 equiv. HCl; and (d) binodals for the systems presented in (a)-(c) at 23 °C.

The effects of HCl added on the binodal curves are displayed in Figure 2.5(d). As the HCl concentrations increased, the binodal curve shifted upward, thereby indicating the requirement of higher concentrations of the polymers for the phase separation to happen. Note that DAPE 11 in the presence of 0.5 and 1 equiv HCl is converted into DAPE 11/zwitterionic/anionic (ZAPE 10) and ZAPE 10, respectively (Scheme 2). The zwitterionic ZAP.

2.4 Conclusions

CPE 8 and a pH-responsive PZE 13 have been synthesized for the first time. The basicity constants of the amine and phosphonate functionalities in salt-free as well as 0.1 N NaCl

have been determined. Despite being a polyzwitterion, PZE **13** was found to be water-soluble owing to steric crowding around the charges. A convenient way was found to convert polymer of the type CPE to PZA, APE, and DAPE, the polymer backbone of which differed in charge types and their densities. PZE **13** was found to be soluble in the presence of Ca^{2+} ions thereby it may find potential application in inhibiting CaCO_3 scale formation. The construction of recyclable PEG-DAPE **11**- H_2O ATPS could be useful in the challenging area of bioproduct purification.^[85, 86] The current work has paved the way to use the newly developed ATPSs in studies involving affinity partitioning of metal ions.

CHAPTER 3: Comparative solution properties of cyclocopolymers having cationic, anionic, zwitterionic and zwitterionic/anionic backbones of similar degree of polymerization

Taken from Shaikh A. Ali, Othman Charles S. Al-Hamouz, Comparative solution properties of cyclocopolymers having cationic, anionic, zwitterionic and zwitterionic/anionic backbones of similar degree of polymerization, *Polymer*, 53, (2012), 3368–3377

Abstract

A new class of ionic copolymers containing amine and phosphonate functionalities has been prepared for the first time. *N,N*-Diallyl-3-(Diethylphosphonato)-methylammonium chloride underwent cyclocopolymerization with SO₂ to give a cationic polyelectrolyte (CPE) in very good yields. Likewise, ethyl 3-(*N,N*-diallylammonio)methanephosphonate/SO₂ cyclocopolymerization afforded the corresponding polyzwitterion-ester (PZE), which on neutralization with NaOH gave the anionic polyelectrolyte (APE). Both CPE and PZE on hydrolysis of the phosphonate ester functionalities gave the same polyzwitterionic acid (PZA). The pH-responsive PZA on treatment with excess NaOH was converted to dianionic polyelectrolyte (DAPE) which on treatment with 1 equivalent HCl afforded the zwitterionic-anionic polyelectrolyte (ZAPE). Solution properties of the CPE, PZE, DAPE, APE and ZAPE having similar degree of polymerization have been studied in some detail. The apparent basicity constants of the amine group in APE have been determined. An aqueous two-phase

system of polyethylene glycol-DAPE-H₂O (0.4 N NaCl) has been constructed for its potential application in selective separation of toxic metal ions since polyphosphonates are expected to be effective chelators.

KEYWORDS: Polyelectrolyte; polyzwitterions; polyphosphonobetaine; basicity constant, aqueous two-phase system; cyclopolymerization.

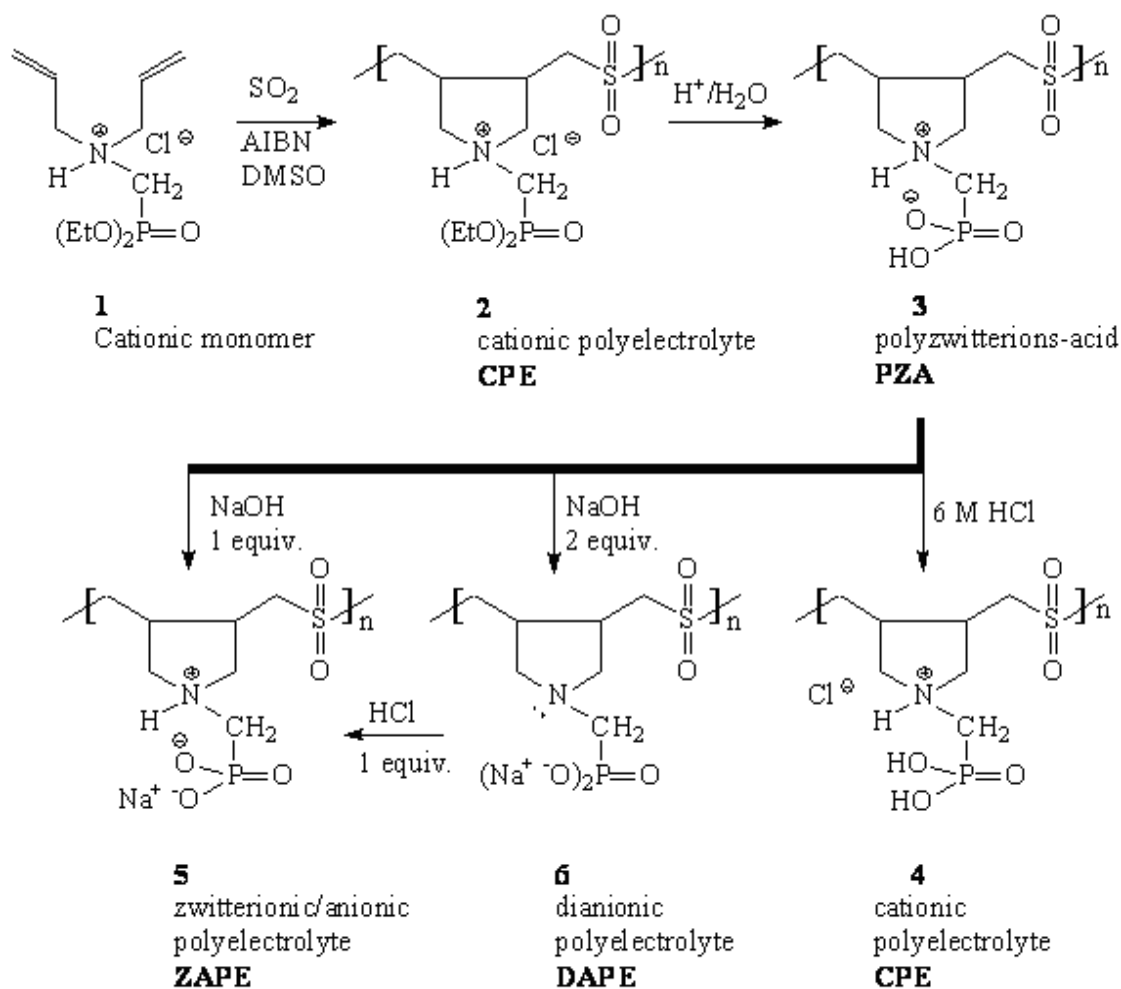
3.1 Introduction

While polymerization of zwitterionic (M^{\pm}) carbo-, phospho- or sulfobetaine monomers having charges of both algebraic signs in the same repeating unit leads to polybetaines (polyzwitterions, PZs)^[46, 87], the presence of both M^+ and M^- with varying proportions in the same polymer chain constitutes a polyampholyte (PA) with or without charge symmetry. Cyclopolymerization reaction^[3, 4, 13, 14] of diallylammonium monomers or their copolymerizations with sulfur dioxide has been an efficient method for the synthesis of PZs. Synthetic PAs and PZs, whose structure and behavior seem to mimic biopolymers like proteins or DNA that mediate life processes, have offered many applications in various industries. PAs and PZs, unlike cationic or anionic polyelectrolytes, are usually insoluble in salt-free water owing to the existence of the polymers in an ionically cross-linked network in a collapsed coil conformation. As such they exhibit anti-polyelectrolyte behavior, i.e., enhancement in viscosity and solubility in the presence of added salts (e.g. NaCl) owing to the neutralization of the ionic cross-links^[4, 8, 9, 11, 14, 65, 88].

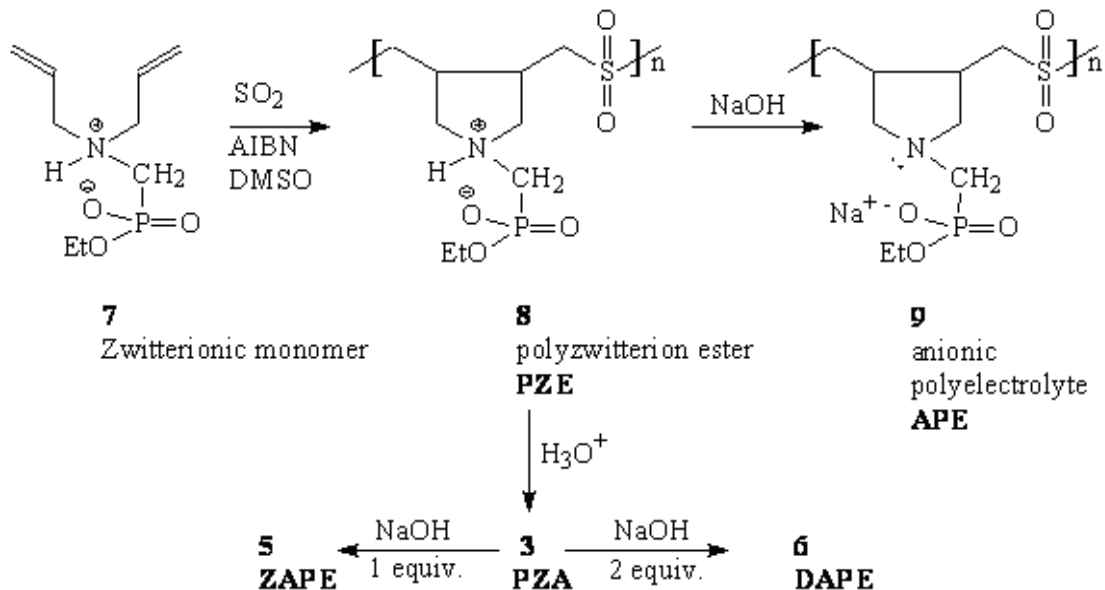
To our knowledge, there are very few reports^[11, 14, 65] and^[88] that describe the cyclopolymerization of phosphorous acid (H₃PO₃) derivatives like diallylaminoalkyl

phosphonic acids to polyphosphobetaines. Extraordinary chelating properties of polymers containing aminomethylphosphonate motifs have attracted attention for removal of heavy metal ion complexes from waste water^[17-19].

In pursuit of tailoring pH-responsive polymers, we have recently reported^[89] the synthesis of diallyl amine salt monomers **1** and **7** (Schemes 1 and 2) and their homocyclopolymers. We describe herein the synthesis of a new series of cationic, anionic, zwitterionic-anionic and zwitterionic polymers *via* cyclocopolymerization of **1** and **7** with SO₂. To the best of our knowledge, cyclocopolymers of diethyl phosphonate **1**/SO₂ and monoethyl phosphonate **7**/SO₂ would represent the first examples of this class of ionic copolymers having a single carbon spacer separating the nitrogen and the phosphonate ester motifs. The new series of pH-responsive polymers would allow us to examine the effects of SO₂ spacer on the solution properties and study the cationic – to – zwitterionic – to zwitterionic/anionic – to – anionic polyelectrolyte transitions involving polymers having identical degree of polymerization.



Scheme 1.



Scheme 2.

Extraction of proteins in aqueous-two phase systems (ATPSs) has received considerable attention owing to the friendly environment they provide for the labile protein products. Recently, there has been considerable interest in the use of polymer-salt based ATPSs in the selective separation of toxic metal ions^[69-75]. In this context, the newly synthesized pH-responsive polyphosphonates would be used for the first time to construct ATPSs that may find application in bioseparation and separation of toxic metal ions.

3.2 Experimental

3.2.1 Physical methods

Elemental analysis was carried out on a Perkin Elmer Elemental Analyzer Series 11 Model 2400. IR spectra were recorded on a Perkin Elmer 16F PC FTIR

spectrometer. ^1H , ^{13}C and ^{31}P NMR spectra were measured in CDCl_3 (using TMS as internal standard) or D_2O at $+25\text{ }^\circ\text{C}$ (using HOD peak at δ 4.65 and ^{13}C peak of dioxane at δ 67.4 ppm as internal standard) on a JEOL LA 500 MHz spectrometer. ^{31}P was referenced with 85% H_3PO_4 in DMSO.

Viscosity measurements were made by Ubbelohde viscometer (having Viscometer Constant of 0.005718 cSt/s at all temperatures) using CO_2 -free water under N_2 in order to avoid CO_2 absorption that may affect the viscosity data. Molecular weights were determined by the GPC measurement performed on an Agilent 1200 series apparatus equipped with a Refractive Index (RI) detector and PL aquagel-OH MIXED column, using polyethylene oxide/glycol as a standard and water as eluent at a flow rate of $1.0\text{ cm}^3/\text{min}$ at $25\text{ }^\circ\text{C}$.

Static light scattering (SLS) experiments were performed using DAWN EOS light-scattering instrument (Wyatt Technology Corporation, CA). Millipore disposable filters of pore size $0.02\text{ }\mu\text{m}$ were used to remove dust particles from solvent (water) and solution of ionic polymers **2**, **5**, and **6**(concentration range: 0.03–0.1 g/dL) in 0.5 N NaCl. Polymer concentrations were corrected to account for the screened polymer by the filtration media. The system light source was a linearly polarized gallium arsenide (GaAs) laser. The laser is positioned so that the incident beam was vertically polarized. An RFM-340 Refractometer (Bellingham & Stanley, UK) was used to measure the differential refractive indices (dn/dc) of different solutions. Measurement of radius of gyration (R_g) of the polymers was conducted using Wyatt DLS correlator at $21\text{ }^\circ\text{C}$. The DLS detector was placed at an angle of 90° to the excitation beam.

3.2.2 Materials

2,2'-Azobisisobutyronitrile (AIBN) from Fluka AG was purified by crystallization from a chloroform–ethanol mixture. Ammonium persulfate (APS) from Fluka AG was used as received. Polyethyleneglycol (PEG) 35000 was purchased from MERCK-Schuchardt. Dimethylsulfoxide (DMSO) was dried over calcium hydride overnight and then distilled at a boiling point of 64–65 °C (4 mmHg). For dialysis, a Spectra/Por membrane with a molecular weight cut-off value of 6000–8000 was purchased from Spectrum Laboratories, Inc.

3.2.3 General procedure for the copolymerization of the monomer **1** with SO₂

All the polymerizations were carried out using conditions as described in Table 3.1. In a typical experiment (Entry 4, Table 3.1), SO₂ (40 mmol) was absorbed in a solution of monomer **1**^[89] (40 mmol) in DMSO (10.0 g). The initiator AIBN (200 mg) was then added under N₂ and stirred at 60 °C for 24 h. The CPE **2** was precipitated in acetone as a white polymer and dried under vacuum at 55 °C to a constant weight. The onset of thermal decomposition (Closed capillary) at 250–260 °C (decomposed, turned black); (Found: C, 37.7; H, 6.8; N, 3.9; S, 9.0. C₁₁H₂₃ClNO₅PS requires C, 37.99; H, 6.67; N, 4.03; S, 9.22%); ν_{\max} (KBr) 3500, 2980, 2908, 1537, 1466, 1397, 1298, 1231, 1123, 1012, 953, 846, 780, and 513 cm⁻¹; ¹H and ¹³C NMR spectra are presented in Figs. 3.1b and 3.2b, respectively. ³¹P NMR (202 MHz, D₂O) signals at δ 6.87 and 13.9 ppm indicated the presence of *cis* and *trans* isomers, respectively (Scheme 3).

Table 3.1. Cyclocopolymerization of the cationic monomer **1 with sulfur dioxide^a to cationic polyelectrolyte (CPE) **2**.**

Entry	AIBN (mg)	Yield (%)	Intrinsic Viscosity ^b (dL g ⁻¹)	\overline{M}_w	(PDI) ^c
1	30	68	0.408	–	–
2	40	78	0.305	61,000	2.01
3	50	81	0.431	–	–
4 ^c	200 ^c	80	0.542	105,000	2.03

^aPolymerization reactions were carried out using 10 mmol each of the monomer and SO₂ in DMSO (2.5 g) in the presence of azoisobutyronitrile (AIBN) at 60 °C for 24 h.

^bViscosity of 1-0.25 % polymer solution in salt-free and 0.1 N NaCl at 30 °C was measured with a Ubbelohde Viscometer (K=0.005718).

^cEntry 3 was repeated in entry 4 in DMSO (10 g) using 40 mmol each of monomer **1** and SO₂.

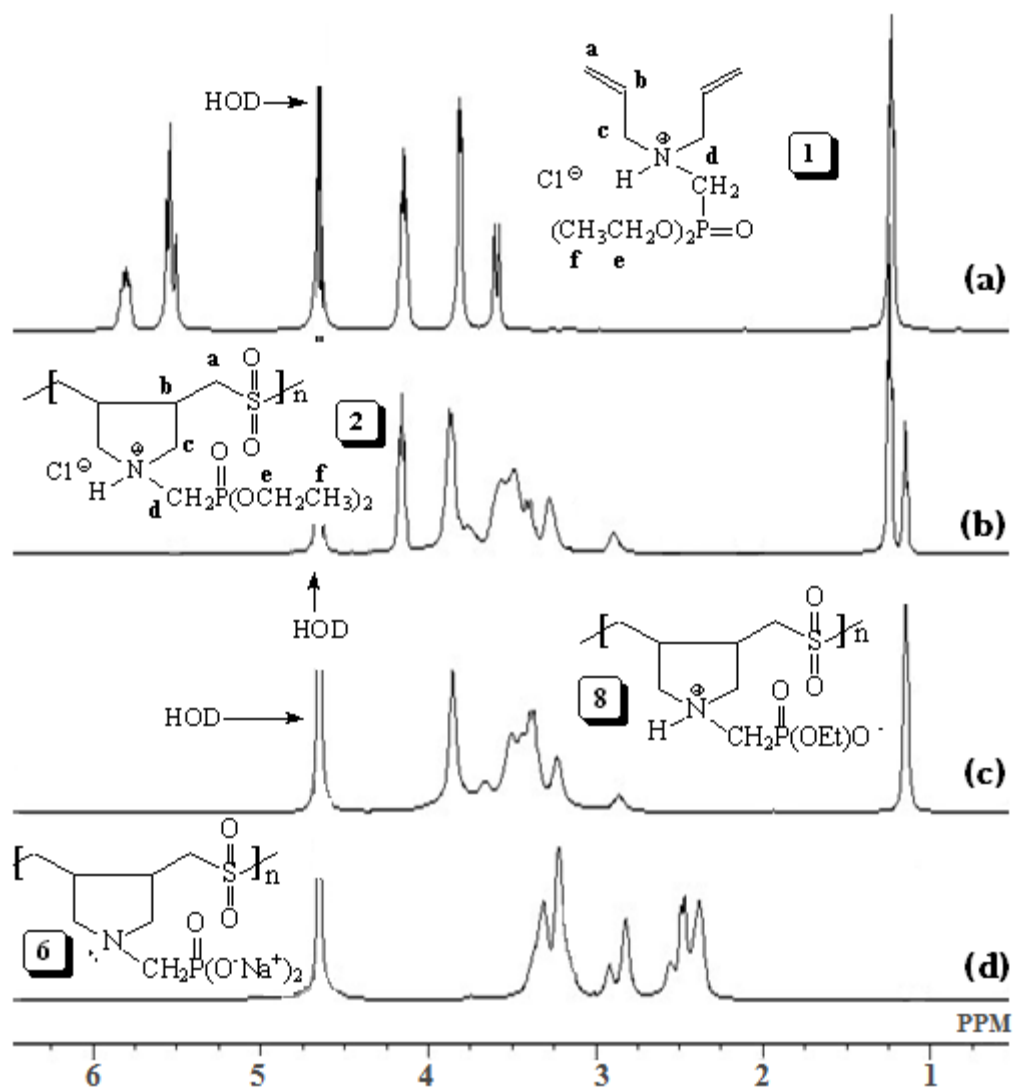


Figure 3.1. ^1H NMR spectrum of (a) 1, (b) 2, (c) 8 and (d) 6 in D_2O .

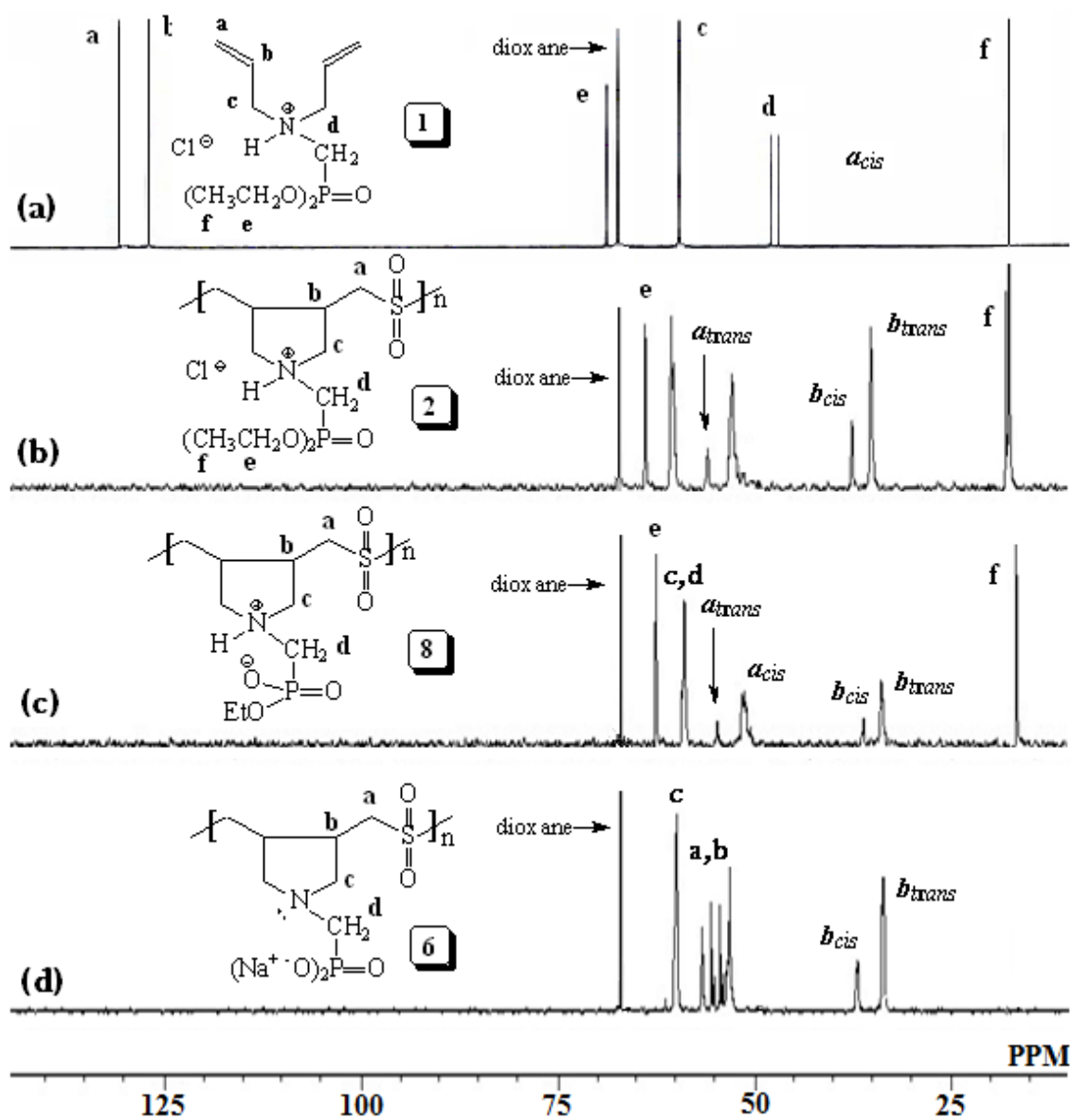
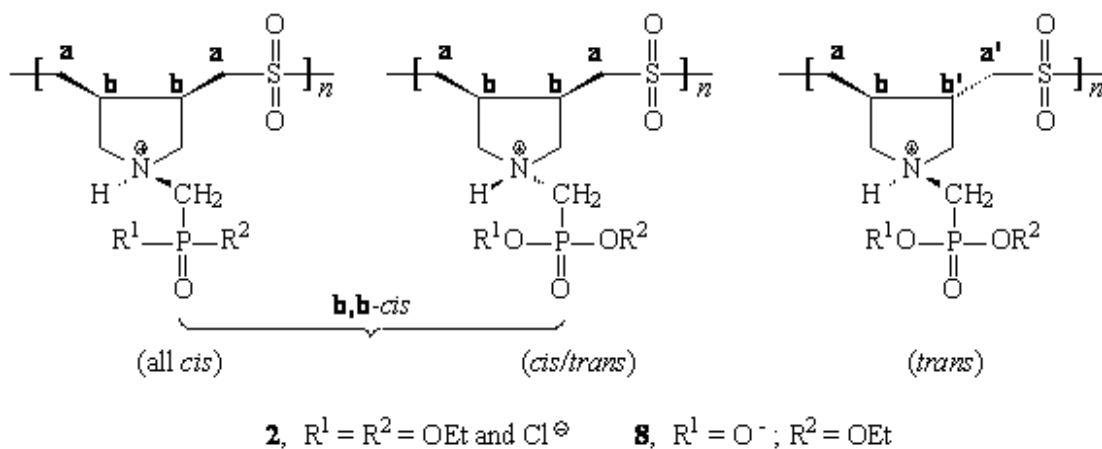


Figure 3.2. ^{13}C NMR spectrum of (a) 1, (b) 2, (c) 8 and (d) 6 in D_2O .



Scheme 3.

3.2.4 Acidic hydrolysis of CPE **2** to polyzwitterionic acid (PZA) **3**

A solution of CPE **2** (6.0 g, 17.3 mmol) in concentrated HCl (65 cm³) and water (45 cm³) (entry 4, Table 3.1) in a closed vessel was hydrolyzed at 90 °C for 24 h. PZA **3** was precipitated in large excess of acetone and the white polymer was dried under vacuum at 50 °C to a constant weight (4.1 g, 92%). The polymer, even though soluble in the reaction mixture in the presence of HCl, was found to be insoluble in water. A portion of the above PZA **3** (0.8 g) was dialyzed against deionized water for three days in order to remove any HCl (the polymer remained insoluble during the dialysis). The resulting solid was dried under vacuum to a constant weight at 55 °C. The onset of thermal decomposition: (Closed capillary) at 250–260 °C (decomposed, turned black). (Found: C, 32.7; H, 5.6; N, 5.4; S, 12.3. C₇H₁₄NO₅PS requires C, 32.94; H, 5.53; N, 5.49; S, 12.56%); ν_{max} (KBr) 3430, 2981, 1426, 1304, 1173, 1128, 1077, 919, 757, 668, and 538 cm⁻¹.

3.2.5 Basification of PZA 3 to dianionic polyelectrolyte (DAPE) 6

PZA 3 (derived from hydrolysis of CPE 2 from entry 4, Table 3.1) (3.06 g, 12 mmol) was dissolved in 1.0 N NaOH (30 cm³, 30 mmol) and immediately precipitated in methanol to obtain DAPE 6 as a white polymer which was dried under vacuum at 55 °C to a constant weight (3.2 g, 89%). The onset of thermal decomposition (Closed capillary): 285–300 °C (decomposed, turned black); (Found: C, 27.9; H, 4.2; N, 4.5; S, 10.4. C₇H₁₂NNa₂O₅PS requires C, 28.10; H, 4.04; N, 4.68; S, 10.72%); ν_{\max} (KBr) 3429 (very broad engulfing the CH stretching vibrations), 1660, 1549, 1529, 1479, 1422, 1298, 1121, 1063, 977, 769, and 562 cm⁻¹; δ_p (202 MHz, D₂O): 11.96. ¹H and ¹³C NMR spectra are presented in Figs. 3.1d and 3.2d, respectively.

3.2.6 Acidification of DAPE 6 to zwitterionic-anionic polyelectrolyte (ZAPE) 5

A 0.0993 N HCl (17.5 cm³, 1.74 mmol) was added to DAPE 6 (derived from entry 4, Table 3.1) (0.50 g, 1.67 mmol). The solution was dialyzed against deionized water for 1.5 h, and freeze dried to obtain ZAPE 5 as a white polymer (0.40 g, 86%). The onset of thermal decomposition: (Closed capillary) 245–270 °C (dark brown, decomposed); (Found: C, 30.0; H, 4.9; N, 4.8; S, 11.3. C₇H₁₃NNaO₅PS requires C, 30.33; H, 4.73; N, 5.05; S, 11.57%); ν_{\max} (KBr) 3200, 2990, 1635, 1468, 1413, 1275, 1111, 1065, 974, 907 and 753 cm⁻¹.

3.2.7 General procedure for the copolymerization of monomer 7 with SO₂

All the polymerizations were carried out using conditions as described in Table 3.2. At the end of the elapsed time, the reaction mixture was dissolved in water and dialyzed against deionized water for 48 h. The resulting solution was freeze dried to

obtain polyzwitterion-ester (PZE) **8** as a white polymer. The onset of thermal decomposition (Closed capillary): 235–245 °C (decomposed, turned black); (Found: C, 37.9; H, 6.5; N, 4.8; S, 11.1. C₉H₁₈NO₅PS requires C, 38.16; H, 6.40; N, 4.94; S, 11.32%); ν_{\max} (KBr) 3430, 2982, 1658, 1427, 1307, 1215, 1129, 1081, 1039, 949, 842, 781, and 538 cm⁻¹; δ_p (202 MHz, D₂O): 6.87 ppm ¹H and ¹³C NMR spectra are presented in Figs. 3.1c and 3.2c.

Table 3.2. Cyclocopolymerization of the zwitterionic monomer 7 with sulfur dioxide^a to PZE 8.

Entry	7 mmol	Initiator (mg)	Temp (°C)	Yield (%)	Intrinsic Viscosity ^b (dl g ⁻¹)	\overline{M}_w	(PDI) ^c
1	8	AIBN (40)	60	43	0.0563	–	–
2	8	AIBN (40)	50	28	0.0547	–	–
3	8	APS (50)	50	88	0.0617	65,500	2.05
4	8	APS (25)	50	81	0.0601	–	–
5 ^c	30	APS (160)	50	76	0.0629	67,600	2.07

^aPolymerization reactions were carried out using 8.0 mmol each of the monomer and SO₂ in DMSO (2.0 g) in the presence of azoisobutyronitrile (AIBN) or ammonium persulfate (APS) for 24 h.

^bViscosity of 1-0.25 % polymer solution in salt-free water at 30 °C was measured with a Ubbelohde Viscometer (K=0.005718).

^cPolymerization in entry 5 was carried out using a larger scale involving 30 mmol each of monomer **7** and SO₂ in DMSO (7.5 g).

3.2.8 Acidic hydrolysis of PZE 8 to PZA 3

PZE 8 (entry 5, Table 3.2) was hydrolyzed to PZA 3 (95% yield) using the procedure described for the conversion of CPE 2 to PZA 3 (*vide supra*).

3.2.9 Basification of PZA 3 (derived from entry 5, Table 3.2) to DAPE 6

PZA 3 (derived from entry 5, Table 3.2) was basified to DAPE 6 (88% yield) using the procedure described for the conversion of PZA 3 to DAPE 6 (*vide supra*).

3.2.10 Basification of PZE 8 to anionic polyelectrolyte (APE) 9

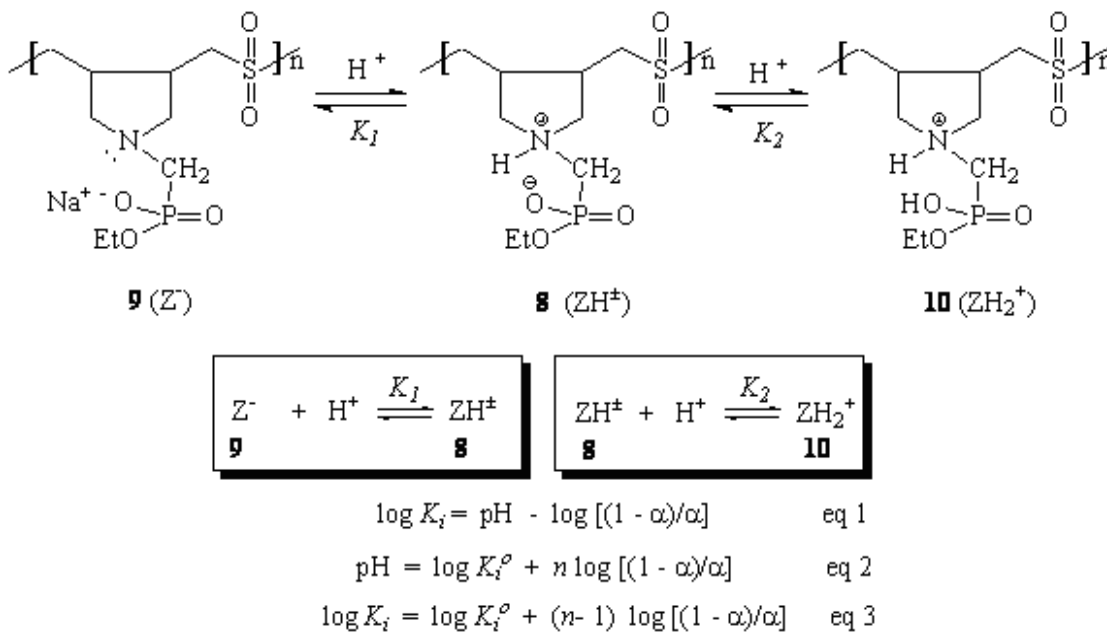
PZE 8 (entry 5, Table 3.2) (283 mg, 1.0 mmol) was dissolved in water (1 cm³) and neutralized with 1.03 N NaOH (1.2 cm³), then precipitated into acetone to obtain APE 9 which was dried under vacuum at 55 °C to a constant weight (257 mg, 93%). The onset of thermal decomposition (Closed capillary): 260–275 °C (decomposed, turned brown); (Found: C, 35.1; H, 5.7; N, 4.4; S, 10.2. C₉H₁₇NNaO₅PS requires C, 35.41; H, 5.61; N, 4.59; S, 10.50%); ν_{\max} (KBr) 3430, 2980, 1654, 1444, 1298, 1193, 1127, 1045, 946 and 786 cm⁻¹ δ_p (202 MHz, D₂O): 17.6 (s, major) and 17.4 (s) ppm.

3.2.11 Potentiometric titrations

The potentiometric titrations were carried out at 23 °C as described elsewhere^[26]. After each addition of the titrant, the pH of the solution was recorded using a Corning pH Meter 220.

The protonation constant of the amine nitrogen, Log K_1 , is calculated at each pH value by the well-known Henderson–Hasselbalch Equation (1) (Scheme 4) where degree of protonation (α) is the ratio $[ZH^{\pm}]_{eq}/[Z]_o$. For the titration with NaOH, the $[Z]_o$ is the initial analytical concentration (mol/L repeating unit) of PZE 8 and $[ZH^{\pm}]_{eq}$ is the concentration of the protonated species 8 at the equilibrium given by

$[ZH^+]_{eq} = [Z]_0 - C_{OH^-} - [H^+] + [OH^-]$, where C_{OH^-} is the concentration of the added NaOH; $[H^+]$ and $[OH^-]$ at equilibrium were calculated from the pH value^[76].



Scheme 4.

The typical electrolytes having apparent basicity constants could be described by the Equation (2) (Scheme 3) where $\log K^0 = \text{pH}$ at $\alpha = 0.5$ and $n = 1$ in the case of sharp basicity constants. The linear regression fit of pH vs. $\log [(1 - \alpha)/\alpha]$ gave $\log K^0$ and 'n' as the intercept and slope, respectively. Simultaneous protonation of the two basic sites is least likely since the basicity constant for the $\text{PO}(\text{OEt})\text{O}^-$ group is less than that of the amine group by about 4–5 orders of magnitude. The second step protonation constant ($\log K_2$) involving the $\text{PO}(\text{OEt})\text{O}^-$ may be calculated by titration of the PZE **8** with HCl as described in ref [26].

The experimental details of the potentiometric titrations are summarized in Table 3.3. Inserting the value of pH from Equation (2) into Equation (1) leads to modified Henderson–Hasselbalch equation (Eq. (3))^[84, 90] (Scheme 4) where $(n - 1)$

gives a measure of the deviation of the studied polymers from the behavior of small molecules showing sharp basicity constants (for molecules having sharp basicity constants, n becomes 1).

Table 3.3. Experimental Details for the potentiometric titration of Polymer PZE 8 (ZH[±]) at 23 °C in Salt-Free Water and in 0.1 N NaCl.

Run	ZH [±] (mmol)	C _T ^a (mol dm ⁻³)	α-range	pH-range	Points ^b	Log K _i ^{o,c}	n _i ^c	R ^{2, d}
<i>Polymer PZE 8 (ZH[±]) in salt-free water</i>								
1	0.1825 (ZH [±])	0.1059	0.88–0.20	5.85–8.88	16	7.65	2.09	0.9981
2	0.2323 (ZH [±])	0.1059	0.86–0.21	5.80–8.69	18	7.57	2.18	0.9935
3	0.2944 (ZH [±])	0.1059	0.89–0.21	5.63–8.70	21	7.59	2.12	0.9973
Average						7.60 (4)	2.13 (5)	
Log K _I ^e = 7.60 + 1.13 log [(1-α)/α]; For the reaction: Z ⁻ + H ⁺ ⇌ ZH [±]								
<i>Polymers PZE 8 (ZH[±]) in 0.1 N NaCl</i>								
1	0.1846 (ZH [±])	0.1059	0.83–0.14	5.64–7.51	15	6.56	1.31	0.9952
2	0.2362 (ZH [±])	0.1059	0.84–0.19	5.62–7.40	17	6.60	1.34	0.9990
3	0.2979 (ZH [±])	0.1059	0.82–0.11	5.64–7.77	21	6.60	1.40	0.9965
Average						6.59 (2)	1.35 (5)	
Log K _I ^e = 6.59 + 0.35 log [(1-α)/α]; For the reaction: Z ⁻ + H ⁺ ⇌ ZH [±]								

^aTitration concentration of NaOH. ^bNumber of data points from titration curve.

^cValues in the parentheses are standard deviations in the last digit.

^dR = Correlation coefficient. ^elog K_i = log K_i^o + (n - 1) log [(1 - α)/α].

3.2.12 Phase compositions and phase diagram of PEG-DAPE 6 (0.4 N NaCl) system

3.2.12.1 The NMR method

Four systems of known compositions (A_{total}) of PEG and DAPE 6 were made in 0.4 N NaCl. The mixtures after thorough shaking were centrifuged for a period of 10 min

to ensure a complete phase separation and kept at 23 °C for 24 h. The volume and the density of the top layers (~1.03 g/cm³) and bottom layers (~1.06 g/cm³) were measured.

The ¹H NMR spectra of the top and bottom layers were measured after exchanging H₂O by D₂O. For a total of twelve protons, the ¹H NMR spectrum of a pure sample of DAPE **6** revealed the area of the signals in the ranges δ2.25–3.0 and δ3.1–3.63 in a respective ratio of 1.23:1. The mole ratio ([PEG]/[DAPE]) of the repeating units of the polymers in each layer was calculated using the integration of the four-proton singlet at δ3.58 for PEG which overlapped with the signals in the range δ3.1–3.63 for DAPE **6**. Weight percent of each polymer is determined by using the Eqs. (4) and (5) as described in our earlier work^[91]:

$$[DAPE_b] = \frac{PEG_0 / 44.03 - (DAPE_0 / 299.19)([PEG]/[DAPE])_t}{V_b \{ ([PEG]/[DAPE])_b - ([PEG]/[DAPE])_t \}} \quad (4)$$

$$DAPE_b = [DAPE_b]V_b \times 299.19 \text{ mg} \quad (5)$$

where, subscript *t* and *b* represent top and bottom phase, respectively. [DAPE] and [PEG] represent concentration of the repeating units in mmol of repeat unit cm⁻³. DAPE₀ and PEG₀ represent the total mass in mg of the polymers and *V* represents the volume in cm³. Molar masses of the repeat units of the DAPE and PEG were taken as 299.19 and 44.03, respectively. The mass of polymer DAPE_b in the bottom phase (Eq. (5)) and the weight percents of the polymers were calculated as described^[91].

3. 2.12.2 The turbidity method

Concentrated solutions of DAPE **6** (~10 %w/w) and PEG (~20 %w/w) in 0.4 N NaCl were used for the construction of binodal at 23 °C using procedure as described

elsewhere^[6, 26]. Points obtained by turbidity method are joined together in the phase diagram.

3.3 Results and discussion

3.3.1 Synthesis of the copolymers

Cationic diethoxyphosphonate **1** and its corresponding zwitterionic ethoxyphosphonate **7** underwent cyclocopolymerization with SO₂ in DMSO in the presence of AIBN or APS to give CPE **2** (Scheme 1, Table 3.1) and PZE **8** (Scheme 2, Table 3.2), respectively, in very good yields. As evident from Table 3.2, changing the initiator from AIBN to APS improved the yield considerably. Acidic hydrolysis of both CPE **2** and PZE **8** to the same phosphonic acid PZA **3** (>90% yield) provided us with the opportunity to compare their sizes by viscometry (*vide infra*). PZA **3** on treatment with excess NaOH afforded DAPE **6** (89%) which upon neutralization with 1 equivalent of HCl gave ZAPE **5** containing an interesting blend of zwitterionic as well as anionic motifs in the same repeating unit.

PZE **8** on treatment with NaOH afforded anionic polyelectrolyte (APE) **9**. CPE **2**, PZE **8** as well as all the other polymers were found to be stable up to 240 °C and thereafter decompose as a result of elimination of SO₂.

3.3.2 Infrared and NMR spectra

The strong absorptions at 1231 and 1012 cm⁻¹ in the IR spectrum of **2** were attributed to the stretching frequency of P=O and P-O-C, respectively. PZE **8** showed the corresponding strong absorptions at 1215 and 1039 cm⁻¹. The two strong bands at around 1300 and 1120 cm⁻¹ were assigned to the asymmetric and symmetric vibrations of SO₂ unit in **2**, **3**, **5**, **6**, **8** and **9**.

^1H and ^{13}C NMR spectra of monomer **1**, CPE **2**, DAPE **6** and PZE **8** are displayed in Figs. 3.1 and 3.2, respectively. The absence of any residual alkene proton or carbon signal in the polymer spectra suggested the chain transfer process [6, 79, 92] for the termination reaction. The ^1H NMR spectrum of CPE **2** (Fig. 3.1b) revealed the presence of two sets of triplets at δ 1.13 and 1.23 ppm in an approximate ratio of 25:75, respectively, attributed to the OCH_2CH_3 protons of the *trans* and *cis* disposed substituents, respectively, in the five-membered ring structure (Scheme 3). The integration of the relevant ^{13}C peaks (Fig. 3.2) yielded the *cis/trans* ratio of the ring substituents to be 75/25 which is similar to that observed for the related polymers derived from quaternary ammonium salts [5, 6, 21, 23, 24, 79-81, 92].

3.3.3 Solubility and critical salt concentrations (CSC)

Zwitterionic PZA **3** was found to be insoluble in water but remained soluble in the presence of HCl as a result of its transformation to cationic polyelectrolyte (CPE) **4** (Scheme 1). DAPE **6** was found to be soluble in salt-free water as expected. Interestingly, ZAPE **5** having zwitterionic as well as anionic motifs was also soluble in salt-free water thereby implying the domination of the anionic motifs in dictating the solubility behavior. The solubility behavior of polymers CPE **2** and PZA **3** are given in Table 3.4. While the former was readily soluble in many different solvents, the later dissolved only in formic acid presumably as a result of its transformation to CPE **4**.

Table 3.4. Solubility^{a,b} of polymer CPE 2, PZA 3 and PZE 8

Solvent	Dielectric constant, ϵ	solubility		
		2	3	8
Formamide	111.0	+	-	+
Water	78.4	+	-	+
Formic acid	58.5	+	+	+
DMSO	47.0	+	-	-
Ethylene glycol	37.3	+	-	-
DMF	37.0	-	-	-
Methanol	32.7	-	-	-
Diethyleneglycol	31.7	+	-	-
Ethanol	24.5	-	-	-
Acetone	21.0	-	-	-
Acetic acid	6.1	+	-	±

^a2%(w/w) of polymer solution was made after heating the mixture at 70°C for 1 h and then cooling to 23°C.

^b‘+’ indicates soluble; ‘-’ indicates insoluble; ‘±’ indicates partially soluble.

PZA 3 was found to be water-soluble in the presence of various salts. The critical minimum salt concentrations (CSCs) required to promote its water solubility are given in Table 3.5. The added electrolytes disrupt the inter- and intra-chain Coulombic interactions in PZA, thus allowing the collapsed coil to expand. For a common K⁺, the sequence of increasing solubility power (decreasing order of CSC values) was found to be: Cl⁻ < Br⁻ << I⁻. The iodide anion is the most polarizable (soft), hence it is particularly effective in neutralizing the cationic nitrogens in the polymer backbone.

Table 3.5. Critical salt concentration (CSC) for aqueous solutions of PZA 3 at 23°C.

Salt	CSC (M)
NaCl	4.73
KCl	4.29
KBr	4.15
KI	2.77
HCl	5.40
CsCl ^a	4.88

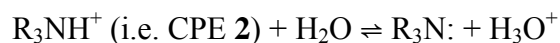
^aIn CsCl the polymer is soluble at 4.88 M, but addition of salt-free water to the polymer solution in 4.88 M CsCl did not give turbid mixture

Even though PZE **8** is a zwitterionic polymer, it was found to be readily soluble in water as well as in protic solvents having higher dielectric constants (Table 3.4); hydrogen bonding with the protic solvents is attributed to the observed solubility behavior. Nonprotic solvents like DMF and DMSO having high dielectric constants failed to dissolve the polymer. PZs are in general expected to be insoluble in water. However, their solubility in water is not unusual; a considerable number of polycarbobetaines having pK_a values of >2.0 , and polysulfobetaines are reported to be soluble in salt-free water^[24, 27, 80]. Steric factor plays a dominant part in the solubility behavior of PZA **3** and PZE **8**; sterically crowded cationic and anionic charges in the later, owing to the presence of an ethoxy group, are unable to move closer to manifest

effective intra- or intermolecular Coulombic interactions, thereby leading to its solubility in water^[13, 81].

3.3.4 Viscosity measurements

Viscosity plots for polymer CPE **2** and DAPE **6** in the presence and absence of added salt NaCl is shown in Fig. 3.3a and b, respectively. Viscosity curve in salt-free water behave like that of a typical polyelectrolyte i.e. concave upwards. However, at lower polymer concentrations, the viscosity values tend to fall as a result of the following equilibrations involving hydrolysis of weak acid (R_3NH^+) and weak base (DAPE **6**):



Where formation of more compact neutral species R_3N and ZAPE **5** induces the polymer backbone to adapt a compact coil conformation owing to a decrease in the repulsion among the like charges.

The viscosity plots became normal in the presence of NaCl, and intrinsic viscosity decreased with increasing NaCl concentrations. Note that dianionic DAPE **6** and monocationic CPE **2** have identical degree of polymerization; however, the former has lower viscosity values (Fig. 3b) than the later (Fig. 3a). One possible rationale behind this observation could be the larger distance among the negative charges on oxygens than the positive charges of the nitrogens in the adjacent repeating units of DAPE **6** and CPE **2**, respectively.

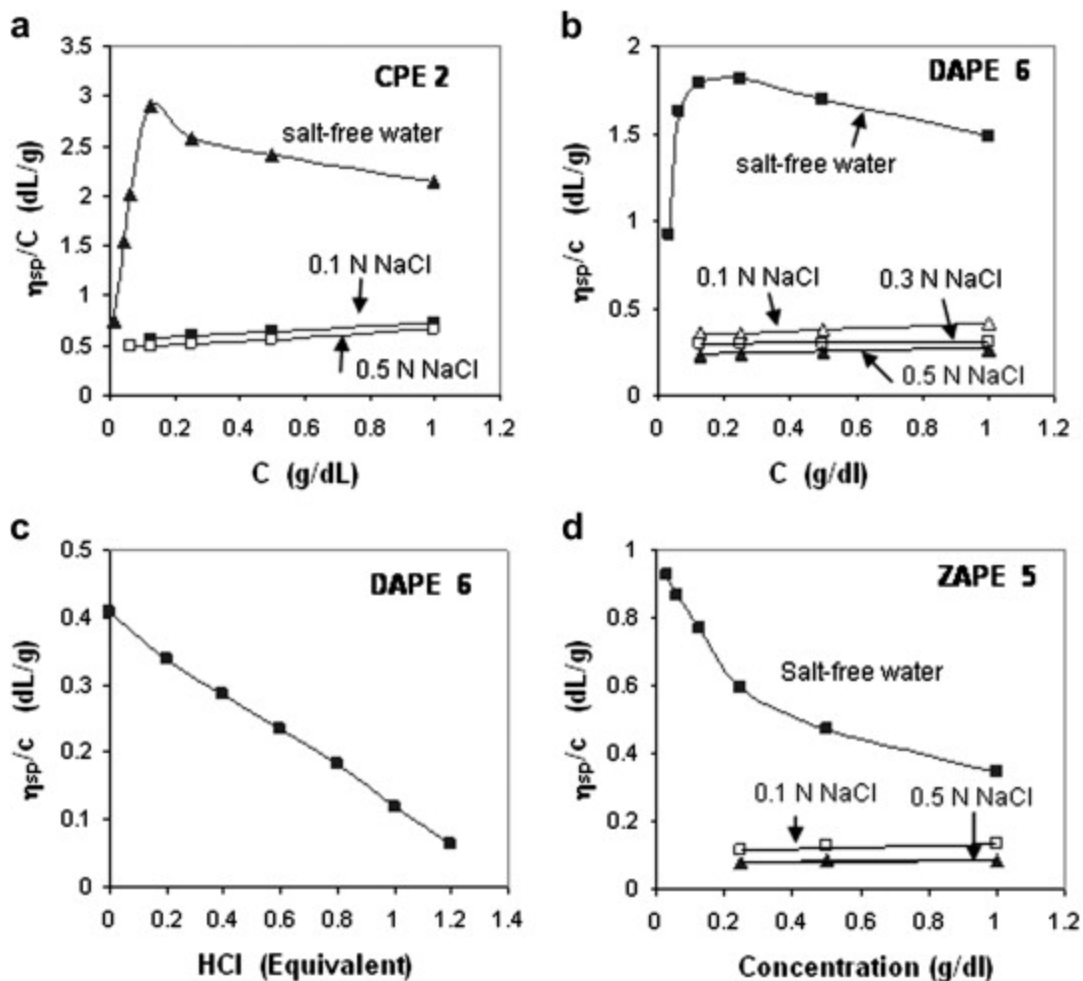


Figure 3.3. Using an Ubbelohde Viscometer at 30 °C: The viscosity behavior of (a) CPE 2 (entry 4, Table 1) in salt-free water, 0.1 N and 0.5 N NaCl, (b) DAPE 6 (prepared from entry 4, Table 1) in salt-free water, 0.1 N, 0.3 and 0.5 N NaCl, (c) a 1.0 g/dL solution of polymer DAPE 6 (prepared from entry 4, Table 1) in salt-free water in the presence of different equivalent of added HCl and (d) ZAPE 5 (prepared from entry 4, Table 1) in salt-free water, 0.1 N and 0.5 N NaCl.

Since the addition of HCl would convert DAPE 6 to a more compact ZAPE 5, the reduced viscosity for 1 g/dL solution of DAPE 6 decreases with the increase in HCl concentrations (Fig. 3.3c). Addition of greater than 1 equivalent of HCl further decreases the viscosity owing to the formation of zwitterionic PZA 3. The PZA3 started to precipitate on addition of greater than 1.2 equivalents of HCl.

The viscosity plots for zwitterionic-anionic ZAPE **5** in the absence and presence of NaCl is shown in Fig. 3.3d. The plots are typical of an anionic polyelectrolyte. It is interesting to note that viscosity values decrease with the increasing concentration of NaCl implying that the anionic motifs dominates over zwitterionic motifs in dictating its viscosity behavior. For the sake of comparison, the viscosity data for CPE **2**, ZAPE **5** and DAPE **6**, all having same degree of polymerization are shown in Fig. 3.4; the sequence of increasing viscosity was found to be: ZAPE **5** ($\pm -$) < DAPE **6** ($--$) < CPE **2** ($+$). (The charges on the repeating unit are written in the parentheses). The viscometric findings were corroborated by the values of radius of gyration (R_g) as measured by light scattering experiments using Wyatt DLS correlator. While the R_g s of ZAPE **5**, DAPE**6**,and CPE **2** in 0.5 N NaCl at 21 °C were determined to be 16, 21, and 28 nm, respectively, the corresponding $[\eta]$ s in 0.5 N NaCl at 30 °C were 0.0784, 0.228, and 0.478 dL/g.

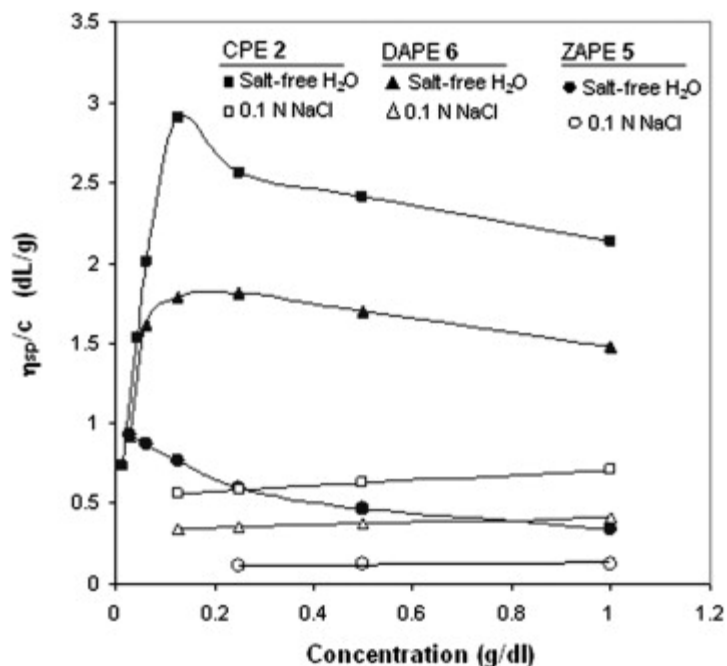


Figure 3.4. The viscosity behavior of CPE 2, DAPE 6 and ZAPE 5 (all from or derived from entry 4, Table 1) in salt-free water, and 0.1 N NaCl at 30 °C using an Ubbelohde Viscometer.

The viscosity data for PZE 8 and APE 9, both having same degree of polymerization, in salt-free and 0.1 N NaCl are shown in Fig. 3.5a. Unlike in the case of a polyelectrolyte, the viscosity plot for PZE 8 in the presence or absence of NaCl remains linear (Fig. 3.5a–iv). The APE 9 and PZE 8 in 0.1 NaCl displayed polyelectrolyte (i.e. decrease in $[\eta]$) and anti-polyelectrolyte behavior (i.e. increase $[\eta]$), respectively. The effect of added salts on the intrinsic viscosity, slope, and Huggins constant, as evaluated by the Huggins equation: $\eta_{sp}/C = [\eta] + k [\eta]^2 C$, are included in Tables 3.2 and 3.6. The $[\eta]$ increases most with NaI (Fig. 3.5b, Table 3.6); the more polarizable iodide is particularly effective in neutralizing the cationic charges on the polymer backbone, thereby leaving the less shielded phosphonate anions to exhibit repulsion hence increase hydrodynamic volume. A decrease in the value for the Huggins constant k in 0.1 N NaI in comparison to NaCl may be associated with an increased polymer–solvent interaction.

The viscosity values almost level off at 0.5 N as a result of near completion of the site and atmospheric binding around the cationic nitrogens^[8]. It is worth mentioning that divalent cation Ca^{2+} , known to precipitate anionic polyelectrolytes from aqueous solution, did not precipitate PZE **8**.

The pH-responsiveness of **8** is demonstrated by the change in the reduced viscosities of a 1.0 g/dL solution of the polymer (entry 5, Table 3.2) (Fig. 3.5c). The addition HCl and NaOH shifts the equilibria towards the more extended polymer backbone of cationic **10** and APE **9**, respectively (Scheme 4). While the NaOH can readily deprotonate **8** ($\text{p}K_{\text{a}} = 7.6$, *vide infra*) to form weakly basic **9** ($\text{p}K_{\text{b}} \approx 6.4$), the relatively higher acidity of the $\text{P}(\text{---O})(\text{OEt})\text{OH}$ ($\text{p}K_{\text{a}} \approx 2$) in CPE **10** preclude its formation to a great extent by the protonation of PZE **8**. This is reflected in the viscosity plots: while a steep increase in the viscosity values is observed on the addition of NaOH, reduced viscosity increases slightly with the addition of HCl.

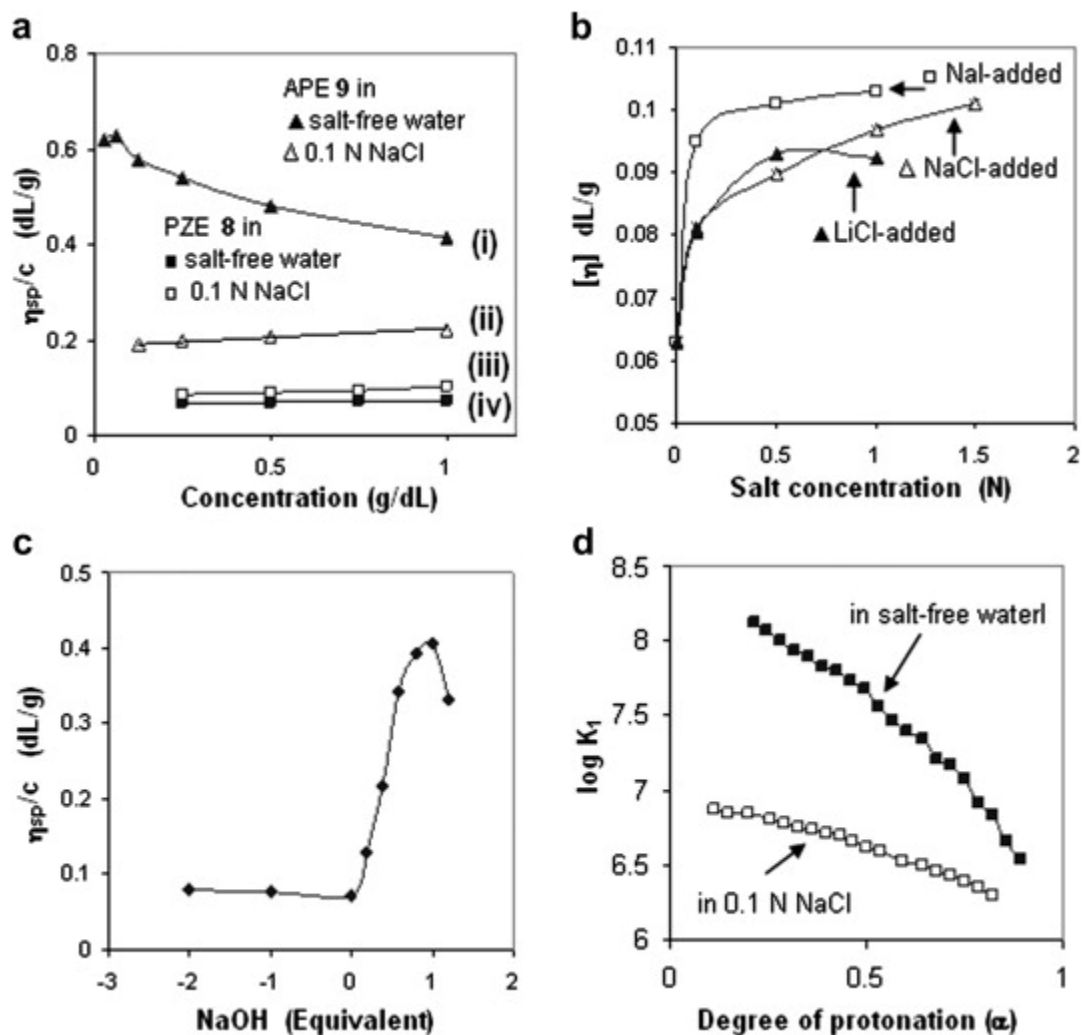


Figure 3.5. Using an Ubbelohde Viscometer at 30 °C: (a) The viscosity behavior of PZE 8 (entry 5, Table 2) and APE 9 (derived from entry 5, Table 2) in salt-free water and 0.1 N NaCl; (b) The intrinsic viscosity $[\eta]$ behavior of PZE 8 (entry 5, Table 2) in the presence of varying concentrations of added salts; (c) Reduced viscosity (η_{sp}/C) of a 1.0 g/dL solution of PZE 8 (entry 5, Table 2) in salt-free water versus equivalent of added NaOH. Negative (-) values indicate the equivalent of added HCl. (d) Plot for the apparent $\log K_1$ versus degree of protonation (α) for PZE 8 (entry 5, Table 2) in salt-free water and 0.1 N NaCl.

Table 3.06. Effect of added salts on the intrinsic viscosity ($[\eta]^a$ and Huggins constant (K') of PZE 8 (entry 5, Table 2).

Solvent	Slope	$[\eta]$	K'
Salt-free H ₂ O	0.0098	0.0629	2.47
0.1 N NaCl	0.0180	0.0811	2.74
0.5 N NaCl	0.0150	0.0897	1.86
1.0 N NaCl	0.0145	0.097	1.54
1.5 N NaCl	0.0128	0.101	1.25
0.1 N NaI	0.00850	0.0948	0.946
0.5 N NaI	0.0208	0.101	2.04
1.0 N NaI	0.0286	0.103	2.69
0.1 N LiCl	0.00900	0.0804	1.39
0.5 N LiCl	0.0143	0.0932	1.65
1.0 N LiCl	0.0344	0.0922	4.05
0.1 N CaCl ₂	0.0100	0.0925	1.17
0.1 N CsCl	0.00420	0.0885	0.536
0.1 N HCl	0.0209	0.0723	4.03

^aViscosity of 1-0.25 % salt-added polymer solution at 30 °C was measured with a Ubbelohde Viscometer ($K=0.005718$).

Finally, CPE 2 (entry 2, Table 3.1) and PZE 8 (entry 5, Table 3.2) have been correlated by their conversions to DAPE 6 via PZA 3. While the $[\eta]$ of CPE 2 is almost four times higher than that of PZE 8, their corresponding DAPE 6 samples were found to

have $[\eta]$ values of 0.181 and 0.201 dL/g, respectively (Table 3.7). The viscosity data are in line with the \overline{M}_w of the two polymers.

Table 3.7. Correlation using intrinsic viscosity in 0.1 N NaCl at 30°C of CPE 2 and PZE 8 and their corresponding DAPE 6.

Sample	$[\eta]_{\text{CPE 2}}$	$[\eta]_{\text{PZE 8}}$	$[\eta]_{\text{DAPE 6}}$	\overline{M}_w
Entry 2, Table 1	0.305	–	0.181	61,000
Entry 5, Table 2	–	0.0811	0.201	67,600

3.3.5 Basicity constants

The “apparent”^[93] nature of the basicity constants $\log K_1$ for the protonation of the trivalent nitrogen of APE **9** (Scheme 4) is demonstrated in Fig. 3.5d, which reveals a change in $\log K_1$ with the degree of protonation (α) in going from one end to the other end of the titration. The n values of 2.13 and 1.35 in salt-free water and 0.1 N NaCl, respectively, reflect a stronger polyelectrolyte effect in the former medium (Table 3.3). The n_1 values of >1 indicates the decrease in the basicity of nitrogens with the increase in α owing to a progressive decrease in the overall negative charge density and electrostatic field force that encourages protonation.

The neutralization process, which transforms the anionic motifs in APE **9** to zwitterionic motifs in PZE **8**, may be described by the viscometric transformation of Fig. 3.5a (i) to 5a (iv) in salt-free water and Fig. 3.5a (ii) to 5a (iii) in 0.1 N NaCl. Viscosity plots thus revealed that APE **9** in salt-free water (Fig. 3.5a–i) is the most expanded hence more hydrated, while PZE **8** in salt-free water (Fig. 3.5a–iv) is the least hydrated. Therefore, as a result of each protonation, the greater number of water

molecules are released in salt-free water than in 0.1 N NaCl thereby leading to an entropy-driven^[83] higher basicity constant and n_1 in the former medium (Table 3.3). The basicity constant ($\log K_1^0$) of the amine group was found to be 7.60 and 6.59 salt-free water and 0.1 N NaCl, respectively.

We were unable to determine the basicity constant $\log K_2^0$ for the protonation of the P(—O)OEtO⁻ group in PZE **8** (Scheme 4); presumably as a result of the presence of ethoxy as well as SO₂ units which may also be protonated and thus interfered with the determination of K_2 . The $\log K_2$ for the protonation of monomer **1** was determined to be 2.11^[89], and PZE **8** is expected to have a similar value.

3.3.6 Phase diagram

Fig. 3.6 shows the phase diagram for a PEG-35000-DAPE **6**-H₂O (0.4 N NaCl) system. Polymer concentrations of the two phases in equilibrium with each other, as determined by ¹H NMR, are connected by tie lines. The turbidity method is used to obtain the binodal curves. The polymers displayed segregative phase separation behavior; the binodal was found to be fairly symmetrical implying that the two polymers may have very similar hydrodynamic volumes^[69, 91]. The top and bottom layers were found to be rich in PEG and DAPE **6**, respectively. The phase separation taking place at relatively low total polymer concentrations of below 10%w/w, could be useful from an industrial point of view.

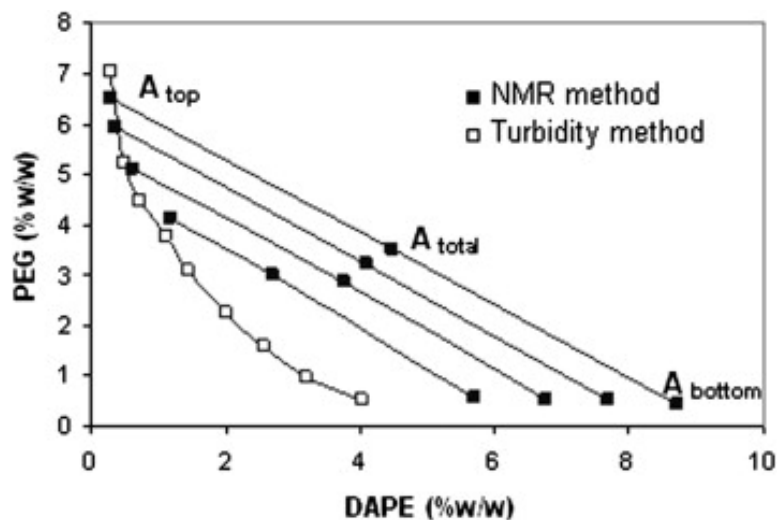


Figure 3.6. Phase diagram of PEG -DAPE 4-Water (0.4 N NaCl) at 23 °C.

3.3.7 Polymer structure versus solubility and basicity constant

The solubility behavior and basicity constant of several polyelectrolytes at 23 °C in salt-free water are listed in Table 3.8. It is evident that the presence of a zwitterionic moiety does not invariably lead to insolubility in salt-free water. While the PZs **8** and **11** having phosphonyl pK_2 s of >2 are water-soluble, carbo-**12** and sulfobetaine **13** are reported to be water-insoluble^[94]. The protonation constant $\log K_1$ of a base (for instance amine nitrogens in **9**) is the pK_1 of its conjugate acid (**8**), and likewise, the $\log K_2$ of $P-O(OEt)O^-$ in **8** is the pK_2 of its conjugate acid $-P=O(OEt)OH$ in **10** (Scheme 4). Note that copolymer **8** has a pK_1 value which is two units lower than that of homopolymer **11**^[89]; the presence of electron-withdrawing SO_2 unit in the former has thus made it more acidic and its conjugate base **9** less basic. The difference in the basicity constants of the conjugate bases of **8** and **11** would indeed be an important factor in exercising selectivity in forming metal ion-complexes.

Table 3.8. Solubility behavior of several PZs and the basicity constants $\log K_i^a$ of their conjugate bases at 23°C in salt-free water.

PZ						
	7	11	8	3	12	13
Solubility ^b	+	+	+	-	-	-
pK_1^c	7.9	9.5	7.6	ND ^e	8.7	8.5
pK_2^d	2.1	2.3	< 2.3	ND ^e	ND ^e	~ -2.1 ^f

^a $\log K_i^a$ of a base (e.g. **9**) = pK_i of its conjugate acid (e. g. **8**) (Scheme 4).

^b '+' indicates soluble; '-' indicates insoluble;

^c pK_1 is for the dissociation of the ammonium moiety of the PZs (e.g. **8**) (Scheme 4).

^d pK_2 is for the dissociation of the protonated i.e. conjugate acid of the PZs (e.g. **10**) (Scheme 4).

^e Not determined as a result of their insolubility.

^f Not determined; the literature value for a SO_3H dissociation is given.

3.4 Conclusions

We have synthesized for the first time an interesting class of pH-responsive phosphonate/ SO_2 copolymers (containing a single carbon spacer between the charges) by cyclopolymerization process. The pH-triggerable amine and phosphonate functionalities permitted us to change the charge type on the polymer backbone to cationic, anionic, zwitterionic-anionic and zwitterionic under the influence of pH. The study demonstrated an interesting correlation between the basicity constant of the amine nitrogens and the viscosity values. While polyzwitterion-acid **3** was insoluble in salt-free water, the corresponding polyzwitterion-ester **8** was soluble as a result of the steric crowding that prevented it from manifesting effective Coulombic interactions. The polymer was found

to be soluble in the presence of Ca^{2+} ions thereby it may find potential application in inhibiting CaCO_3 scaling. The construction of PEG-DAPE **6**- H_2O ATPS could be useful in the area of affinity partitioning of metal ions. Note that the DAPE **6** at lower pH values can be converted into water-insoluble PZA **3**, and thus removed from the system and recycled.

CHAPTER 4: Aqueous two-phase systems of pH-responsive diallylammoniomethanephosphonate-*alt*-sulfur dioxide cyclopolymer with polyethylene glycol

Taken from **Othman Charles S. Al-Hamouz**, Shaikh A. Ali, Aqueous two-phase systems of pH-responsive polydiallylammoniomethanephosphonate-*alt*-sulfur dioxide cyclopolymer with polyethylene glycol, *Journal of Chemical Engineering and Data*, Minor revision.

Abstract

Aqueous two phase systems (ATPSs) composed of polyethylene glycol (PEG) and a pH-responsive dianionic polyelectrolytes (DAPE) having aminomethylphosphonate motifs have been investigated. The effects of HCl and salt (sodium chloride) on the binodal of the phase diagrams have been examined. With the increase in the concentration of sodium chloride, the binodals shifted downwards, thus requiring lower amount of polymers needed to form the ATPSs. The presence of trivalent nitrogen and negative oxygens in each repeat unit of the DAPE permitted the change of the charge types and their densities in the polymer chain, whose conformations can thus be fine-tuned for potential separation and purification of biomaterials in ATPSs. The phase separation happened at relatively low total polymer concentrations (below than 10%) which could be useful from the industrial point of view. The solubility behavior of the DAPE makes it a suitable component for the construction of recycling ATPSs since the polymer can be effectively removed at a lower pH by its conversion to a water-insoluble polyzwitterion (PZ) and thus recycled.

KEY WORDS: Aqueous two-phase system; pH-responsive polymer; Polyethylene glycol; phase diagram; polyaminophosphonate

4.1 Introduction

Aqueous two-phase systems (ATPSs) comprising two water-soluble polymers in the presence or absence of inorganic salt are of tremendous industrial importance^[95-99]. The high water content and low interfacial tension in ATPSs provide a benign and compatible environment for efficient purification as well as selective separation of a variety of industrially important labile biomolecules such as proteins^[100-103]. The added advantage of such inexpensive liquid-liquid extraction systems is that they can be readily scaled-up. The separation technique is also becoming increasingly important in non-biotechnology areas such as industrial waste remediation: Notable examples include the utilization of ATPSs in the removal of color from textile plant wastes^[104], and metal ions^[105] and organic pollutants from the environment^[106]. ATPSs based on poly(ethylene glycol) (PEG) and dextran are the most commonly used polymers in separation process^[70, 107-109]. However, purified dextran is quite expensive and biodegradable^[110]. There have been efforts to develop environment-friendly novel green ATPSs based on ionic liquids^[111, 112].

The ATPSs based on hydrophobically modified acrylamide/styrene copolymer-PEG^[113] and poly(diallylammonioethanoate-*alt*-sulfur dioxide)-PEG^[85, 86] have been successfully examined in the study of protein partitioning. Recently the coexistence curves for a variety of ATPSs involving pH-responsive hydrophobically modified ionic

cyclocopolymers of diallylammonioethanoate/sulphur and urethanized polyvinyl alcohol (UPVA) have been reported ^[114].

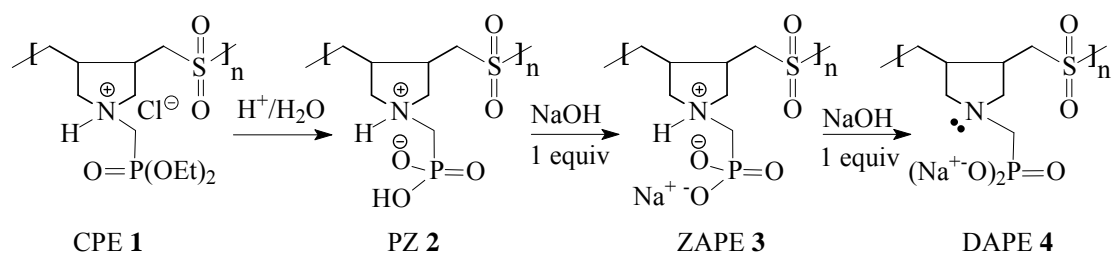
Ionic polymers including PZs and polyampholytes have the potential to be effective components in the construction of ATPSs. The ATPSs involving PZs, which seem to mimic biomolecules like proteins, is expected to impart greater influence in bioseparation involving monomeric amino acids or proteins. With this in mind, herein we report, the effect of pH and salt concentration on the phase diagram data of new ATPSs involving pH-responsive dianionic polyelectrolytes (DAPE) **4** and PEG. The charge types and their densities on the polymer chains of the DAPE can be controlled by allowing it to equilibrate with the polyzwitterions (PZ) **2** and zwitterionic/anionic polyelectrolyte (ZAPE) **3** under the influence of added HCl. Note that ZAPE **3** has an interesting blend of zwitterionic and anionic motifs in the same repeating unit. The solubility behaviors of the polymers dictate that DAPE **4** could be a promising component for the construction of recycling ATPS since the pH-responsive polymer can be precipitated at a lower pH value by its conversion to water-insoluble PZ **2**.

4.2 Experimental

4.2.1 Materials

The synthesis of the pH- responsive polymer DAPE **4** *via* CPE **1** have been carried out as described elsewhere (Scheme 1) ^[115]. The intrinsic viscosity $[\eta]$ of CPE **1** is determined to be 0.531 dL g⁻¹ in 0.1 N NaCl at 30°C. Molecular weight (\overline{M}_w) of a sample of CPE **1** with an $[\eta]$ value of 0.542 dL g⁻¹ has been reported to be 105,000 (PDI: 2.03) determined by the GPC measurement using polyethylene oxide/glycol as a standard and water as eluent. Since CPE **1**, prepared for the current work, has a similar intrinsic

value, its (\overline{M}_w) is also expected to be around $\sim 100,000 \text{ g mol}^{-1}$. The repeating units of CPE **1** and DAPE **4** have molar masses of 347.79 and $299.19 \text{ g mol}^{-1}$, respectively; thus the (\overline{M}_w) and \overline{M}_n for the DAPE **4** is calculated to be $86,000$ and $42,400 \text{ g mol}^{-1}$, respectively for a PDI of 2.03 . The reduced and intrinsic viscosities of ZAPE **3** and DAPE **4** in the presence of HCl in different salt concentrations are mentioned in Table 4.1. Polyethylene glycol (PEG) of number average molecular weight (\overline{M}_n) of 35000 was purchased from MERCK-Schuchardt. All solvents used were of analytical grade.



Scheme 1.

Table 4.01. Viscosity of ZAPE 3 and DAPE 4.

Polymer	Reduced viscosity ^a (η_{sp}/C) dL g ⁻¹	Intrinsic viscosity [η] ^b dL g ⁻¹		
		0.1 N NaCl	0.25 N NaCl	0.4 N NaCl
DAPE 4	0.401	0.331	0.291	0.256
DAPE + 0.5 equiv HCl	0.259	–	–	–
DAPE + 1 equiv HCl	0.120	–	–	–
DAPE + 1.2 equiv HCl	0.0630	–	–	–
DAPE + 1.4 equiv HCl	Precipitate	–	–	–
ZAPE 3	–	0.112	0.0989	0.0847

^aViscosity of 1% (i.e. 1 dL g⁻¹) polymer solution in salt-free and 0.1 N NaCl at 30 °C was measured with a Ubbelohde Viscometer (K=0.005718).

^bViscosity of 1-0.125 % polymer solution in salt-free and 0.1 N NaCl at 30 °C was measured with a Ubbelohde Viscometer (K=0.005718). ^bViscosity of 1-0.125 % polymer solution in salt-free and 0.1 N NaCl at 30 °C was measured with a Ubbelohde Viscometer (K=0.005718).

4.2.2 Phase compositions and phase diagram of PEG –DAPE systems

4.2.2.1 The NMR Method

The stock solutions of DAPE 4 (10-20 %w/w) and PEG (20 %w/w) were prepared in salt-free water. Several total-systems (~7 cm³) of known compositions (A_{total}) as described in Tables 4.2-4.8 were made. The equivalent amount of NaCl, generated in the presence of HCl, is taken into account in the determination of the final salt (NaCl) concentration. The mixtures were shaken thoroughly and centrifuged for a period of 10-20 min to ensure a complete phase separation. After equilibration at 23°C for 24 h, the volume and the density of the top layers (~1.03 g/cm³) and bottom layers (~1.06 g/cm³) were measured. The ¹H NMR spectra of both layers were measured after exchanging H₂O

by D₂O (Figure 4.1). The top and bottom layers were found to be overwhelmingly rich in PEG and DAPE, respectively. The ¹H NMR spectra of (a) DAPE **4**, (b) sample from the bottom phase of **system 2** of Fig. 4.2c (Table 4.4) (*vide infra*), and (c) sample from top phase of **system 3** of Fig. 4.2c (Table 4) (*vide infra*), are displayed in Fig. 4.1.

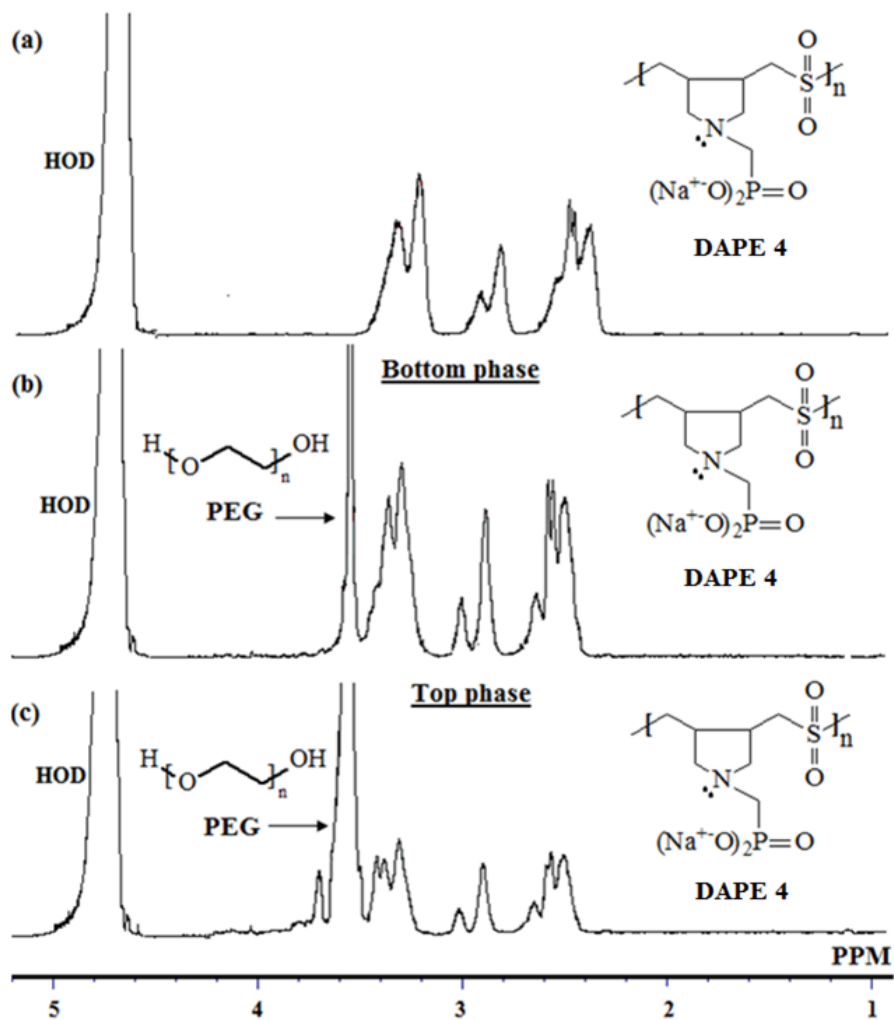


Figure 4.1. ¹H NMR spectra of (a) DAPE **4**. (b) Bottom phase, system 2: (DAPE **4**, PEG, 0.4N NaCl, 0.0 equiv. HCl). (c) Top Phase, system 3: (DAPE **4**, PEG, 0.4N NaCl, 0.0 equiv. HCl).

The ^1H NMR signals for the twelve protons of DAPE **4** appeared in the ranges δ 2.45 - 3.05 and 3.10-3.60 ppm while the partially overlapping four-proton singlet at δ 3.6 were attributed to the PEG (Fig. 4.1b & 4.1c). Careful integration of the signals in the ranges 2.25 - 3.05 and 3.10-3.60 ppm revealed their respective areas in a 1.23:1.00 ratio (Fig. 4.1a). Note that the signals in the range 2.45 - 3.05 is free of any overlapping signal and its area (A) is used to calculate the area (B) under 3.10-3.60 attributed to DAPE **4** as $A \times (1.00/1.23)$. The area (C) under four-proton overlapping singlet at δ 3.6 for the PEG was calculated as $[D - A \times (1.00/1.23)]$ where D is the total area in the range δ 3.10-3.60 ppm belonging to the PEG as well as a part of DAPE **4**. So, the area for a single H for DAPE **4** and PEG becomes $[A + B]/12$ and $C/4$, respectively. The mole ratio of PEG/DAPE **4** (i.e. the ratio of area of single H of PEG and DAPE) thus becomes:

$$\frac{\text{mol PEG}}{\text{mol DAPE}} = \frac{\text{Area of 1H of PEG}}{\text{Area for 1H of DAPE}} = \frac{C/4}{[A + B]/12} \quad (1)$$

^1H NMR measurements allowed us to determine the mole ratios. The tie lines were constructed using the systems in Tables 4.2-4.8. Weight percent of each polymer is determined by using the Equations 2 and 3 as described in our earlier work^[26, 91].

$$[DAPE]_b = \frac{PEG_0 / 44.03 - (DAPE_0 / MW_{DAPE}) ([PEG]/[DAPE])_t}{V_b \{ ([PEG]/[DAPE])_b - ([PEG]/[DAPE])_t \}} \quad (2)$$

Where, subscript t and b represent top and bottom phase, respectively. $[DAPE]$ and $[PEG]$ represent concentration of the repeating units in mmol of repeat unit cm^{-3} . $DAPE_0$ and PEG_0 represent total mass in mg of the polymers and V represents the volume in cm^3 . Molar masses of the repeat units of the DAPE and PEG were taken as 299.19 and 44.05,

respectively. [PEG]/[DAPE] represents molar ratio of the polymers as determined by ^1H NMR integration. The mass of polymer DAPE in the bottom phase is then calculated using:

$$\text{DAPE}_b = [\text{DAPE}_b]V_b \times 299.19 \text{ mg} \quad (3)$$

Once one of the polymer concentrations is known in a phase, then the rest of the concentrations and weight percents of the polymers in the two phases are easily calculated from the known volume, density and mass of the two phases.

4.2.2.2 Binodals by turbidity method

The turbidity method: The turbidity experiments were carried out at 23°C as described elsewhere ^[26, 91]. Thus about 1.5 g of a stirred solution (~10-15 %w/w) of DAPE **4** in x N NaCl ($x = 0, 0.1$ or 0.4 N) was titrated with a known weight of a concentrated solution (~20 %w/w) of the PEG in x N NaCl until the transparent system turned turbid. Then a known weight of an x N NaCl solution was added until the system became transparent again. At this point, the composition of the two polymers corresponds to a point on the binodal curve. The process was repeated to obtain more points using more PEG to make the mixture turbid followed by addition of x N NaCl to make it transparent. In order to obtain points on the other end of the binodal, the concentrated solution of the PEG was titrated with the DAPE **4** solution using same way as described above.

Table 4.2 Phase Composition of the PEG – DAPE 4 System at 23°C, (0.0 equiv. HCl, 0.1N NaCl) shown in figure 4.2a.

NMR method							
System	Total system		Top phase		Bottom phase		Volume ratio ^a
	PEG	DAPE	PEG	DAPE	PEG	DAPE	
	%w/w	%w/w	%w/w	%w/w	%w/w	%w/w	
1	5.46	5.98	13.89	0.65	0.65	9.15	0.65
2	5.19	5.12	12.53	1.02	0.79	7.71	0.88
3	4.90	4.60	10.50	1.40	1.20	6.80	0.95
4	4.41	4.25	8.53	2.04	2.26	5.48	0.57

Turbidity method					
System	Binodal data		System	Binodal data	
	PEG	DAPE		PEG	APE
	%w/w	%w/w		%w/w	%w/w
a	13.29	0.65	e	3.70	3.44
b	8.05	1.83	f	3.10	3.80
c	5.70	2.40	g	2.60	4.30
d	4.50	2.92	h	2.01	5.01

^aVolume ratio of top and bottom phase

Table 4.3 Phase Composition of the PEG – DAPE 4 System at 23°C, (0.0 equiv. HCl, 0.25N NaCl) shown in figure 4.2b.

NMR method							
System	Total system		Top phase		Bottom phase		Volume ratio ^a
	PEG	APE	PEG	APE	PEG	APE	
	%w/w	%w/w	%w/w	%w/w	%w/w	%w/w	
1	7.72	4.51	14.2	0.33	0.47	9.37	1.17
2	4.71	5.21	12.7	0.45	0.79	7.71	0.51
3	4.32	4.31	10.5	0.61	0.97	6.32	0.54
4	3.98	3.75	8.52	0.96	1.23	5.48	0.6

Turbidity method					
System	Binodal data		System	Binodal data	
	PEG	DAPE		PEG	APE
	%w/w	%w/w		%w/w	%w/w
a	10.1	0.464	f	3.31	2.37
b	8.14	0.765	g	2.73	2.77
c	6.52	1.15	h	2.11	3.45
d	5.13	1.56	i	1.56	4.15
e	4.11	2.06	j	1.41	4.53

^aVolume ratio of top and bottom phase

Table 4.4. Phase Composition of the PEG – DAPE 4 System at 23°C, (0.0 equiv. HCl, 0.4N NaCl) shown in Figure 4.2c.

NMR method

System	Total system		Top phase		Bottom phase		Volume ratio ^a
	PEG	DAPE	PEG	DAPE	PEG	DAPE	
	%w/w	%w/w	%w/w	%w/w	%w/w	%w/w	
1	3.50	4.50	6.50	0.30	0.45	8.70	0.97
2	3.18	4.10	5.94	0.36	0.51	7.68	0.98
3	2.85	3.77	5.10	0.63	0.59	6.75	0.99
4	2.95	2.69	4.03	1.18	0.69	5.71	2.06

Turbidity method

System	Binodal data		System	Binodal data	
	PEG	DAPE		PEG	APE
	%w/w	%w/w		%w/w	%w/w
a	7.02	0.29	f	2.26	2.01
b	5.25	0.50	g	1.57	2.58
c	4.50	0.74	h	0.99	3.19
d	3.77	1.11	I	4.00	0.51
e	3.08	1.45			

^aVolume ratio of top and bottom phase

Table 4.5. Phase Composition of the PEG – DAPE 4 system at 23°C,(0.5 equiv. HCl, 0.25NaCl) shown in figure 4.3a.

NMR method

System	Total system		Top phase		Bottom phase		Volume ratio ^a
	PEG	DAPE	PEG	DAPE	PEG	DAPE	
	%w/w	%w/w	%w/w	%w/w	%w/w	%w/w	
1	5.47	9.00	14.97	0.23	0.19	14.00	0.58
2	5.10	7.80	13.00	0.30	0.34	12.22	0.57
3	4.89	6.60	11.3	0.34	0.45	11.1	0.71
4	3.68	6.15	9.00	0.82	0.55	8.93	0.53

Turbidity method

System	Binodal data		System	Binodal data	
	PEG	DAPE		PEG	APE
	%w/w	%w/w		%w/w	%w/w
a	1.20	5.03	f	4.23	1.55
b	1.65	4.06	g	5.30	1.23
c	2.47	3.02			
d	3.08	2.36			
e	3.48	2.01			

^aVolume ratio of top and bottom phase

Table 4.06. Phase Composition of the PEG – DAPE 4 system at 23°C (1 equiv. HCl, 0.25 N NaCl) shown in figure 4.3b.

NMR method

System	Total system		Top phase		Bottom phase		Volume ratio ^a
	PEG	DAPE	PEG	DAPE	PEG	DAPE	
	%w/w	%w/w	%w/w	%w/w	%w/w	%w/w	
1	3.80	5.90	6.12	1.02	0.53	13.00	1.48
2	3.60	5.20	5.40	1.20	0.73	11.50	1.60
3	2.61	6.62	5.02	0.98	0.81	10.86	0.74
4	2.80	5.93	4.74	1.58	1.05	10.37	1.00

Turbidity method

System	Binodal data		System	Binodal data	
	PEG	DAPE		PEG	APE
	%w/w	%w/w		%w/w	%w/w
a	1.67	6.54	f	3.35	3.02
b	2.03	5.50	g	3.71	2.55
c	2.21	4.90	h	4.00	2.24
d	2.70	4.00	I	4.20	1.94
e	3.10	3.50	J	4.50	1.69

^aVolume ratio of top and bottom phase

Table 4.7. Phase Composition of the PEG – DAPE 4 system at 23°C (0.5 equiv. HCl, 0.4N NaCl) shown in figure 4.3c.

NMR method							
System	Total system		Top phase		Bottom phase		Volume ratio ^a
	PEG	DAPE	PEG	DAPE	PEG	DAPE	
	%w/w	%w/w	%w/w	%w/w	%w/w	%w/w	
1	3.90	5.70	8.30	0.15	0.05	10.7	0.91
2	3.295	5.31	7.45	0.36	0.10	9.57	0.85
3	2.57	4.06	5.14	0.85	0.40	6.78	0.86
4	3.17	3.26	5.04	0.96	0.40	6.74	1.50

Turbidity method					
System	Binodal data		System	Binodal data	
	PEG	DAPE		PEG	APE
	%w/w	%w/w		%w/w	%w/w
a	0.53	4.70	e	2.80	1.60
b	0.80	3.70	f	3.40	1.35
c	1.15	3.01	g	4.20	1.01
d	1.77	2.30			

^aVolume ratio of top and bottom phase

Table 4.8. Phase Composition of the PEG – DAPE 4 system at 23°C, (1 equiv. HCl, 0.4N NaCl) shown in figure 4.3d.

NMR method							
System	Total system		Top phase		Bottom phase		Volume ratio ^a
	PEG	DAPE	PEG	DAPE	PEG	DAPE	
	%w/w	%w/w	%w/w	%w/w	%w/w	%w/w	
1	4.24	7.42	8.64	0.36	0.12	14.58	1.00
2	3.67	5.93	6.49	0.497	0.20	12.58	1.17
3	2.90	5.50	5.20	0.76	0.47	10.4	1.02
4	2.63	4.74	4.20	1.57	0.88	8.78	1.24

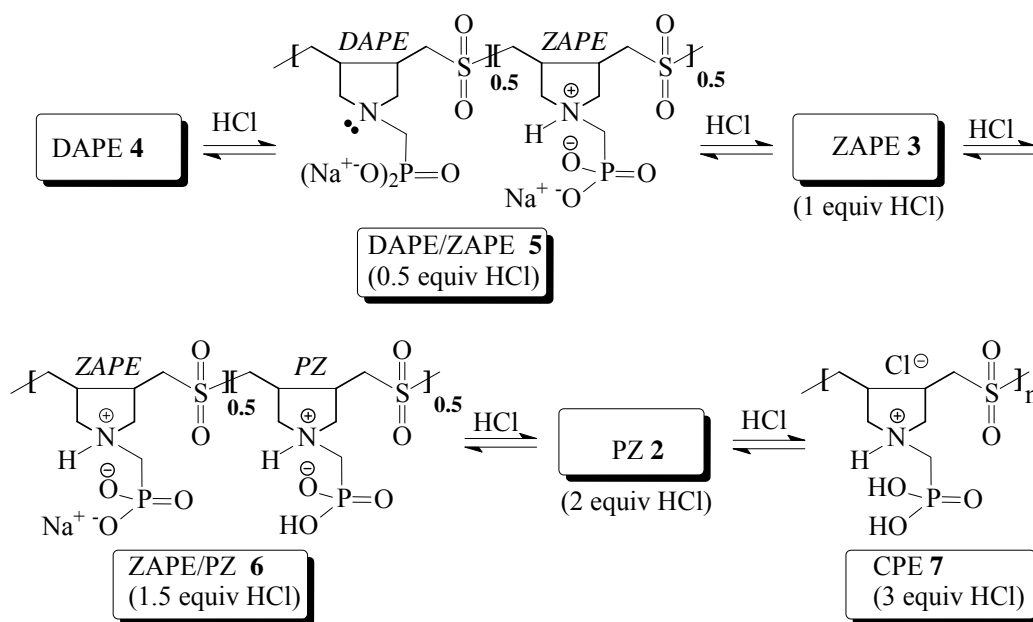
Turbidity method					
System	Binodal data		System	Binodal data	
	PEG	DAPE		PEG	APE
	%w/w	%w/w		%w/w	%w/w
a	1.20	5.90	f	2.88	2.13
b	1.45	5.10	g	3.33	1.53
c	1.67	4.40	h	3.47	1.29
d	2.11	3.50	I	4.00	0.87
e	2.50	2.76			

^aVolume ratio of top and bottom phase

4.3 Results and Discussion

4.3.1 Solution properties

Before the construction of an ATPS using DAPE **4** as a component, it seems prudent to examine the solubility and viscosity behaviors of the polymer. DAPE **4** is a pH-responsive polyelectrolyte owing to the presence of the two negative oxygens and a nitrogen having unquenched valency that permits several equilibrations involving DAPE/ZAPE **5**, ZAPE **3**, ZAPE/PZ **6**, PZ **2**, and CPE **7** (Scheme 2).



Scheme 2.

The dominance of a particular form would depend on the pH of the medium. Note that the The type of charges and their densities on the polymer backbone can be controlled by addition of NaOH or HCl. In the presence of 0, 0.5, 1, 2, and 3 equivalents of HCl, the dominant form in the equilibrations is expected to be DAPE **4**, DAPE/ZAPE **5**, ZAPE **3**, PZ **2**, and CPE **7**, respectively (Scheme 2). Note that all the forms are soluble in salt-free water except PZ **2**, in which the zwitterionic interactions are so strong that it

requires a critical salt concentration (CSC) of 4.73 M NaCl to disrupt the intra- and interchain attractive interactions and permit its water solubility. DAPE **4** upon addition of 1.2 equiv HCl gives water-soluble **6** with a ZAPE/PZ ratio of 80:20, while the form of **6** with a ZAPE/PZ ratio of 60:40, obtained after addition of 1.4 equiv of HCl, becomes water-insoluble as a result of increasing proportion of zwitterionic fraction (Table 4.1). One of the important advantage of having DAPE as a component in an ATPS is that it can be used as a water-soluble polymer in the form of **4**, **3** above a certain minimum pH and below which it can be recycled by precipitating out in the form of water-insoluble PZ **2**. The solubility behavior (as presented above) and its relationship with the hydrodynamic volume of a polymer chain can be rationalized using eq 4. The screening of the attractive polyampholytic interactions between opposite charges and repulsive Coulombic interactions between similar charges can be described mathematically^[116-119] by the first and second term of eq 4, respectively:

$$v^* = - \frac{\pi(fI_B)^2}{\kappa_S} + \frac{4\pi I_B \Delta f^2}{\kappa_S^2} \quad (4)$$

where v^* is the electrostatic excluded volume, I_B is the Bjerrum length, f is the total fraction of charged monomers, Δf is the charge imbalance, and κ_S is the Debye-Huckel screening parameter. The solution behavior of ionic polymers with or without charge symmetry is then described by v^* : a negative and a positive excluded volume implies contraction and expansion of a polymer chain, respectively. For a electroneutral (\pm)PZ **2**, the solution behavior is described by the screening of the attractive polyampholytic interactions since the second term of eq. 4 becomes zero as a result of $\Delta f = 0$. The negative v^* electrostatic excluded volume indicates contraction to a collapsed polymer

chain. The electroneutrality of (\pm) PZ **2** cannot be maintained in the presence of added salt NaCl; it acquires an overall anionic charge since the cationic nitrogens are more effectively screened by Cl^- ions, than the anionic PO_3^- by the Na^+ [8]. As a result, the presence of NaCl makes v^* value a less negative thus helping the polymer coil to expand thereby resulting in increased solubility of the polymer.

As the DAPE **4** travels through DAPE/ZAPE **5**, ZAPE **3**, ZAPE/PZ **6** to electroneutral PZ **2**, the charge imbalance Δf decreases progressively. The decreasing importance of the second term in eq 4 with decreasing Δf thus leads to the contraction of polymer coil. This correlates well with the viscosity data: DAPE **4** has higher viscosity than ZAPE **3** whereas the PZ **2** becomes water-insoluble as a result of its being in a collapsed chain conformation (Table 4.1). The viscosity values were found to be decreasing with the increase in NaCl concentration, indicating that Δf decreases and the repulsive contribution by the second term decreases thereby leading to the contraction of the polymer chain. The negative oxygens in DAPE **4** and in the anionic fraction of ZAPE **3** are screened by the Na^+ ions from the added NaCl and as a result the charge imbalance Δf is minimized.

4.3.2 Effect of NaCl and HCl on the binodal of DAPE 4-PEG ATPS

The phase diagrams of DAPE **4**-PEG- H_2O systems are shown in Figs 4.2 and 4.3. In the phase diagrams, the %w/w of the polymer rich in the top and bottom phase is assigned the y- and x-axis, respectively. The PEG and DAPE preferred to stay at the top and bottom phase, respectively. The tie lines in the phase diagrams for each total system of composition A_{total} were constructed by ^1H NMR method which is used to determine the compositions A_{top} and A_{bottom} of the polymers in equilibrium in the top and bottom

phases, respectively. The tie lines are helpful in the construction of APTS with suitable volume ratio of the top and bottom phases as determined by the ratio of the tie line lengths of $A_{total}-A_{bot}$ and $A_{total}-A_{top}$. The binodal curves were obtained by the turbidity method. The experimental data are shown in Tables 4.2-4.8.

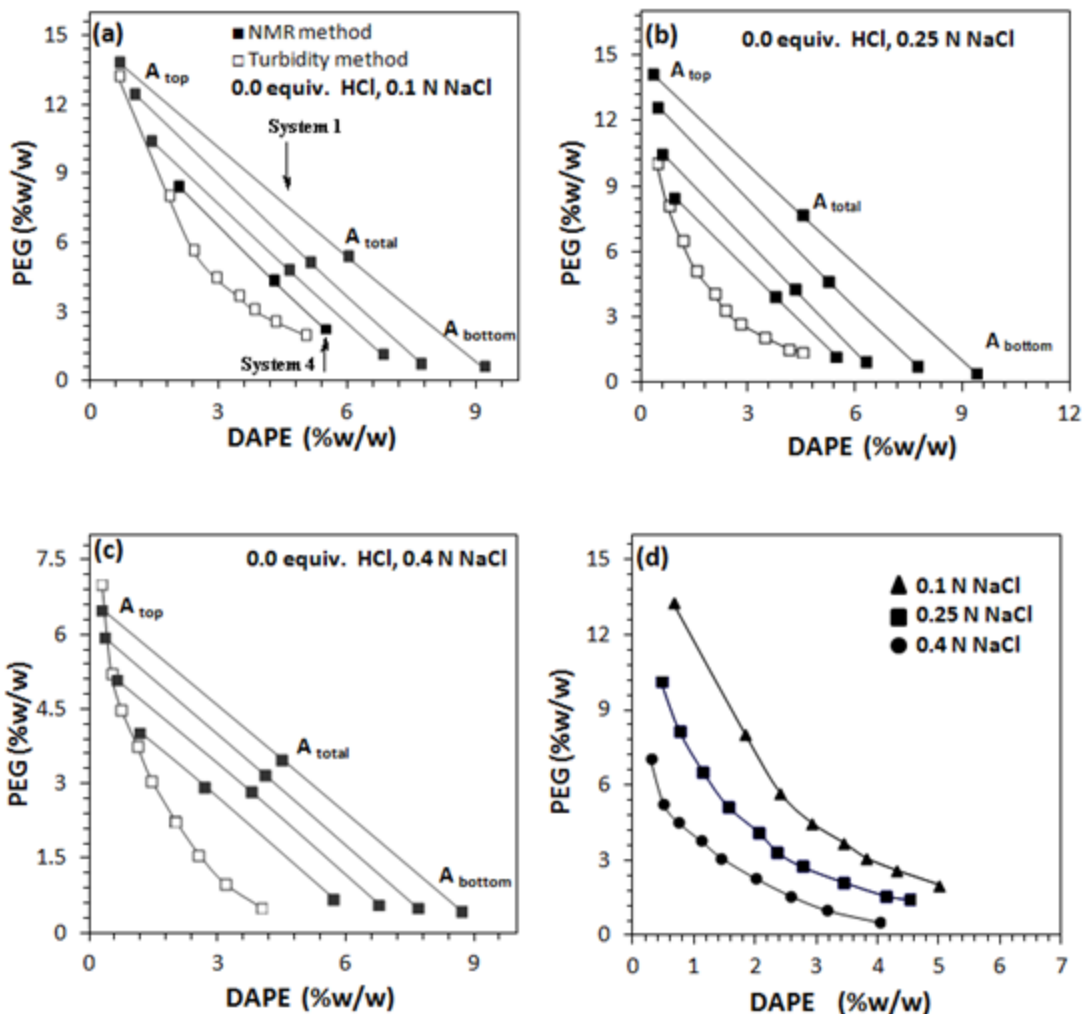


Figure 4.2. Phase diagram of PEG-DAPE 4-H₂O in the presence of (a) 0.0 equiv. HCl, 0.1 N NaCl; (b) 0.0 equiv. HCl, 0.25 N NaCl; (c) 0.0 equiv. HCl, 0.4 N NaCl; (d) The effect of salt concentration on the binodal curve of PEG-DAPE 4-H₂O system.

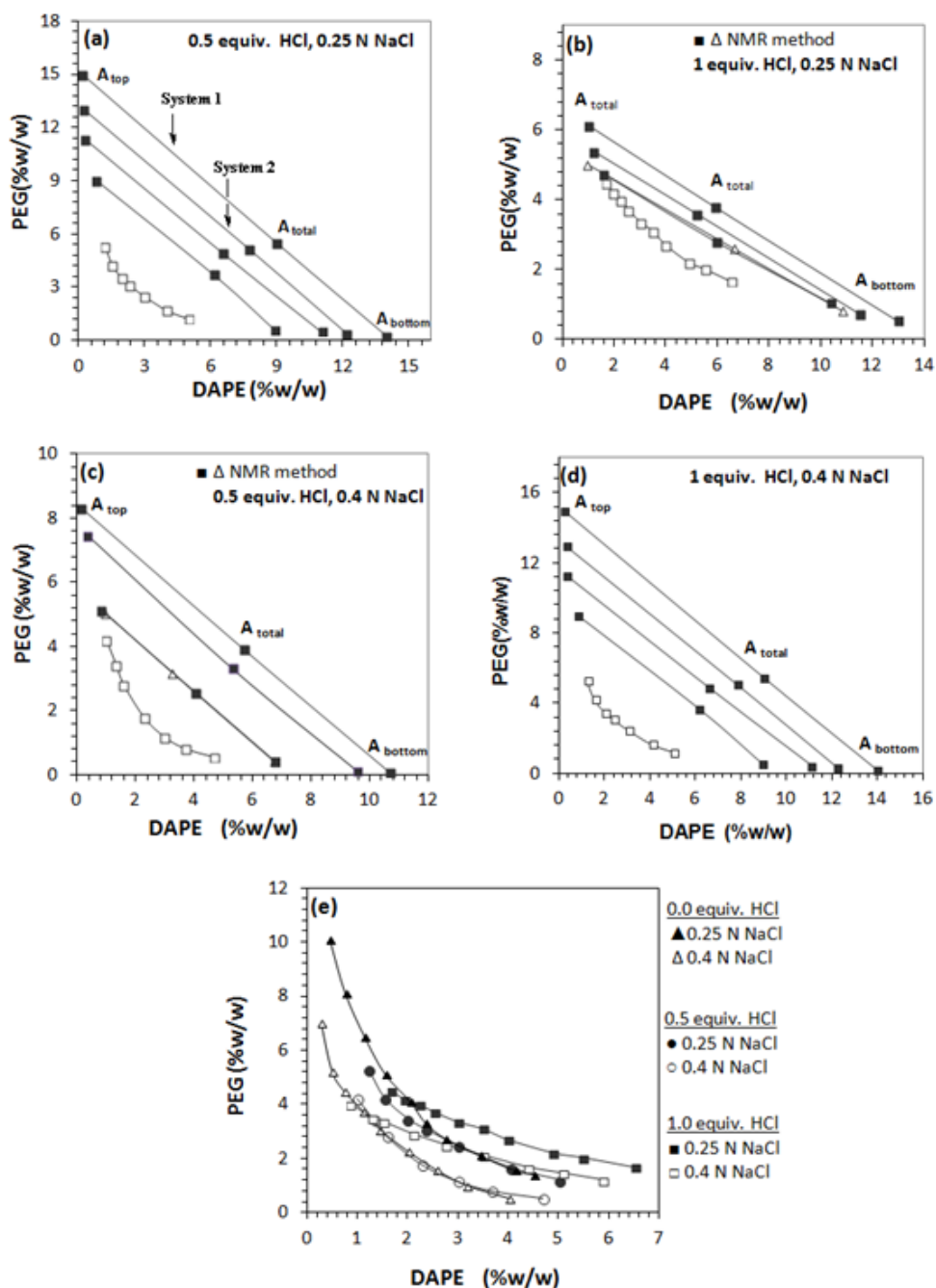


Figure 4.3. Phase diagram of PEG-DAPE 4-H₂O in the presence of (a) 0.5 equiv. HCl, 0.25 N NaCl; (b) 1.0 equiv. HCl, 0.25 N NaCl; (c) 0.5 equiv. HCl, 0.4 N NaCl; (d) 1.0 equiv. HCl, 0.4N NaCl.(e) Effect of HCl and NaCl concentration on the binodal curves of DAPE 4/ PEG/H₂O ATPSs.

The binodals ascertain the segregative phase separation behavior of the polymers, and their symmetrical shape imply that the two polymers may have very similar

hydrodynamic volumes [64, 95]. The phase formation happening at total polymer concentrations of below 10 %w/w, could be useful from an industrial point of view. The effect of salt concentration on the binodals is shown in Fig. 4.2d. The binodal curves are shifted downward with the increase in concentration of NaCl. The increase in the salt concentration leads to a decrease in electrostatic repulsion between the poly-electrolyte chains^[82, 120-122] leading to a compact coiled structure (Fig. 4.4.) For DAPE **4**, addition of salt is thus expected to decrease the hydrodynamic volume of the polymer chain, which in turn makes it less compatible with the PEG thereby requiring lesser amounts of polymers for phase separation to occur. Changing the NaCl concentration from 0.1 N to 0.4 N, leads to a greater contraction of polymer chain of DAPE **4** as evidenced by the reduced $[\eta]$ (Table 4.1). As a result of the greater mismatch of size with the PEG, the polymers become the least compatible in 0.4 N NaCl.

The effects of NaCl concentration and the types of backbone charges (depending on the amount of added HCl) on the binodal curves are displayed in Fig. 4.3e. The binodal curves are also shifted downward with the increase in concentration of NaCl from 0.25 N to 0.4 N in the presence of 0.5 or 1.0 equivalent of HCl (Fig. 4.3e). Note that the DAPE **4** (~100% negative charge) in the presence of 0.5 and 1 equivalent HCl becomes DAPE/ZAPE (=)/(± -) **5** and ZAPE (± -) **3** with a respective charge imbalance (Δf) of 0.60 and 0.33 in favor of the negative charges. The size of the polymer chain decreases with the decrease in Δf and leads to greater size-mismatch in the case of ZAPE **3** thereby making it the least compatible with the PEG. Since all three species (i.e. **3**, **4** and **5**) have excess negative charges in the polymer backbone, the addition of added salt (NaCl) has

thus demonstrated polyelectrolyte effect (Fig. 4.4) by decreasing the hydrodynamic volume of the polymers.

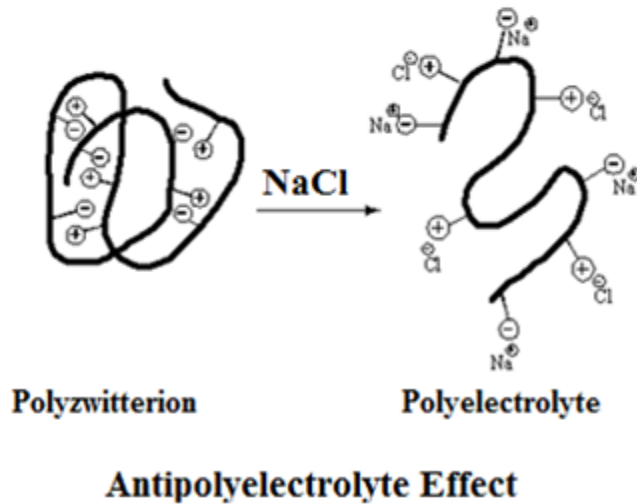
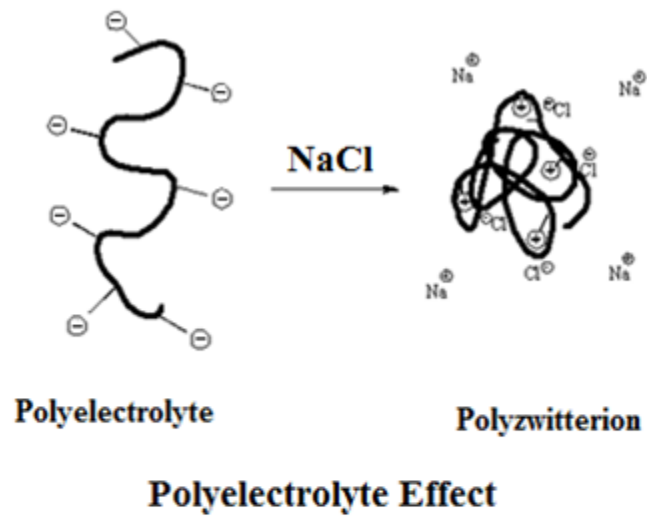


Figure 4.4. Effect of added salt on the conformation of polyelectrolytes and polyelectrolytes.

4.3.3 The Correlation of the Phase Diagrams Using the Method of Diamond and Hsu

The consistency of the tie-lines of the [DAPE 4-PEG-H₂O (NaCl)] systems was checked using the following correlation developed by Diamond & Hsu ^[123, 124] based on Flory- Huggins theory:

$$\ln K_1 = A_1(w_1'' - w_1') \quad (5)$$

And

$$\ln K_2 = A_2(w_2'' - w_2') \quad (6)$$

where w'' and w' are the polymer weight percent in the top and bottom phase, respectively, the slopes A_1 and A_2 are functions of the polymer molecular weight and the interactions between the polymers and water, K_1 and K_2 represent the partition coefficient (C_t/C_b) of the polymer between the top and bottom phase, and the subscripts 1 and 2 represent polymer 1 (DAPE 4) and polymer 2 (PEG). Straight line plots for the correlation results ascertain the satisfactory representation of the phase behaviour by this model (Figure 4.5).

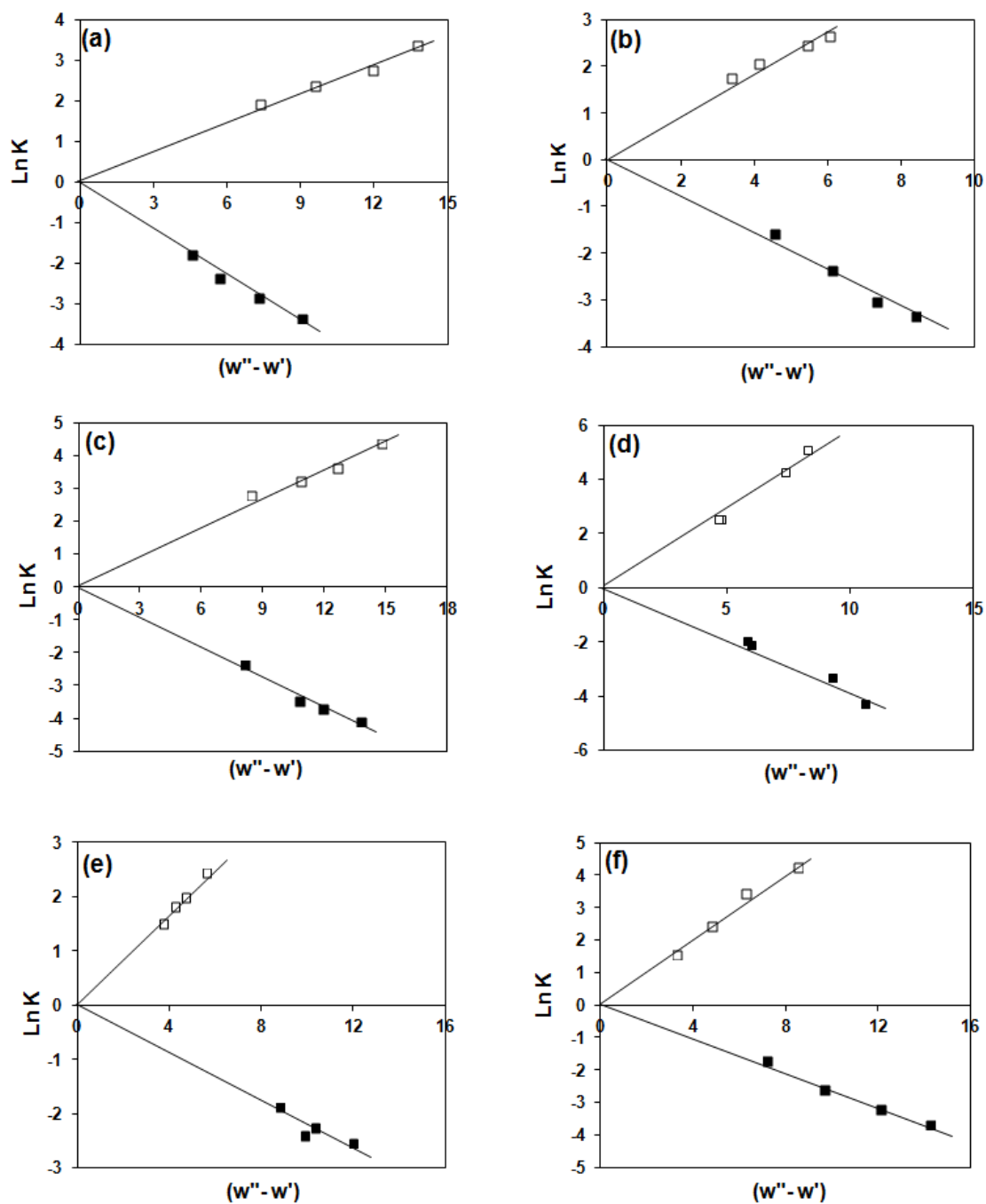


Figure 4.5. Correlation of the phase diagrams of DAPE 4- PEG-HCl systems using the method of Diamond and Hsu: using the tie line data of : (a) fig. 4.2b; (b) fig. 4.2c; (c) fig. 4.3a; (d) fig. 4.3c; (e) fig. 4.3b; (f) fig. 4.3d.

4.4 Conclusions

In this work a pH-responsive polyaminophosphonate DAPE **4** was used in the construction of aqueous two-phase systems with PEG. The effect of pH and salt on the binodal curves was investigated. The two polymers were found to form ATPS at low concentrations, where the addition of HCl changed the charge types and their densities on the polymer chains. The increasing concentration of NaCl shifted the binodals downward thereby requiring lesser concentration of the polymers to form ATPS. One of the most gratifying aspects of DAPE **4** is its almost zero solubility in water in the presence of HCl which transforms the polymer to PZ **2**. The solubility behavior thus makes it a suitable component for the construction of recycling ATPSs where the polymer can be effectively removed and recycled. The aminophosphonate residues in **3** and **4** mimic biomolecules like proteins, and as such the ATPSs may be used in their bioseparation. Variable charge densities in the polymer backbone may be exploited in selecting and separating certain proteins using the newly developed ATPSs. The constructed ATPSs may also be helpful for selective removal of toxic metal ions since the polymers having aminophosphonate motifs are known to have extraordinary chelating properties. We do believe that the Data presented in the article will add significant experimental knowledge in the construction of ATPS using ionic polymers.

CHAPTER 5: Synthesis and Cyclopolymerization of Diallylammoniomethanesulfonate

Taken from Shaikh. A. Ali, Othman Charles S. Al-Hamouz, Synthesis and Cyclopolymerization of Diallylammoniomethanesulfonate, *Polymer Engineering and Science*, In Press (2013).

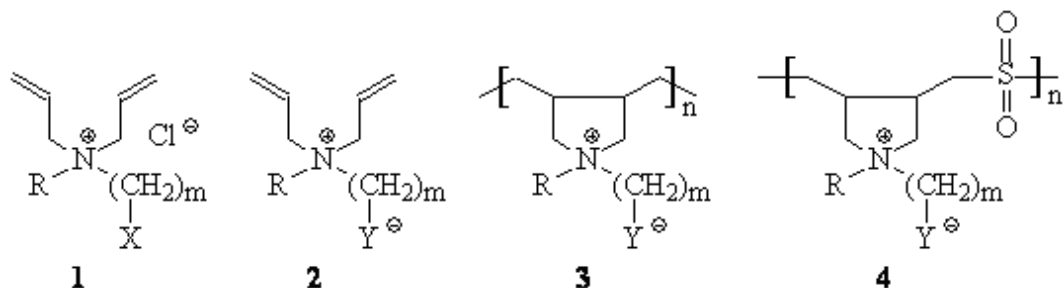
Abstract

N,N-diallylammoniomethanesulfonate, a new zwitterionic monomer having a sulfobetaine (SB) motif, has been synthesized by reacting diallylamine with formaldehyde and sodium bisulfite. While the monomer underwent cyclopolymerization to give the unstable polysulfobetaine (PSB) in low yields, copolymerization with sulfur dioxide gave the stable PSB/SO₂ copolymer in excellent yields. The polymers, as a consequence of having unquenched nitrogen valency in the repeating units, are pH-responsive. The PSB/SO₂ copolymer, upon treatment with sodium hydroxide, was converted into a water-soluble anionic polyelectrolyte (APE). The strong zwitterionic interactions inherent in the PSB/SO₂ made it insoluble in salt-free water; the presence of large concentration (>3 M) of low molecular weight salts (e.g., NaCl, KI etc.) was required to neutralize the intragroup zwitterionic interactions and promote dissolution. The PSB/SO₂ represents the first example of a sulfobetaine polymer having a single methylene spacer separating the charge centers. The stability of the copolymer is explained in terms of electron density on the nitrogens.

KEYWORDS: Polyelectrolyte; cyclopolymerization; polysulfobetaine; pH-responsive; polyzwitterions; salt effects.

5.1 Introduction

In addition to the synthesis of a variety of polyelectrolytes, Butler's cyclopolymerization^[2, 7, 20, 46, 125] involving diallylammonium salts has also been a convenient protocol to generate polyzwitterions (PZs)^[3, 4, 14, 35, 115, 126, 127] and polyampholytes (PAs)^[128] (Scheme 1).



Scheme 1.

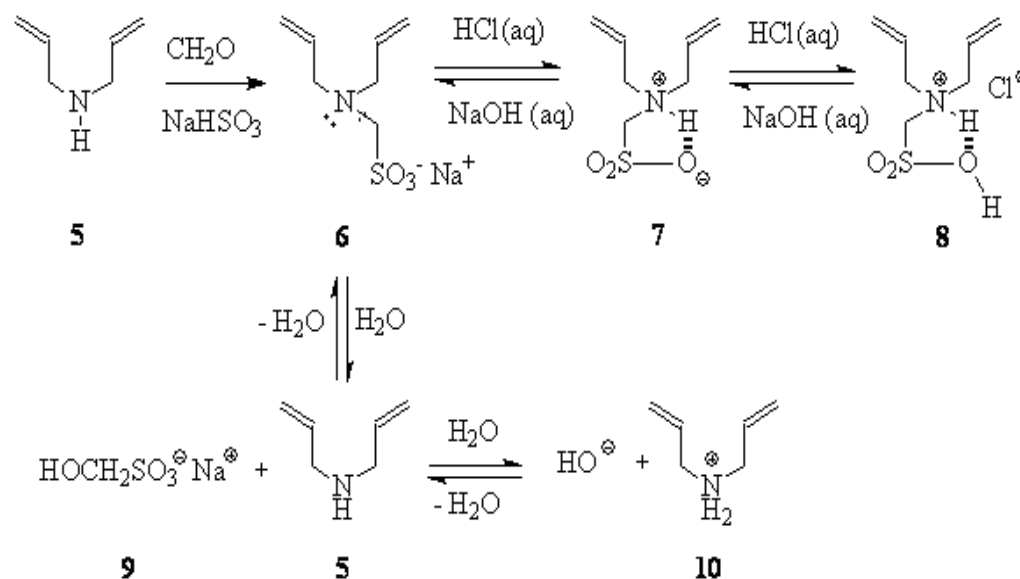
Cyclocopolymerization of diallylammonium salts with sulfur dioxide have also been reported to lead to the synthesis of alternate copolymers^[20, 25, 129]. While the PZs have charges of both algebraic signs on the same repeating unit, the PAs have the presence of cationic and anionic motifs on different repeating units in the same polymer chain with or without charge symmetry^[128]. The cyclopolymers having five-membered ring embedded into the polymer architecture represent the eighth most important structural feature for synthetic polymers^[128, 130, 131].

Butler's cyclopolymers are of tremendous scientific and technological interest; the cationic polyelectrolyte poly(diallyldimethylammonium chloride) alone accounts for over 1000 patents and publications^[20]. The PZs and PAs, whose structure and behavior seem to mimic biopolymers like proteins or DNA that mediate life processes, have offered many new applications in medicine, biotechnology, hydrometallurgy, and oil industry^[1].

^{10, 86]}. The permanent dipole of amphoteric PZs or PAs, unlike polyelectrolytes, can exhibit antipolyelectrolyte behavior i.e., enhancements of viscosity and solubility in the presence of added electrolytes (e.g., NaCl) owing to the neutralization of the ionically crosslinked network in a collapsed coil conformation ^[8, 9, 33, 81, 118, 132, 133]. The high dipole moment of PZs renders the properties of excellent polar host matrix in which only target ions can migrate^[134, 135]. The stoichiometric blends of some polyzwitterions with alkali metal salts have produced excellent matrices having high ionic conductivity ^[136]. The unique “antipolyelectrolyte” behavior makes PZs attractive candidates for application in enhanced oil recovery, drag reduction, personal care products, cosmetics, and pharmaceuticals^[137-139]. The PZs have been utilized for efficient separations of biomolecules^[87] and to develop procedures for DNA assay^[140]. They have also drawn attention in the field of ion exchange; their abilities to chelate toxic trace metal ions (Hg²⁺, Cd²⁺, Cu²⁺, and Ni²⁺) have been exploited in wastewater treatment^[46, 137].

For the synthesis of PZs **3** or the zwitterions/sulfur dioxide copolymer **4**, monomer may either be cationic (+) **1** or zwitterionic (\pm) **2**; the pendent substituent ‘X’ (e.g. CO₂R) in the former could then be converted into Y⁻ (e.g. CO₂⁻) so as to provide entry to polycarbo (Y⁻ = CO₂⁻) [33,34], phosphono (Y⁻ = P[OR][=O]O⁻) [35,36], and sulfobetaines (Y⁻ = SO₃⁻) [37,38] (Scheme 1). A polysulfobetaine (PSB) remains zwitterionic over a wide range of pH owing to the strong acid nature of the sulfonic acid [pK_a: (-) 2.1], while a polycarbobetaine (PCB) or polyphosphonobetaine (PPB), because of the weak acid nature of the carboxylic or phosphonic acid group, can be rendered cationic by lowering the pH of the aqueous medium^[87]. The pH-responsive PSBs and PCBs having unquenched valency of nitrogens can also be changed to polyanions having trivalent

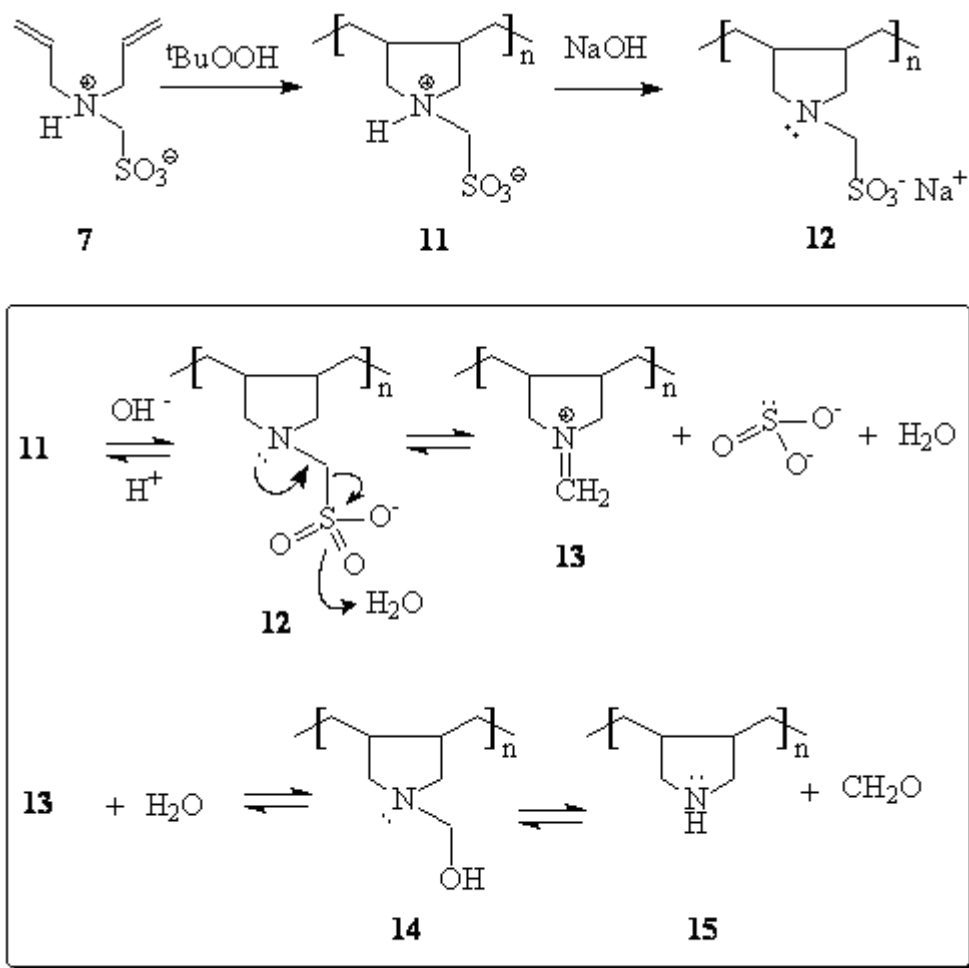
nitrogens by neutralization of the ammonio proton in **3** or **4** (R=H)^[14, 115, 126, 127]. The synthesis of copolyzwitterions incorporating 25 mol % carboxybetaine and 75 mol % sulfobetaine and its interesting pH-dependent solution properties have been reported^[141]. Nearly monodisperse PZs have been synthesized by group transfer polymerization (GTP) of 2-(dimethylamino)ethyl methacrylate (DMAEMA) followed by quantitative betainization using 1,3-propanesultone^[142].



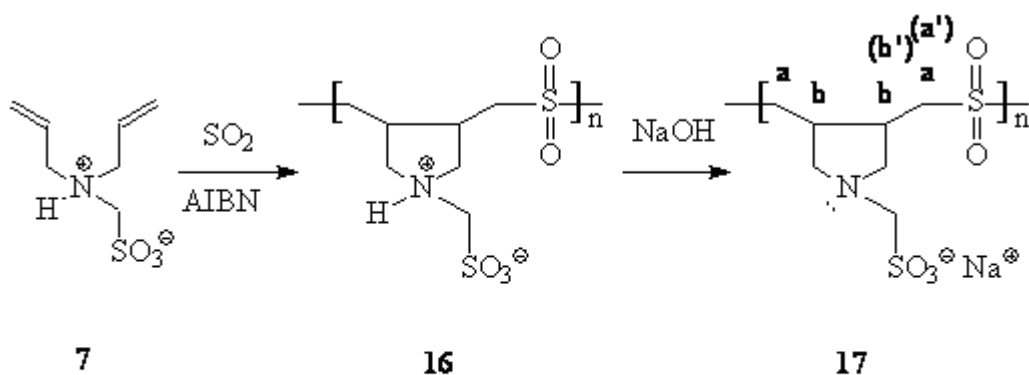
Scheme 2.

While the PZs having carboxylate and phosphonate moieties in the α -position with respect to the positive nitrogens as in **3** ($m=1$) are reported^[26, 141], the corresponding polysulfobetaine (PSB) (**3**, $m = 1$, $Y^- = \text{SO}_3^-$) is not known to date. Even outside the domain of cyclopolymers, the literature lacks, to our knowledge, any report that describes a PSB having a single methylene spacer separating the zwitterionic charges. We report herein the synthesis and cyclopolymerization of a new sulfobetaine (SB) monomer **7** (Scheme 2) having a single methylene spacer to produce homo-(**11**) (Scheme 3) and

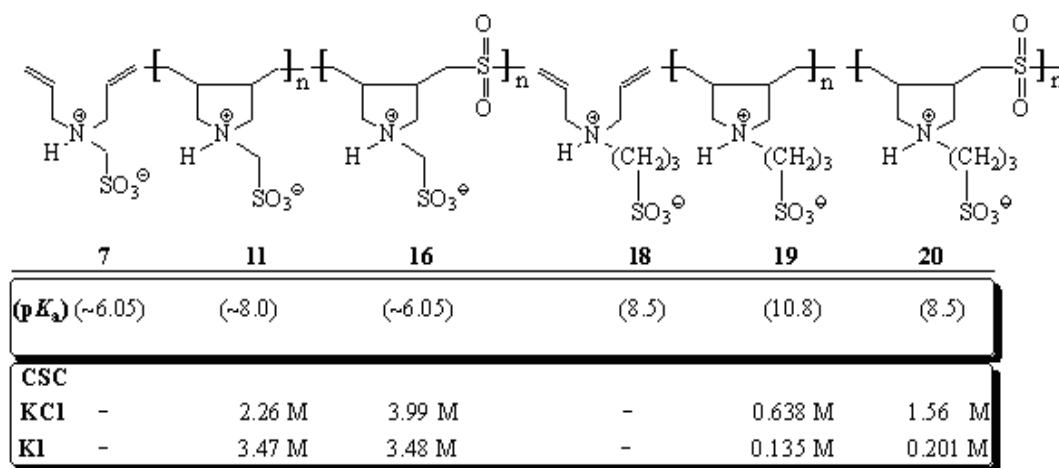
copolymer **(16)** (Scheme 4) with an intent to examine and compare their solution properties with the corresponding PSBs **19** and **20** (Scheme 5) having $(\text{CH}_2)_3$ spacer separating the charges in the zwitterionic motifs^[30, 94].



Scheme 3.



Scheme 4.



Scheme 5.

The newly synthesized polymers are expected to demonstrate interesting solution properties as a result of the closer proximity of the charges in the zwitterionic unit.

5.2 Experimental

5.2.1 Physical Methods

Melting points were recorded in a calibrated Electrothermal-IA9100- Digital Melting Point Apparatus. Elemental analysis was carried out on a Perkin Elmer Elemental Analyzer Series II Model 2400. IR spectra were recorded on a Perkin Elmer

16F PC FTIR spectrometer. ^1H and ^{13}C NMR spectra were measured in CDCl_3 (using TMS as internal standard) or D_2O at $+25\text{ }^\circ\text{C}$ (using HOD signal at 4.65 and dioxane ^{13}C peak at $\delta 67.4$ as internal standards) on a JEOL LA 500 MHz spectrometer. Viscosity measurements were made with an Ubbelohde viscometer (viscometer constant = 0.005718 cSt/s at all temperatures) with CO_2 -free water under N_2 to avoid CO_2 absorption, which could affect the viscosity data.

5.2.2 Materials

t-Butylhydroperoxide (TBHP) (80% in ditertiarybutylperoxide), ammonium persulfate (APS), paraformaldehyde, diallyl amine (**5**) from Fluka Chemie AG (Buchs, Switzerland) were used as received. Sodium bisulfite was purchased from Fisher Scientific Company. Dimethylsulfoxide (DMSO) was dried over calcium hydride overnight and then distilled under reduced pressure at a bp of $64\text{--}65^\circ\text{C}$ (4 mmHg). For dialysis, a Spectra/Por membrane with a MW cut-off value of 6000-8000 was purchased from Spectrum Laboratories, Inc.

5.2.3 Sodium diallylaminomethanesulfonate (**6**)

To a stirring heterogeneous mixture of NaHSO_3 (31.2 g, 0.3 mol) and paraformaldehyde (9.0 g, 0.3 mol) in water (50 cm^3) was added diallylamine (**5**) (29 g, 0.3 mol) at 20°C . The exothermic reaction ensued, and the resultant homogeneous reaction mixture was stirred for 1 h, after which cooled to room temperature. The solution was then freeze-dried to obtain sodium diallylaminomethanesulfonate (**6**) (61 g, 95%) which was used without further purification for the subsequent step. The ^1H NMR spectrum revealed the product as very pure. However an analytical sample was prepared by washing the white salt with acetone/ether. (Found: C, 39.2; H, 5.8; N, 6.4; S, 14.9.

$C_7H_{12}NNaO_3S$ requires C, 39.43; H, 5.67; N, 6.57; S, 15.04 %); mp 135 °C - started to melt; did not melt completely; ~220 °C expands as yellowish solid; 320 °C turned to black powder; ν_{\max} (KBr): 3438, 3076, 2978, 2843, 1645, 1423, 1191 (very strong), 1048 (strong), 995, 910, 848 and 788 cm^{-1}

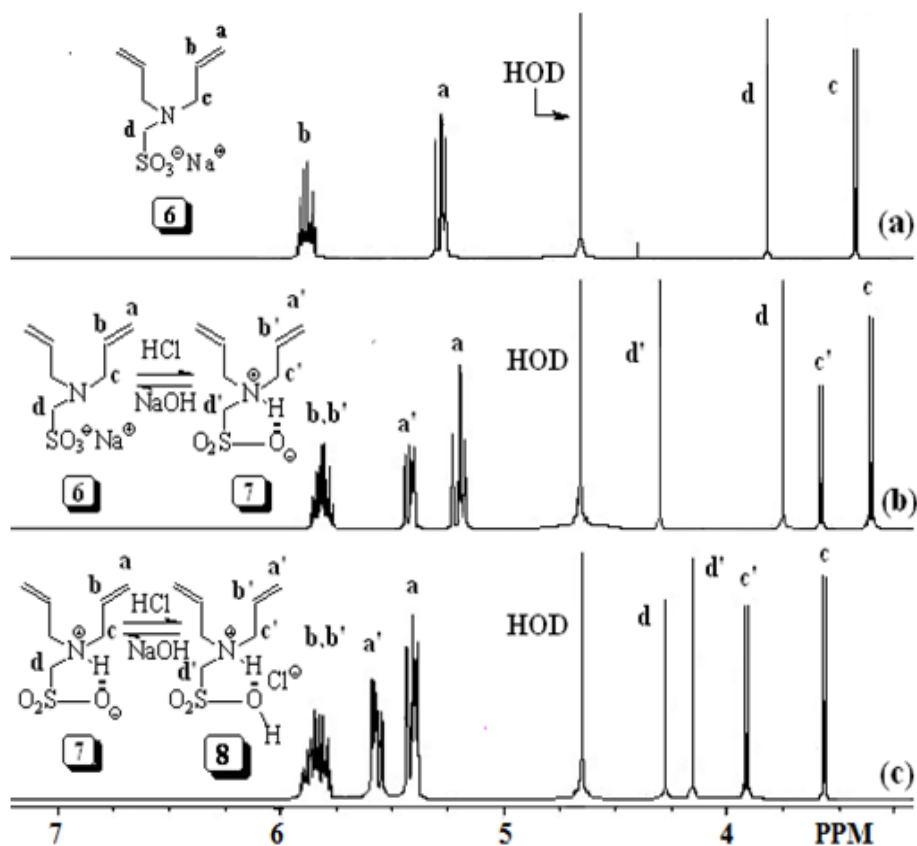


Figure 5.1. 1H NMR spectra of (a) 6, (b) 6/7 (60:40), and (c) 7/8 (60:40) in D_2O .

δ_H (D_2O): 3.43 (6H, d, J 6.8 Hz), 3.82 (2 H, s), 5.28 (4 H, m), 5.88 (2 H, m), (HOD: 4.65). δ_C (D_2O): 56.5, 68.8, 120.5 ($=CH_2$), 134.7 ($-CH=$), (dioxane, 67.40 ppm). ^{13}C spectral assignments of the alkene carbons were supported by DEPT 135 NMR analysis. The 1H and ^{13}C NMR spectra are displayed in Figs. 5.1a and 5.2a, respectively.

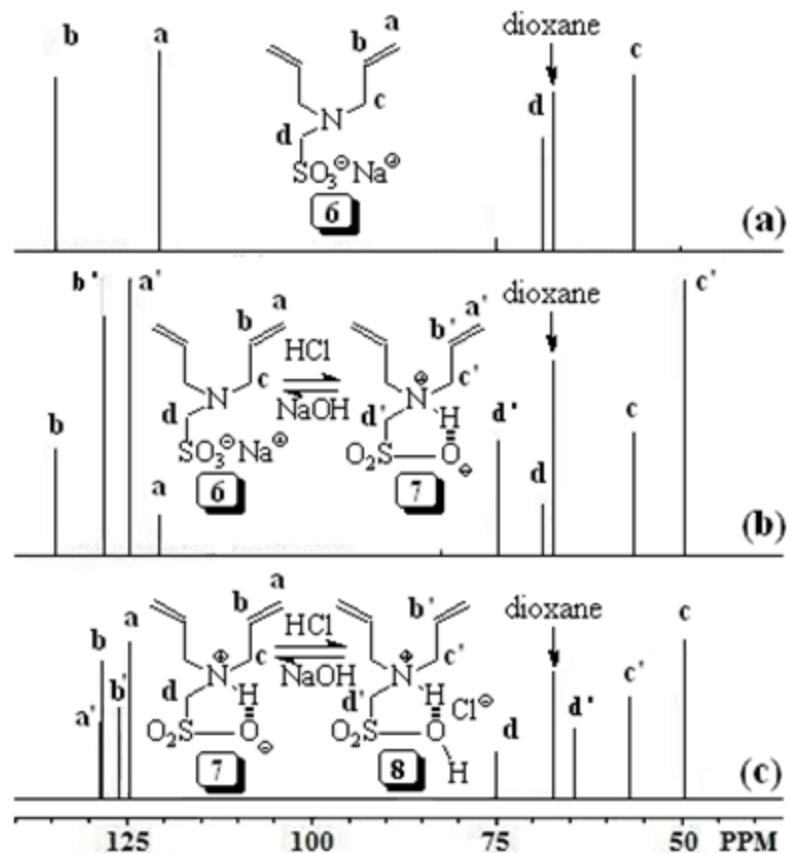


Figure 5.2. ^{13}C NMR spectra of (a) **6**, (b) **6/7** (60:40), and (c) **7/8** (60:40) in D_2O .

5.2.4 Diallylammoniomethanesulfonate (**7**)

To a solution of above salt **6** (0.25 mmol diallylamine) in water (75 cm^3) was added dropwise concentrated HCl until the pH became 1.5 (it required about 21 cm^3 concentrated HCl). The resulting solution was then freeze-dried. The residual thick liquid was triturated with ethanol (100 cm^3) and filtered to remove NaCl. After removal of ethanol, the residue was dried under vacuum at $40\text{ }^\circ\text{C}$ to a constant weight to obtain **7** (44.5 g, 85%) as a thick liquid which solidified upon cooling inside a freezer. The spectral data revealed that the above product contained a mixture of **7** and **8** in a 1:1 ratio. The average molar mass of **7** and **8** was used in the percent yield calculation. Since it is a mixture, its elemental analysis was not carried out.

ν_{\max} (neat): 3417, 3003, 2784, 1645, 1452, 1203 (very strong), 1037 (strong), 996, 949, 782 and 603 cm^{-1} . The ^1H NMR spectrum revealed the following signals for **7** and **8**:

7: δ_{H} (D_2O): 3.63 (6H, d, $J = 6.6$ Hz), 4.23 (2 H, s), 5.46 (4 H, m), 5.90 (2 H, m), (HOD: 4.65). δ_{C} (D_2O): 49.5, 75.0, 124.6 ($=\text{CH}_2$), 128.2 ($-\text{CH}=\text{}$) (dioxane, 67.4 ppm). ^{13}C spectral assignments of the alkene carbons were supported by DEPT 135 NMR analysis.

8: δ_{H} (D_2O): 3.97 (6H, d, $J = 7.3$ Hz), 4.34 (2 H, s), 5.64 (4 H, m), 5.90 (2 H, m), (HOD: 4.65). δ_{C} (D_2O): 57.0, 64.5, 125.9 ($-\text{CH}=\text{}$), 128.6 ($=\text{CH}_2$) (dioxane, 67.4 ppm). ^{13}C spectral assignments of the alkene carbons were supported by DEPT 135 NMR analysis. The ^1H and ^{13}C NMR spectra are displayed in Figs. 5.1 and 5.2, respectively.

5.2.5 General Procedure for the Homopolymerization of a mixture of **7** and **8**

All the polymerizations were carried out using conditions as described in Table 5.1. In a typical experiment, a solution of the monomer **7/8** (1:1) in a suitable solvent in a small round bottomed flask was purged with N_2 , and after adding the required amount of the initiator, the mixture was stirred in the closed flask at the specified temperature for 48 h. For instance in entry 10 (Table 5.1), when monomer **7/8** (15 mmol) in DMSO (3.0 g) and APS (375 mg) was heated at 65°C for 48 h, followed by precipitation in acetone, gave a yellow polymeric powder (50%). The polymer was dissolved in water in the presence of NaCl and dialyzed against deionized water for 24 h. During dialysis, the polymer **11** precipitated which was dried under vacuum at 55°C to a constant weight (10%). The water-soluble material after freeze-drying also gave intractable mixture of polymeric materials (34%). When the water-soluble polymer was again dialyzed against water for longer duration (72 h), only a small amount of polymer (6%) was recovered.

Table 5.1 Homopolymerization of the monomer 7.^a

Entry	Initiator (mg)	Solvent (g)	Temp(°C)	Yield ^b (%)
1	AIBN (45)	DMSO (1.5 g)	70	trace
2	AIBN (75)	DMSO (3.8 g)	60	4
3	AIBN (75)	DMSO (1.5 g)	70	4
4	AIBN (150)	DMSO (2.3 g)	65	5
5	AIBN (225)	DMSO (2.3 g)	60	8 ^c
6	AIBN (270)	DMSO (2.4 g)	70	9 ^d
7	AIBN (300)	DMSO (2.7 g)	60	5
8	APS (75)	DMSO (3.8 g)	60	6
9	APS (150)	DMSO (3.8 g)	60	8
10	APS (375)	DMSO (3.0 g)	65	10 ^e
11	APS (400)	DMSO (3.0 g)	65	11 ^f
12	APS (450)	DMSO (2.7 g)	40	trace
13	APS (80)	Water (1.2 g)	65	trace
14	TBHP(25)	6 M HCl (1.2 g)	65	trace ^g
15	TBHP(135)	1 N NaCl (1.2 g)	65	trace ^g

^aPolymerization reactions were carried out in a solution of monomer **7** (15 mmol) in solvent DMSO or water (in the presence or absence of NaCl or HCl) using initiator APS or TBHP or AIBN for 48 h.

^byield for the water-insoluble polymer.

^cTotal yield for water soluble + water insoluble polymer = 33%.

^dTotal yield for water soluble + water insoluble polymer = 48%.

^eTotal yield for water soluble + water insoluble polymer = 50%.

^fTotal yield for water soluble + water insoluble polymer = 50%.

^gExothermic reaction set in immediately after addition of the initiator at 20°C with evolution of gas.

When the polymerization of 1:1 mixture of monomers **7/8** was carried out in 1 N NaCl or 6 M HCl with the monomer/solvent wt ratio of 70:30 using initiator TBHP, an immediate exothermic reaction set in at 20°C, and the solution turned brown. After

heating at 65°C for 48 h it gave a trace amount of polymeric material which was insoluble in methanol but soluble in water.

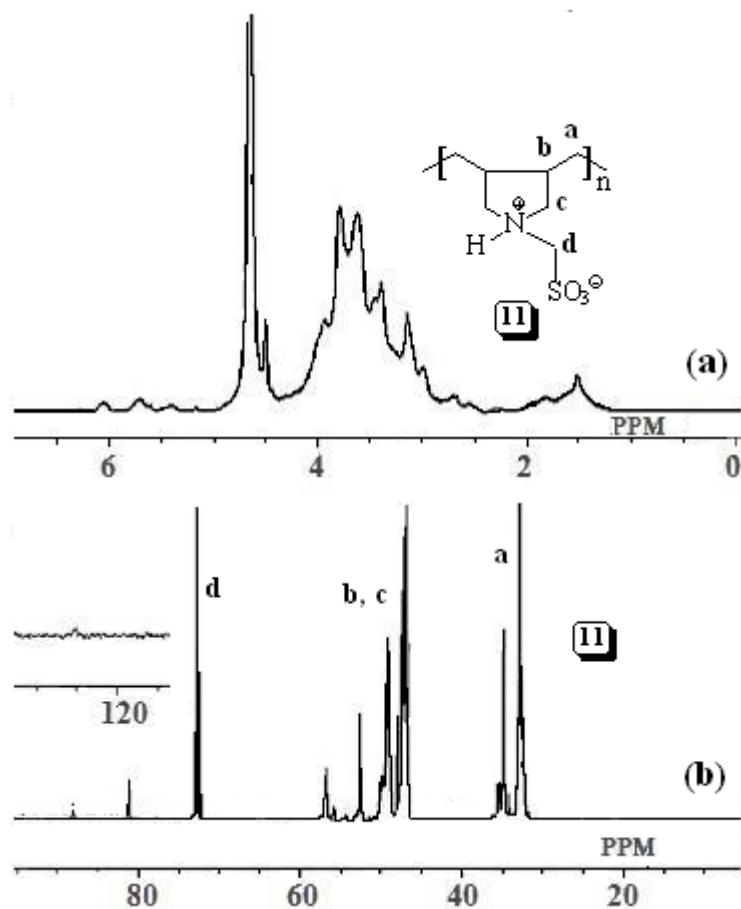


Figure 5.3. (a) 1H and (b) ^{13}C NMR spectra of 11 in ($D_2O + NaCl$).

PZ 11: The onset of thermal decomposition (Closed capillary): mp 255 °C (brown)-265 °C (black); ν_{max} (KBr): 3433 (very broad), 2970, 2927, 2749 (br), 1635, 1467, 1421, 1307, 1214, 1126, 1038, 853, 779, 593 and 518 cm^{-1} . (Found: C, 44.5; H, 7.3; N, 7.7; S, 16.1. $C_7H_{13}NO_3S$ requires C, 43.96; H, 6.85; N, 7.32; S, 16.76 %). The 1H and ^{13}C NMR spectra are displayed in Fig. 5.3.

5.2.6 General Procedure for the Copolymerization of 1:1 mixture of monomers 7/8 with SO₂

All the polymerizations were carried out using conditions as described in Table 5.2. In a typical experiment, SO₂ was absorbed in a solution of the monomers 7/8 in DMSO. The required amount of the initiator (AIBN) was then added under N₂ and the closed flask was stirred using magnetic stir-bar at 60°C for 24 h. Within hours, the magnetic bar stopped stirring, and initial reaction mixture became a solid mass of white polymer. At the end of the elapsed time, the polymerization mixture was dropped into water. The polymer was crushed to powder and filtered.

White copolymer **16** was dried under vacuum at 60 °C to a constant weight. The onset of thermal decomposition (Closed capillary): mp 235 °C (brown)- 260 °C (black), effervescence of SO₂; ν_{\max} (KBr): 3700-2500 (very broad), 1639, 1462, 1418, 1304, 1214, 1125, 1041, 775 and 618 cm⁻¹. (Found: C, 32.7; H, 5.3; N, 5.3; S, 24.8. C₇H₁₃NO₅S₂ requires C, 32.93; H, 5.13; N, 5.49; S, 25.12 %). The ¹H and ¹³C NMR spectra are displayed in Fig. 5.4 and 5.5, respectively.

Table 5.02 Cyclocopolymerization^a of the monomer 7 with SO₂.

Entry	7 (mmol)	Initiator (mg)	DMSO (g)	Yield (%)	$[\eta]^b$ (dL g ⁻¹)	\overline{M}_n
1	6.0	AIBN (32)	1.5	60	0.0567	67,500
2	6.0	AIBN (32)	2.1	87	0.0553	65,000
3	6.0	AIBN (32)	3.1	83	0.0512	62,500
4	6.0	AIBN (18)	1.5	82	0.0572	67,000
5	52	AIBN (156)	13	80	0.0545	64,000

^aPolymerization reactions were carried out in a solution of monomer 7 in DMSO using initiator AIBN at 60°C for 24 h.

^bViscosity of 1.5-0.5 % polymer solution of 5 in the presence of 1 equivalent NaOH in 0.1 N NaCl at 30°C was measured with Ubbelohde Viscometer (K=0.005718).

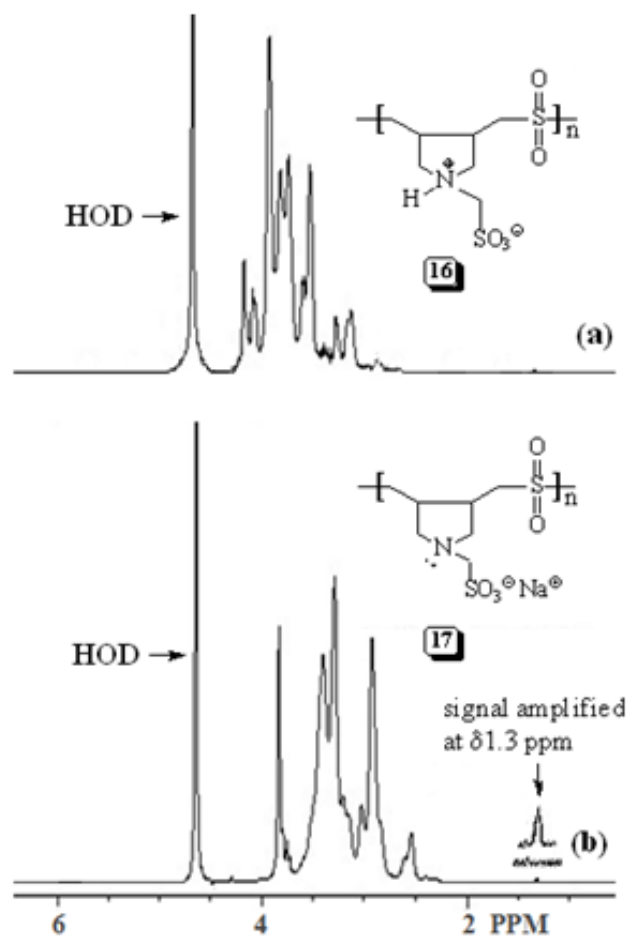


Figure 5.4 ^1H NMR spectra of (a) 16 in ($\text{D}_2\text{O} + \text{KCl}$) and (b) 17 in D_2O .

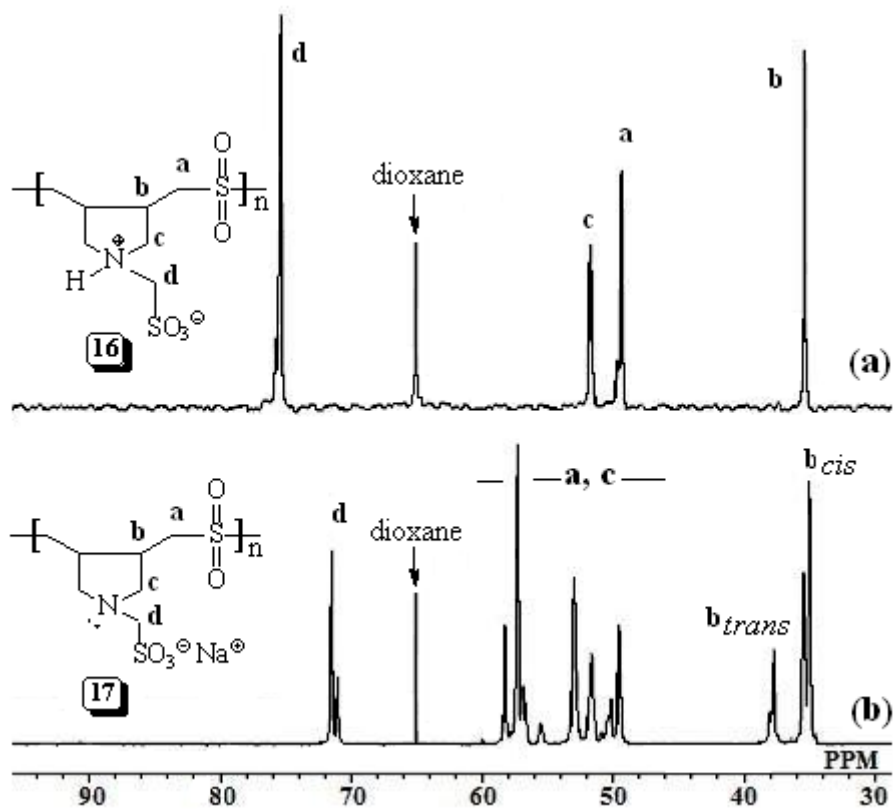


Figure 5.5 ^{13}C NMR spectra of (a) 16 in ($\text{D}_2\text{O} + \text{KCl}$) and (b) 17 in D_2O .

5.2.7 Conversion of PSB 16 to Anionic Polyelectrolyte (APE) 17

To a stirred heterogeneous mixture of PSB **16** (1.53 g, 6.0 mmol) in water (5 cm³) at 5-10° C was added powdered NaOH (240 mg, 6.0 mmol) in 3 portions (ca. 5 min). After the mixture became homogeneous, another part of solid NaOH (240 mg, 6.0 mmol) was added, briefly stirred (30 sec), and precipitated into methanol (30 cm³). APE **17** thus generated was filtered, washed with methanol and dried under vacuum at 55°C to a constant weight (1.38 g, 83%). The onset of thermal decomposition (Closed capillary); 225° C (brown)- 245 °C effervescence of SO₂ ; (Found: C, 30.0; H, 4.5; N, 4.9; S, 22.8. C₇H₁₂NNaO₅S₂ requires C, 30.32; H, 4.36; N, 5.05; S, 23.12 %).

5.2.8 Reconversion of (APE) 17 to PSB 16

To a stirred mixture of APE **17** (0.278 g, 1.0 mmol) in water (1 cm³) at 20° C was added 1 N HCl (1.2 mL, 1.2 mmol). The precipitate thus formed was kept under stirring for 2 h after which it was filtered and dried under vacuum at 55° C to a constant weight of PSB **16** (0.237 g, 93%).

5.2.9 Solubility Measurements and Cloud Point Titrations in Aqueous Salt Solutions

The Critical (minimum) Salt Concentration (CSC) required to promote water solubility of PSB **11** or **16** at 23 °C was measured by titration of 1% w/w polymer solution at sufficiently high salt concentration with deionized water. The accuracy of the CSC values, obtained by visual determination of the first cloud point, was approximately ±2-4%. The results of the solubility and CSC values are given in Table 5.3.

Table 5.3 Critical Salt Concentration for Aqueous Solutions of Polysulfobetaines 11 and 16 at 23 °C.

Salt	CSC (M) for 11	CSC (M) for 16
NaCl	3.06	insoluble
KCl	2.26	3.99
KBr	3.28	3.78
KI	3.47	3.48

5.3 Results and discussion

5.3.1 Monomer Synthesis

Zwitterionic diallylammoniomethanesulfonate (**7**), a sulfobetaine (SB), was prepared using procedure described for the synthesis of dimethylammoniomethanesulfonate ($\text{Me}_2\text{NH}^+\text{CH}_2\text{SO}_3^-$)^[143]. Diallyl amine (**5**), on treatment with paraformaldehyde and sodium bisulfite, afforded sodium diallylaminomethanesulfonate (**6**), which on treatment with HCl gave a mixture of diallylammoniomethanesulfonate (**7**) and its corresponding sulfonic acid **8** in excellent yield (Scheme 2). The IR spectra of **6** and a mixture of **7** and **8** indicate the presence of the sulfonate group by its characteristic bands at ~ 1200 and ~ 1040 cm^{-1} . ^1H and ^{13}C NMR spectrum of **6-8** are displayed in Figures 5.1 and 5.2, respectively. Figures 5.1a and 5.2a confirm the structure of monomer precursor **6** having four types of hydrogens and carbons. Sodium salt **6** upon addition of about 0.4 equivalent of HCl generated a mixture of **6** and **7** as indicated by the NMR spectra presented in Figures 5.1b and 5.2b. New sets of four signals attributed to **7** appeared in the spectra. The synthesis of SB **7** in the current

study led to a mixture of **7** and **8** in a 1:1 as described in the experimental section. The analysis of the NMR spectra (Figures 5.3c and 5.3d) led to this conclusion. It is interesting to note that the NMR signals for the apparently equilibrating mixture of **6/7** (Figures 5.1b, 5.2b) and **7/8** (Figures 5.1c, 5.2c) were distinct for each species. For instance, the signal of carbon or protons marked d and d' should appear at an average chemical shifts as expected for a fast equilibrating mixture. The observation that they appear at two different chemical shifts led us to rationalize that the specie **6** and **7** are either frozen or equilibrating slowly with respect to NMR time scale. Slow equilibration makes sense since for the species **7**, equilibration must involve breaking of the H-bond followed by deprotonation to **6**. The equilibration for the pair involving **7** and **8** also seems to be frozen.

5.3.2 Homocyclopolymerization

A 1:1 mixture of monomers **7/8** was subjected to cyclopolymerization (Scheme 3) under various conditions using a variety of initiators to give water-insoluble polysulfobetaine (PSB) **11** in very low yields as given in Table 5.1. In entry 10, for instance, a polymeric powder was obtained in 50% yield of which the water-insoluble polymer **11** only accounted for 10%, while the remainder being water-soluble. The water-soluble portion constituted polymer of low molecular mass as it escaped the dialysis bag (of MWCO 6000-8000) upon prolonged dialysis. PSB **11**, upon neutralization with sodium hydroxide, was converted into the corresponding unstable APE **12** which could not be reconverted to PSB **11** upon acidification. Generally, the bisulfite compounds are unstable; the reactions which lead to their formation are readily reversible and markedly influenced by acids and alkalis.

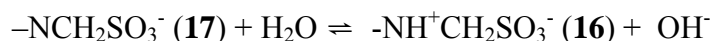
The ^1H and ^{13}C NMR spectra of water-insoluble **11** are displayed in Fig. 5.3. The spectra are approximately consistent with the polymer structure. The water-soluble fraction of the polymer as described before did not show the NMR signal attributed to the CH_2 (marked 'd') group (not shown using a Figure). In some samples it was completely absent whereas in other cases incomplete hydrolysis led to the presence of CH_2SO_3^- dependent to variable extents as indicated by the lower intensities of the CH_2 (marked 'd') signals. Even in the polymer spectra of water-insoluble **11** given in Fig 5.3, the intensity of the CH_2 (d) carbon seems to be less than the other carbons. The elemental analysis was not that satisfactory. The results are rationalized in terms of structural instability of the bisulphite/formaldehyde addition product. As outlined in Scheme 3, the breakdown of **12** to immonium salt **13** is the consequence of electron push from the trivalent nitrogen to the bisulfite leaving group. The formation of H_2O addition product **14** followed conversion to **15** and formaldehyde. The appearance of a minor signal around $\delta 81$ ppm could be attributed to the NCH_2OH carbon of **14** (Figure 5.3b).

5.3.4 Cocyclopolymerization with SO_2

While we were dismayed by the synthetic results to obtain homopolymer **11** which represents the first example of a PSB with a single methylene spacer, we were delighted to synthesize effectively the sulfur dioxide copolymer. The 1:1 monomer mixture of **7/8** in the presence of 1 molar equivalent of SO_2 was subjected to polymerization in DMSO using AIBN as the initiator to give water-insoluble PSB **16** in excellent yields (Scheme 4). The results of the polymerization under various conditions molar masses of PSB **16** and intrinsic viscosities in the presence of 1 equivalent NaOH are given in Table 5.2. The polymer precipitated during the polymerization process. The neutralization of PSB

16 with an excess of NaOH followed by precipitation into methanol afforded water-soluble APE **17** which, on addition of 1 equivalent of HCl, reverted to PSB **16** in 93% yield. The IR spectrum of PSB **16** indicates the presence of the sulfonate group by its characteristic bands at ~1200 and ~1040 cm⁻¹. The two strong bands at ~1300 and ~1120 cm⁻¹ were assigned to the asymmetric and symmetric vibrations of SO₂ unit.

Thermal degradation of PSB **16** appeared to happen at around 230-250°C and is attributed to the loss of sulfur dioxide. The ¹H and ¹³C spectra are displayed in Figs. 5.4 and 5.5, respectively. The absence of any residual alkene proton or carbon signal in the spectra indicated the chain transfer process for the termination reaction involving the macroradical abstracting the labile allylic hydrogen of monomer **7**^[79, 92, 144]. Note that the NMR signals of PSB **16** are shifted downfield than that of APE **17** as a result of the former having the presence of electron withdrawing positive nitrogens (Figure 5.4). The ¹³C NMR spectrum of PSB **16** (Fig. 5.5a) revealed the presence of four types of signals as expected. However, for APE **17**, the carbon 'b' appeared as two signals in a respective ratio of 80:20, attributed to the symmetrical major *cis* (b,b) and unsymmetrical minor *trans* (b,b') disposed substituents in the five-membered ring structure (Fig. 5.5b, Scheme 4)^[14]. The integration of the relevant ¹³C peaks yielded the *cis/trans* ratio which is similar to that observed for the related cyclopolymers^[5, 14, 91]. Note that while the ¹³C spectrum of the structurally frozen PSB **16** is much simpler than that of mobile APE **17** as a result of the equilibration:



Molar masses of the copolymers were determined using end group analysis. In cyclopolymerization reaction, the termination involves degradative chain transfer

reaction involving the abstraction of the labile allylic hydrogens; the resultant stable allylic radical cannot reinitiate polymerization. In that scenario, it would be a good approximation to assume that each polymer chain will have one initiator fragment (i.e., the primary radical $\text{Me}_2\dot{\text{C}}(\text{CN})$) as an end group^[26]. The end group hydrogens of the initiator fragment in PSB **16** or APE **17** appeared as a broad singlet at $\delta 1.3$ ppm (Figure 5.4b). The area (A) at $\delta 1.3$ thus integrates for six protons of the initiator fragment, while the area (B) for rest of the signals at $\delta 2-4$ ppm belongs to all the twelve protons of the repeating units. The degree of polymerization (DP) is then calculated as the ratio of the area of a single proton of the repeating unit and initiator fragment [i.e., $\text{DP} = (\text{B}/12)/((\text{A}/6))$]. The number average M_n of PSB **16** was then obtained by multiplying the DP with the molar mass (255.30) of each repeating unit. The molar masses are reported in Table 5.2.

5.3.5 Solubility behaviors of the homo-and copolymers

Like the overwhelming majority of reported polyzwitterions, PSB **11** was found to be insoluble in water^[4, 134, 135]. However, as anticipated for zwitterionic polymers, it was found to be soluble in the presence of added salts. The low molecular weight anions and cations of the added electrolyte enter and partially neutralize a portion of the intra-chain interactions in PSB, thus allowing the collapsed coil in pure water to expand in the presence of small ions. For various salts, the critical minimum salt concentrations (CSCs) required to promote water solubility of PSB **11** at 23 °C are shown in Table 5.3. For a common cation, K^+ , the sequence of increasing solubility power (i.e., decreasing order of CSC values) was found to be:



It is interesting to note that the order is the reverse of solubility power known for various PSBs^[8, 30, 143]. The iodide anion is the most polarizable (soft), hence it is anticipated to be the most effective in neutralizing ionic crosslinks thus increasing the solubility of the PSB. We are at this stage unable to rationalize the apparent anomaly in the solubility behaviour for the current polymer **11**. There is a considerable difference in the concentration of common electrolytes required to promote solubility of PSB **11** having a CH_2SO_3^- pendent. For instance, a much lower concentration of 0.638 M KCl is required to promote solubility of PSB **19** containing longer $(\text{CH}_2)_3\text{SO}_3^-$ pendent^[30], whereas the CSC of KCl required for the solubility of **11** was found to be 2.26 M (Scheme 5, Table 5.3). Increasing spacer length is thus found to decrease the CSC values. It is interesting to note that the corresponding polycarbobetaine having a CH_2CO_2^- pendent is readily soluble in salt-free water^[26]. The $\text{p}K_a$ of polyelectrolytes having $-\text{NH}^+\text{CH}_2\text{CO}_2\text{H}$ motifs is reported^[26] to be 2.5 and that of sulfonic acid group in $-\text{NH}^+\text{CH}_2\text{SO}_3\text{H}$ is expected to be or even lower than -2.1, the normal $\text{p}K_a$ of a sulfonic acid. The sulfobetaine moiety ($\text{NH}^+\text{CH}_2\text{SO}_3^-$), having more dispersed charges and thus being less hydrated, is able to exert stronger zwitterionic interactions. The negative charges on the carbobetaines ($\text{NH}^+\text{CH}_2\text{CO}_2^-$), having higher carboxyl $\text{p}K_a$ values are expected to be less dispersed, hence more hydrated^[5, 24, 26] and as such tend to exhibit weaker Coulombic interactions with the cationic charges on the nitrogens^[80] thus imparting solubility in salt-free water.

For various salts, the CSC required to promote water solubility of PSB **16** at 23 °C are shown in Table 5.3. For a common cation, K^+ , the sequence of increasing solubilizing power (i.e., decreasing CSC values) was determined to be:



To our knowledge, the zwitterionic interaction is the largest ever reported in literature for a polyzwitterion; it required a huge amount of KI (3.48 M) to break the zwitterionic interaction and thus promote solubility. A much lower concentration of 0.201 M KI was required to promote solubility of the corresponding PSB **20** containing longer $(\text{CH}_2)_3\text{SO}_3^-$ pendent. The intercharge distances of $\text{Et}_3\text{N}^+(\text{CH}_2)_n\text{SO}_3^-$ have been derived from their dipole moments and evaluated to be 3.90 Å (for $n = 2$) and 4.80 Å (for $n = 3$)^[50]. Using calibration curve, the distance separating the charges of the unknown zwitterions ($n = 1$) has been estimated to be 3.05 Å which is lower than the minimum of 3.18 Å required for the ion-pair conformation^[145]. The higher CSC values are consistent with the development of strong electrostatic attractive interactions between the charges of opposite algebraic signs as well as dipolar interactions promoting intragroup, intra- and interchain associations (Figure 5.6)^[46]. The linear increase of dipole moment μ with the increase in n values in $\text{Et}_3\text{N}^+(\text{CH}_2)_n\text{SO}_3^-$ is more in favour of an extended conformation than a curled one. It has been reported that for $n = 2$ or 3, the zwitterion is expected to be practically in its fully extended conformation and has very little possibility of coiling especially in the case of $n = 2$. Increasing the number of methylene units between the charged centres increases the dipole moment and thus hydrophilicity and solubility^[2, 145, 146].

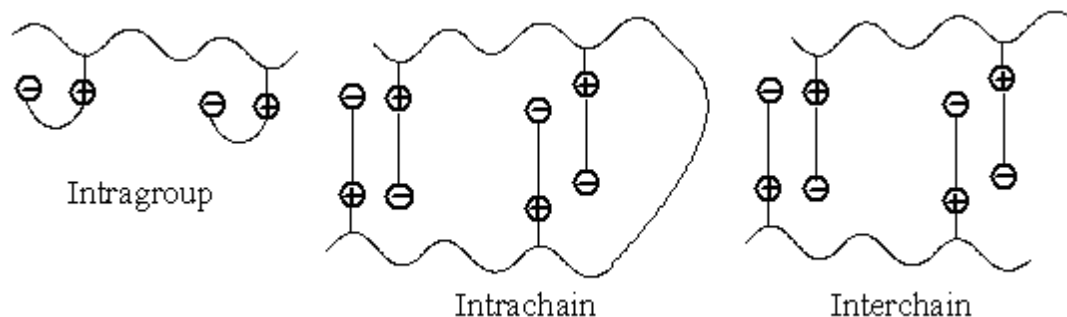


Figure 5.06 Depiction of intragroup, intrachain, and interchain attractions in polyzwitterions

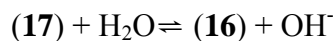
The higher CSC value for the polymer **16** (with a single methylene spacer between the charge centres separated by 3.05 Å) than the corresponding copolymer **20** having a spacer of three methylene units is attributed to the formation of intra group ion pair (thus imparting more covalent character and lesser solubility in aqueous media). For the copolymer with $n = 3$, the intra- and interchain zwitterionic interactions seem to be the dominant interactions (Figure 5.6).

5.3.6 Estimated pKa Values of the PSBs

We were unable to determine the pK_a of SB **7** (i.e., Log [protonation constant K] of the conjugate base **6**) by potentiometry as described elsewhere^[89]. The gradual addition of titre HCl (0.1 M) to a 2.5×10^{-3} M (molarity of the repeating units) solution (200 mL) of **6** led to a decrease in pH; however, considerable hydrolysis at around pH 6 led to higher pH values which cannot be justified by the amount of HCl added. As described in Scheme 2, hydrolysis of **6** led to the formation of basic diallylamine (**5**) which upon acid-base reaction with H_2O generates OH^- thereby increasing the pH. Similar hydrolysis was noted for dimethylammoniomethanesulfonate (DAMS), $Me_2NH^+CH_2SO_3^-$, which is reported^[143] to have an approximate pK_a value of 6.05 as determined using 1H NMR

technique. Monomer SB **7** is also expected to have a similar pK_a value since both DAMS and **7** have single methylene spacer separating the zwitterions. The pK_a value of **18** having a longer $(CH_2)_3$ spacer separating the zwitterions is reported to be 8.5 which is almost ~ 2.5 units higher than that of **7** (Scheme 5)^[30].

Zwitterionic attraction is so prominent in PSB **16** that we were unable to determine the protonation constant, K , for the amine nitrogen in APE **17** using potentiometry^[89]. Thus addition of even 2 drops of titre HCl (0.1 M) to a 200 mL of 2.0×10^{-3} M solution (molarity of the repeating units) of **17** led to a cloudy solution followed by precipitation. Note that for the above solution containing 0.4 mmol of **17**, a volume of 4.0 mL of 0.1 M HCl (i.e., 0.4 mmol HCl) would be the acid equivalent to the basic nitrogens in it. The pK_a values of monomer **18** and its SO_2 -copolymer **20** are similar (Scheme 5); as such the corresponding pair **7/16** is also assigned the same pK_a value of 6.05. Based on the amine pK_b value of 7.95 of **17** (i.e., 14 - ammonium pK_a value of 6.05 of **16**), the following equilibration:

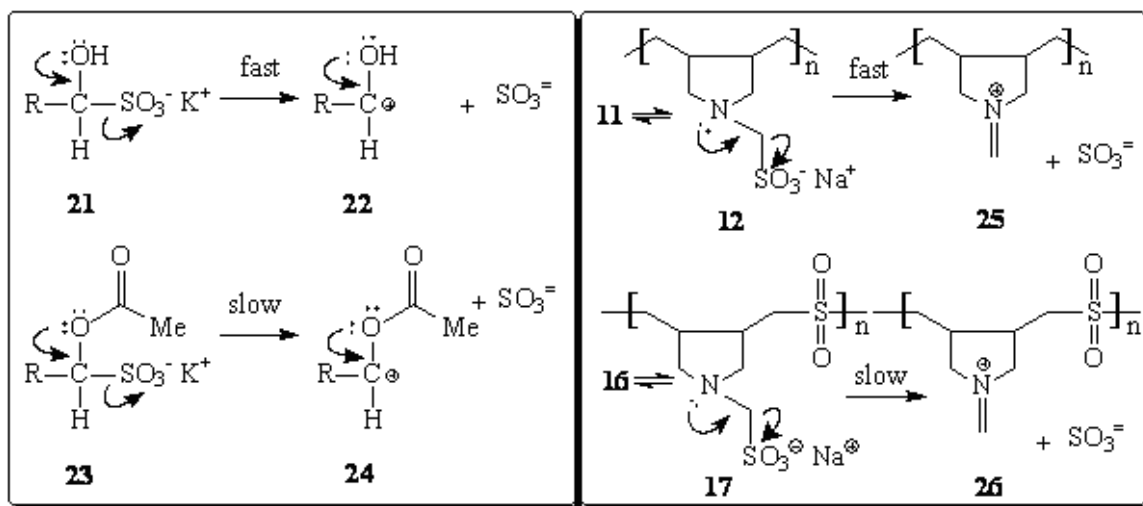


is calculated to contain only 0.24 mol % of **16**. A slight increase in its concentration led to precipitation thus demonstrating superior zwitterionic interactions operating in **16**.

5.3.7 Comparative Stability of Homopolymer **11** versus Copolymer **16**

The question remains: why is homopolymer **11** unstable while copolymer **16** is stable? The reversible nature of the aldehyde/bisulfite addition reaction is well known. While the addition product **21** undergoes relatively faster desulfonation to **22**, the acetyl protected **23** on the other hand is quite stable (Scheme 6). Since the electron push from

the oxygen, as shown in the Scheme, facilitates the removal of the sulfite group, the stability of **23** could be attributed to the lesser electron density on oxygen as a result of electron-withdrawing acetyl group. In a similar fashion, the stability of copolymer **17** (the conjugate base of **16**) may thus be rationalized in terms of depleted electron charge density on the nitrogen as result of the presence of electron withdrawing SO₂ units in the polymer backbone. Note that the presence of SO₂ does indeed deplete electron density as indicated by the lower pK_a value of copolymer **20** than that of homopolymer **19** by a significant 2.3 units (Scheme 5). The trivalent nitrogen in copolymer **17** is thus more electronegative hence less basic or nucleophilic than its counterpart in homopolymer **12**, thereby imparting greater stability to the copolymer as it is unable to push the electrons required for decomposition to **26** as depicted in Scheme 6.



Scheme 6.

5.4 Conclusions

A convenient synthesis of the new zwitterionic monomer **7** has been achieved. The work described in this paper represents the first example of a cyclopolymerization-

derived PSBs having zwitterionic charges separated by a single methylene spacer. While the homopolymer **11** was unstable, the corresponding SO₂ copolymer **16** was found to be stable owing to the depleted electron charge density on the trivalent nitrogens in **17**. The PSBs demonstrated very strong zwitterionic interactions as a result of the proximity of the charges of opposite algebraic signs leading to the formation of the ion-pairs.

The current challenge in the field of polymers is the construction of stimuli responsive advanced materials of polyzwitterions (PZs) that have high added-value applications in drug delivery systems, separation materials, sensors, catalysts, etc. Numerous applications of PZs also include their uses as fungicides, fire-resistant polymers, lubricating oil additives, emulsifying agents, bioadherent coatings ^[145, 147, 148] drilling-mud additives ^[149] and chelator of toxic trace metals (Hg, Cd, Cu, and Ni) in wastewater treatment^[139]. The current PSB's effectiveness in some of such applications has to be tested.

CHAPTER 6: Removal of heavy metal ions using a novel cross-linked polyzwitterionic phosphonate

Taken from **Othman Charles S. Al Hamouz**, Shaikh. A. Ali, Removal of heavy metal ions using a novel cross-linked polyzwitterionic phosphonate, *Separation and Purification Technology*, 98 (2012) 94–101.

ABSTRACT

A novel cross-linked polyzwitterionic acid (CPZA) was synthesized via cyclocopolymerization of diallylaminomethylphosphonic acid and 1,1,4,4-tetraallylpiperazinium dichloride (10 mol%), a cross-linker, in the presence of tert-butylhydroperoxide in aqueous solution at 85 °C. CPZA, upon treatment with NaOH, was converted into a cross-linked anionic polyelectrolyte (CAPE). The experimental data for the adsorption of Pb^{2+} and Cu^{2+} on CAPE fitted Lagergren second-order kinetic model and Langmuir as well as Freundlich isotherm models. The adsorption capacity of Pb^{2+} was higher than that of Cu^{2+} while the rate of adsorption was found to be higher for Cu^{2+} . The adsorption process was spontaneous and endothermic in nature with negative and positive values for ΔG and ΔH , respectively. The low activation energies of 12.8 and 17.9 kJ/mol for Cu^{2+} and Pb^{2+} , respectively, indicated the adsorption as a favorable process. The excellent adsorption and very good desorption efficiencies implied the efficacy of the resin in removing as well as recovering the metal ions from aqueous solution. An efficient synthetic access to the resin would enable its use in the treatment of contaminated waste water.

KEY WORDS: adsorption; desorption; cross-linked polyphosphonate; cross-linked polyzwitterion; heavy metal ions.

6.1 Introduction

The presence of heavy metal ions, such as Pb^{2+} , Cu^{2+} , etc., in natural and waste water systems is a matter of great concern due to their negative effects on the environment and human health. These toxic pollutants are nonbiodegradable and can accumulate in the human body causing a variety of diseases and disorders^[49, 50, 67, 68, 150]. Various techniques, like adsorption, precipitation, dialysis, ion exchange, reverse osmosis, and extraction, have been developed in the past for the removal of metal contaminants from water resources. One of the most attractive among these techniques is presumably the adsorption process due to the availability of different types of low-cost and environment-friendly adsorbents^[48, 52, 53, 56, 151]. Inorganic/organic polymer hybrid adsorbents have been widely investigated; their efficacies in metal ion removal are attributed to the formation of a stronger chemical bonding between M^{n+} and, for instance, amine motifs in the hybrid materials^[54, 55, 57, 58, 152]. Recently, the researchers have focused on the syntheses of zwitterionic cross-linked inorganic/organic hybrid materials for the removal of heavy metal ions via electrostatic effects^[59, 60, 153-155].

A titania-phosphonate hybrid porous material was found to have a large capacity for selective adsorption of Cd^{2+} ions^[61]. Considerable attention has been given to synthesize chelating agents containing aminomethylphosphonate motif owing to its extraordinary chelating properties in extracting heavy metal ions from waste water^[65]. In this paper, a novel cross-linked polymer containing aminomethylphosphonate motifs has been

synthesized and tested for its efficiency as an adsorbent for the removal of heavy metal ions like Pb^{2+} and Cu^{2+} ions from aqueous solutions. Desorption of the metal ions from the cross-linked polymer has also been investigated for the recovery of the metal ions and recycling of the polymer.

6.2 Experimental

6.2.1 Physical Methods

Elemental analysis was carried out on a Perkin Elmer Elemental Analyzer Series II Model 2400. IR spectra were recorded on a Perkin Elmer 16F PC FTIR spectrometer. ^1H spectra were measured in D_2O at $+25\text{ }^\circ\text{C}$ (using HOD peak at δ 4.65) on a JEOL LA 500 MHz spectrometer. Scanning electron microscopy images were taken by TESCAN LYRA 3 (Czech Republic).

6.2.2 Materials

Diallylamine, tertiary butylhydroperoxide (TBHP) (70% in water), paraformaldehyde and phosphorous acid from Fluka Chemie AG (Buchs, Switzerland) were used as received. All solvents used were of analytical grade.

6.2.3 Synthesis of monomers

6.2.3.1 Diallylaminomethylphosphonic acid 2

The synthesis of monomer **2** was carried out as described with some modifications in the isolation procedure^[65]. Thus, diallylamine (**1**) (0.50 mol) was added dropwise for 45 min to a stirred mixture of phosphorous acid (0.50 mol), water (50 mL), and concentrated hydrochloric acid (50 mL) under ice cooling. The reaction mixture was then refluxed for 1 h during which paraformaldehyde (1.0 mol) was added in several portions (ca. 20 min). The resulting solution was refluxed for an additional hour and thereafter evaporated to

dryness to obtain the crude product **2** (122 g). A ^1H NMR spectrum of a mixture containing a known mass of this crude product and a known mass of ethanol in D_2O revealed the purity of the product. Integration of the proton signals of $\text{CH}_2\text{P-}$ of **2** at $\delta 3.11$ versus CH_2O of ethanol at $\delta 3.40$ helped us to determine the purity of the crude product. The crude product (122 g) contained 0.42 mol of **2** (84%). The crude sample of 0.290 g was thus found to have 1 mmol (0.191 g) of **2** (i.e. the crude product contained 66 %w/w monomer **2**; the rest of the materials may include HCl , H_2O etc). The ^1H NMR spectrum was very clean and free of undesired products. Monomer **2** was used in the subsequent polymerization without further purification.

6.2.3.2 1,1,4,4-tetraallylpiperazinium dichloride 3

Monomer **3**, a cross-linker, was prepared as described^[64].

6.2.4 General procedure for the copolymerization of 2 and 3

All the polymerizations were carried out using the conditions described in Table 6.1. In a typical experiment (entry 5), monomer **2** (9 mmol i.e. 2.61 g of 66 %w/w purity) and cross-linker **3** (0.319 g, 1.0 mmol) were dissolved in deionized water (1.577 g). Initiator TBHP (190 mg) was added, and the reaction mixture in the closed flask under N_2 stirred using a magnetic stir-bar at the specified temperature for 24 h at 85°C . Within 6-8 h the stir-bar stopped moving; the reaction mixture became a transparent swelled gel. At the end of the elapsed time, the swelled gel of the cross-linked polyzwitterionic acid (CPZA) **4** was soaked in water (1-3 h) with replacement of water several times. The swelled gel was then poured onto acetone. The resin was filtered and dried under vacuum at 70°C to a constant weight.

Table 6.01 Copolymerization of monomers 2 and 3^a.

Entry No	Initiator (mg)	Monomer 2 (mmol)	Monomer 3 (mmol)	Monomer Concentration ^b (%w/w)	Yield (%)
1	90	9.0	1.0	80	33
2	90	9.0	1.0	75	44
3	90	9.0	1.0	65	48
4	90	9.3	0.70	65	44
5	180	9.0	1.0	65	76
6	1400	70	7.8	65	78

^aPolymerization reactions were carried out in an aqueous solution in the presence tertiary butylhydroperoxide (TBHP) for 24 h. Entry 5 was repeated in Entry 6 on a large scale.

^bCombined weight of impure monomer 2 and monomer 3 is considered in calculating the required %w/w of deionized water

The onset of thermal decomposition (Closed capillary): The resin was stable up to 350 °C, thereafter its colour changed to pale yellow; (Found: C, 45.1; H, 7.6; N, 7.2. A copolymer from monomer 2 $C_7H_{13}NO_3P$ (90 mol%) and monomer 3 $C_{16}H_{28}Cl_2N_2$ (10 mol%) requires C, 45.60; H, 7.53; N, 7.47); ν_{max} (KBr) 3500, 2876, 2817, 2779, 2700, 2626, 2375, 2279, 1657, 1464, 1086, 974, 762, 553, and 477 cm^{-1} .

6.2.5 Basification of CPZA 4 to cross-linked anionic polyelectrolyte (CAPE) 5

A mixture of CPZA 4 (8.0 g, ~ 34 mmol) and a solution of NaOH (3 g, 75 mmol) in water (100 mL) was stirred at room temperature for 1 h. The resin was then filtered and washed with water until a neutral filtrate was obtained. The resulting cross-linked

polyanion **5** was then freeze-dried, and further dried under vacuum at 70°C to a constant weight (6.82 g). The onset of thermal decomposition (Closed capillary): The resin was stable up to 350 °C, thereafter its colour changed to pale yellow.

6.2.6 Sample characterizations

FT-IR spectra were recorded on a Perkin Elmer 16F PC FTIR spectrometer in the region of 4000-400 cm⁻¹. Ion exchange capacity (IEC) was determined by titremetric analysis method. The weighed polymer CAPE **5** (100 mg) was immersed in a 0.1 mol dm⁻³ HCl (50 mL) for 24 h. The decrease in acidity was determined by titration with a 0.1 mol dm⁻³ NaOH solution. The IEC can be calculated by Eq. (1):

$$IEC = \frac{mmol_i - mmol_f}{W} \quad (1)$$

where mmol_i and mmol_f are the initial and final amount of HCl in mmol, respectively, *W* is the weight of the polymer in g^[156].

6.2.7 Adsorption experiments

The procedure for the adsorption experiments of the cross-linked polymer CAPE **5** for Pb²⁺ ions can be described briefly as follows: a mixture of CAPE **5** (50 mg) in a 0.1 mol dm⁻³ aqueous Pb(NO₃)₂ solution (20 mL) was stirred using a magnetic stir-bar at different pH for 24 h. The resin was filtered and carefully washed with deionized water. The combined filtrate was titrated with a 0.1 mol dm⁻³ aqueous EDTA solution to determine the amount of Pb²⁺ remained. The adsorption capacity ($q_{Pb^{2+}}$) can be calculated using Eq. (2):

$$q_{Pb^{2+}} = \frac{(C_0 - C_f)V}{W} \text{ mmol/g} \quad (2)$$

where C_0 and C_f are the initial and final concentration of Pb^{2+} ions, respectively, W is the weight of the polymer in g, and V is the volume of the solution in mL. Data presented are average of triplicate runs and varied by less than 4% in all the cases studied.

For adsorption kinetic studies, the resin sample was stirred in a 0.1 mol dm^{-3} $Pb(NO_3)_2$ solution for different adsorption times at a preferred pH. The adsorption isotherm was constructed by changing the concentration of $Pb(NO_3)_2$ from 0.02 to 0.1 mol dm^{-3} at $25 \text{ }^\circ\text{C}$ for 24 h. Based on the adsorption data from experiments carried out at different temperatures, the thermodynamic parameters ΔG , ΔH , and ΔS for Pb^{2+} removal were calculated.

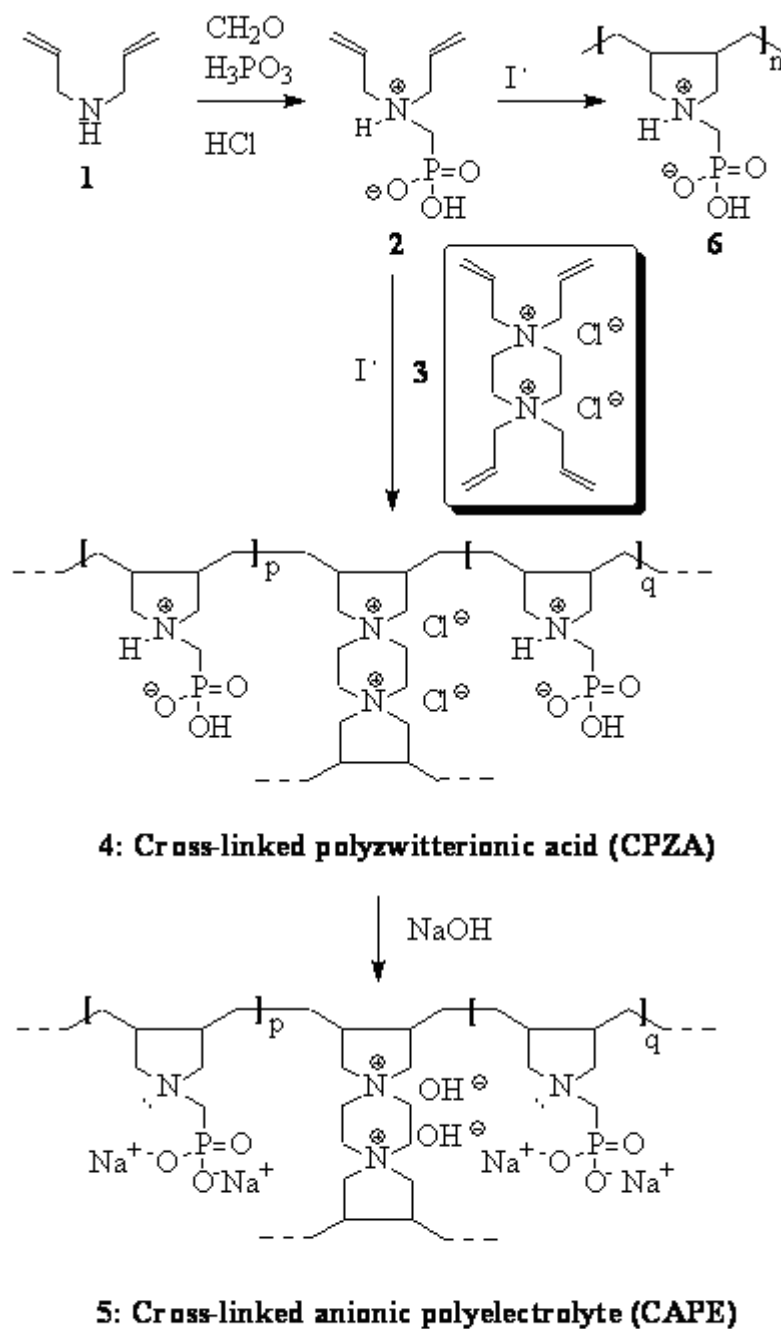
Similar experiments, as presented above, were conducted for the adsorption of Cu^{+2} ions in a 0.1 mol dm^{-3} aqueous $Cu(NO_3)_2$ solution. The amount of Cu^{2+} ions remained in the solution was determined by iodometric titration using excess KI and a 0.1 mol dm^{-3} aqueous $Na_2S_2O_3$ solution [47, 60]. Finally, the desorption efficiencies of Pb^{2+} and Cu^{2+} ions were measured using a 1 mol dm^{-3} HNO_3 .

6.3 Results and discussion

6.3.1 Synthesis of cross-linked polymer 4 and 5

Diallylaminomethylphosphonic acid **2**, a zwitterionic acid (ZA) monomer, was synthesized using a modified procedure^[65]. Butler's cyclopolymerization of **2** has been reported to give cyclopolymer **6**, a polyzwitterionic acid (PZA) (Scheme 1)^[65]. In fact, the cyclopolymerizations of a variety of *N,N*-diallylammonium salts led to the synthesis of an array of scientifically and technologically important water-soluble cationic

polyelectrolytes^[88, 91, 157-160]. The polymer-architecture, having the five-membered cyclic units embedded in the backbone, has been recognized as the eighth major structural type of synthetic polymers. Over 33 million pounds of poly(diallyldimethylammonium chloride) alone are sold annually for water treatment and another 2 million pounds are used for personal care formulation^[20].



Scheme 1. Synthesis of monomer and cross-linked polymers.

An aqueous solution of monomer ZA **2** (90 mol%) and cross-linker **3** (10 mol%) underwent cyclocopolymerization in the presence of initiator TBHP to give novel CPZA **4** in very good yields (Scheme 1). The results of the polymerization under various

conditions are given in Table 6.1. The polymer yields were almost doubled by doubling the concentration of the initiator (*cf.* entries 3 and 4 vs. 5 and 6). Higher concentration of the initiator was required since the presence of diallyl moiety could result in the extensive degradative chain transfer between the polymer radicals and the monomers^[79]. To the best of our knowledge, the synthesis of CPZA **4** represents the first example of a cross-linked polymer (containing aminomethylphosphonate motifs) by the cyclopolymerization protocol.

CPZA **4** was found to swell in water while shrank upon soaking in acetone owing to the removal of water. Its basification with excess NaOH led to cross-linked anionic polyelectrolyte (CAPE) **5** in excellent yield. Elemental analysis of CPZA **4** revealed the incorporation of monomers **2** and **3** to CPZA **4** in an approximate mol ratio of 90:10, which is the same as the feed ratio (Table 6.1).

6.3.2 Ion-exchange properties of CAPE **5**

The ion exchange capacity (IEC) of CAPE **5** was found to be 6.98 mmol/g, which ascertained the excellent ability of the resin to adsorb metal ions (M^{2+}) as a result of the presence of chelating ligands of $-N^{\ominus}$ and phosphonate motifs $-P(=O)O_2^{-2}$. The bands in the IR spectrum of the resin **5** in the region of 900–1150 cm^{-1} are attributed to the phosphonate P–O vibrations (Fig. 6.1A)^[161-163]. IR spectra of CAPE **5** loaded with Cu^{2+} and Pb^{2+} (Fig. 6.1B and C) revealed the increase in the intensity and broadness of the phosphonate P–O vibrations as a result of the adsorption of the metal ions^[164]. The C–N absorption was found in near $\sim 1460\text{ cm}^{-1}$. The peaks around 1650 cm^{-1} were ascribed to the H–O–H bending vibration. The appearances of new strong bands at 1326 (Fig. 6.1B) and 1384 cm^{-1} (Fig. 6.1C) were attributed to the presence of ionic nitrate group since the

adsorption process was carried out in the presence of lead and copper nitrates [165]. Interestingly, the presence of these strong bands implies the ability of the resin to act also as an anion exchanger. Note that the absorption band attributed to the nitrate ion is absent in the IR spectrum of the unloaded resin **5** (Fig. 6.1A).

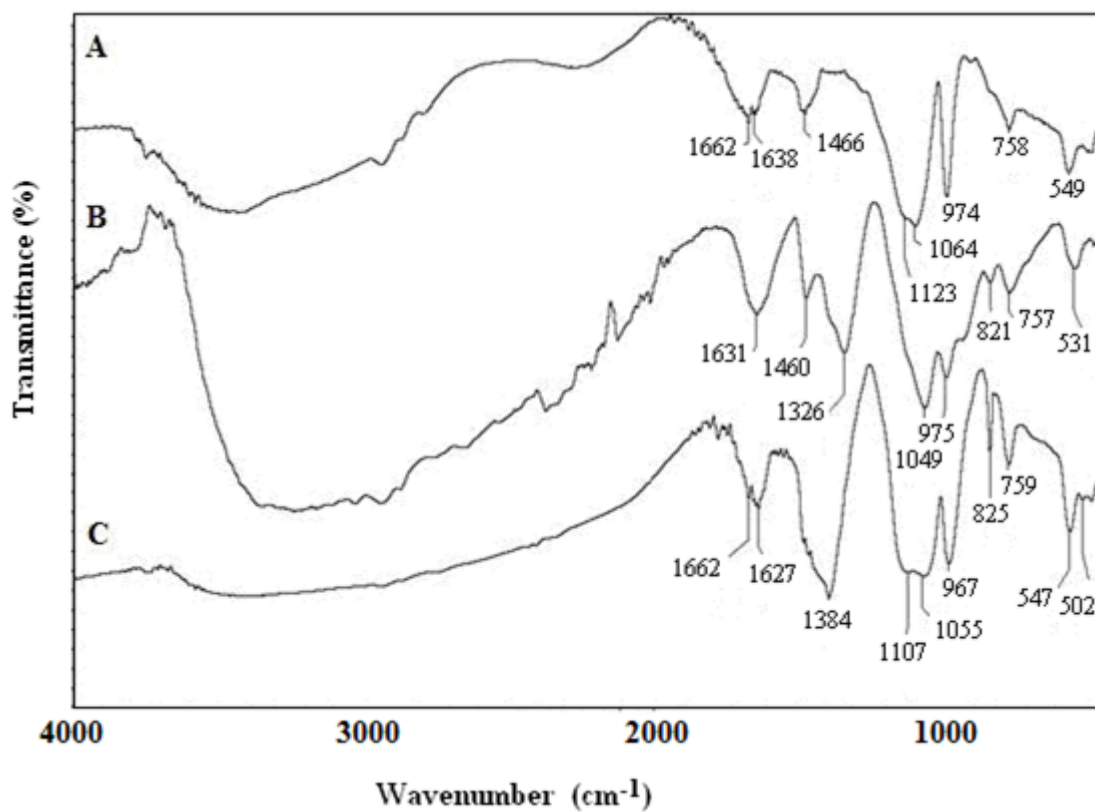


Figure 6.1 IR spectra of (A) Cross-linked polyanion **5**, (B) Cross-linked polyanion **5** loaded with Cu^{2+} and (C) Cross-linked polyanion **5** loaded with Pb^{2+} .

6.3.3 Adsorption kinetics

The adsorption kinetics, as described by the relationship between adsorption capacity and adsorption time, are presented in Fig. 6.2. It was found that the adsorption of Cu^{2+} ions by CAPE **5** reached to equilibrium in about 1 h, while more than 5 h were needed for Pb^{2+} ions. It is reported that Lagergren adsorption kinetic model is a suitable

tool to investigate the adsorption properties of a polymer^[166]. The following equations express the linearly first-order and second-order kinetic equations [Eqs. (3) and (4)] for the Lagergren model, respectively:

$$\log (q_e - q_t) = \log q_e - \frac{k_1 t}{2.303} \quad (3)$$

$$\frac{t}{q_t} = \frac{1}{k_2 q_e^2} + \frac{t}{q_e} \quad (4)$$

where k_1 and k_2 are the first-order and second-order rate constant, respectively, q_t and q_e are the adsorption capacity of the metal ions at a time t and at equilibrium, respectively.

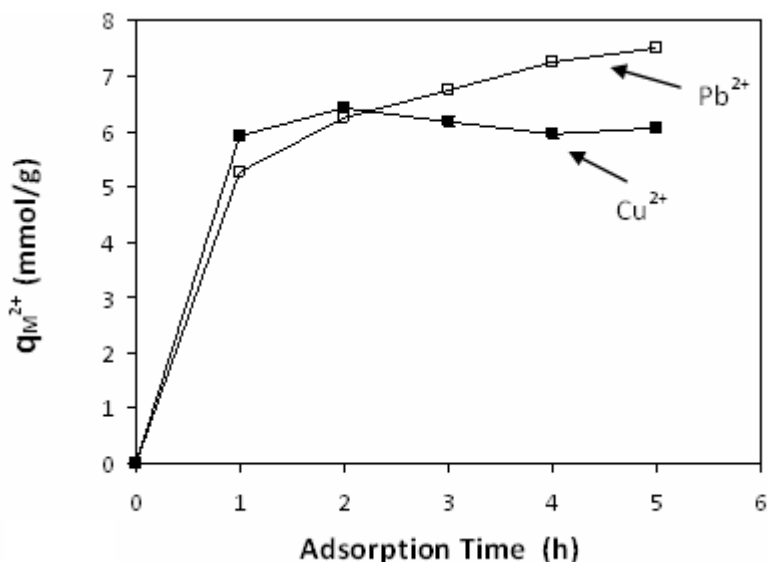


Figure 6.2. Adsorption kinetic curves of Cu^{2+} and Pb^{2+} in 0.1 M solution at pH 4 at 25°C.

Neither Pb^{2+} nor Cu^{2+} fitted the first-order Lagergren kinetic model, so the graphs representing the kinetic model have not been displayed. The second-order Lagergren kinetic model (Fig. 6.3), however, fitted well for the adsorption of both Cu^{2+} and Pb^{2+} ions on CAPE 5; suggesting that the adsorption process might be chemical adsorption^[167]. The values reported in Table 6.2. show that the rate constant (k_2) for the

removal of Cu^{2+} is much higher than that for Pb^{2+} ; however, CAPE 5 adsorbs a larger amount of Pb^{2+} at the longer periods of time (Fig. 6.2, Table 6.2).

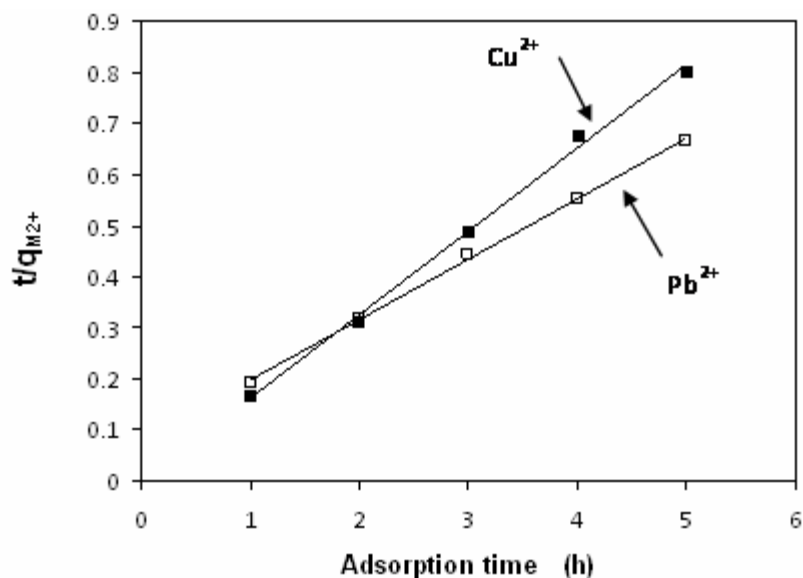


Figure 6.3. Lagergren second-order kinetic model for adsorption of Cu^{2+} and Pb^{2+} on CAPE 5.

In a recent article, the opposite trend was observed for the adsorption of Cu^{2+} and Pb^{2+} ions by a negatively charged carboxylate hybrid copolymer^[168]. The adsorption kinetics of metal ions is governed by many a complex factor like adsorption mechanism, electrostatic effect, ionic radii, electronegativity, the sorbent functional groups' preference for certain metal ions, etc^[169, 170].

Table 6.02 Lagergren second-order kinetic model parameters for Cu^{2+} and Pb^{2+} adsorption.

Entry No	Metal ion	k_2 (h g mmol^{-1})	h^a (h g mmol^{-1})	q_e (mmol g^{-1})	$q_{e,\text{exp}}$ (mmol g^{-1})	R^2
1	Cu^{2+}	88.13	3333.3	6.150	6.05	0.9963
2	Pb^{2+}	0.177	12.822	8.446	7.50	0.9987

^aInitial adsorption rate $h = k_2 q_e^2$.

It is reported that the smaller the effective ionic radius, the more closely and strongly is the ion adsorbed ^[171]. As such Cu²⁺ (0.087 nm) having a smaller effective ionic radius than that of Pb²⁺ (0.143 nm) is expected to have a faster rate of adsorption^[172]. However, the higher hydrated ionic radius of Cu²⁺ (0.419 nm) as compared to Pb²⁺ (0.401 nm) keeps it farther away from the adsorbing surface leading to weaker adsorption with lower adsorption capacity^[173]. The difference in the Pb²⁺ and Cu²⁺ ions' affinity for the aminophosphonate motifs in CAPE **5** is another important factor to be taken into account in order to rationalize the observed adsorption kinetics.

The adsorption capacity of Pb²⁺ is found to be larger than that of Cu²⁺. The experimental data so far revealed that the resin is an efficient adsorbent for the removal of both lead and copper ions from aqueous solutions.

6.3.4 Effect of initial concentration on the adsorption of Cu²⁺ and Pb²⁺ ions

As shown in Fig. 6.4, the adsorption capacity of CAPE **5** increases with the increase in initial concentration of Cu²⁺ and Pb²⁺ ions. To further explore the adsorption mechanism, Langmuir and Freundlich isotherm models were used to analyze the adsorption data.

The Langmuir isotherm equation can be expressed by Eq. (5) where it assumes the mechanism of the adsorption process as a monolayer adsorption on the surface of the polymer:

$$\frac{C_e}{q_e} = \frac{C_e}{Q_m} + \frac{1}{Q_m b} \quad (5)$$

where C_e and q_e are the concentrations of metal ion in the solution and resin, respectively, Q_m and b are the Langmuir constants.

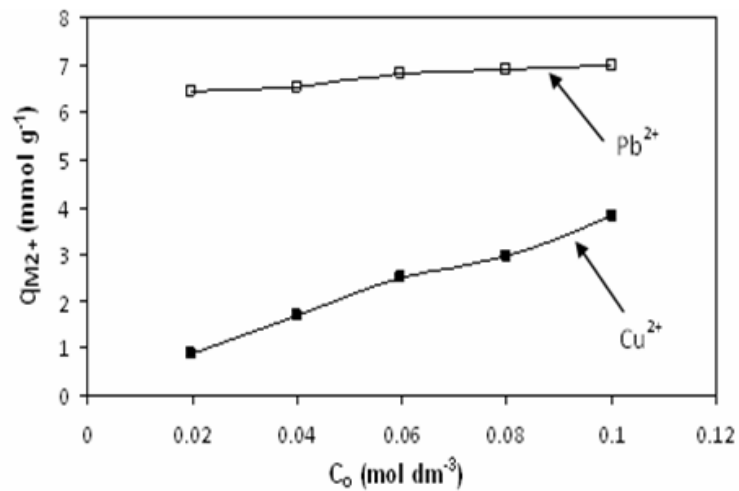


Figure 6.4 The effect of initial concentration on the adsorption capacity of CAPE 5 at pH 4 for 24 h at 25°C.

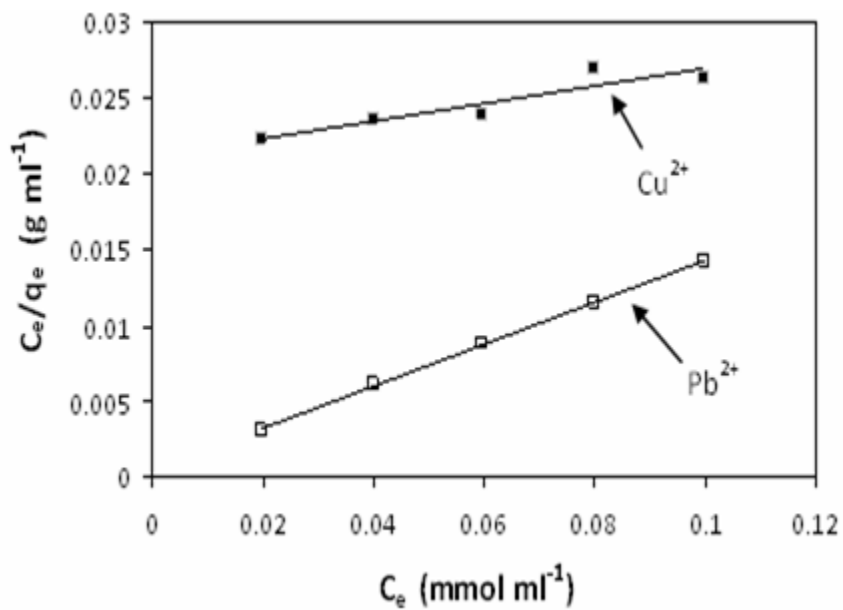


Figure 6.5 Langmuir isotherm of the adsorption of Cu²⁺ and Pb²⁺ ions on CAPE 5.

Figure 6.5 illustrates the Langmuir plot of C_e/q_e versus C_e , enabling the calculation of Langmuir constants from the intercept and slope of the linear plot. Freundlich isotherm model, on the other hand, describes the adsorption occurring on a heterogeneous surface with uniform energy; Eqs. (6) and (7) express the model:

$$q_e = k_f C_e^{1/n} \quad (6)$$

$$\log q_e = \log k_f + \frac{1}{n} \log C_e \quad (7)$$

where q_e and C_e are the equilibrium concentrations of metal ion in the adsorbed and liquid phase, respectively, k_f and n represent the Freundlich constants, which can be calculated from the slope and intercept of the linear plot of $\log q_e$ versus $\log C_e$ as presented in Figure 6.6.

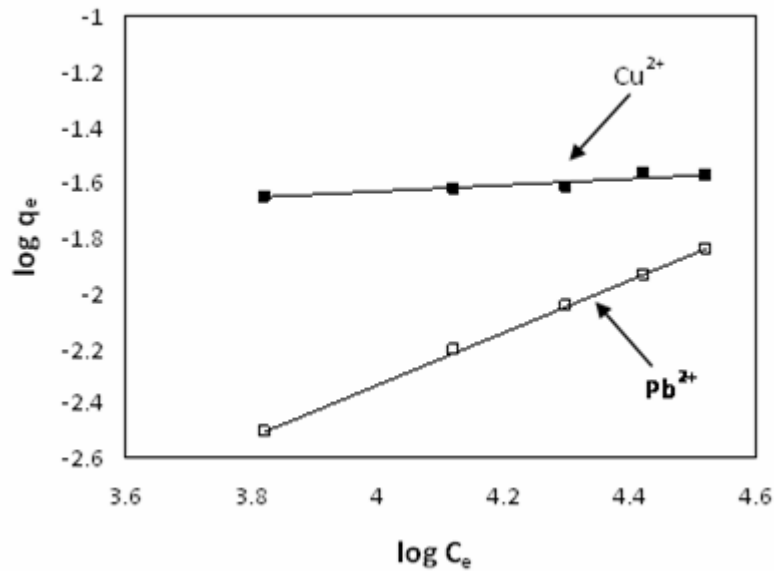


Figure 6.6 Freundlich isotherm of the adsorption of Cu^{2+} and Pb^{2+} ions on CAPE 5.

Figs. 6.5 and 6.6 illustrate that the adsorption of Pb^{2+} ions fitted well with both the Langmuir as well as Freundlich isotherm models, thereby implying that the adsorption may occur as a monolayer as well as a heterogeneous surface adsorption. For the adsorption of Cu^{2+} , the experimental data gave similar fit with both the models, albeit with poor regression coefficients (R^2). While the Pb^{2+} undergoes chemical adsorption as a result of the formation of a more stable Pb^{2+} complex with the sorbent functional groups, the poor stability of Cu^{2+} complex^[169] may encourage both physical and chemical adsorption of the ions thereby giving poor fitting with the adsorption models.

Table 6.3 Langmuir and Freundlich isotherm model constants for Cu^{2+} and Pb^{2+} adsorption.

Langmuir isotherm model				
Entry No	Metal ion	Q_m (mmol g ⁻¹)	b (dm ³ mmol ⁻¹)	R^2
1	Cu^{2+}	17.0	2.792	0.8610
2	Pb^{2+}	7.19	347.8	0.9994
Freundlich isotherm model				
Entry No	Metal ion	k_f	n	R^2
1	Cu^{2+}	0.00235	4.577	0.8483
2	Pb^{2+}	7.62×10^{-7}	1.047	0.9996

The Langmuir and Freundlich isotherm model constants are given in Table 6.3. At a pH of 4, the zwitterionic phosphonate motifs [i.e. $\text{NH}^+\cdots\text{P}(=\text{O})(\text{OH})\text{O}^-$] in CPZA **4** may partially change to zwitterionic/anionic motifs [i.e. $\text{NH}^+\cdots\text{P}(=\text{O})(\text{O}^-)^2$] which can influence the adsorption of metal ions on the resin surface by electrostatic adsorption that follows Langmuir adsorption model.

For the Langmuir isotherm model, separation factor or equilibrium parameter (R_L) can be used to describe the favorability of adsorption on the polymer surface by Eq. (8) [47].

$$R_L = \frac{1}{(1+bC_0)} \quad (8)$$

where C_0 is the initial M^{2+} concentration and b is the Langmuir equilibrium constant. A favorable adsorption is indicated when the R_L value is between $0 < R_L < 1$, whereas the value outside the range describes an unfavorable adsorption. The R_L values for the adsorption of both metal ions are given in Table 6.4, which reveals that the values fall in the preferred region (i.e. $0 < R_L < 1$). The results thus certify that CAPE **5** is a promising adsorbent for the removal of heavy metal ions in aqueous solutions.

Table 6.4 The R_L values based on the Langmuir isotherm model

C_0 (mol dm ⁻³)	R_L value	
	Cu^{2+}	Pb^{2+}
0.02	0.9471	0.1257
0.04	0.8995	0.06706
0.06	0.8565	0.04573
0.08	0.8174	0.03469
0.10	0.7817	0.02795

6.3.5 Effect of pH and temperature on adsorption

The effect pH (in the range 3-6) on the uptake of Pb^{2+} and Cu^{2+} were investigated at a fixed concentration (0.1 M) and time of 24 h. The pH of the solution was controlled by using an acetate buffer ($\text{CH}_3\text{COONa}/\text{CH}_3\text{COOH}$). Results of metal uptake at different pH are shown in Fig. 6.7. Optimum pH was found to be 4 and 6 for the adsorption of Pb^{2+} and Cu^{2+} , respectively; at higher pH values, the hydrolysis of the metal ions occurs to different extent by the formation of metal hydroxides, which compete with the metal ion uptake by the resin^[174].

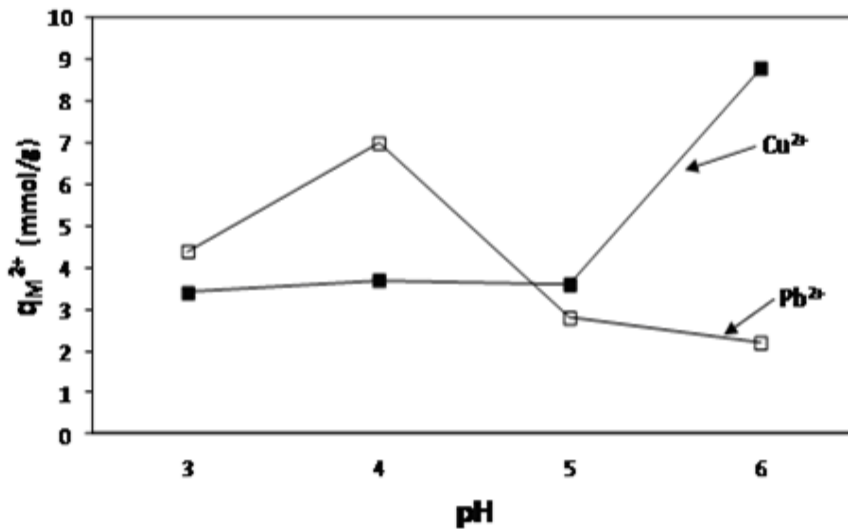


Figure 6.7 pH dependence of metal uptake by CAPE 5.

Adsorption experiments were also performed to obtain the thermodynamic parameters; the results are illustrated in Fig. 6.8.

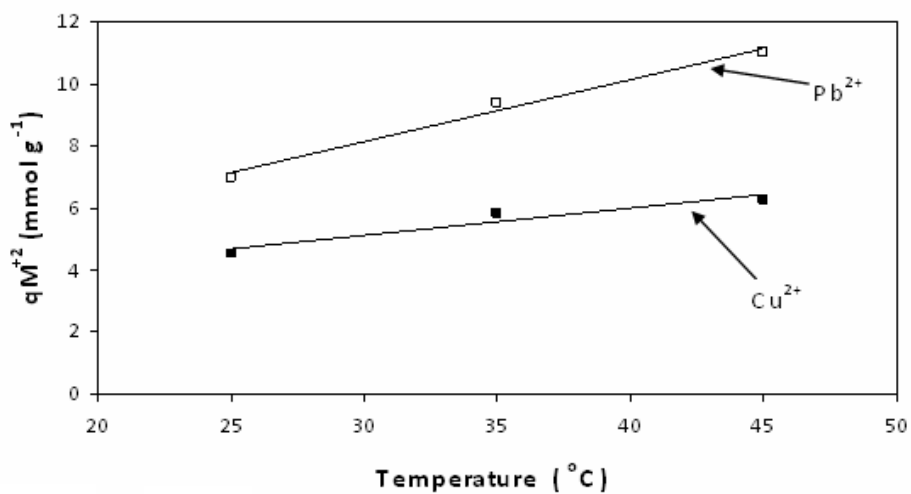


Figure 6.08 Effect of temperature on the adsorption capacity of CAPE 5.

As can be seen from the Fig., the adsorption capacity increases with the increase in temperature, suggesting that the adsorption process is endothermic, and the increased swelling of the resin permits greater diffusion of the metal ions ^[163]. The activation energy of the adsorption process can be calculated by plotting $\log q_e$ versus $1/T$ as shown in Fig. 6.9.

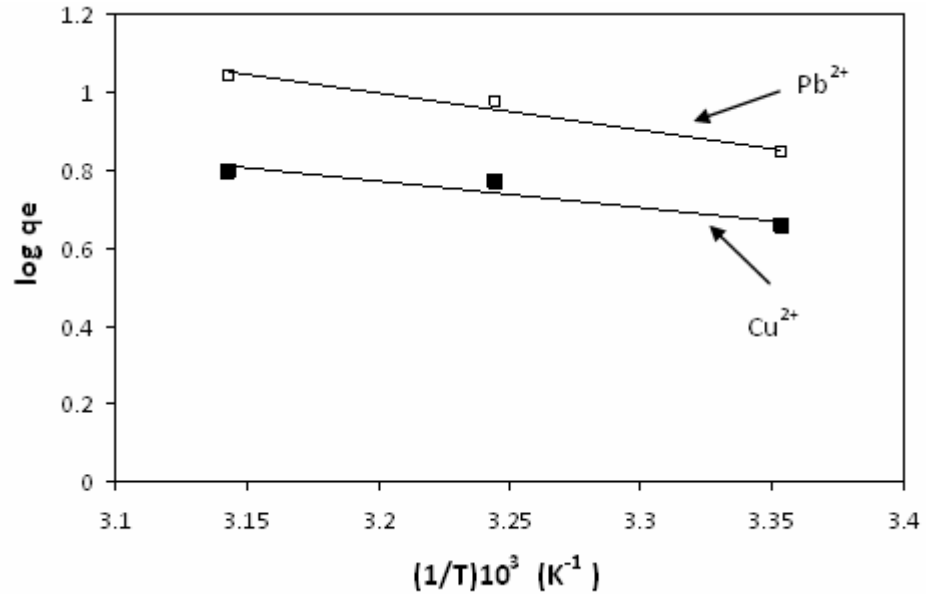


Figure 6.09 Plots of $\log q_e$ versus $(1/T) \times 10^3$.

Using Arrhenius equation [Eq. (9)], the activation energies were found to be 12.8 and 17.9 kJ/mol for the adsorption of Cu^{2+} and Pb^{2+} , respectively. These E_a values are relatively low in comparison to typical chemical reactions with activation energies of 65 – 250 kJ/mol, thereby indicating that the adsorption of the metal ions is relatively easy and a favored process^[175].

$$\log q_e = -\frac{E_a}{2.303RT} + \text{constant} \quad (9)$$

A plot of $\log (q_e/C_e)$ versus $1/T$ is displayed in Fig. 6.10. The thermodynamic parameters ΔG , ΔH and ΔS were calculated using Vant-Hoff equation [Eq. (10)], and are

tabulated in Table 6.5 ^[167]. The negative ΔG values ascertain the spontaneity of the adsorption process.

$$\log\left(\frac{q_e}{C_e}\right) = -\frac{\Delta H}{2.303RT} + \frac{\Delta S}{2.303R} \quad (10)$$

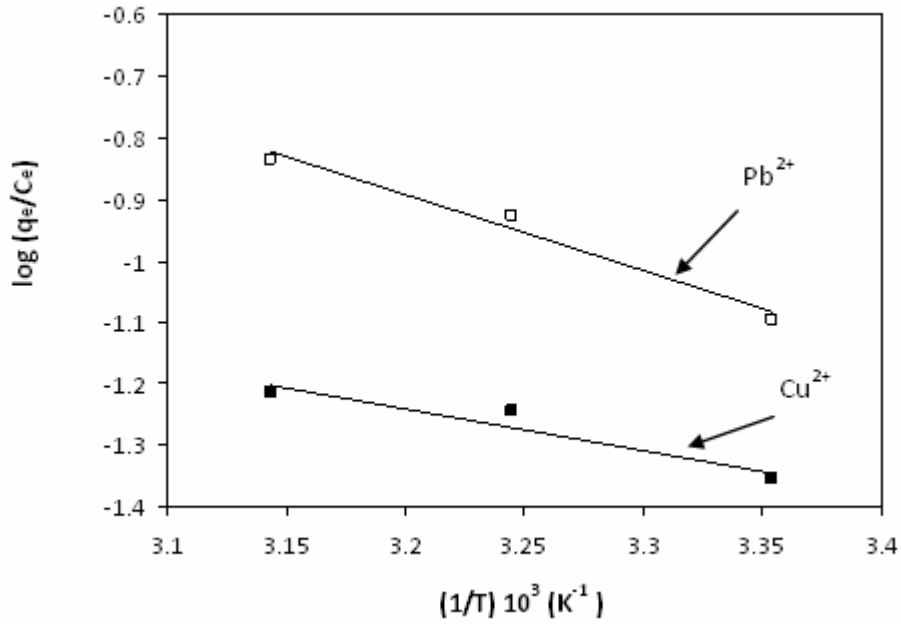


Figure 6.010. Plots of $\log(q_e/C_e)$ versus $(1/T) \times 10^3$.

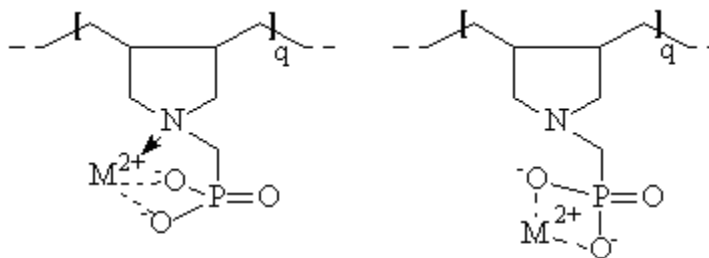
Table 6.5 Thermodynamic data for Pb²⁺ and Cu²⁺ adsorption.

Metal ion	Temp. (K)	ΔG (kJ/mol)	ΔH (kJ/mol)	ΔS (J/mol K)	R ²
Pb ²⁺	298	-17.3			
	308	-17.8	23.5	58.0	0.9774
	318	-18.4			
Cu ²⁺	298	-5.09			
	308	-5.26	12.8	17.1	0.9103
	318	-5.44			

As the temperature increases, the ΔG values become more negative, thereby indicating that the adsorption is more favorable at the higher temperatures. Favorable adsorption at higher temperatures is attributed to the greater swelling of the resin and increased diffusion of metal ions into the resin. Greater dissociation of zwitterionic phosphonate motifs, $\text{NH}^+\cdots\text{P}(=\text{O})(\text{OH})\text{O}^-$ to zwitterionic/anionic motifs, $\text{NH}^+\cdots\text{P}(=\text{O})(\text{O}^-)^2$, at elevated temperatures is also expected to increase the electrostatic attractions between the metal ions and ion exchange groups. The positive values of ΔH certify that the adsorption is an endothermic process. In addition, it can be found in Table 6.5 that the ΔS values are positive, suggesting that the randomness increased during the adsorption of metal ions as a result of the release of water molecules from their large hydration shells.

As reported in the literature^[164, 165, 176], the aminomethylphosphonate motifs are potentially tridentate ligands, having one coordination site at the nitrogen and two bonding sites at the phosphonate motif. Towards the weak acid range the formation of metal-complex using the aminophosphonate motif as a tridentate ligand (especially at low

loads) is depicted in Scheme 2. At high loads, complexes without the amino group would result using phosphonate motif as a bidentate ligand.



Scheme 2. Metal-complex: aminomethylphosphonate as tridentate and bidentate ligand.

6.3.6 Scanning electron microscopy (SEM)

Unloaded and loaded CAPE **5** were investigated by scanning electron microscopy. Unloaded CAPE **5** was immersed in 0.1 M $\text{Pb}(\text{NO}_3)_2$ and 0.1 M $\text{Cu}(\text{NO}_3)_2$ for 24 h at pH of 4, filtered, and dried under vacuum until constant weight was achieved. Loaded and unloaded polymers were then sputter-coated for 6 min with a thin film of gold. CAPE **5** SEM images (Fig. 6.11) showed that it adsorbed both metals, and the adsorption process happened on the surface and throughout the polymer (EDX analysis).

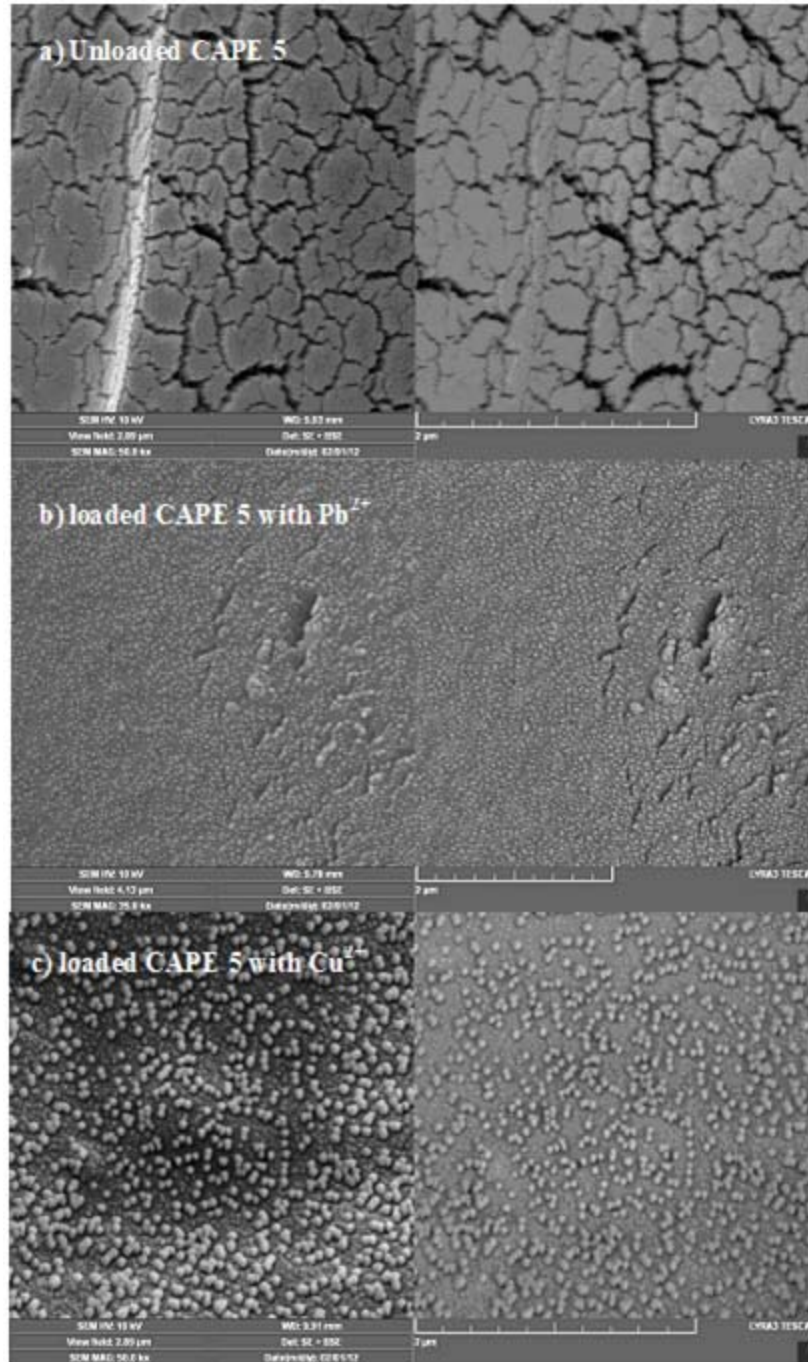


Figure 6.11 SEM images for unloaded and loaded CAPE 5 with Pb²⁺ and Cu²⁺.

6.3.7 Desorption experiment

One of the important criteria for the effective usage of adsorbent in industry is the recycling and reuse of the adsorbent. For this purpose, an experiment was conducted by immersing 100 mg resin in 20 mL of 0.1 mol dm⁻³ Cu(NO₃)₂ (or Pb(NO₃)₂) for 24 h. The loaded resin was then filtered and immersed in 1 mol dm⁻³ HNO₃ for 30 min. After filtration, the amount of Cu²⁺ ions desorbed in the filtrate was determined; the efficiency of the desorption process was calculated by the ratio of desorbed amount of Cu⁺² ions to the amount of adsorbed Cu⁺² ions in the resin. The results indicated that the percentage efficiency of the desorption process to be 77.8% and 68.3% for Cu²⁺ and Pb²⁺ ions, respectively. Based on the above findings it can be concluded that the novel cross-linked polymer used in this work is a promising candidate as an adsorbent for separation and recovery of metal ions from wastewater.

6.4 Conclusion

A novel cross-linked polyphosphonate was prepared in excellent yield from inexpensive starting materials. The resin was found to have an excellent adsorption capacity for Pb²⁺ and Cu²⁺ ions. The adsorption followed Lagergren second-order kinetic model and Langmuir as well as Freundlich isotherm models. The negative ΔG s and positive ΔH s ensured the spontaneity and the endothermic nature of the adsorption process. The excellent adsorption and very good desorption efficiencies implied the efficacy of the resin in removing as well as the recovery of the metal ions from aqueous solution. The effective recycling of the resin would enable it to be used in the treatment of contaminated water in industry. A comparison of CAPE 5 with those of different types

of sorbents in recent references reveals the excellent metal removal capacity of the current resin (Table 6.6).

Table 6.6 Comparison of CAPE 5 with those of different types of sorbents in References.

Adsorbent	Q _m for Pb ²⁺ mg/g (mmol/g)	Q _m for Cu ²⁺ mg/g (mmol/g)	Ref.
metal-complexed chitosans	105 (0.51)	–	[175]
magnetic chelating resin	597 (2.88)	–	[176]
magnetic chelating resin	–	10.4 (0.16)	[177]
fructose-mediated [poly(ethylene glycol)/chitosan] membrane	185 (0.89)	–	[178]
Cassia grandis seed gum-graft-poly(methyl methacrylate)	127 (0.61)	–	[179]
Papaya seed	–	213 (3.35)	[180]
poly(methylmethacrylate methacryloylamidoglutamic acid) beads	65.2 (0.32)	92.6 (1.46)	[181]
negatively charged hybrid adsorbents	814 (3.93)	–	[182]
negatively charged hybrid adsorbents	–	4.13 (0.065)	[183]
Novel cross-linked polyphosphonate	1488 (7.19)	1080 (17.0)	This work

CHAPTER 7: Removal of Zinc and Cadmium Ions Using a Cross-linked Polyaminophosphonate

Taken from **Othman Charles S. Al-Hamouz**, S. A. Ali, Removal of Zinc and Cadmium Ions Using a Cross-linked Polyaminophosphonate, Journal of Macromolecular Science: Pure and Applied Chemistry, 50(4) (2013) 375-384

ABSTRACT

A cross-linked polyzwitterionic acid (CPZA) containing aminophosphonic acid motifs was synthesized *via* cyclocopolymerization of diallylaminomethylphosphonic acid and cross-linker 1,1,4,4-tetraallylpiperazinium dichloride (10 mol%) using tert-butylhydroperoxide as the initiator. The CPZA upon treatment with NaOH was converted to a cross-linked anionic polyelectrolyte (CAPE 5). The adsorption of Zn^{2+} and Cd^{2+} on CAPE 5 showed that the experimental data fit the Lagergren second-order kinetic model and Langmuir, as well as Freundlich isotherm models. The adsorption capacity of Zn^{2+} was found to be higher than that of Cd^{2+} , and the adsorption process was spontaneous and endothermic in nature. The low activation energy of 11.3 and 9.3 kJ/mol for Zn^{2+} and Cd^{2+} , respectively indicated the adsorptions as a favorable process. The resin demonstrated excellent adsorption efficiency in removing the metal ions from aqueous solution.

KEY WORDS: adsorption; cross-linked polyaminophosphonate; heavy metal ions.

7.1 Introduction

Contamination from toxic metal ions has attracted significant attention owing to their negative effects on the environment. These toxic pollutants are non-biodegradable and can accumulate in the human body causing a variety of diseases and disorder^[184, 185]. The release of many metal ions from various industries poses the greatest danger to the environment and is a matter of grave concern. Metals such as zinc and cadmium are used in mining, metal coating, and battery production. Contamination by Zn^{2+} is considered a priority by the Environmental Protection Agency (EPA) because it gives rise to serious poisoning cases leading to dehydration, stomachache, dizziness and incoordination in muscles^[186]. Cd^{2+} , on the other hand, causes kidney failure, nervous system damage, bone damage, as well as other serious illness^[187].

Several techniques have been proposed for the removal of toxic metal ions such as adsorption, precipitation, dialysis, ion exchange, reverse osmosis and extraction. One of the most attractive techniques is the adsorption process due to the availability of different types of effective adsorbents^[48, 49, 52, 55, 188]. Inorganic/organic polymer hybrid adsorbents have been widely investigated, and their efficacy in the removal of metal ions has been attributed to the formation of a stronger chemical bonding between M^{n+} and, for instance, amine motifs in the hybrid materials^[61, 189-192]. Recently researchers have focused on the synthesis of zwitterionic cross-linked inorganic/organic hybrid materials in removing heavy metal ions via electrostatic effects^[59, 60, 62, 184, 193].

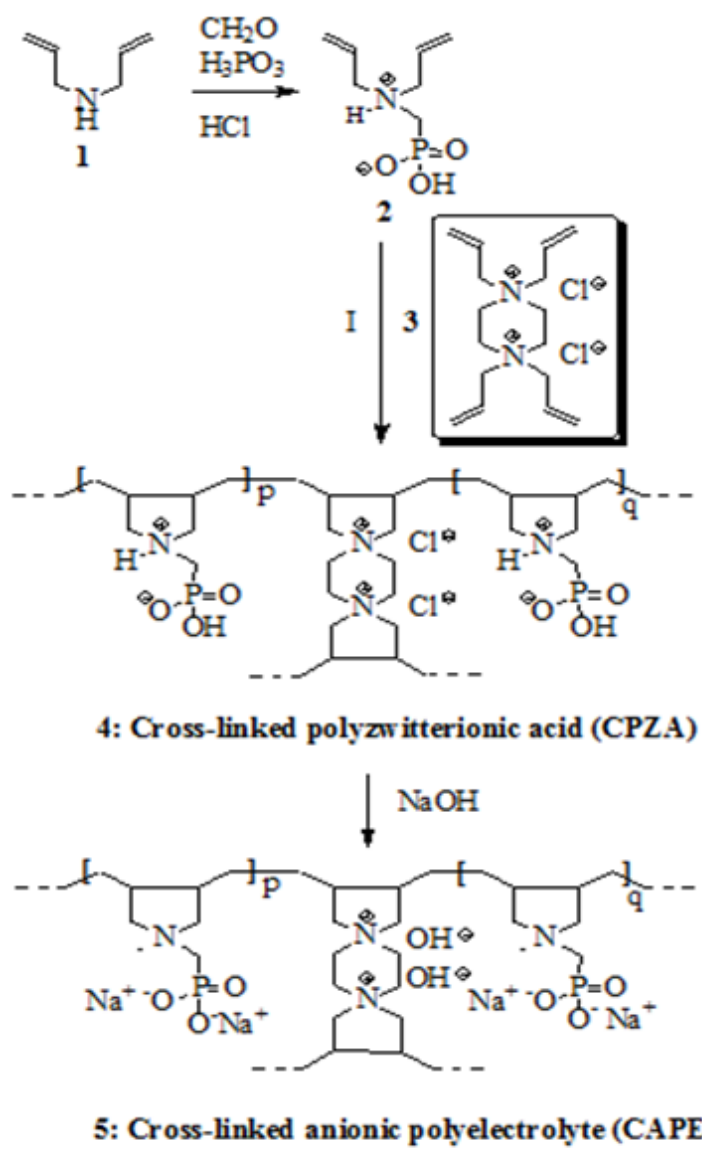
A titania-phosphonate hybrid porous material has been found to have a large capacity for selective adsorption of Cd^{2+} ions^[61, 192]. Considerable attention has been given to synthesize chelating agents containing aminomethylphosphonate motifs owing to its extraordinary chelating properties in extracting heavy metal ions from waste

water^[65]. Recently, we have synthesized novel cross-linked polymer (CAPE 5) containing aminomethylphosphonate motifs and examined its excellent efficacy as an adsorbent for the removal of toxic metal ions like Pb^{2+} and Cu^{2+} ions from aqueous solutions (Sch. 1)^[194]. In this paper, we report the efficiency of CAPE 5 in the removal of toxic metal ions Zn^{2+} and Cd^{2+} from aqueous solutions.

7.2 Experimental

7.2.1 Physical Methods

IR spectra were recorded on a Perkin-Elmer 16F PC FTIR spectrometer. Scanning electron microscopy images were taken by TESCAN LYRA 3 (Czech Republic) Equipped with Oxford, energy-dispersive X-ray spectroscopy (EDX) detector model X-Max. Thermogravimetric analysis (TGA) was performed using a thermal analyzer (STA 429) manufactured by Netzsch (Germany). The polymer sample to be tested (usually ~5 mg) was placed in a platinum crucible. Aluminum oxide (Al_2O_3 ; ~4 mg) was placed in an identical platinum crucible as a reference sample. With the sample carrier system, which had two sets of 10% Pt–Pt/Rh thermocouples, the sample carrier was placed in the middle of the vertical furnace, which was programmed and controlled by a microprocessor temperature controller. The temperature was raised at a uniform rate of 10°C/min. The analyses were made over a temperature range of 20–800°C in an air atmosphere flowing at a rate of 100 mL/min.



Scheme 1.

7.2.2 Materials

Diallyl amine, tertiary butylhydroperoxide (TBHP) (70% in water), paraformaldehyde and phosphorous acid from Fluka Chemie AG (Buchs, Switzerland) were used as received. All solvents used were of analytical grade.

7.2.3 Synthesis of Monomers and Polymers

Diallylaminomethylphosphonic acid **2**^[65] and the cross-linker **3**^[64] have been synthesized as described in the literature. The synthesis of cross-linked polyzwitterionic acid (CPZA) **4** and its transformation to cross-linked anionic polyelectrolyte (CAPE) **5** have been described elsewhere^[194]. Thus, monomer **2** (90 mol%) and **3** (10 mol%) in water (monomers/water wt% 65:35) using TBHP as the initiator at 85°C for 24 h afforded CPZA **4** (78%), which upon treatment with NaOH, gave CAPE **5** in the form of powder.

7.2.4 Sample Characterization

FT-IR spectra have been recorded on a Perkin-Elmer 16F PC FTIR spectrometer in the region of 4000-400 cm⁻¹. Ion exchange capacity (IEC) was determined by the titrimetric analysis method ((Eq. (1)). The weighed polymer (100 mg) was immersed in 50 ml of 0.1 M hydrochloric acid for 24 h. The ion exchange capacity was determined from the decrease in acidity by titration with 0.1 M NaOH solution.

$$IEC = \frac{mmol_i - mmol_f}{W} \quad (1)$$

Where $mmol_i$ and $mmol_f$ are the initial and final amount of HCl in mmol, respectively; W is the weight of the polymer in g^[156]. Thermal stability of CAPE **5** was determined by Thermogravimetric analysis (TGA).

7.2.5 Adsorption Experiments

The adsorption properties of the cross-linked polymer CAPE **5** for Zn^{2+} and Cd^{2+} ions were determined by titration; the procedure for Zn^{2+} adsorption was as follows: A mixture of CAPE **5** (50 mg) in 20 ml of 1000 ppm Zn^{2+} solution [prepared from $Zn(NO_3)_2$] was stirred using a magnetic stir-bar at different pH for 24 h. The resin was filtered and carefully washed with deionized water. The combined filtrate was titrated with 0.1 M EDTA solution to find out the amount of Zn^{2+} remained. The adsorption capacity ($q_{Zn^{2+}}$) can be calculated using Equation 2:

$$q_{Zn^{2+}} = \frac{(C_o - C_f)V}{W} \quad (2)$$

Where C_o and C_f are the initial and final concentration of Zn^{2+} ions in $mg\ L^{-1}$, respectively, W is the weight of the polymer in g and V is the volume of the solution in L.

The adsorption kinetic curves were determined by inserting the polymer in solution (1000 ppm metal ion) at a preferred pH for different times. Adsorption isotherm was constructed by changing the initial solution concentration from 200 to 1000 ppm of Zn^{2+} at 25°C for 24 h. Thermodynamic parameters ΔG , ΔH and ΔS were calculated using data from experiments carried out at different temperatures. Similar procedure was conducted for the adsorption of Cd^{2+} using $Cd(NO_3)_2$ solutions^[195].

7.3 Results and Discussion

The synthesis of CAPE **5** involved the Butler's cyclopolymerization process using monomer **2** and crosslinker **3**^[194]. Butler's cyclopolymerization protocol gives polymers having five-membered ring embedded in the backbone (Sch. 1). The polymer architecture thus obtained has been classified as the eighth major structural feature of synthetic high polymers^[196]. To our knowledge, so far there is only one report^[194] that describes the use of the cross-linked cyclopolymer of the type **5** in the adsorption of toxic ions like Cu²⁺ and Pb²⁺.

7.3.1 Ion Exchange Properties and Thermal Stability of CAPE **5**

The ion exchange capacity (IEC) of CAPE **5** was found to be 6.98 mmol/g, which ascertained the excellent ability of the resin to adsorb metal ions (M²⁺) as a result of the presence of chelating ligands of -N: and phosphonate motifs -P(=O)O₂²⁻. IR spectra (Fig. 7.1) shows a shift of the -P=O and -P-O bands at 1049 and 969 cm⁻¹ of the unloaded resin upward to 1140 and 1073 in the case of Zn²⁺ and to 1179 and 1021 cm⁻¹ in the case of Cd²⁺ with an increase in the intensity and broadness of the peaks^[185]. The C-N absorption was found in near ~1450 cm⁻¹. The peaks around 1650 cm⁻¹ were ascribed to the H-O-H bending vibration. The appearances of new strong bands at 1384 cm⁻¹ were attributed to the presence of ionic nitrate group since the adsorption process was carried out in the presence of metal nitrates^[165]. The presence of these strong bands thereby implies the ability of the resin to act as an anion exchanger at pH 4. At pH 4, there will be considerable amount of NH⁺...P(=O)(O⁻)₂ and NH⁺...P(=O)(OH)₂ motifs which can act as an anion exchanger. Note that the absorption band attributed to the nitrate ion is absent in the unloaded resin (Fig. 7.1).

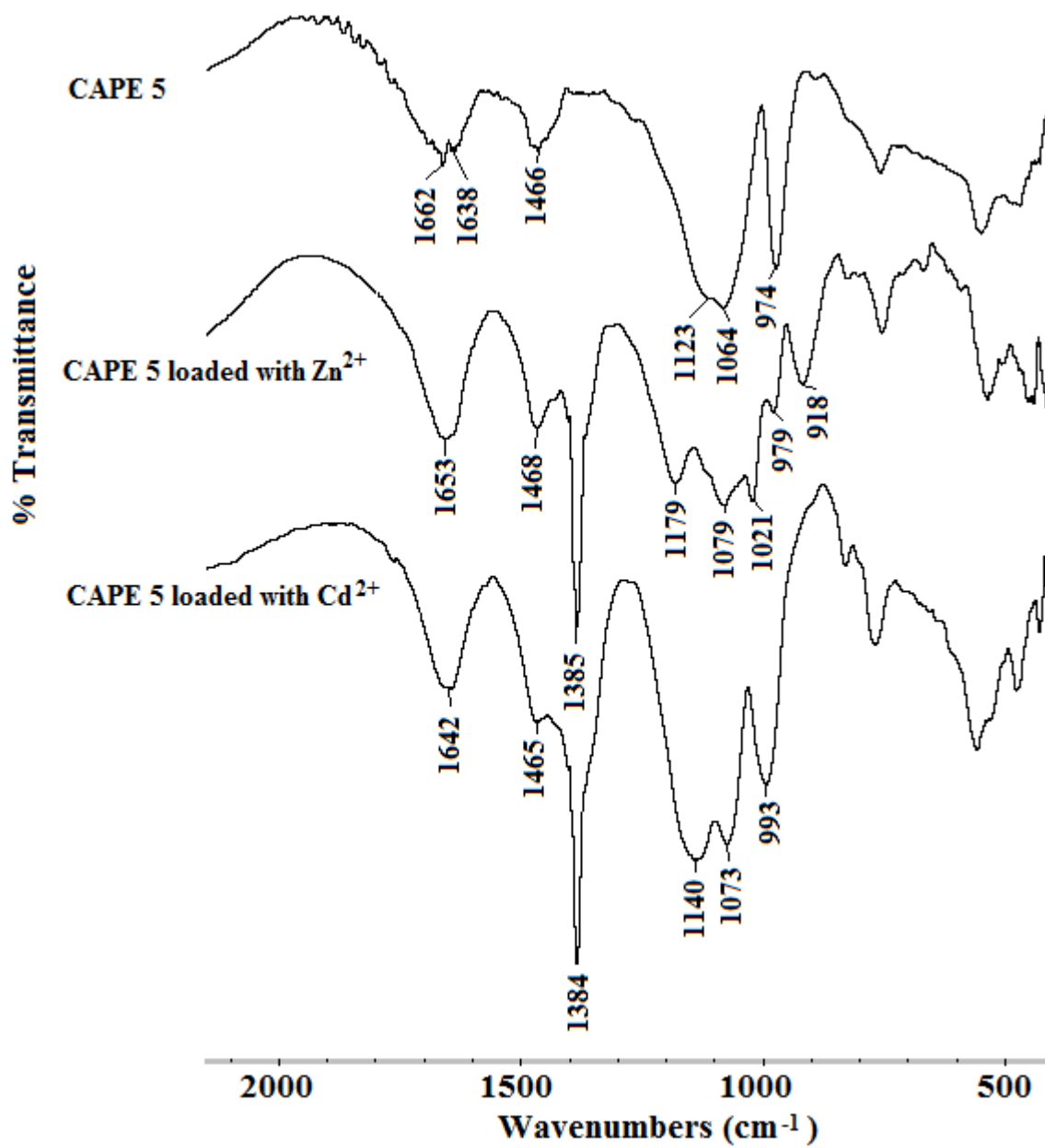


Figure 7.1 FT-IR of unloaded and loaded CAPE 5 with Zn²⁺ and Cd²⁺.

Thermogravimetric analysis (TGA) curve of the cross-linked polymer (Fig. 7.2) showed two fractions in weight loss, the first slow weight loss of 6% was attributed to the loss of trapped water in the cross-linked polymer, the second major loss was 48.8%, which is due to the combustion of nitrogenated organic fraction with the release of CO₂, NO_x and H₂O gases, the residual mass at 800°C was found to be 45.2% which may be attributed to Na₂O.1.5P₂O₅^[163].

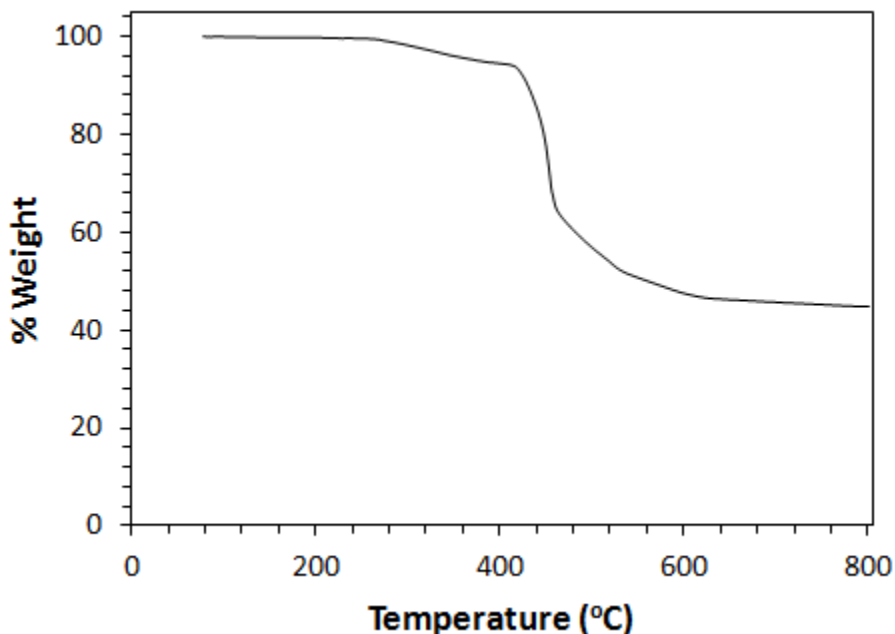


Figure 7.02 TGA curve for CAPE 5.

7.3.2 Adsorption Kinetics

Figure 7.3a shows the adsorption rate of the metal ions at different times. The adsorption rate for both Zn²⁺ and Cd²⁺ increases for 2 h, then reaches equilibrium showing a fast adsorption process that can be useful for industrial application. It has been reported that the Lagergren adsorption kinetic model is a suitable tool to investigate the

adsorption properties of a polymer^[47]. The following equations express the linearly first-order and second-order kinetic equations (Eqs. 3 and 4) for the Lagergren model, respectively:

$$\log (q_e - q_t) = \log q_e - \frac{k_1 t}{2.303} \quad (3)$$

$$\frac{t}{q_t} = \frac{1}{k_2 q_e^2} + \frac{t}{q_e} \quad (4)$$

Where k_1 and k_2 are the first-order and second-order rate constant, respectively; q_t and q_e are the adsorption capacity of the metal ions at a time t and at equilibrium, respectively. Neither Zn^{2+} nor Cd^{2+} fit the first-order Lagergren kinetic model, so the graph representing the kinetic model has not been displayed, while the second-order Lagergren kinetic model (Fig. 7.3b, Table 7.1) fit the adsorption of both Zn^{2+} and Cd^{2+} ions. The data fit with the second-order model suggesting that the adsorption is a chemical adsorption process^[197, 198]. The resin was found to be an efficient adsorbent for removing both zinc and cadmium ions from aqueous solutions; the rate of adsorption and adsorption capacity of Zn^{2+} was found to be larger than that of Cd^{2+} (Table 7.2)^[199]. A metal ion loses water ligands and becomes the bare cations when it enters into interlayer of the resin. A comparison of the several characteristic parameters of Zn^{2+} and Cd^{2+} ions reveals that the difference in their adsorption behaviour lie with the notable difference in their ionic radii. The larger ionic radius of Cd^{2+} should cause a quick saturation of adsorption sites because of steric effects.

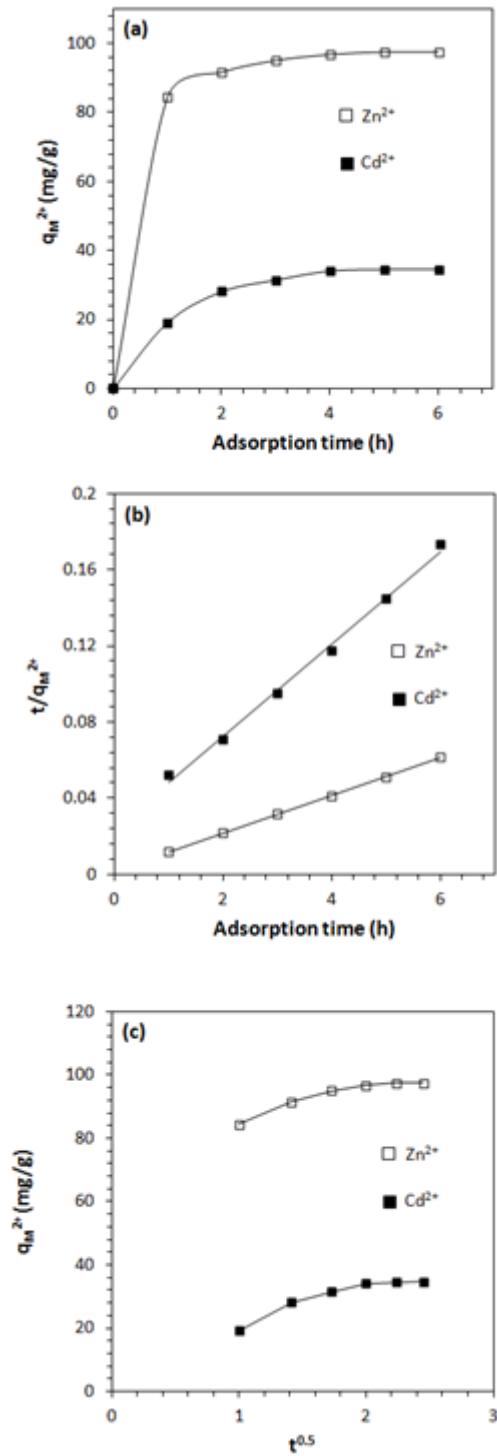


Figure 7.03. (a) Effect of time on the adsorption capacity; (b) Lagergren second-order kinetic model.(c) intraparticle diffusion model.

Table 7.1 Lagergren second-order kinetic model parameters for Zn²⁺ and Cd²⁺ adsorption.

CAPE	Temp (K)	q_e, exp (mg g ⁻¹)	k_2 (h ⁻¹ g mg ⁻¹)	h^a (h ⁻¹ g ⁻¹ mg)	q_e, cal (mg g ⁻¹)	R^2	E_a (kJ mol ⁻¹)
Zn ²⁺	298	98	0.0516	526.3	101	0.9999	11.3
	308	120	0.0611	909.1	122	1.0000	
	323	137	0.0741	1428.6	138	0.9998	
Cd ²⁺	298	35	0.0242	41.3	41	0.9951	9.30
	308	45	0.0275	70.9	51	1.0000	
	323	51	0.0324	101.0	56	0.9991	

^aInitial adsorption rate $h = k_2 q_e^2$.

Table 7.02 Ionic radius, effective hydrated ionic radius, hydration energy, electronegativity, and hardness Index of Zn²⁺ and Cd²⁺ ions

Metal ion	Ionic radius (nm)	Hydration energy (kJ mol ⁻¹)	Hydration radius (nm)	Electronegativity (Pauling)	Hardness Index
Zn ²⁺	0.083	-2057	0.276	1.65	0.115
Cd ²⁺	0.097	-1827	0.263	1.69	0.081

The adsorption data may also be described by some adsorption diffusion models which are always constructed on the basis of three consecutive steps: (1) film diffusion (i.e., diffusion across the liquid film surrounding the adsorbent particles); (2) intraparticle diffusion (i.e., diffusion in the liquid contained in the pores and/or along the pore walls); and (3) mass action (i.e., physical adsorption and desorption between the adsorbate and active sites). The intraparticle diffusion model assumes that the metal ions are transported from the solution through an interface between the solution and the adsorbent (i.e., film diffusion) followed by a rate-limiting intraparticle diffusion step which bring them into

the pores of the particles in the adsorbent. The following equation expresses the relation of the adsorption capacity and time^[200, 201]:

$$q_t = x_i + k_p t^{0.5} \quad (5)$$

Where q_t is the adsorption capacity at time t , k_p is the rate constant of intraparticle diffusion, x_i is related to boundary layer thickness. The adsorption process is governed by the intraparticle diffusion in the case of a straight line fit for the plot of q_t vs. $t^{0.5}$. The curves in Figure 7.3c, however, show that the adsorption happens via a rapid diffusion within 2 h, then reaches equilibrium. The poor regression coefficients of 0.8787 and 0.8673 for Zn^{2+} and Cd^{2+} , respectively, conclude that the rate determining step is not governed by intraparticle diffusion alone.

7.3.3 Effect of Initial Concentration on the Adsorption of Copper and Lead Ions

As shown in Figure 7.4a, the adsorption capacity of CAPE 5 increased with increasing the concentrations of Zn^{2+} and Cd^{2+} ions. Two isotherm models were applied; Langmuir isotherm model which can be expressed by Equation 6, where it assumes the mechanism of the adsorption process as a monolayer adsorption on the surface of the polymer:

$$\frac{C_e}{q_e} = \frac{C_e}{Q_m} + \frac{1}{Q_m b} \quad (6)$$

Where C_e and q_e are the concentration of metal ions in the solution and on the resin, respectively, Q_m and b are the Langmuir constants. Figure 7.4b represents the plot of C_e/q_e vs. C_e . The Freundlich isotherm model, on the other hand, describes the adsorption occurring on a heterogeneous surface with uniform energy; Equations 7 and 8 express the model:

$$q_e = k_f C_e^{1/n} \quad (7)$$

$$\log q_e = \log k_f + \frac{1}{n} \log C_e \quad (8)$$

Where q_e and C_e are the equilibrium concentrations of metal ions on the adsorbed and in the liquid phase, respectively; k_f and n represent the Freundlich constants, which can be calculated from the slope and intercept of Figure 7.4c which shows the plot of $\log q_e$ vs. $\log C_e$.

Figures 7.4(b and c) illustrate that adsorption of Zn^{2+} and Cd^{2+} ions fit well with both Langmuir and Freundlich isotherm models (Table 7.3). The maximum adsorption capacity (Q_m) found by the Langmuir isotherm model was very close to the experimental data supporting that the adsorption mechanism could be monolayer adsorption. The fitness of data with Freundlich isotherm model could also support that the adsorption occurred on a heterogeneous surface.

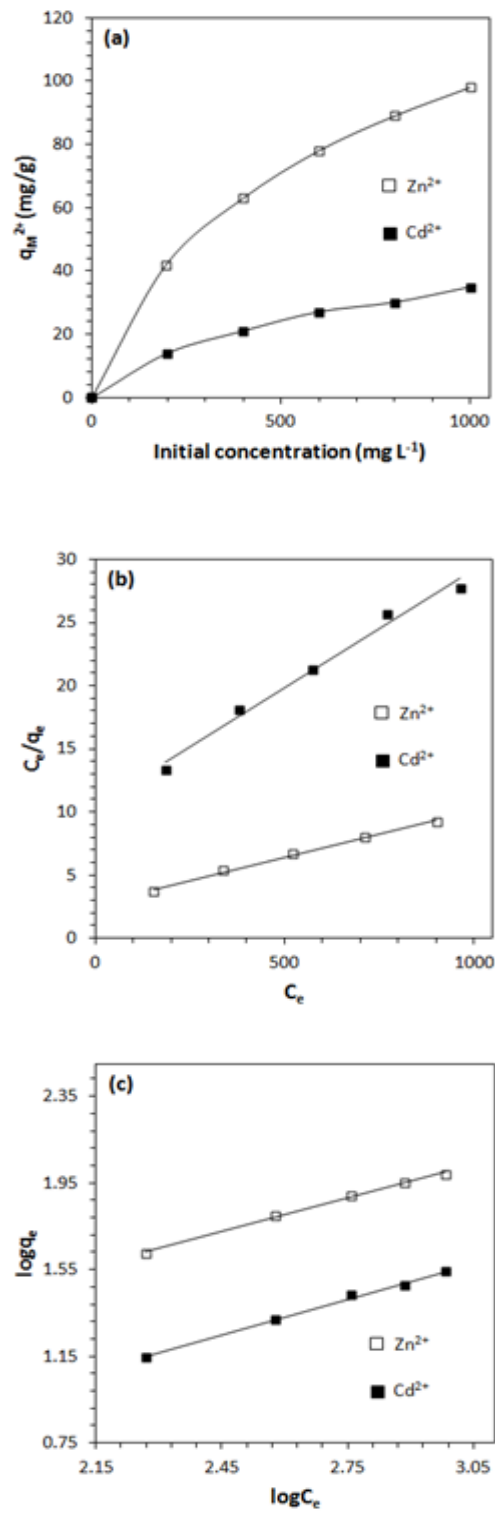


Figure 7.4 (a) Effect of initial concentration on the adsorption capacity; (b) Langmuir isotherm plot; (c) Freundlich isotherm plot.

Table 7.3 Langmuir and Freundlich isotherm model constants for Zn²⁺ and Cd²⁺ adsorption.

Langmuir Isotherm Model				
Entry No	Metal ion	Q _m (mg g ⁻¹)	b (dm ³ mg ⁻¹)	R ²
1	Zn ²⁺	136.97	2.67×10 ⁻³	0.9949
2	Cd ²⁺	53.48	1.79×10 ⁻³	0.9857

Freundlich Isotherm Model				
Entry No	Metal ion	k _f	n	R ²
1	Zn ²⁺	2.868	1.935	0.9966
2	Cd ²⁺	0.807	1.825	0.9966

For the Langmuir isotherm model, separation factor or equilibrium parameter (R_L) can be used to describe the favorability of adsorption on the polymer surface by Equation 9 [47, 184].

$$R_L = \frac{1}{(1 + bC_0)} \quad (9)$$

Where C_0 is the initial M^{2+} concentration and b is the Langmuir equilibrium constant. A favorable adsorption is indicated when the R_L value is between $0 < R_L < 1$, whereas the R_L values outside the range describes an unfavorable adsorption. The R_L values for the adsorption of both metal ions are given in Table 7.4, which reveals that R_L values fall in the preferred region ($0 < R_L < 1$). The results thus certify that CAPE 5 is a promising adsorbent for the removal of heavy metal ions in aqueous solutions.

Table 7.4 The R_L values based on the Langmuir isotherm model.

C_o ($mg L^{-1}$)	R_L value	
	Zn^{2+}	Cd^{2+}
200	0.6517	0.7364
400	0.4834	0.5828
600	0.3842	0.4822
800	0.3187	0.4112
1000	0.2723	0.3584

7.3.4 Effect of pH on Adsorption

Adsorption experiments at different pHs (3–6) have been carried out; the optimum pH was found to be 4 for adsorption of both the metal ions. As shown in Figure 7.5, the adsorption capacity increased by increasing the pH, which could be due to the increase of the anionic motifs [i.e., $NH^+ P(=O)(O^-)_2$ and $NP(=O)(O^-)_2$] that would impart stronger attraction to the metal ions. Whereas, at lower pH (pH=3), the increased amount of cationic motifs (i.e. $NH^+ \cdots P(=O)(OH)_2$) discourages the adsorption of metal cations, thereby leading to lower adsorption capacity. At higher pH, metal hydrolysis occurs owing to the formation of metal hydroxides which interfere in the determination of the adsorption capacity^[174].

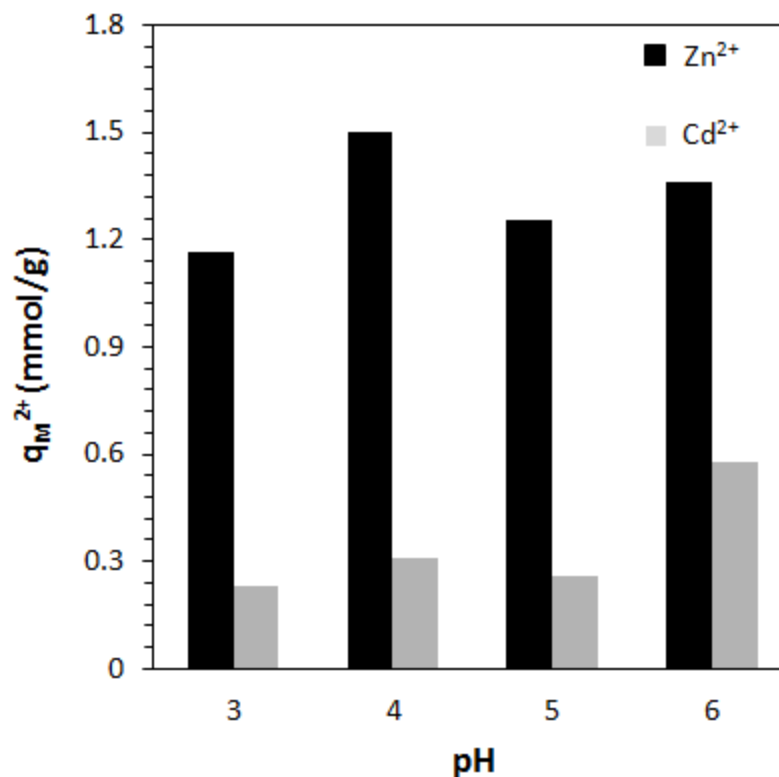


Figure 7.05 Effect of pH on the adsorption capacity.

7.3.5 Effect of Temperature on Adsorption

Adsorption experiments were performed to study the effect of temperature on the adsorption capacity (Fig. 7.6a). Increased adsorption capacity at higher temperatures suggests the adsorption as an endothermic process. Swelling of the polymer at higher temperatures permits greater diffusion of metal ions^[161]. Using the Arrhenius equation (Eq. 10), a plot of $\ln k_2$ vs. $1/T$ (Fig. 7.6b) can be used to calculate the activation energies which were found to be 11.3 and 9.30 kJ/mol for the adsorption of Zn^{2+} and Cd^{2+} , respectively. These E_a values are relatively low in comparison to typical chemical

reactions with activation energies of 65 –250 kJ/mol, thereby indicating that the adsorption of the metal ions is relatively easy and a favored process^[174].

$$\ln k_2 = - \frac{E_a}{RT} + \text{constant} \quad (10)$$

Thermodynamic parameters ΔG , ΔH and ΔS were calculated using the Vant-Hoff equation (Eq. 11). A plot of $\log (q_e/C_e)$ vs. $1/T$ is displayed in Figure 7.6c and are tabulated in Table 7.5^[174, 175]. The negative ΔG values ascertain the spontaneity of the adsorption process.

$$\log \left(\frac{q_e}{C_e} \right) = - \frac{\Delta H}{2.303RT} + \frac{\Delta S}{2.303R} \quad (11)$$

As the temperature increases the ΔG values become more negative thereby indicating that the endothermic adsorption is more favorable at higher temperatures. Favorable adsorption at higher temperatures is attributed to the greater swelling of the resin and increased diffusion of metal ions into the resin. Greater dissociation of zwitterionic phosphonate motifs, $\text{NH}^+\cdots\text{P}(=\text{O})(\text{OH})\text{O}^-$ to zwitterionic/anionic motifs, $\text{NH}^+\cdots\text{P}(=\text{O})(\text{O}^-)_2$, at elevated temperatures is also expected to increase the electrostatic attractions between the metal ions and ion exchange groups. The positive values of ΔH certify that the adsorption is an endothermic process. In addition, it can be found in Table 7.5 that the ΔS values are positive, suggesting that the randomness increased during adsorption of metal ions as a result of release of water molecules from the large hydration shells of the metal ions.

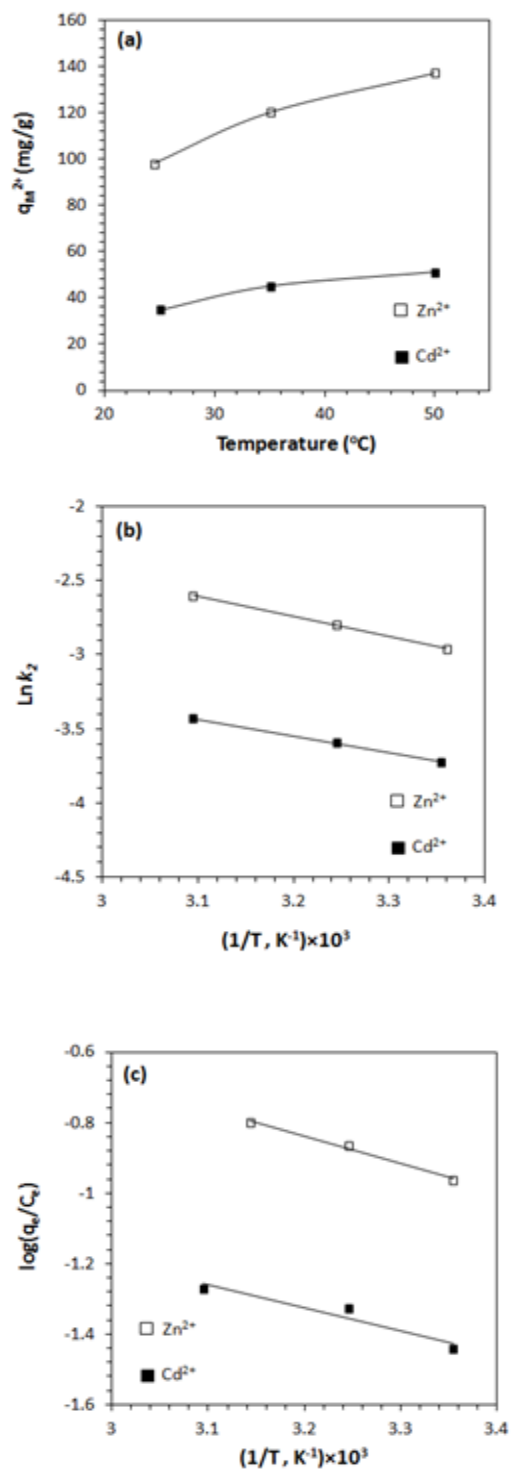
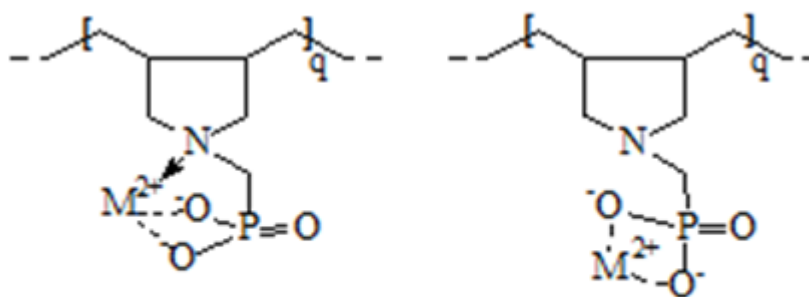


Figure 7.6 (a) Effect of temperature on the adsorption capacity; (b) Arrhenius plot; (c) Vant-Hoff plot.

Table 7.05 Thermodynamic Data for Zn²⁺ and Cd²⁺ adsorption.

Metal ion	Temp. (K)	ΔG (kJ/mol)	ΔH (kJ/mol)	ΔS (J/mol K)	R ²
Zn ²⁺	298	-9.50			
	308	-9.80	15.0	31.9	0.9909
	323	-10.3			
Cd ²⁺	298	-4.29			
	308	-4.44	12.5	14.4	0.9197
	323	-4.65			

As reported in the literature ^[165, 167, 185], the aminomethylphosphonate motifs are potentially tridentate ligands, having one coordination site at the nitrogen and two bonding sites at the phosphonate motif. Towards the weak acid range, the formation of metal-complex using the aminophosphonate motif as a tridentate ligand (especially at low loads) is depicted in Scheme 2. At high loads, complexes without the amino group would result using phosphonate motif as a bidentate ligand.



Scheme 2.

7.3.6 Scanning Electron Microscopy (SEM)

Unloaded and loaded CAPE **5** were investigated by scanning electron microscopy. Unloaded CAPE **5** was immersed in each 1000 ppm solution of Zn(II) and Cd(II) for 24 h at pH 4, filtered, and dried under vacuum until constant weight was achieved. Loaded and unloaded polymers were then sputter-coated for 4 min with a thin film of gold. CAPE **5** SEM images (Fig. 7.7) showed that it adsorbed both metals, and the adsorption process happened on the surface as well as throughout the polymer which was confirmed by Energy-dispersive X-ray spectroscopy (EDX analysis).

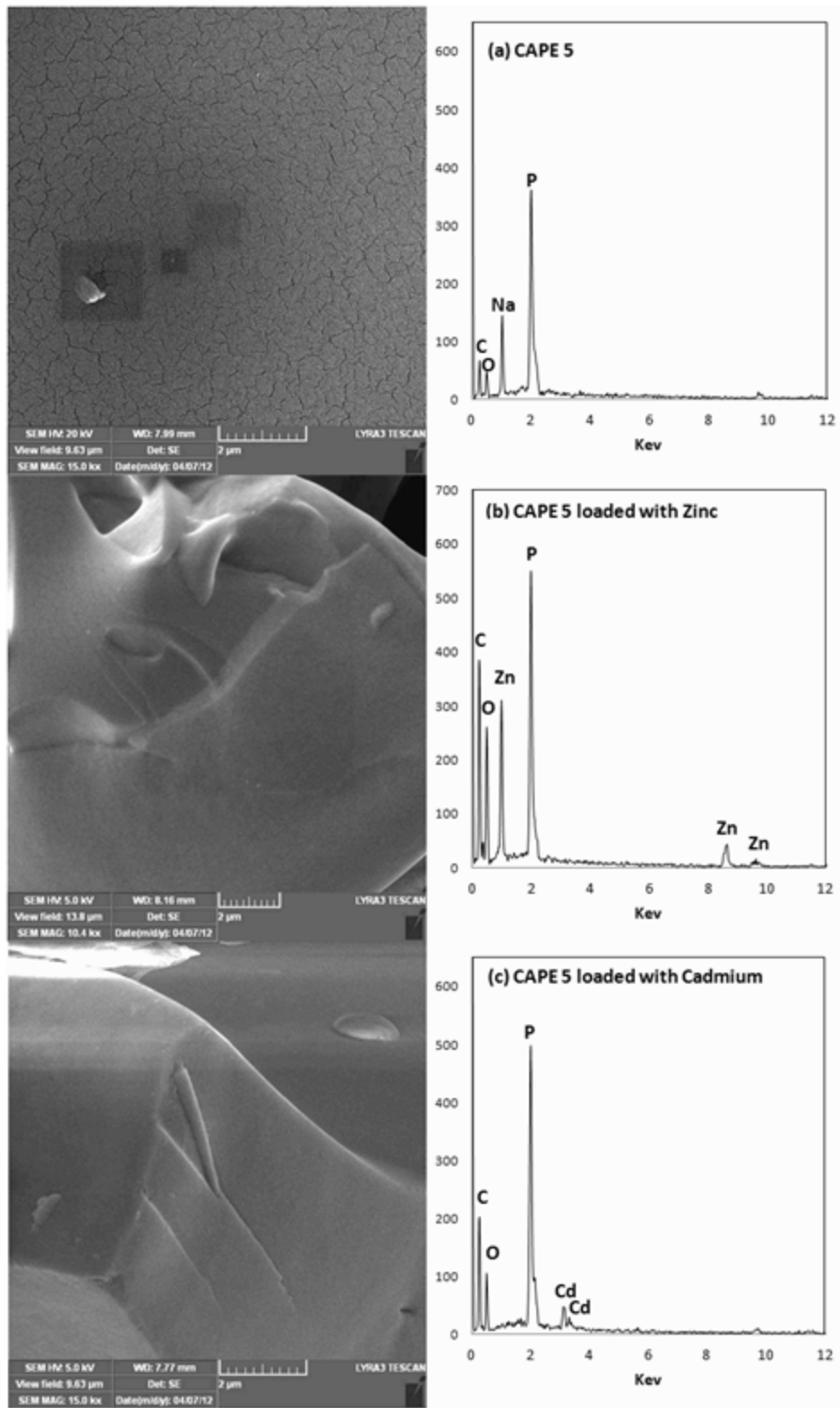


Figure 7.07. SEM images and EDX analysis for:(a) CAPE 5; (b) CAPE 5 loaded with Zinc; (c) CAPE 5 loaded with Cadmium.

7.4 Conclusions

The cross-linked polyphosphonate **5** was found to have an excellent adsorption capacity for Zn^{2+} and Cd^{2+} ions. The adsorption followed the Lagergren second-order kinetic model and Langmuir as well as the Freundlich isotherm models. The negative ΔGs and positive ΔHs ensured the spontaneity and the endothermic nature of the adsorption process, respectively. The adsorption capacities of CAPE **5** for Zn^{2+} and Cd^{2+} ions are compared with those of various types of sorbents in Table 7.6 which ascertains the excellent efficacy of the current resin for the removal of the metal ions.

Table 7.06 Comparison of CAPE 5 with those of different types of sorbents in References.

Adsorbent	Zn^{2+} ($mg\ g^{-1}$)	Cd^{2+} ($mg\ g^{-1}$)	Refs
Na-Montmorillonite	3.6	5.2	[202]
Coffee residue-clay	13.4	39.5	[203]
Blast-furnace slag	103	–	[204]
red mud	14.9	10.6	[205]
manganese ore	98.0	59.2	[206]
Activated carbon	–	8.0	[207]
CAPE 5	137	53.4	This work

CHAPTER 8: A Novel Cross-linked Polyphosphonate for the Removal of Pb²⁺ and Cu²⁺ from Aqueous Solution

Taken from **Othman Charles S. Al-Hamouz**, Shaikh A. Ali, Novel Cross-linked Polyphosphonate for the Removal of Pb²⁺ and Cu²⁺ from Aqueous Solution, Industrial & Engineering Chemistry Research, 51(43) (2012) 14178–14187.

Abstract

A novel cross-linked polyzwitterionic acid (CPZA) was synthesized via cyclopolymerization of diallylaminomethylphosphonic acid (90 mol %) and 1,1,4,4-tetraallylpiperazinium dichloride (10 mol%), a cross-linker, with sulfur dioxide in the presence of azoisobutyronitrile (AIBN) in dimethylsulfoxide (DMSO) at 65 °C. CPZA, upon treatment with NaOH, was converted into a cross-linked anionic polyelectrolyte (CAPE). The experimental data for the adsorption of Pb²⁺ and Cu²⁺ on CAPE fitted Lagergren second-order kinetic model and Langmuir as well as Freundlich isotherm models. The adsorption capacity of Pb²⁺ was higher than that of Cu²⁺ and the rate of adsorption of both metals was found to be almost equal. The maximum adsorption capacity of Pb²⁺ and Cu²⁺ were determined to be 2.76 and 2.22 mmol g⁻¹, respectively. The adsorption process was spontaneous and endothermic in nature with negative and positive values for ΔG and ΔH , respectively. The relatively low activation energies of 25.5 and 27.1 kJ/mol for Pb²⁺ and Cu²⁺, respectively, indicated the adsorption as a favorable process. The excellent adsorption and very good desorption efficiency implied the efficacy of the resin in removing as well as recovering the metal ions from aqueous solution. An efficient synthetic access to the resin would enable its use in the treatment of contaminated waste water.

KEYWORDS: adsorption, desorption, cross-linked polyphosphonate, heavy metal ions

8.1 Introduction

The presence of heavy metal ions, such as Pb^{2+} , Cu^{2+} , etc., in natural and waste water systems is a matter of great concern due to their negative effects on the environment and human health. These toxic pollutants are nonbiodegradable and can accumulate in the human body causing a variety of diseases and disorders^[66-68, 208, 209]. Various techniques, like adsorption, precipitation, dialysis, ion exchange, reverse osmosis, and extraction, have been developed in the past for the removal of metal contaminants from water resources. One of the most attractive among these techniques is presumably the adsorption process due to the availability of different types of low-cost and environment-friendly adsorbents^[48, 52, 151, 188]. Inorganic/organic polymer hybrid adsorbents have been widely investigated; their efficacies in metal ion removal attributed to the formation of a stronger chemical bonding between M^{n+} and, for instance, amine motifs in the hybrid materials^[54, 58, 152, 190, 210]. Recently, the researchers have focused on the syntheses of zwitterionic cross-linked inorganic/organic hybrid materials for the removal of heavy metal ions *via* electrostatic effects^[47, 59, 60, 153, 211]. A titania-phosphonate hybrid porous material was found to have a large capacity for selective adsorption of Cd^{2+} ions^[61]. Considerable attention has been given to synthesize chelating agents containing aminomethylphosphonate motif owing to its extraordinary chelating properties in extracting heavy metal ions from waste water^[65, 212-215].

In this paper, a novel cross-linked anionic polyelectrolyte (CAPE) **5** containing aminomethylphosphonate motifs has been synthesized *via* Butler's cyclopolymerization

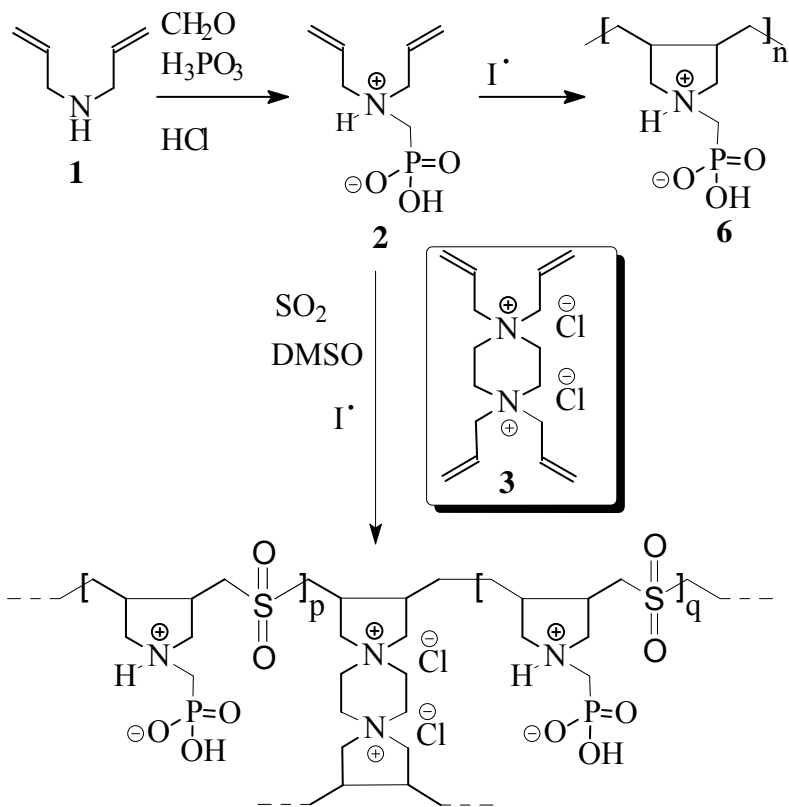
protocol (Scheme 1)^[20]. The polymer-architecture, having the five-membered cyclic units embedded in the backbone, has been recognized as the eighth major structural type of synthetic polymers^[130, 131]. To our knowledge, the synthesis of the cross-linked SO₂ terpolymer **5**, would represent the first example of this new class of resin containing strongly chelating amine and phosphonate ligands as well as weakly chelating SO₂ units. The new resin has been tested for its efficiency as an adsorbent for the removal of heavy metal ions like Pb²⁺ and Cu²⁺ ions from aqueous solutions. Desorption of the metal ions from the cross-linked polymer has also been investigated for the recovery of the metal ions and recycling of the polymer.

8.2 Experimental

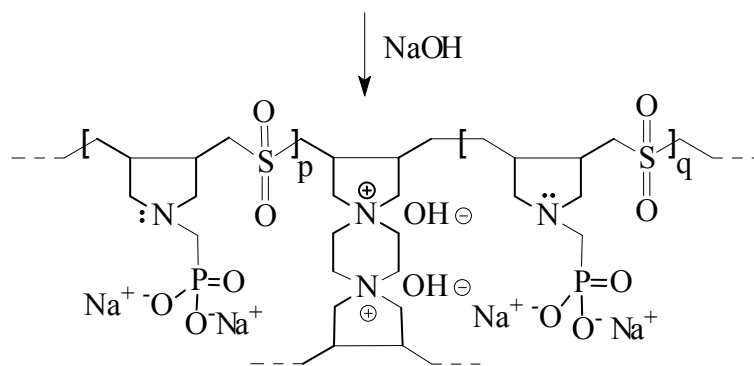
8.2.1 Physical Methods

Elemental analysis was carried out on a Perkin Elmer Elemental Analyzer Series II Model 2400. IR spectra were recorded on a Perkin Elmer 16F PC FTIR spectrometer. ¹H spectra were measured in D₂O at +25 °C (using HOD peak at δ 4.65) on a JEOL LA 500 MHz spectrometer. Scanning electron microscopy images were taken by TESCAN LYRA 3 (Czech Republic) Equipped with Oxford, energy-dispersive X-ray spectroscopy (EDX) detector model X-Max. Thermogravimetric analysis (TGA) was performed using a thermal analyzer (STA 429) manufactured by Netzsch (Germany). The polymer sample to be tested (usually ~5 mg) was placed in a platinum crucible. Aluminum oxide (Al₂O₃; ~4 mg) was placed in an identical platinum crucible as a reference sample. With the sample carrier system, which had two sets of 10% Pt–Pt/Rh thermocouples, the sample carrier was placed in the middle of the vertical furnace, which was programmed and

controlled by a microprocessor temperature controller. The temperature was raised at a uniform rate of 10 °C/min. The analyses were made over a temperature range of 20–800 °C in an air atmosphere flowing at a rate of 100 mL/min. The specific surface area of the CAPE **5** was measured by Brunauer–Emmett–Teller (BET) N₂ method using a Micrometrics ASAP 2020 BET surface area analyzer. Samples were degassed under high vacuum for 6 h at 80 °C. Specific surface area of CAPE **5** was calculated by the Brunauer–Emmett–Teller (BET) method and pore volumes were taken at the P/P₀ = 0.974 single point. Pore size diameter was determined by the BJH method.



4: Cross-linked polyzwitterionic acid (CPZA)



5: Cross-linked anionic polyelectrolyte (CAPE)

Scheme 1.

8.2.2 Material

2,2'-Azobisisobutyronitrile (AIBN) from Fluka AG was purified by crystallization from a chloroform-ethanol mixture. Diallylamine, paraformaldehyde, phosphorous acid, and sulfur dioxide from Fluka Chemie AG (Buchs, Switzerland) were used as received. Dimethylsulfoxide (DMSO) from Sigma-Aldrich (USA) was dried over calcium hydride overnight and then distilled at a boiling point of 64-65 °C (4 mmHg). All solvents used were of analytical grade.

8.2.3 Synthesis of monomers

8.2.3.1 Diallylaminomethylphosphonic acid **2**

The synthesis of monomer **2** was carried out as described with some modifications in the isolation procedure^[65]. Thus, diallylamine (**1**) (0.50 mol) was added dropwise for 45 min to a stirred mixture of phosphorous acid (0.50 mol), water (50 mL) and concentrated hydrochloric acid (50 mL) under ice cooling. The reaction mixture was then refluxed for 1 h during which paraformaldehyde (1.0 mol) was added in several portions (ca. 20 min). The resulting solution was refluxed for an additional hour and thereafter evaporated to dryness to obtain the crude product **2** (122 g). An ¹H NMR spectrum of a mixture containing a known mass of this crude product and a known mass of ethanol in D₂O revealed the purity of the product. Integration of the proton signals of CH₂P- of **2** at δ3.11 versus CH₂O of ethanol at δ3.40 helped us to determine the purity of the crude product. The crude product (122 g) contained 0.42 mol of **2** (84%). The crude sample of 0.290 g was thus found to have 1 mmol (0.191 g) of **2** (i.e. the crude product contained 66 %w/w monomer **2**; the rest of the materials may include HCl, H₂O etc). The ¹H NMR spectrum was very clean and free of undesired products. Monomer **2** was used in the subsequent polymerization without further purification.

8.2.3.2 1,1,4,4-tetraallylpiperazinium dichloride **3**

Monomer **3**, a cross-linker, was prepared as described^[64].

8.2.4 General procedure for the terpolymerization of **2** and **3** with sulfur dioxide.

To a solution of monomer **2** (27 mmol i.e. 7.86 g of 66 %w/w purity), cross-linker **3** (3 mmol, 0.96 g) in DMSO (9.00 g) in a round bottom flask (50 ml), was absorbed SO₂ (30 mmol, 1.92 g) (from a cylinder) by gentle blowing it over the stirred surface of the solution. After the initiator AIBN (200 mg) was added, the reaction mixture was stirred at 65 °C under N₂ for 24 h. Within 3-5 h, the magnetic stir-bar stopped moving; the reaction mixture became a transparent swelled gel. At the end of the elapsed time, the swelled gel of the cross-linked polyzwitterionic acid (CPZA) **4** was soaked in water (48 h) with replacement of water several times. The swelled gel was then poured onto acetone. The resin was filtered and dried at 70°C under vacuum to a constant weight (7.76 g, 96%). (Found: C, 34.1; H, 5.9; N, 5.4; S, 11.8%). A terpolymer from monomer **2** C₇H₁₃NO₃P (90 mol%) and monomer **3** C₁₆H₂₈Cl₂N₂ (10 mol%) and SO₂ (100 mol%) requires C, 34.66; H, 5.71; N, 5.67; S, 12.14); ν_{\max} (KBr) 3419, 2921, 2847, 1655, 1479, 1423, 1303, 1124, 1056, 975, 779, 639, 560, 514 and 477 cm⁻¹.

8.2.5 Basification of CPZA **4** to cross-linked anionic polyelectrolyte (CAPE) **5**

A mixture of CPZA **4** (5.34 g, ~ 20 mmol) and a solution of NaOH (1.60 g, ~40 mmol) in water (150 mL) was stirred at room temperature for 1 h. The resin was dropped onto 200 ml methanol (containing 10 mmol NaOH to insure complete exchange with Na⁺), the resultant CAPE **5** was filtered and dried at 65 °C under vacuum to a constant weight (5.42 g). The TGA curve (Figure 8.1) shows that the initial decomposition began around 200 °C.

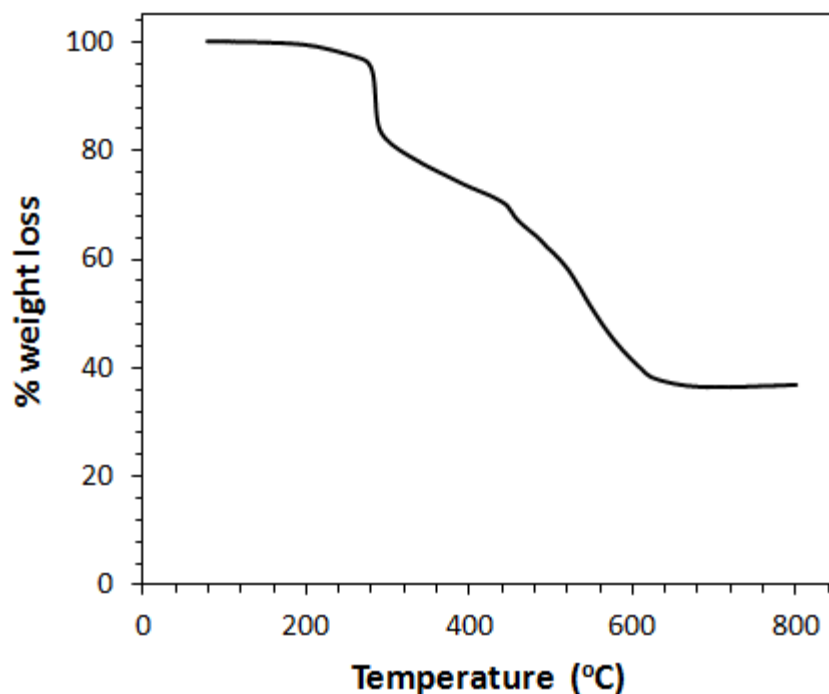


Figure 8.01. TGA curve of CAPE 5.

8.2.6 Sample characterizations

FT-IR spectra were recorded on a Perkin Elmer 16F PC FTIR spectrometer in the region of 4000-400 cm^{-1} . Ion exchange capacity (IEC) was determined by titrimetric analysis method. Polymer CAPE **5** (100 mg) was immersed in a 0.1 mol dm^{-3} HCl (50 mL) for 24 h. The decrease in acidity was determined by titration with a 0.1 mol dm^{-3} NaOH solution. The IEC can be calculated by Eq. (1):

$$IEC = \frac{mmol_i - mmol_f}{W} \quad (1)$$

where $mmol_i$ and $mmol_f$ are the initial and final amount of HCl in mmol, respectively, W is the weight of the polymer in g^[156].

8.2.7 Adsorption experiments

The procedure for the adsorption experiments of CAPE **5** for Pb^{2+} ions can be described briefly as follows: a mixture of CAPE **5** (50 mg) in a solution (20 mL) of 0.1 mol dm^{-3} aqueous $\text{Pb}(\text{NO}_3)_2$ was stirred using a magnetic stir-bar at different pH for 24 h. The resin was filtered and carefully washed with deionized water. The combined filtrate was titrated with a 0.1 mol dm^{-3} aqueous EDTA solution to determine the amount of Pb^{2+} remained. The adsorption capacity ($q_{\text{Pb}^{2+}}$) in mmol g^{-1} can be calculated using Eq. (2):

$$q_{\text{Pb}^{2+}} = \frac{(C_0 - C_f)V}{W} \quad (2)$$

where C_0 and C_f are the initial and final concentration of Pb^{2+} ions in mol dm^{-3} , respectively, W is the weight of the polymer in g, and V is the volume of the solution in mL. Data presented are average of triplicate runs and varied by less than 4% in all the cases studied.

For adsorption kinetic studies, the resin sample was stirred in a 0.1 mol dm^{-3} $\text{Pb}(\text{NO}_3)_2$ solution for different adsorption times at a preferred pH. The adsorption isotherm was constructed by changing the concentration of $\text{Pb}(\text{NO}_3)_2$ solution from 0.02 to 0.1 mol dm^{-3} at $25 \text{ }^\circ\text{C}$ for 24 h. Based on the adsorption data from experiments carried out at different temperatures, the activation energy for the adsorption process and thermodynamic parameters ΔG , ΔH and ΔS for Pb^{2+} removal were calculated.

Similar experiments, as presented above, were conducted for the adsorption of Cu^{2+} ions in a 0.1 mol dm^{-3} aqueous $\text{Cu}(\text{NO}_3)_2$ solution. The amount of Cu^{2+} ions remained in the solution was determined by iodometric titration using excess KI and a 0.1 mol dm^{-3}

aqueous Na₂S₂O₃ solution^[47, 211]. Finally, the desorption efficiencies of Pb²⁺ and Cu²⁺ ions were measured using a 0.1 mol dm⁻³ HNO₃.

8.3 Results and discussion

8.3.1 Synthesis and characterization of cross-linked polymers 4 and 5

Diallylaminomethylphosphonic acid **2**, a zwitterionic acid (ZA) monomer, was synthesized using a modified procedure^[65]. Butler's cyclopolymerization of **2** has been reported to give cyclopolymer **6**, a polyzwitterionic acid (PZA) (Scheme 1)^[65]. In fact, the cyclopolymerizations of a variety of *N,N*-diallylammonium salts led to the synthesis of an array of scientifically and technologically important water-soluble cationic polyelectrolytes^[88, 157, 158]. The polymer-architecture, having the five-membered cyclic units embedded in the backbone, has been recognized as the eighth major structural type of synthetic polymers. Over 33 million pounds of poly(diallyldimethylammonium chloride) alone are sold annually for water treatment and another 2 million pounds are used for personal care formulation^[20].

Monomer ZA **2** (90 mol %), cross-linker **3** (10 mol %) and sulphur dioxide (100 mmol %) in DMSO as a solvent, underwent cyclocopolymerization in the presence of initiator AIBN to give the novel cross-linked terpolymer CPZA **4** (Scheme 1). Elemental analysis of CPZA **4** revealed the incorporation of monomers **2** and **3** to CPZA **4** in an approximate mol ratio of 90:10, which is the same as the feed ratio. Sulfur dioxide is well known to take part in cyclopolymerization process as a comonomer to yield alternate copolymers with diallylammonium salts^[14]. Elemental analyses of CPZA **4** ascertained the molar ratio of (**2+3**) and SO₂ as 1:1.

CPZA **4** was found to swell in water while shrank upon soaking in acetone owing to the removal of water. Its basification with excess NaOH led to CAPE **5** in excellent yield. Thermogravimetric analysis (TGA) curve of the cross-linked polymer (Figure 8.1) showed two major loss in weight, first sharp weight loss was 14.6 % which is due to the loss of sulphur dioxide, the second major loss was 39.7 % which is due to the combustion of nitrogenated organic fraction with the release of CO₂, NO_x and H₂O gases, the residual mass at 800 °C was found to be 45.7 % which may be attributed to Na₂O.1.5P₂O₅.^[163] The surface area, pore size diameter, and total pore volume were found to be 5.5 m² g⁻¹, 32.0 nm, and 0.032 cm³ g⁻¹, respectively.

8.3.2 Adsorption properties of CAPE **5** and IR spectroscopy

The ion exchange capacity (IEC) of CAPE **5** was found to be 6.29 mmol/g, which ascertained the excellent ability of the resin to adsorb metal ions (M²⁺) as a result of the presence of chelating ligands of amine nitrogens and phosphonate motifs -P(=O)(O⁻)₂. The two strong bands at 975 cm⁻¹ and 1065 cm⁻¹ in the IR spectrum of the resin **5** are attributed to the phosphonate P-O vibrations^[161, 163] and the absorptions at 1124 cm⁻¹ and 1303 cm⁻¹ were assigned to the asymmetric and symmetric vibrations of SO₂ unit (Figure 8.2A). The C-N absorption was found in near ~1460 cm⁻¹. The peaks around 1650 cm⁻¹ were ascribed to the H-O-H bending vibration. The appearances of new strong bands 1385 (Figure 8.2B) and 1384 cm⁻¹ (Figure 8.2C) were attributed to the presence of ionic nitrate group since the adsorption process was carried out in the presence of lead and copper nitrates^[165]. Interestingly, the presence of these strong bands implies the ability of the resin to act also as an anion exchanger. Note that the absorption band

attributed to the nitrate ion is absent in the IR spectrum of the unloaded resin **5** (Figure 8.2A)

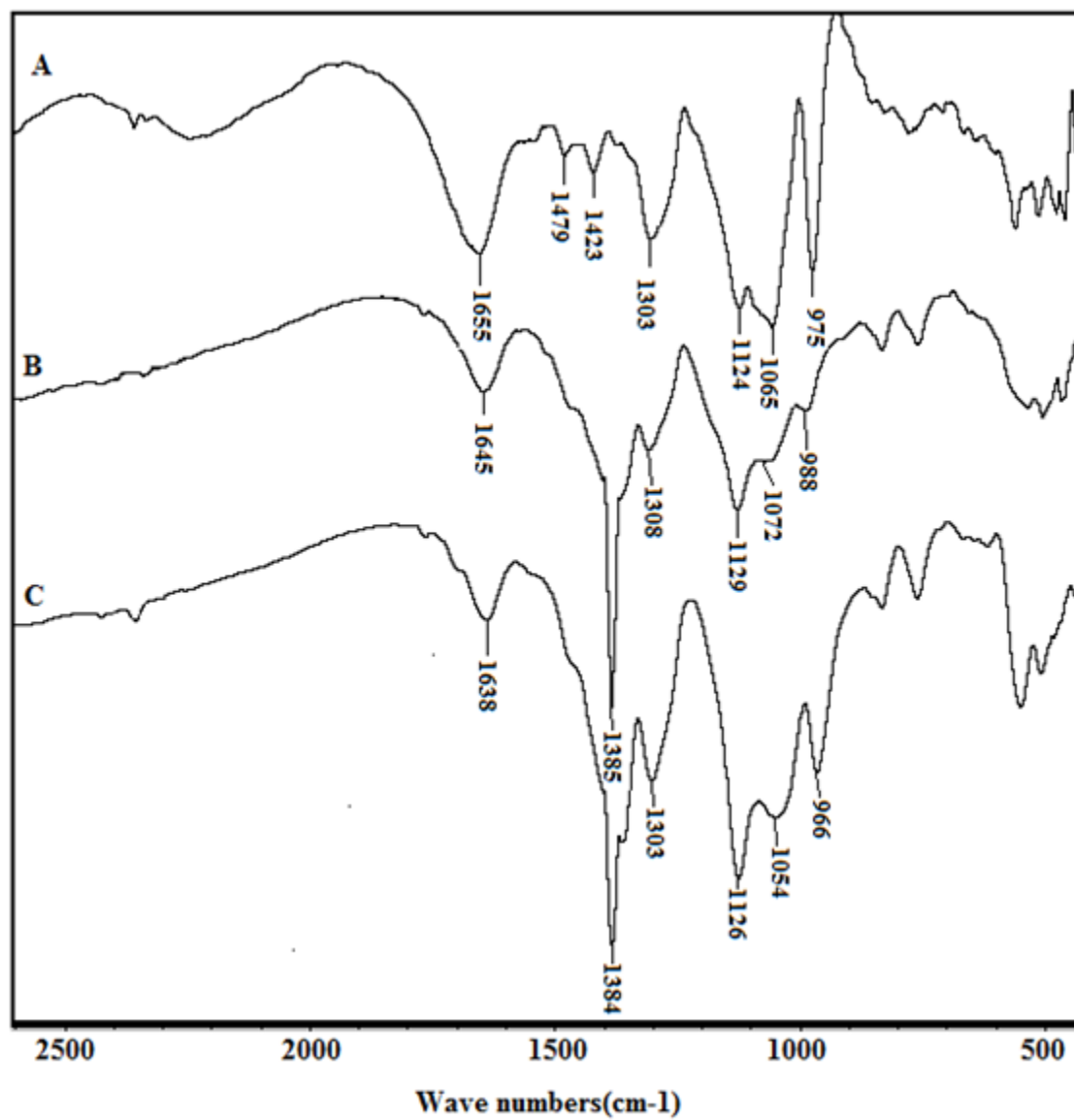


Figure 8.02. IR spectra of (A) Cross-linked polyanion **5**, (B) Cross-linked polyanion **5** loaded with Cu²⁺ and (C) Cross-linked polyanion **5** loaded with Pb²⁺.

A comparison of the IR spectra of CAPE **5** and Cu²⁺ and Pb²⁺-loaded CAPE **5** (Figure 8.2) reveals strong perturbations of the P-O peaks implying a direct bond between metal ions and the phosphonate group. The spectra revealed the increase in the intensity and broadness of the phosphonate P–O vibrations as a result of the adsorption of the metal ions^[164, 216].

8.3.3 Adsorption kinetics

The adsorption kinetics, as described by the relationship between adsorption capacity and adsorption time, are presented in Figure 8.3a. It was found that the adsorption of Cu²⁺ and Pb²⁺ ions by CAPE **5** reached to equilibrium in about 2 h. It is reported that Lagergren adsorption kinetic model is a suitable tool to investigate the adsorption properties of a polymer^[67].

The following equations express the linearly first-order and second-order kinetic equations [Eqs. (3) and (4)] for the Lagergren model, respectively:

$$\mathbf{log} (q_e - q_t) = \mathbf{log} q_e - \frac{k_1 t}{2.303} \quad (3)$$

$$\frac{t}{q_t} = \frac{1}{k_2 q_e^2} + \frac{t}{q_e} \quad (4)$$

where k_1 and k_2 are the first-order and second-order rate constant, respectively, q_t and q_e are the adsorption capacity of the metal ions at a time t and at equilibrium, respectively.

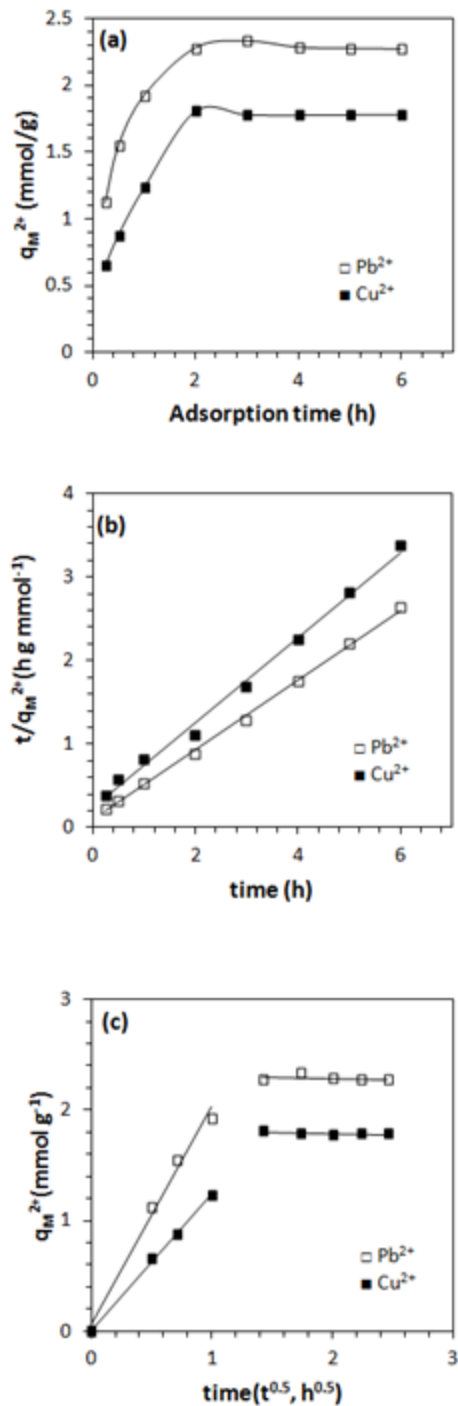


Figure 8.3. (a) Adsorption kinetic curves of Cu^{2+} and Pb^{2+} in 0.1 M solution at pH 4 at 25°C; (b) Lagergren second-order kinetic model for adsorption of Cu^{2+} and Pb^{2+} on CAPE 5; (c) Intraparticle diffusion model.

Neither Pb^{2+} nor Cu^{2+} fitted the first-order Lagergren kinetic model, so the graphs representing the kinetic model have not been displayed. The second-order Lagergren kinetic model (Figure 8.3b), however, fitted well for the adsorption of both Cu^{2+} and Pb^{2+} ions on CAPE 5; suggesting that the adsorption process might be chemical adsorption^[167]. The values reported in Table 8.1 show that the rate constants (k_2) for the removal of Pb^{2+} at various temperatures are higher than those Cu^{2+} . The adsorption capacity of Pb^{2+} is found to be larger than that of Cu^{2+} (Figure 8.3a, Table 8.1). The rationale for such a difference could be attributed to the lower effective ionic radii of Pb^{2+} (4.5 Å) as compared to Cu^{2+} (6 Å) and differences in the affinity of the phosphonate motifs in the resin for the metal ions^[217]. The experimental data so far revealed that the resin is an efficient adsorbent for the removal of both lead and copper ions from aqueous solutions.

The adsorption data may also be described by some adsorption diffusion models which are always constructed on the basis of three consecutive steps: (1) film diffusion (i.e., diffusion across the liquid film surrounding the adsorbent particles); (2) intraparticle diffusion (i.e., diffusion in the liquid contained in the pores and/or along the pore walls); and (3) mass action (i.e., physical adsorption and desorption between the adsorbate and active sites).

Since the adsorption step is very rapid, the overall rate of adsorption process, therefore, will be controlled by either surface diffusion or intraparticle diffusion. The intraparticle diffusion model assumes that the metal ions are transported from the solution via film diffusion followed by a rate-limiting intraparticle diffusion step which bring

them into the pores of the particles in the adsorbent. Following equation expresses the relation of the adsorption capacity and time^[200, 201]:

$$q_t = x_i + k_p t^{0.5} \quad (5)$$

where q_t is the adsorption capacity at time t , k_p is the rate constant of intraparticle diffusion, x_i is related to boundary layer thickness^[218]. According to the Weber–Morris model, intraparticle diffusion is involved in the rate-limiting step^[218-220] in the case of a straight line fit for the plot of q_t versus $t^{0.5}$; and if the plot passes through the origin then it becomes the sole rate-limiting step^[221]. Since the initial linear plot did pass through the origin, intraparticle diffusion within the pores of the resins was the only rate-limiting step (Figure 8.3c). The value of the square of regression (R^2) for Pb^{2+} and Cu^{2+} plots were found to be 0.9962 and 0.9992, respectively. Note that the second linear section represents the final equilibrium stage.

Table 8.01 Lagergren Second–Order Kinetic Model Parameters for Pb^{2+} and Cu^{2+} Adsorption

CAPE 5	Temp (K)	$q_{e, \text{exp}}$ (mmol g ⁻¹)	k_2 (h ⁻¹ g mmol ⁻¹)	h^a (h ⁻¹ g ⁻¹ mmol)	$q_{e, \text{cal}}$ (mmol g ⁻¹)	R^2	E_a (kJ mol ⁻¹)
Pb^{2+}	298	2.20	2.01	11.42	2.38	0.9983	
	310	2.50	2.90	19.16	2.57	0.9995	25.46
	319	2.72	4.05	31.35	2.78	0.9998	
Cu^{2+}	298	1.78	1.18	4.47	1.95	0.9952	
	306	1.92	1.76	7.39	2.05	0.9995	27.10
	324	2.27	2.90	16.50	2.39	0.9987	

^aInitial adsorption rate $h = k_2 q_e^2$.

8.3.4 Effect of initial concentration on the adsorption of Cu²⁺ and Pb²⁺ ions

As shown in Figure 8.4a, the adsorption capacity of CAPE 5 increases with the increase in initial concentration of Cu²⁺ and Pb²⁺ ions. To further explore the adsorption mechanism, Langmuir and Freundlich isotherm models were used to analyze the adsorption data. The Langmuir isotherm equation can be expressed by Eq. (6) where it assumes the mechanism of the adsorption process as a monolayer adsorption on the surface of the polymer:

$$\frac{C_e}{q_e} = \frac{C_e}{Q_m} + \frac{1}{Q_m b} \quad (6)$$

where C_e and q_e are the concentrations of metal ion in the solution and resin, respectively, Q_m and b are the Langmuir constants. Figure 8.4b illustrates the Langmuir plot of C_e/q_e versus C_e , enabling the calculation of Langmuir constants from the intercept and slope of the linear plot. Freundlich isotherm model, on the other hand, describes the adsorption occurring on a heterogeneous surface with uniform energy; Eqs. (7) and (8) express the model:

$$q_e = k_f C_e^{1/n} \quad (7)$$

$$\log q_e = \log k_f + \frac{1}{n} \log C_e \quad (8)$$

where q_e and C_e are the equilibrium concentrations of metal ion in the adsorbed and liquid phase, respectively, k_f and n represent the Freundlich constants, which can be calculated from the slope and intercept of the linear plot of $\log q_e$ versus $\log C_e$ as presented in Figure 8.4c.

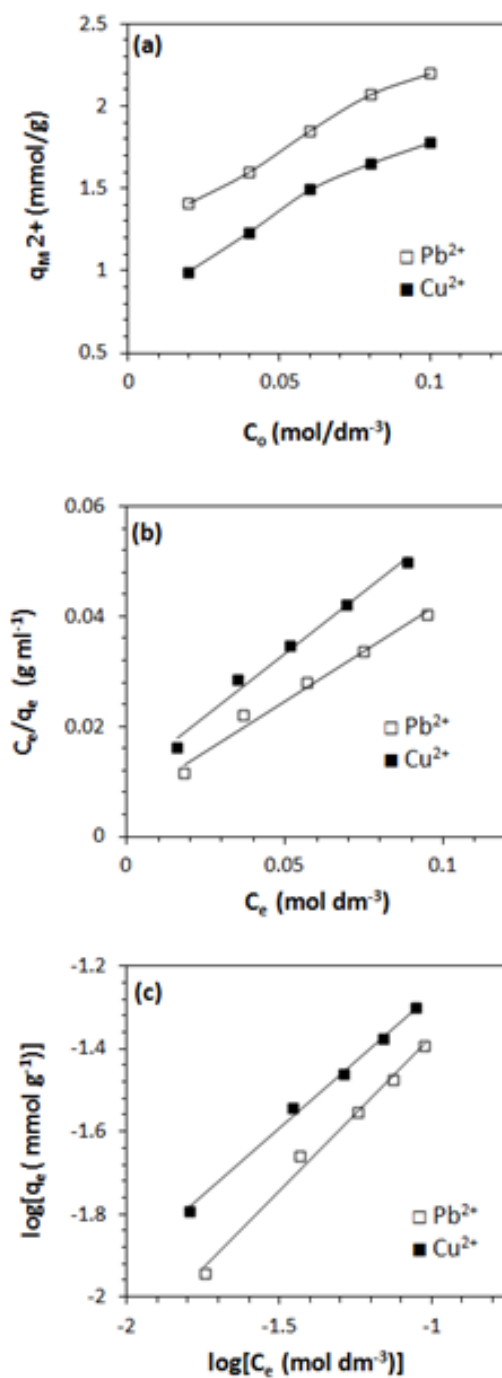


Figure 8.4. (a) The effect of initial concentration on the adsorption capacity of CAPE 5 at pH 4 for 24 h at 25°C; (b) Langmuir and (c) Freundlich isotherm of the adsorption of Cu²⁺ and Pb²⁺ ions on CAPE 5.

Figures 8.4b and 8.4c illustrate that the adsorption of Pb^{2+} and Cu^{2+} ions fitted well with both the Langmuir as well as Freundlich isotherm models, thereby implying that the adsorption may occur as a monolayer as well as a heterogeneous surface adsorption. The Langmuir and Freundlich isotherm model constants are given in Table 8.2. At a pH of 4, the zwitterionic aminophosphonate motifs [i.e. $\text{NH}^+\cdots\text{P}(=\text{O})(\text{OH})\text{O}^-$] in CPZA **4** may partially change to zwitterionic/anionic aminophosphonate motifs [i.e. $\text{NH}^+\cdots\text{P}(=\text{O})(\text{O}^-)_2$] which can influence the adsorption of metal ions on the resin surface by electrostatic adsorption that follows Langmuir adsorption model.

Table 8.2 Langmuir and Freundlich isotherm model constants for Cu^{2+} and Pb^{2+} adsorption.

Langmuir isotherm model				
Entry No	Metal ion	Q_m (mmol g ⁻¹)	b (dm ³ mmol ⁻¹)	R^2
1	Cu^{2+}	2.22	42.1	0.9875
2	Pb^{2+}	2.76	54.9	0.9843
Freundlich isotherm model				
Entry No	Metal ion	k_f	n	R^2
1	Cu^{2+}	0.240	1.542	0.9968
2	Pb^{2+}	0.237	1.340	0.9909

For the Langmuir isotherm model, separation factor or equilibrium parameter (R_L) can be used to describe the favorability of adsorption on the polymer surface by Eq. (9):^[47]

$$R_L = \frac{1}{(1+bC_0)} \quad (9)$$

where C_0 is the initial M^{2+} concentration and b is the Langmuir equilibrium constant. A favorable adsorption is indicated when the R_L value is between $0 < R_L < 1$, whereas the value outside the range describes an unfavorable adsorption. The R_L values for the adsorption of both metal ions are given in Table 8.3, which reveals that the values fall in the preferred region (i.e. $0 < R_L < 1$). The results thus certify that CAPE 5 is a promising adsorbent for the removal of heavy metal ions in aqueous solutions.

Table 8.3 The R_L values based on the Langmuir isotherm model

C_0 (mol dm ⁻³)	R_L value	
	Cu^{2+}	Pb^{2+}
0.02	0.5428	0.4765
0.04	0.3725	0.3128
0.06	0.2835	0.2328
0.08	0.2289	0.1854
0.10	0.1919	0.1540

8.3.5 Effect of pH and temperature on adsorption.

The effect pH (in the range 3-6) on the uptake of Pb^{2+} and Cu^{2+} were investigated at a fixed concentration (0.1 M) and time of 24 h. The pH of the solution was controlled by using an acetate buffer (CH_3COONa/CH_3COOH). Results of metal uptake at different pH are shown in Figure 8.5. Optimum pH was found to be 4; at higher pH values, the hydrolysis of the metal ions occur by the formation of metal hydroxides, which compete with the metal ion uptake by the resin^[174].

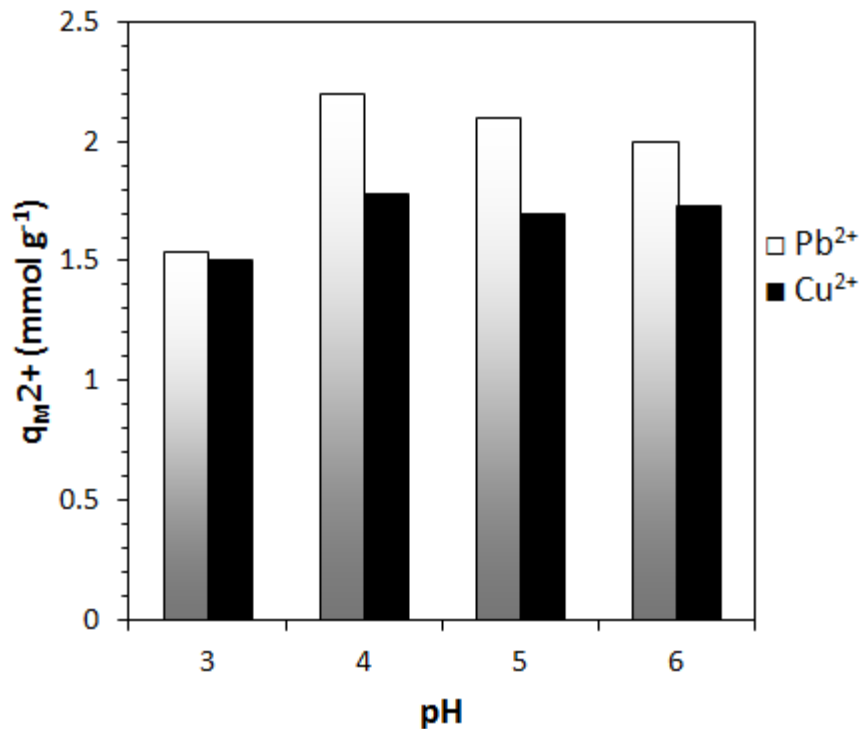


Figure 8.05. pH dependence of metal uptake by CAPE 5.

Adsorption experiments were also performed to obtain the thermodynamic parameters; the results are illustrated in Figure 8.6a. As can be seen from the Figure, the adsorption capacity increases with the increase in temperature, suggesting that the adsorption process is endothermic, and this can be explained that at higher temperature swelling of the resin increases which permits greater diffusion of the metal ions^[163]. The activation energy of the adsorption process can be calculated by plotting $\ln k_2$ versus $1/T$ as shown in Figure 8.6b. Using Arrhenius equation [Eq. (10)], the activation energies were found to be 27.1 and 25.5 kJ/mol for the adsorption of Cu²⁺ and Pb²⁺, respectively.

These E_a values are relatively low in comparison to typical chemical reactions with activation energies of 65 – 250 kJ/mol, thereby indicating that the adsorption of the metal ions is relatively easy and a favored process^[175].

$$\ln k_2 = -\frac{E_a}{RT} + \text{constant} \quad (10)$$

A plot of $\log (q_e/C_e)$ versus $1/T$ is displayed in Figure 8.6c. The thermodynamic parameters ΔG , ΔH and ΔS were calculated using Vant-Hoff equation [Eq. (11)], and are tabulated in Table 8.4.^[167, 217] The negative ΔG values ascertain the spontaneity of the adsorption process.

$$\log \left(\frac{q_e}{C_e} \right) = -\frac{\Delta H}{2.303RT} + \frac{\Delta S}{2.303R} \quad (11)$$

As the temperature increases, the ΔG values become more negative, thereby indicating that the adsorption is more favorable at the higher temperatures. Favorable adsorption at higher temperatures is attributed to the greater swelling of the resin and increased diffusion of metal ions into the resin. Greater dissociation of zwitterionic phosphonate motifs, $\text{NH}^+\cdots\text{P}(=\text{O})(\text{OH})\text{O}^-$ to zwitterionic/anionic motifs, $\text{NH}^+\cdots\text{P}(=\text{O})(\text{O}^-)_2$, at elevated temperatures is also expected to increase the electrostatic attractions between the metal ions and ion exchange groups. The positive values of ΔH certify that the adsorption is an endothermic process. In addition, it can be found in Table 8.4 that the ΔS values are positive, suggesting that the randomness increased during the adsorption of metal ions as a result of the release of water molecules from their large hydration shells.

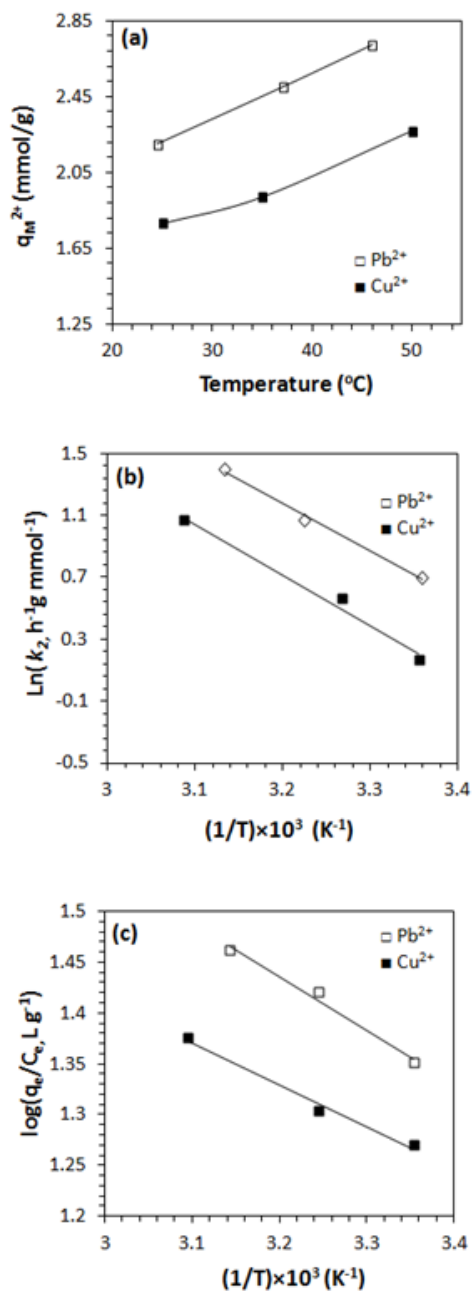
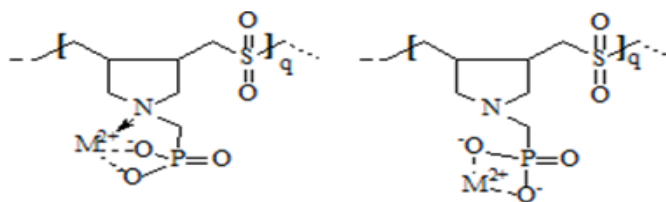


Figure 8.06. (a) Effect of temperature on the adsorption capacity of CAPE 5; (b) Arrhenius plot; (c) Vant-Hoff plot.

Table 8.4 Thermodynamic Data for Pb²⁺ and Cu²⁺ adsorption.

Metal ion	Temperature (K)	ΔG (kJ/mol)	ΔH (kJ/mol)	ΔS (J/mol K)	R ²
Pb ²⁺	298	-17.4			
	310	-18.1	9.67	58.3	0.9767
	319	-18.6			
Cu ²⁺	298	-15.1			
	308	-15.6	7.65	50.6	0.9961
	323	-16.3			

As reported in the literature,^[164, 165, 176] the aminomethylphosphonate motifs are potentially tridentate ligands, having one coordination site at the nitrogen and two bonding sites at the phosphonate motif. Towards the weak acid range the formation of metal-complex using the aminophosphonate motif as a tridentate ligand (especially at low loads) is depicted in Scheme 2. At high loads, complexes without the amino group would result using phosphonate motif as a bidentate ligand.

**Scheme 2.**

8.3.6 Scanning electron microscopy (SEM)

The surface morphology of the unloaded and loaded CAPE **5** was investigated by scanning electron microscopy. Unloaded CAPE **5** was immersed in 0.1 M $\text{Pb}(\text{NO}_3)_2$ and 0.1 M $\text{Cu}(\text{NO}_3)_2$ for 24 h at a pH of 4, filtered, and dried under vacuum to constant weight. Loaded and unloaded polymers were then sputter-coated for 6 min with a thin film of gold. The elemental composition of the resin before and after the metal adsorption was determined by randomly selecting areas on the solid surfaces and analyzing by energy dispersive X-ray (EDX) in conjunction with SEM. The EDX spectrum for unloaded CAPE **5** indicated the presence of C, O, Na, P, and S in the structure (Fig. 8.7a); whereas the spectra in Fig. 8.7b and 8.7c revealed the presence of characteristic peaks for Cu and Pb, respectively. The cation exchange with Na^+ ions is ascertained by the absence of its signal in the spectra of the loaded samples. The surface of the unloaded sample shows cracks thus allowing it to have higher area for adsorption, whereas the loaded samples show more uniform structure owing to the adsorption of metal ions. Visible changes in the surface morphology of CAPE **5** before and after loading of metal ions indicated that sorption took place. The SEM images thus showed that CAPE **5** adsorbed both the metals, and the adsorption process happened on the surface and throughout the polymer which was confirmed by Energy-dispersive X-ray spectroscopy (EDX analysis).

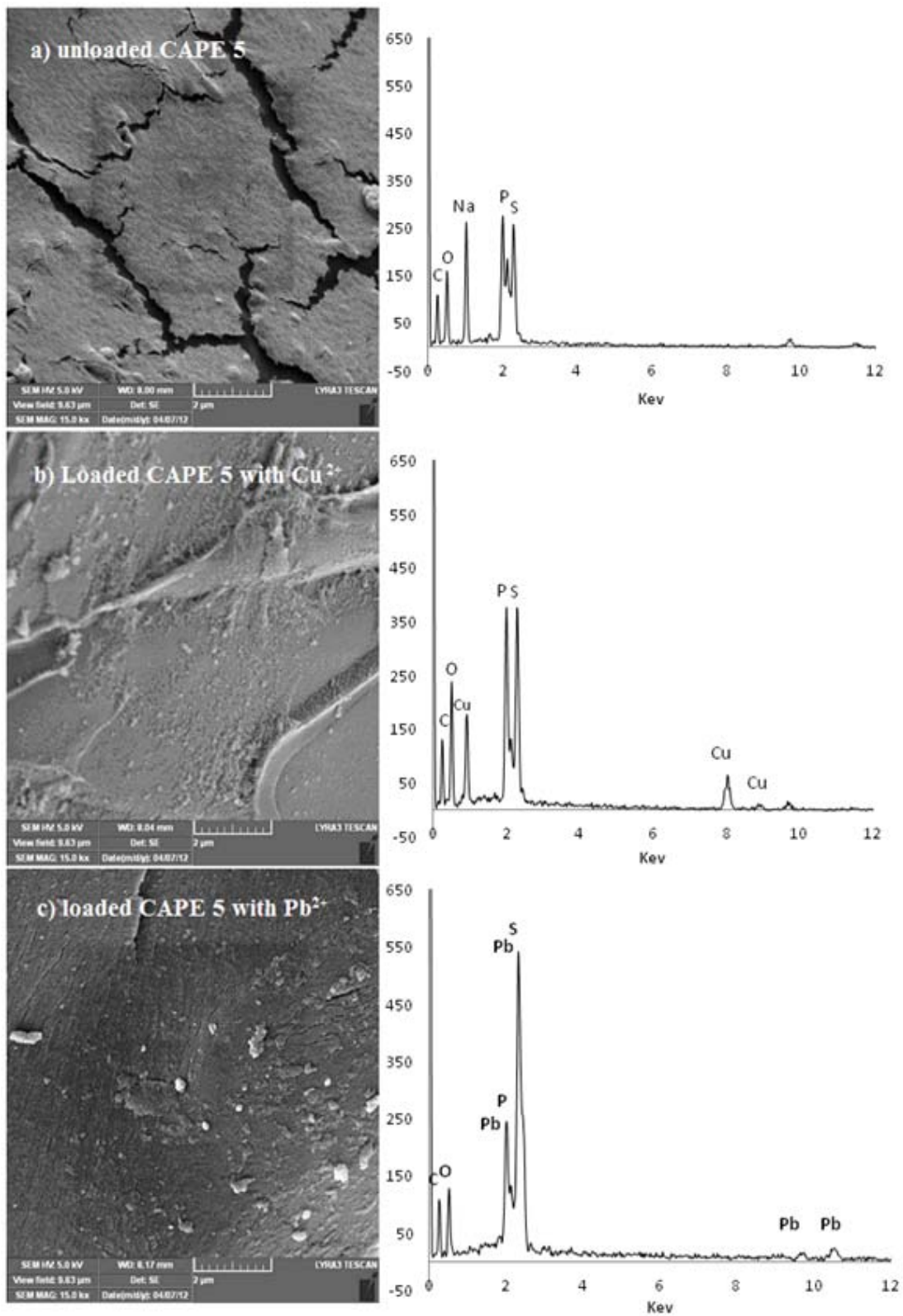


Figure 8.07. SEM images for unloaded and loaded CAPE5 with Pb^{2+} and Cu^{2+} .

8.3.7 Desorption experiment.

One of the important criteria for the effective usage of adsorbent is the recycling and reuse of the adsorbent. For this purpose, an experiment was conducted by immersing 50 mg resin in 20 mL of 0.1 mol dm^{-3} $\text{Cu}(\text{NO}_3)_2$ (or $\text{Pb}(\text{NO}_3)_2$) for 24 h. The loaded resin was then filtered and immersed in 0.1 mol dm^{-3} HNO_3 for 3 h. After filtration, the amount of metal ions desorbed in the filtrate was determined; the efficiency of the desorption process was calculated by the ratio of desorbed amount of M^{2+} ions to the amount of adsorbed Cu^{2+} ions in the resin. The results indicated that the percentage efficiency of the desorption process to be 81% and 63% for Cu^{2+} and Pb^{2+} ions, respectively. The above findings indicates an effective regeneration cycle, which concludes that the above cross-linked anionic polyelectrolyte can be a potential adsorbent for the removal of Cu^{2+} and Pb^{2+} from aqueous solutions.

8.4 Conclusion

A novel cross-linked polyphosphonate was prepared in excellent yield from inexpensive starting materials. The resin was found to have a very good adsorption capacity for Pb^{2+} and Cu^{2+} ions. The adsorption followed Lagergren second-order kinetic model and Langmuir as well as Freundlich isotherm models. The negative ΔG s and positive ΔH s ensured the spontaneity and the endothermic nature of the adsorption process. The good adsorption and desorption efficiencies implied the efficacy of the resin in removing as well the recovery of the metal ions from aqueous solution. The effective recycling of the resin would enable it to be used in the treatment of contaminated water in industry. A comparison of CAPE 5 with those of different types of sorbents in recent references reveals the excellent metal removal capacity of the current resin (Table 8.5).

Table 8.5 Comparison of CAPE 5 with those of different types of sorbents in References.

Adsorbent	Q _m for Pb ²⁺ mg/g (mmol/g)	Q _m for Cu ²⁺ mg/g (mmol/g)	Ref.
metal-complexed chitosans	105 (0.51)	–	[217]
magnetic chelating resin	597 (2.88)	–	[201]
magnetic chelating resin	–	10.4 (0.16)	[200]
fructose-mediated [poly(ethylene glycol)/chitosan] membrane	185 (0.89)	–	[218]
Cassia grandis seed gum-graft-poly(methyl methacrylate)	127 (0.61)	–	[181]
Dowex 50X8-200	-	66.1 (1.04)	[176]
poly(methylmethacrylate methacryloylamidoglutamic acid) beads	65.2 (0.32)	92.6 (1.46)	[183]
negatively charged hybrid adsorbents	–	4.13 (0.065)	[200]
Novel cross-linked polyphosphonate	571 (2.76)	141 (2.22)	This work

CHAPTER 9: Removal of zinc and cadmium ions using a cross-linked polyzwitterionic phosphonate/sulfur dioxide terpolymers

Taken from **Othman Charles S. Al-Hamouz**, S. A. Ali, Removal of zinc and cadmium ions using a cross-linked polyzwitterionic phosphonate/sulfur dioxide terpolymer, Separation Science and Technology, submitted.

ABSTRACT

A cross-linked polyzwitterionic acid was synthesized *via* cycloterpolymerization of diallylaminomethylphosphonic acid, cross-linker 1,1,4,4-tetraallylpiperazinium dichloride, and SO₂. The adsorption of Zn²⁺ and Cd²⁺ by the resin showed that the experimental data fitted Lagergren second-order kinetic model and Langmuir as well as Freundlich isotherm models. The maximum adsorption capacity of Zn²⁺ and Cd²⁺ at 25°C was found to be 79 and 81 mg g⁻¹, respectively; and the adsorption process was spontaneous and endothermic in nature as revealed by the negative and positive values of ΔG and ΔH , respectively. The resin demonstrated excellent adsorption efficiency in removing the metal ions from aqueous solution.

Key words: adsorption; cross-linked polyphosphonate; toxic metal ions.

9.1 Introduction

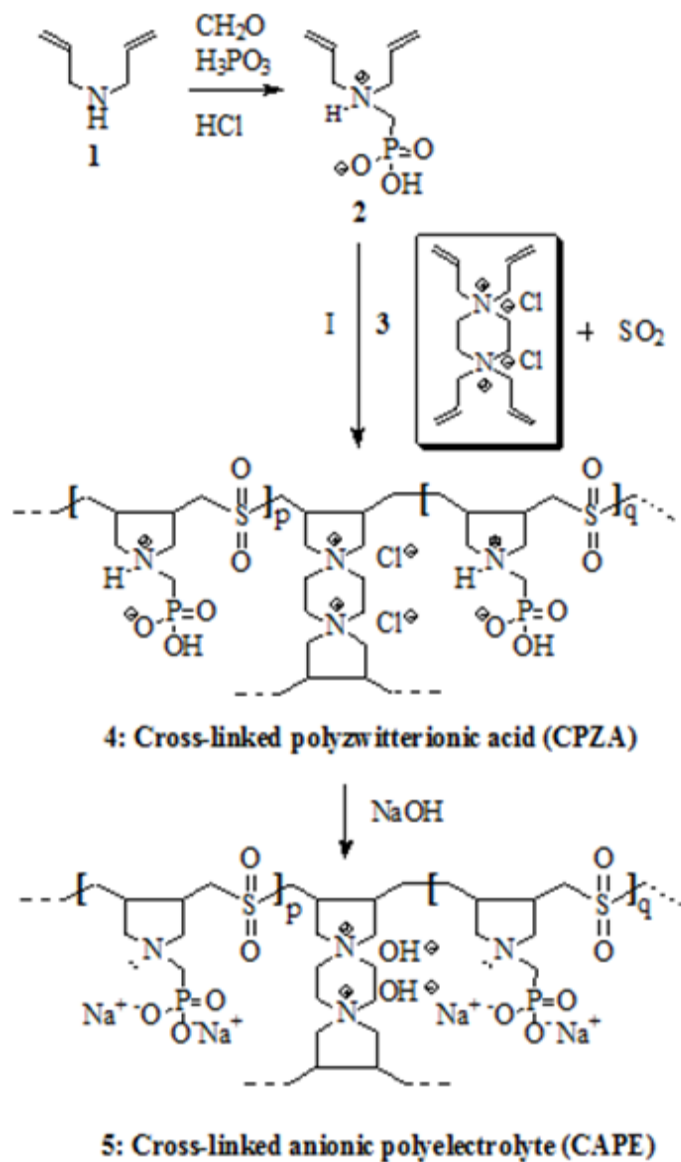
Pollution caused by toxic metal ions is a matter of great concern due to their negative effects on the environment and human health. These nonbiodegradable pollutants on accumulation in the human body can cause a variety of diseases and disorders^[67, 68]. Metal pollutants like zinc and cadmium are used in a variety of industrial processes such as mining, metal coating, and battery production. Due to their hazardous effects governmental agencies such as the Environmental Protection Agency (EPA) considered Zn^{2+} as a priority because it gives rise to serious poisoning cases leading to dehydration, stomachache, dizziness and incoordination in muscles^[186]. Cd^{2+} , on the other hand, causes kidney failure, nervous system damage, bone damage, as well as other serious illness^[187].

For Cd, the drinking water guideline value recommended by WHO is 0.003 mg Cd/L^[222]. It is difficult for chemical precipitation methodologies to treat economically low concentration (less than 5 mg/L) of cadmium. Ion exchange and reverse osmosis have been effective in achieving the metal concentration limits but have high operation and maintenance costs^[223]. Contamination by Zn^{2+} is considered a priority by the Environmental Protection Agency (EPA) because it gives rise to serious poisoning cases leading to dehydration, stomachache, dizziness and incoordination in muscles^[186].

One of the most attractive techniques for the removal of toxic metal ions is the adsorption process due to the availability of different types of adsorbents^[48, 52, 151, 188]. Inorganic/organic polymer hybrid adsorbents have been widely investigated, and their efficacy in the removal of metal ions has been attributed to the formation of a stronger

chemical bonding between M^{n+} and, for instance, amine motifs in the hybrid materials [54, 58, 152, 190, 210]. Recently researchers have focused on the synthesis of zwitterionic cross-linked inorganic/organic hybrid materials in removing heavy metal ions via electrostatic effects [47, 59, 60, 193].

A titania-phosphonate hybrid porous material has been found to have a large capacity for selective adsorption of Cd^{2+} ions [54]. Considerable attention has been given to synthesize chelating agents containing aminomethylphosphonate motifs owing to its extraordinary chelating properties in extracting heavy metal ions from waste water [65]. Recently we have synthesized two novel cross-linked polymers containing aminomethylphosphonate motifs and examined its excellent efficacy as an adsorbent for the removal of toxic metal ions like Pb^{2+} and Cu^{2+} ions from aqueous solutions [194, 224]. In this paper we report the efficiency of cross-linked anionic polyelectrolyte (CAPE 5) in the removal of toxic metal ions Zn^{2+} and Cd^{2+} from aqueous solutions (Scheme 1).



Scheme 1.

9.2 Experimental

9.2.1 Physical Methods

IR spectra were recorded on a Perkin Elmer 16F PC FTIR spectrometer. Scanning electron microscopy (SEM) images were taken by TESCAN LYRA 3 (Czech Republic) Equipped with Oxford, energy-dispersive X-ray spectroscopy (EDX) detector model X-Max.

9.2.2 Materials

2,2'-Azobisisobutyronitrile (AIBN) from Fluka AG was purified by crystallization from a chloroform-ethanol mixture. Diallylamine, paraformaldehyde and phosphorous acid from Fluka Chemie AG (Buchs, Switzerland) were used as received. All solvents used were of analytical grade.

9.2.3 Synthesis of monomers and cross-linked polymers

Diallylaminomethylphosphonic acid **2**^[65] and the cross-linker **3**^[64, 65] have been synthesized as described in the literature. The synthesis of cross-linked polyzwitterionic acid (CPZA) **4** and its transformation to cross-linked anionic polyelectrolyte (CAPE) **5** have been described elsewhere^[224]. Thus a solution of monomer **2** (27 mmol i.e. 7.86 g of 66 %w/w purity), cross-linker **3** (3 mmol, 0.96 g) and SO₂ (30 mmol, 1.92 g) in DMSO (30 mmol, 9.00 g) was polymerized in the presence of initiator AIBN (200 mg) at 65°C for 24 h to obtain cross-linked polyzwitterionic acid (CPZA) **4** which was converted to cross-linked anionic polyelectrolyte (CAPE) **5** upon treatment with NaOH.

9.2.4 Sample characterization

FT-IR spectra have been recorded on a Perkin Elmer 16F PC FTIR spectrometer in the region of 4000-400 cm⁻¹. Ion exchange capacity (IEC) was determined by titremetric

analysis method [Eq. (1)]. The dried and weighed polymer (100 mg) was immersed in 50 ml of 0.1 M hydrochloric acid for 24 h. The ion exchange capacity was determined from the decrease in acidity by titration with 0.1 M NaOH solution.

$$IEC = \frac{mmol_i - mmol_f}{W} \quad (1)$$

Where $mmol_i$ and $mmol_f$ are the initial and final amount of HCl in mmol, respectively; W is the weight of the polymer in g [194, 224].

9.2.5 Adsorption experiments

The adsorption properties of the cross-linked polymer CAPE **5** for Zn^{2+} and Cd^{2+} ions were determined by titration; the procedure for Zn^{2+} adsorption was as follows: A mixture of CAPE **5** (50 mg) in 20 ml of 1000 ppm Zn^{2+} solution [prepared from $Zn(NO_3)_2$] was stirred using a magnetic stir-bar at different pH for 24 h. The resin was filtered and carefully washed with deionized water. The combined filtrate was titrated with 0.1 M EDTA solution to find out the amount of Zn^{2+} remained. The adsorption capacity ($q_{Zn^{2+}}$) can be calculated using Eq. (2):

$$q_{Zn^{2+}} = \frac{(C_0 - C_f)V}{W} \quad (2)$$

Where C_0 and C_f are the initial and final concentration of Zn^{2+} ions, respectively, W is the weight of the polymer in g and V is the volume of the solution in mL.

The adsorption kinetic curves were determined by inserting the polymer in solution (1000 ppm metal ion) at a preferred pH of 4 at various times (*vide infra*). Adsorption isotherm was constructed by changing the solution concentration from 200 to 1000 ppm

of Zn^{2+} at 25°C for 24 h. Thermodynamic parameters ΔG , ΔH and ΔS were calculated using data from experiments carried out at different temperatures. Similar procedure was conducted for the adsorption of Cd^{2+} using $\text{Cd}(\text{NO}_3)_2$ solutions^[195].

9.3 Results and Discussion

The synthesis of CAPE **5** involved the Butler's cyclopolymerization process using monomer **2**, cross-linker **3** and SO_2 ^[224]. Butler's cyclopolymerization protocol gives polymers having five-membered ring embedded in the backbone (Scheme 1). The polymer architecture thus obtained has been classified as the eighth major structural feature of synthetic high polymers^[196]. To our knowledge, so far there is only two reports^[194, 224] that describes the use of the cross-linked cyclopolymer of the type **5** in the adsorption of toxic ions like Cu^{2+} and Pb^{2+} .

9.3.1 Ion exchange properties and FTIR spectroscopy of CAPE **5**

The ion exchange capacity (IEC) of CAPE **5** was found to be 6.29 mmol/g, which ascertained the excellent ability of the resin to adsorb metal ions (M^{2+}) as a result of the presence of chelating ligands of $-\text{N}^-$ and phosphonate motifs $-\text{P}(=\text{O})\text{O}_2^-$. For FTIR study, CAPE **5** was immersed in 1000 ppm solution of Zn(II) or Cd(II) for 24 h at pH 4, filtered, and dried under vacuum until constant weight was achieved. The bands in the IR spectrum of the resin **5** in the region of $900\text{--}1056\text{ cm}^{-1}$ are attributed to the phosphonate P–O vibrations and the two strong absorptions at ~ 1120 and ~ 1300 were assigned to the asymmetric and symmetric vibrations of SO_2 unit.

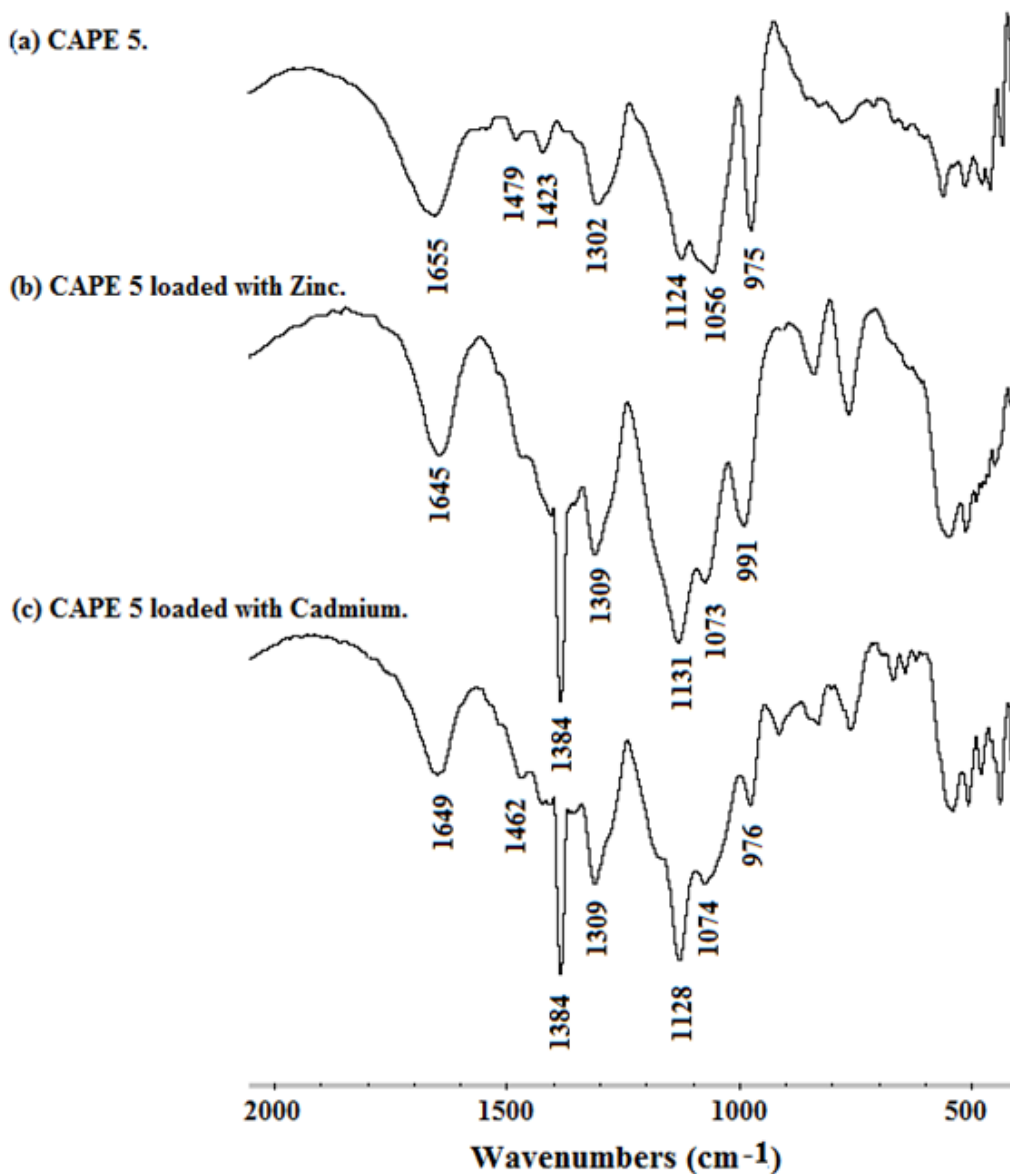
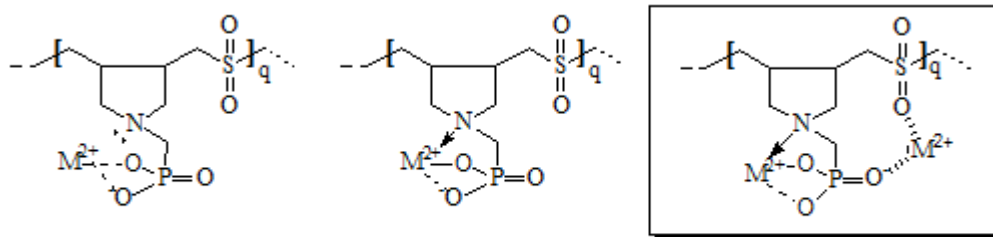


Figure 9.01 FT-IR of unloaded and loaded CAPE 5 with Zn²⁺ and Cd²⁺.

The IR spectra (Fig. 9.1) shows a shift of the -P=O and -P-O bands at 1056 and 975 cm⁻¹ of the unloaded resin upward to 1073 and 991 in the case of Zn²⁺ and to 1074 and 976 cm⁻¹ in the case of Cd²⁺ with an increase in the intensity and broadness of the peaks [185]. The SO₂ peaks also shifted to upward form 1124 and 1302 to 1131 and 1309

in the case of Zn^{2+} and to 1128 and 1309 in the case of Cd^{2+} meaning the involvement of SO_2 group in the adsorption of metal ions [Scheme 2].



Scheme 2.

The peaks around 1650 cm^{-1} were ascribed to the H-O-H bending vibration. The appearances of new strong bands at 1384 cm^{-1} were attributed to the presence of ionic nitrate group since the adsorption process was carried out in the presence of metal nitrates [165, 197]. The presence of these strong bands thereby implies the ability of the resin to act as an anion exchanger at pH 4. Note that the absorption band attributed to the nitrate ion is absent in the unloaded resin (Fig. 9.1).

9.3.2 Adsorption kinetics

Figure 9.2a shows the adsorption rate of the metal ions at different times. The adsorption rate for both Zn^{2+} and Cd^{2+} increases up for 2 h, then reaches equilibrium showing a fast adsorption process that can be useful for industrial application (Fig. 9.2a). It has been reported that Lagergren adsorption kinetic model is a suitable tool to investigate the adsorption properties of a polymer^[67].

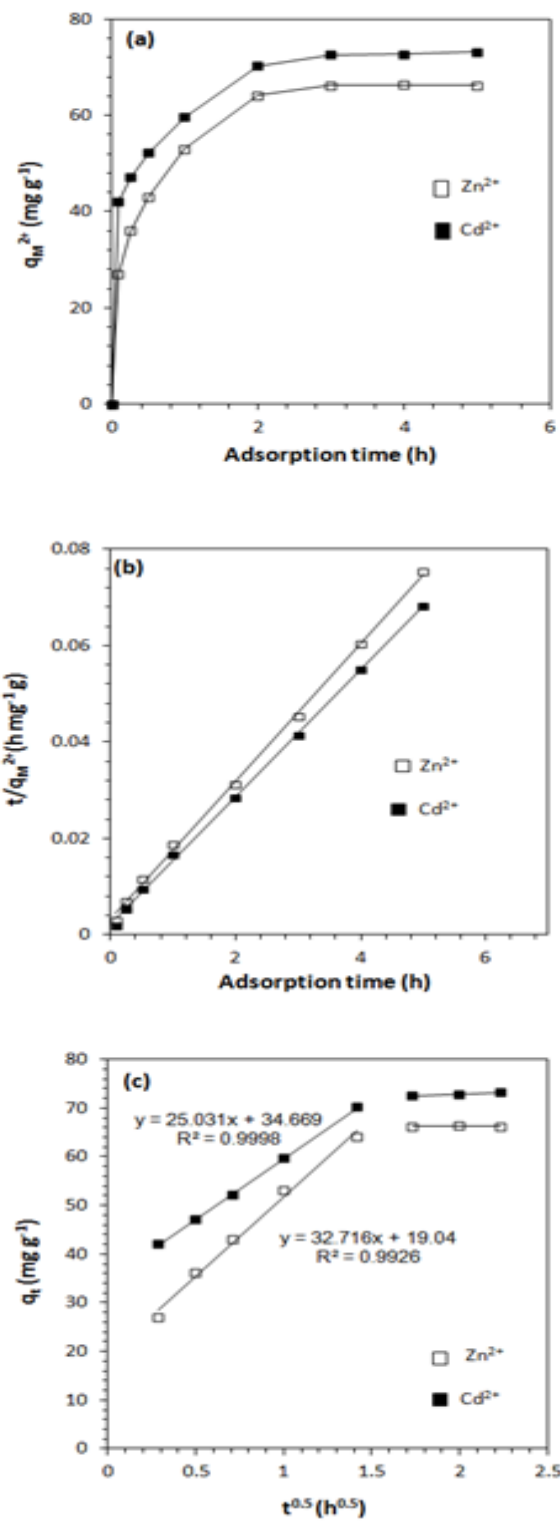


Figure 9.02. (a) Effect of time on the adsorption capacity; (b) Lagergren second-order kinetic model.(c) Intraparticle diffusion model.

The following equations express the linearly first-order and second-order kinetic equations (Eqs. 3 and 4) for the Lagergren model, respectively:

$$\log (q_e - q_t) = \log q_e - \frac{k_1 t}{2.303} \quad (3)$$

$$\frac{t}{q_t} = \frac{1}{k_2 q_e^2} + \frac{t}{q_e} \quad (4)$$

where k_1 and k_2 are the first-order and second-order rate constant, respectively; q_t and q_e are the adsorption capacity of the metal ions at a time t and at equilibrium, respectively. Neither Zn^{2+} nor Cd^{2+} fitted the first-order Lagergren kinetic model, so the graph representing the kinetic model has not been displayed, while the second-order Lagergren kinetic model (Fig. 9.2b, Table 9.1) fitted the adsorption of both Zn^{2+} and Cd^{2+} ions.

Table 09.1 Lagergren second-order kinetic model parameters for Zn^{2+} and Cd^{2+} adsorption.

CAPE	Temp (K)	$q_{e, \text{exp}}$ (mg g ⁻¹)	k_2 (h ⁻¹ g mg ⁻¹)	h^a (h ⁻¹ g ⁻¹ mg)	$q_{e, \text{cal}}$ (mg g ⁻¹)	R^2	E_a (kJ mol ⁻¹)
Zn^{2+}	298	66.2	0.0620	303	68.5	0.9986	13.4
	308	72.2	0.0769	435	74.6	0.9994	
	323	79.1	0.0946	625	81.0	0.9998	
Cd^{2+}	298	73.2	0.0792	455	75.8	0.9989	12.2
	308	79.3	0.0946	625	81.3	0.9993	
	323	89.0	0.116	833	84.7	0.9995	

^aInitial adsorption rate $h = k_2 q_e^2$.

The data fitted with the second-order model suggesting that the adsorption is a chemical adsorption process^[198, 199]. The resin was found to be an efficient adsorbent for

removing both zinc and cadmium ions from aqueous solutions; the rate of adsorption as well as the adsorption capacity of Cd^{2+} was found to be larger than that of Zn^{2+} . The adsorption process is influenced by various factors like ionic radius, hydration energy, electronegativity, hardness index, etc., among which some factors may dominate over the others. The factor that influences the adsorption most seems to be the hydration energy; the metal ion has to be dehydrated prior adsorption and as such the Zn^{2+} ions having higher hydration energy is less like to be adsorbed than Cd^{2+} (Table 9.2)^[201].

Table 09.02. Ionic radius, effective hydrated ionic radius, hydration energy, electronegativity, and hardness Index of Zn^{2+} and Cd^{2+} ions

Metal ion	Ionic radius (nm)	Hydration energy (kJ mol^{-1})	Hydration radius (nm)	Electronegativity (Pauling)	Hardness Index
Zn^{2+}	0.083	-2057	0.276	1.65	0.115
Cd^{2+}	0.097	-1827	0.263	1.69	0.081

Another model that can be used to study the effect of the adsorption rate is the intraparticle diffusion model which assumes that the metals transport from the solution through an interface between the solution and the adsorbent into the pores of the particles in the adsorbent (Eq. 5), and can be expressed by the relation of the adsorption capacity and time ^[200, 220].

$$q_t = x_i + k_p t^{0.5} \quad (5)$$

where q_t is the adsorption capacity at time t , k_p is the rate constant of intraparticle diffusion, x_i is related to boundary layer thickness. If the data plot of q_t versus $t^{0.5}$ gives a straight line then the adsorption process is governed by the intraparticle diffusion. Since the initial linear plot did not pass through the origin, that is, there is an intercept which

indicates that rapid adsorption occurs within a short period of time (Fig. 9.2c). The intercept x_i of the linearized line was used to define the initial adsorption factor (R_i) as:

$$R_i = 1 - \frac{x_i}{q_e} \quad (6)$$

where x_i is the initial adsorption amount and q_e the final adsorption amount at the longer time. The respective x_i and q_e values of 19.0 and 66.2 mg g⁻¹ for Zn²⁺ at 25°C, and the corresponding values of 34.7 and 73.2 mg g⁻¹ for Cd²⁺ (Table 9.1, Fig. 9.2c), led to R_i values of 0.713 and 0.526 for Zn²⁺ and Cd²⁺, respectively. For the Cd²⁺, for instance, the R_i value of 0.526 indicate the relatively strong rapid initial adsorption has already reached (1- 0.526)×100 i.e. 47.4% before the first adsorption data was collected at a time of 5 min. The other 52.6% of adsorption is governed by intraparticle diffusion as indicated by the linear relation with an excellent square of correlation coefficient (R^2) of 0.9998 (Fig. 9.2c). In this case, the intraparticle diffusion within the pores of the resins becomes the rate-limiting step. Note that the horizontal asymptote represents the final equilibrium stage.

9.3.3 Effect of initial concentration on the adsorption of Zinc and Cadmium ions

As shown in Fig. 9.3a the adsorption capacity of CAPE 5 increased with increasing the concentrations of Zn²⁺ and Cd²⁺ ions. Two isotherm models were applied; Langmuir isotherm model, which can be expressed by Eq. (7), assumes the mechanism of the adsorption process as a monolayer adsorption on the surface of the polymer:

$$\frac{C_e}{q_e} = \frac{C_e}{Q_m} + \frac{1}{Q_m b} \quad (7)$$

where C_e and q_e are the concentration of metal ions in the solution and on the resin, respectively, Q_m and b are the Langmuir constants. Fig. 9.3b represents the plot of C_e/q_e versus C_e .

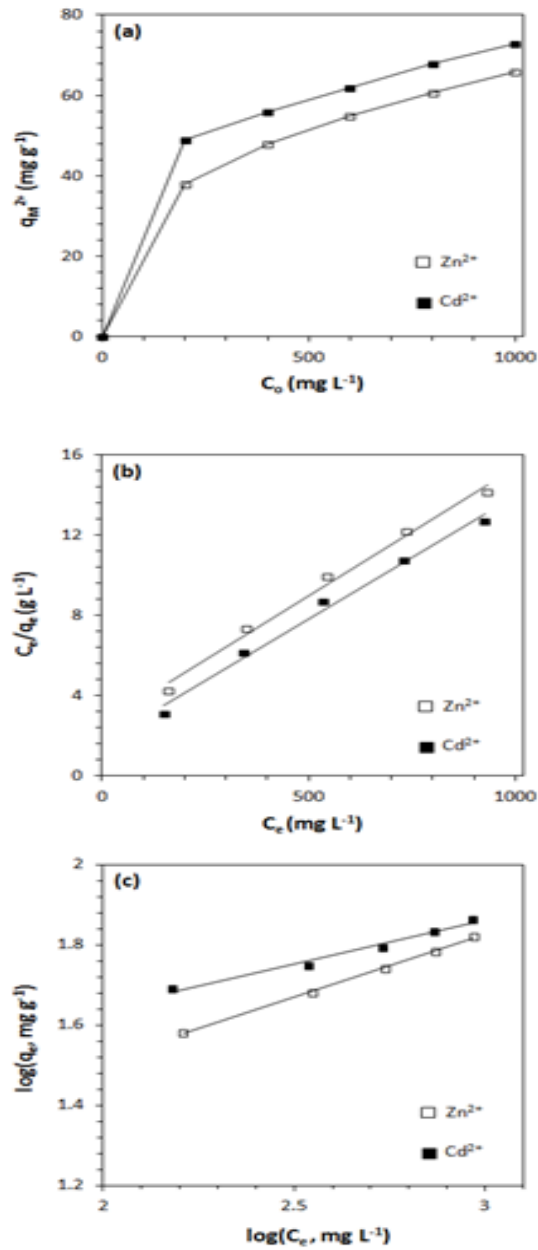


Figure 9.03. (a) Effect of concentration on the adsorption capacity; (b) Langmuir isotherm plot ; (c) Freundlich isotherm plot.

Freundlich isotherm model, on the other hand, describes the adsorption occurring on a heterogeneous surface with uniform energy; Eqs. **8** and **9** express the model:

$$q_e = k_f C_e^{1/n} \quad (8)$$

$$\log q_e = \log k_f + \frac{1}{n} \log C_e \quad (9)$$

where q_e and C_e are the equilibrium concentrations of metal ions on the adsorbed and in the liquid phase, respectively; k_f and n represent the Freundlich constants, which can be calculated from the slope and intercept of Fig. 9.3c which shows the plot of $\log q_e$ versus $\log C_e$. Figs. 9.3b and 9.3c illustrate that adsorption of Zn^{2+} and Cd^{2+} ions fitted well with both Langmuir and Freundlich isotherm models (Table 9.3). The maximum adsorption capacity (Q_m) found by the Langmuir isotherm model was close to the experimental data supporting that the adsorption mechanism could be monolayer adsorption.

The fitness of data with Freundlich isotherm model could also support that the adsorption occurred on a heterogeneous surface.

For the Langmuir isotherm model, separation factor or equilibrium parameter (R_L) can be used to describe the favorability of adsorption on the polymer surface by Eq. **(10)** [47].

$$R_L = \frac{1}{(1+bC_0)} \quad (10)$$

Where C_0 is the initial M^{2+} concentration and b is the Langmuir equilibrium constant. A favorable adsorption is indicated when the R_L value is between $0 < R_L < 1$, whereas the R_L

values outside the range describes an unfavorable adsorption. The R_L values for the adsorption of both metal ions are given in Table 4, which reveals that R_L values fall in the preferred region ($0 < R_L < 1$).

Table 09.3 Langmuir and Freundlich isotherm model constants for Zn²⁺ and Cd²⁺ adsorption at 25°C.

Langmuir isotherm model				
Entry No	Metal ion	Q_m (mg g ⁻¹)	b (dm ³ mg ⁻¹)	R^2
1	Zn ²⁺	78.7	4.87×10^{-3}	0.9916
2	Cd ²⁺	81.3	7.44×10^{-3}	0.9903
Freundlich isotherm model				
Entry No	Metal ion	k_f	n	R^2
1	Zn ²⁺	7.69	3.19	0.9992
2	Cd ²⁺	16.1	4.59	0.9790

Table 9.4 The R_L values based on the Langmuir isotherm model

C_o (mg L ⁻¹)	R_L value	
	Zn ²⁺	Cd ²⁺
200	0.5064	0.4012
400	0.3391	0.2516
600	0.2549	0.1831
800	0.2042	0.1439
1000	0.1703	0.1185

The more favorable adsorption is reflected by lower R_L values; as seen in Table 9.4, the R_L values decreased with increasing the initial concentration, indicating more favorable adsorption at higher concentration of metal ions.

For the Freundlich isotherm model, the values of n were determined to be higher than 1; values lying in the range 1 to 10 are considered for classification as favorable adsorption^[225, 226]. The slope ($1/n$) range of 0 - 1 is known to be a measure of adsorption intensity or surface heterogeneity, becoming more heterogeneous as its value gets closer to zero. A $1/n$ value below unity is indicative of chemisorption process, whereas $1/n$ above one implies cooperative adsorption (Table 9.3)^[227]. For the adsorption of Cd^{2+} ions, the higher value of the constant k_f , which is related to adsorption capacity (q), indicates higher affinity of the ions to the adsorbent in comparison to Zn^{2+} adsorption.

9.3.4 Effect of pH on adsorption

Adsorption experiments at different pHs (3 – 6) have been carried out; as seen from Fig. 9.4. The maximum adsorption was found to be pH = 4 for adsorption of both the metal ions. As shown in Figure 9.4, the adsorption capacity increased by increasing the pH which could be due to the increase of the anionic motifs [i.e. $\text{N}^{\cdots}\text{P}(=\text{O})(\text{O}^-)_2$] that would impart stronger attraction to the metal ions. Whereas, at lower pH (pH = 3) the increased amount of cationic motifs [i.e. $\text{NH}^+\cdots\text{P}(=\text{O})(\text{OH})_2$] discourages the adsorption of metal cations thereby leading to lower adsorption capacity. At higher pH, metal hydrolysis occurs owing to the formation of metal hydroxides which interfere in the determination of the adsorption capacity^[161]. This is why the study was not conducted at pH 6 even though it gave higher adsorption capacity.

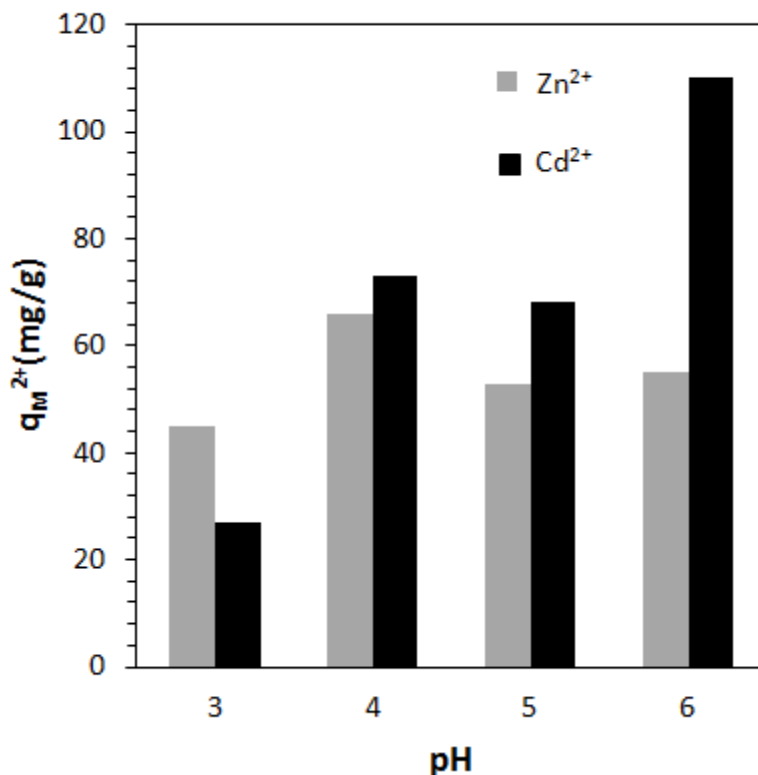


Figure 9.4. Effect of pH on the adsorption capacity.

9.3.5 Effect of Temperature on adsorption

Adsorption experiments were performed to study the effect of temperature on the adsorption capacity (Fig. 9.5a). Increased adsorption capacity at higher temperatures suggests the adsorption as an endothermic process. Swelling of the polymer at higher temperatures permits greater diffusion of metal ions. Using Arrhenius equation (Eq. 11), a plot of $\ln k_2$ (table 9.1) versus $1/T$ (Fig. 9.5b) can be used to calculate the activation energies which were found to be 13.4 and 12.2 kJ/mol for the adsorption of Zn^{2+} and Cd^{2+} , respectively^[167].

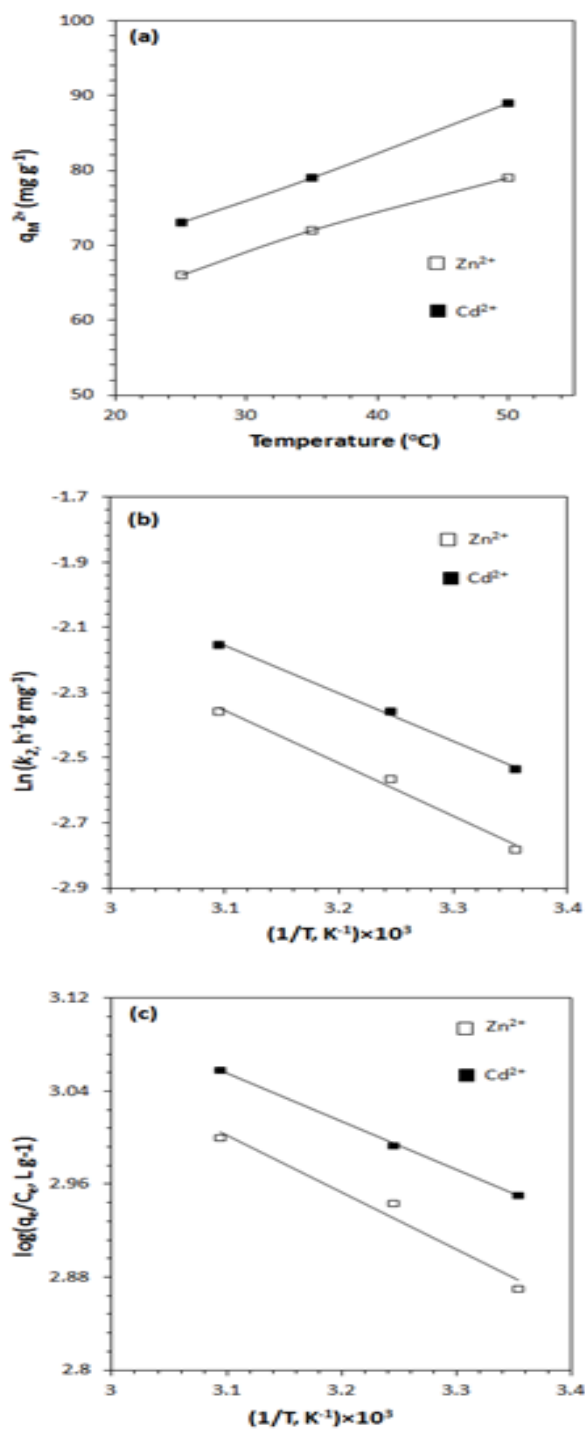


Figure 9.5. (a) Effect of temperature on the adsorption capacity; (b) Arrhenius plot; (c) Vant-Hoff plot.

These E_a values are relatively low in comparison to typical chemical reactions with activation energies of 65 – 250 kJ/mol, thereby indicating that the adsorption of the metal ions is relatively easy and a favored process^[175].

$$\ln k_2 = -\frac{E_a}{RT} + \text{constant} \quad (11)$$

Thermodynamic parameters ΔG , ΔH and ΔS were calculated using Vant-Hoff equation (Eq. 12). A plot of $\log (q_e/C_e)$ versus $1/T$ is displayed in Fig. 9.5c and are tabulated in Table 9.5^[175]. The negative ΔG values ascertain the spontaneity of the adsorption process.

$$\log \left(\frac{q_e}{C_e} \right) = -\frac{\Delta H}{2.303RT} + \frac{\Delta S}{2.303R} \quad (12)$$

As the temperature increases the ΔG values become more negative thereby indicating that the endothermic adsorption is more favorable at higher temperatures. Favorable adsorption at higher temperatures is attributed to the greater swelling of the resin and increased diffusion of metal ions into the resin. Greater dissociation of zwitterionic phosphonate motifs, $\text{NH}^+\cdots\text{P}(=\text{O})(\text{OH})\text{O}^-$ to zwitterionic/anionic motifs, $\text{NH}^+\cdots\text{P}(=\text{O})(\text{O}^-)_2$, at elevated temperatures is also expected to increase the electrostatic attractions between the metal ions and ion exchange groups. The positive values of ΔH certify that the adsorption is an endothermic process. In addition, it can be found in Table 9.5 that the ΔS values are positive, suggesting that the randomness increased during adsorption of metal ions as a result of release of water molecules from the large hydration shells of the metal ions.

Table 9.05 Thermodynamic Data for Zn²⁺ and Cd²⁺ adsorption.

Metal ion	Temp. (K)	ΔG (kJ/mol)	ΔH (kJ/mol)	ΔS (J/mol K)	R ²
Zn ²⁺	298	-16.4			
	308	-17.3	9.44	86.7	0.9722
	323	-18.6			
Cd ²⁺	298	-16.8			
	308	-17.7	7.98	83.3	0.9991
	323	-18.9			

As reported in the literature^[165, 185] the aminomethylphosphonate motifs are potentially tridentate ligands, having one coordination site at the nitrogen and two bonding sites at the phosphonate motif. Towards the weak acid range the formation of metal-complex using the aminophosphonate motif as a tridentate ligand (especially at low loads) is depicted in Scheme 2. At high loads, complexes without the amino group would result using phosphonate motif as a bidentate ligand.

9.3.6 Scanning electron microscopy (SEM)

Unloaded and loaded CAPE **5** were investigated by scanning electron microscopy. Unloaded CAPE **5** was immersed in each of 1000 ppm solution of Zn(II) and Cd(II) for 24 h at pH 4, filtered, and dried under vacuum until constant weight was achieved. Loaded and unloaded polymers were then sputter-coated for 4 min. with a thin film of gold. CAPE **5** SEM and EDX images (Figure 9.6) shows the composition of the unloaded resin which contains: C, O, Na, P, S which is similar to the designed resin (Figure 9.6a, scheme 1). Whereas, Figure 9.6b and 9.6c shows the disappearance of Na ions which

were displaced with zinc and cadmium ions, indicating that the adsorption occurred on CAPE 5 as shown by Energy-dispersive X-ray spectroscopy (EDX analysis).

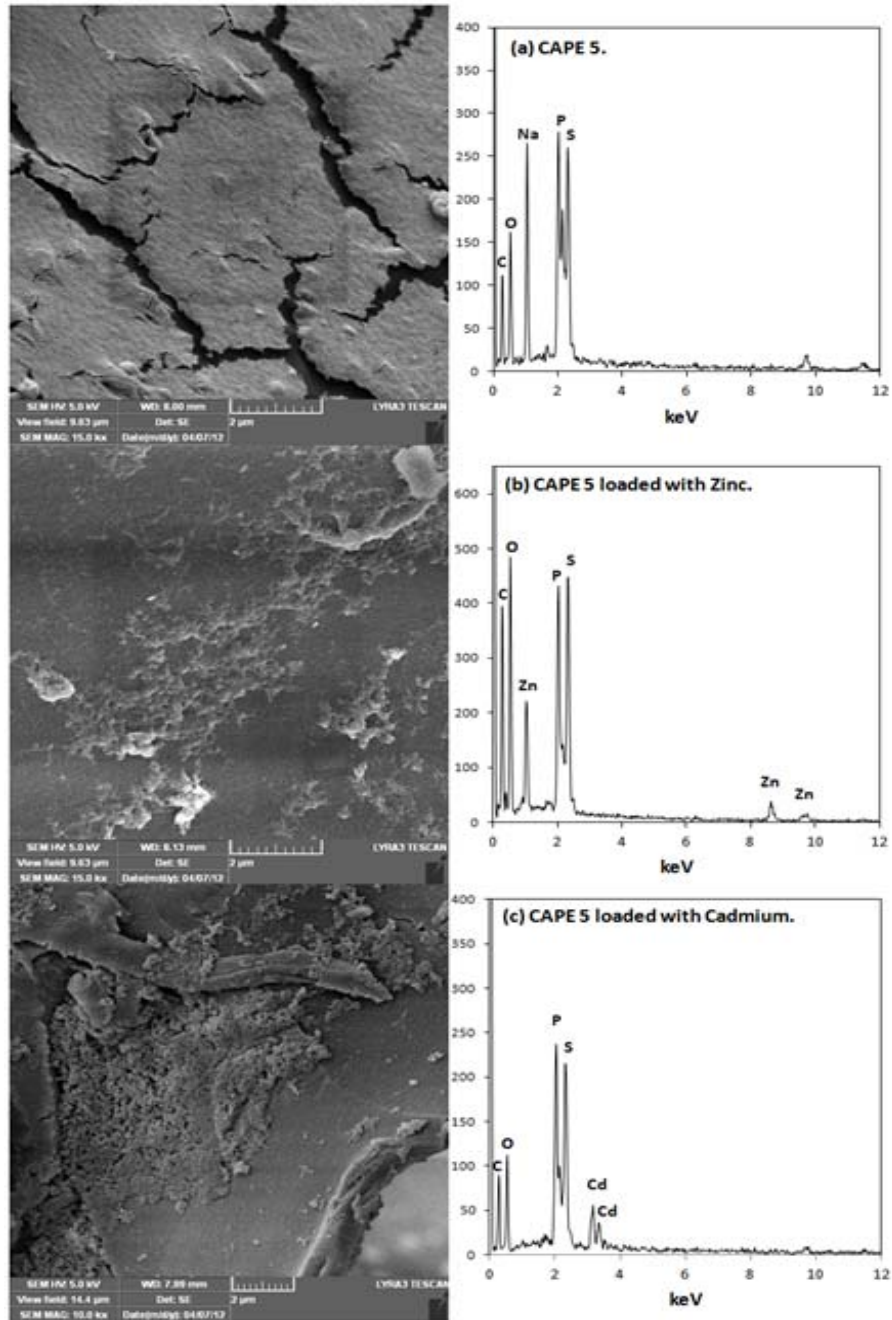


Figure 9.6. SEM images and EDX analysis for:(a) CAPE 5; (b) CAPE 5 loaded with Zinc; (c) CAPE 5 loaded with Cadmium.

9.4 Conclusion

The cross-linked polyphosphonate **5** was found to have an excellent adsorption capacity for Zn²⁺ and Cd²⁺ ions. The adsorption followed Lagergren second-order kinetic model and Langmuir as well as Freundlich isotherm models. The negative ΔG s and positive ΔH s ensured the spontaneity and the endothermic nature of the adsorption process, respectively. The adsorption capacities of CAPE **5** for Zn²⁺ and Cd²⁺ ions are compared with those of various types of sorbents in Table 9.6 which ascertains the excellent efficacy of the current resin for the removal of the metal ions.

Table 9.06 Comparison of CAPE 5 with those of different types of sorbents in References.

Adsorbent	Zn ²⁺ (mg g ⁻¹)	Cd ²⁺ (mg g ⁻¹)	Refs
Na-Montmorillonite	3.6	5.2	[202]
Coffee residue-clay	13.4	39.5	[203]
red mud	14.9	10.6	[205]
manganese ore	98.0	59.2	[206]
Activated carbon	-	8.0	[207]
CAPE 5	78.7	81.3	This work

CHAPTER 10: Novel cross-linked polymers having pH-responsive amino acid residues for the removal of Cu²⁺ from aqueous solution at low concentrations

Taken from S. A. Ali, **Othman Charles S. Al-Hamouz**, N. M. Hassan, Novel cross-linked polymers having pH-responsive amino acid residues for the removal of Cu²⁺ from aqueous solution at low concentrations, *Journal of Hazardous Materials*, 248-249 (2013) 47-58.

ABSTRACT

Two novel cross-linked anionic polyelectrolytes (CAPE) **I** and **II** containing pH-responsive amino acid residues have been synthesized *via* cyclo- and terpolymerization of a monomer having diallylammonioethanoate motif (90 mol%) and a cross-linker 1,1,4,4-tetraallylpiperazinium dichloride (10 mol%) in the absence and presence of SO₂ (100 mol%), respectively. The experimental data for the adsorption of Cu²⁺ on the CAPES fitted Lagergren second-order kinetic model thereby indicating the chemical nature of the adsorption process. The fitness order of Freundlich > Langmuir > Temkin for the isotherm models for CAPE **I** showed the favorability of adsorption on a heterogeneous surface, whereas for CAPE **II** the fitness order of Langmuir > Freundlich > Temkin certified the favorability toward monolayer adsorption. The adsorption process was spontaneous and endothermic in nature with negative and positive values for ΔG and ΔH , respectively. For the sorbents CAPE **I** and CAPE **II**, the efficiency of Cu²⁺ removal at an initial metal concentration of 200 ppb was found to be 77.5 and 99.4%, respectively. Desorption efficiencies were found to be 88 and 93% for CAPE **I** and CAPE **II**,

respectively. Treatment of real wastewater samples spiked with Cu^{2+} ions showed the excellent ability of the resins to adsorb metal ions.

KEY WORDS: adsorption, cross-linked polyaminocarboxylate, heavy metal.

10.1 Introduction

Removal of toxic metal ions is a matter of great importance due to their negative effects on the environment and human health. Nonbiodegradable Cu^{2+} ions in typical concentrations of several thousand ppm to less than 1 ppm are produced as waste in various chemical industries, such as smelting, mining, printed circuit board manufacturing, electroplating, wire drawing, copper polishing, and paint manufacturing. The accumulation of copper in the human body can cause a variety of diseases and disorders. High intake of copper can be fatal: a concentration of 1.3 ppm can cause immediate effects on infants and adults as well in the form of vomiting, diarrhea, nausea; at higher concentrations; for infants, it can cause liver and kidney damage^[228, 229]. According to WHO standards, the maximum allowable concentration of copper in drinking water is 0.2 mg/l^[230], while it is 0.2 and less than 2 ppm for agriculture irrigation and ponds fish farming, respectively^[231]. In order to protect humans and the environment, it is of utmost importance to remove copper ions from environments.

Various techniques, like adsorption, precipitation, dialysis, ion exchange, reverse osmosis, and extraction, have been developed in the past for the removal of metal contaminants from water resources. One of the most attractive among these techniques is presumably the adsorption process due to the availability of different types of low-cost and environment-friendly adsorbents^[48, 52, 151, 188]. Inorganic/organic polymer hybrid adsorbents have been widely investigated; their efficacies in metal ion removal are

attributed to the formation of a stronger chemical bonding between M^{n+} and, for instance, amine motifs in the hybrid materials^[54, 58, 152, 190, 210]. Recently, the researchers have focused on the syntheses of zwitterionic cross-linked inorganic/organic hybrid materials for the removal of heavy metal ions *via* electrostatic effects^[47, 59, 60, 67, 153, 193].

There are many sorbent materials to remove larger concentration of metal ions; however, it remains challenging to develop new materials for removing copper ions at ppb-levels. In the current study, two novel cross-linked polymers containing aminomethylcarboxylate motifs (i.e., aminoacid residues) have been synthesized and tested for their efficiencies as adsorbents for the removal of Cu^{2+} ions at low concentrations from aqueous solutions.

10.2 Experimental

10.2.1 Apparatus

Elemental analysis was carried out on a Perkin Elmer Elemental Analyzer Series II Model 2400. IR spectra were recorded on a Perkin Elmer 16F PC FTIR spectrometer. 1H and ^{13}C spectra were measured on a JEOL LA 500 MHz spectrometer using HOD signal at δ 4.65 and dioxane signal at 67.4 ppm as internal standards, respectively. The specific surface area for CAPE **6** and CAPE **9** were measured by Burnauer–Emmett–Teller (BET) N_2 method using a Micrometrics ASAP 2020 BET surface area analyzer. Samples were degassed under high vacuum for 6 h at 80 °C. Specific surface area for both CAPEs were calculated by the Brunauer–Emmett–Teller (BET) method and pore volumes were taken at the $P/P_0 = 0.974$ single point. Pore size diameter was determined by the BJH method. Scanning electron microscopy images were taken by TESCAN LYRA 3 (Czech Republic) equipped with Oxford, energy-dispersive X-ray spectroscopy (EDX) detector

model X-Max. Inductively coupled plasma analysis was performed on ICP-MS XSERIES-II (Thermo Scientific), Thermogravimetric analysis (TGA) was performed using a thermal analyzer (STA 429) manufactured by Netzsch (Germany). The polymer sample to be tested (usually ~5 mg) was placed in a platinum crucible. Aluminum oxide (Al_2O_3 ; ~4 mg) was placed in an identical platinum crucible as a reference sample. With the sample carrier system, which had two sets of 10% Pt–Pt/Rh thermocouples, the sample carrier was placed in the middle of the vertical furnace, which was programmed and controlled by a microprocessor temperature controller. The temperature was raised at a uniform rate of 10 °C/min. The analyses were made over a temperature range of 20–800 °C in an air atmosphere flowing at a rate of 100 mL/min.

10.2.2 Materials

Azoisobutyronitrile (AIBN) from Fluka AG was purified by crystallization from a chloroform-ethanol mixture. Diallylamine, t-butylhydroperoxide (TBHP) (70% aqueous solution), from Fluka Chemie AG (Buchs, Switzerland) were used as received. All solvents used were of analytical grade.

10.2.3 Synthesis of monomers

10.2.3.1 Ethyl diallylaminoethanoate (1)

Amine **1** was prepared as described^[26].

10.2.3.2 Sodium diallylaminoethanoate (2)

A mixture of **1** (50.0 g, 0.273 mol) and sodium hydroxide (12.4 g, 0.31 mol) in methanol (100 ml) was stirred at 20 °C for 24 h. After removal of the solvent, the residual solid was washed with ether and dried under vacuum at 55 °C to a constant weight (45.3 g, 94%). Mp 295 – 297 °C; (Found: C, 54.0; H, 6.9; N, 7.7%. $\text{C}_8\text{H}_{12}\text{NNaO}_2$ requires C,

54.23; H, 6.83; N, 7.91%); ν_{\max} (KBr) $\nu(-C(=O)O^-)$ 1594, 1408 cm^{-1} ; $\nu(\text{C-N})$ 1157 cm^{-1} ; $\nu(\text{C=C})$, 1645, 994, 914 cm^{-1} . δ_{H} (D_2O) 2.99 (2H, s), 3.09 (4H, d, J 7.1 Hz), 5.11 (4H, m) and 5.75 (2H, m); δ_{C} (D_2O) 56.91, 57.26 (2C), 120.04 (2C, $=\text{CH}_2$), 134.96 (2C, $\text{CH}=\text{}$) and 179.61. ^{13}C spectral assignments were supported by DEPT 135 NMR analysis.

10.2.3.3 Diallylammonioethanoate (3)

Concentrated HCl (20 mL, 0.24 mol) was added dropwise (*ca.* 5 min) to a solution of **2** (40 g, 0.23 mol) in water (30 mL). The mixture was then freeze dried, and the residual solid was dissolved in ethanol (45 ml). The precipitated NaCl was filtered off washed with a 1:1 ethanol/ether mixture. Removal of the solvents followed by drying at 55 °C under vacuum to a constant weight afforded the zwitterionic monomer **3** (32 g, 90%). Mp 85-89 °C closed capillary; (Found: C, 61.6; H, 8.6; N, 8.7%. $\text{C}_8\text{H}_{13}\text{NO}_2$ requires C, 61.91; H, 8.44; N, 9.03%); ν_{\max} (KBr) $\nu(\text{C=O})$ 1734 cm^{-1} , $\nu(\text{C(=O)O}^-)$ 1644, 1396 cm^{-1} ; $\nu(\text{C-N})$ 1154 cm^{-1} ; $\nu(\text{C=C})$, 1646, 998, 885 cm^{-1} ; δ_{H} (D_2O) 3.54 (2H, s), 3.69 (4H, br, s), 5.45 (4H, m) and 5.81 (2H, m); δ_{C} (D_2O) 55.03, 57.48 (2C), 126.63 (2C, $\text{CH}=\text{}$), 127.42 (2C, $=\text{CH}_2$) and 171.33. ^{13}C spectral assignments were supported by DEPT 135 NMR analysis.

10.2.3.4 1,1,4,4-tetraallylpiperazinium dichloride (4)

Monomer **4**, a cross-linker, was prepared as described^[64].

10.2.3.5 N,N-diallyl-N-carboethoxymethylammonium chloride (7)

Monomer **7** was prepared as described^[26].

10.2.4 Copolymerization of monomer 3 and 4 to form cross-linked polyzwitterion (CPZA) 5

The initiator TBHP (610 mg) was added to a homogeneous mixture of monomer 3 (8.0 g, 51.5 mmol) and cross-linker 4 (1.82 g, 5.7 mmol) in water (5.29 g). The reaction mixture under N₂ in the closed flask was stirred using a magnetic stir-bar at 87 °C for 24 h. Within 3-5 h, the magnetic stir-bar stopped moving; the reaction mixture became a transparent swollen gel. At the end of the elapsed time, the swelled gel of the CPZA 5 was soaked in water (48 h) with replacement of water several times. The swelled gel was then poured onto acetone. The resin was filtered and dried under vacuum at 70°C to a constant weight (5.6 g, 57%). The yield is based on incorporation of the monomers 3/4 in a ratio of 90:10 which is same as the feed ratio. (Found: C, 61.1; H, 8.6; N, 8.8%. Monomer 3 C₈H₁₃NO₂ (90 mol%) and monomer 4 C₁₆H₂₈Cl₂N₂ (10 mol%) requires C, 61.73; H, 8.48; N, 9.00 %); ν_{\max} (KBr) $\nu(\text{C}=\text{O})$ 1715 cm⁻¹, $\nu(\text{CO}_2^-)$ 1593, 1403 cm⁻¹; $\nu(\text{C}-\text{N})$ 1135 cm⁻¹.

10.2.4.1 Basification of CPZA 5 to cross-linked anionic polyelectrolyte (CAPE 6)

A mixture of CPZA 5 (4.04 g, ~ 23.5 mmol) and a solution of NaOH (1.88 g, 47 mmol) in water (100 mL) was stirred at room temperature for 24 h. CAPE 6 was dropped onto methanol (200 ml) and allowed to soak in it for 5 h after which it was filtered and dried under vacuum at 65°C to a constant weight (3.1 g, 70%). TGA analysis show initial decomposition begins around 200°C. The surface area and total pore volume were found to be 2.15 m² g⁻¹ and 0.0022 cm³ g⁻¹, respectively.

10.2.5 Terpolymerization of **4**, **7**, and sulfur dioxide to cross-linked cationic polyelectrolyte (CCPE **8**)

Sulfur dioxide (1.92 g, 30 mmol) was absorbed in a mixture of **7** (5.93 g, 27 mmol) and cross-linker **4** (3.0 mmol, 0.96 g) in DMSO (6.0 g). Initiator AIBN (150 mg) was then added, and the mixture was stirred at 65 °C for 48 h during which it became viscous. At the end of the elapsed time, the viscous product was soaked in water for 24 h, with frequent changing of water, and finally freeze-dried (6.34 g, 72%). The yield is based on incorporation of the monomers **3/4/SO₂** in a ratio of 90:10:100 which is same as the feed ratio. (Found: C, 42.8; H, 6.6; N, 4.9; S, 10.7 %). A terpolymer from monomer **7** C₁₀H₁₈ClNO₂ (90 mol%) and monomer **4** C₁₆H₂₈Cl₂N₂ (10 mol%) and SO₂ (100 mol%) requires C, 43.11; H, 6.49; N, 5.18; S, 11.01 %); ν_{\max} (KBr) $\nu(\text{C}=\text{O})$ 1746 cm⁻¹; $\nu(\text{C}-\text{O}-\text{C})$ 1232 cm⁻¹; $\nu(\text{S}(\text{=O})_2)$ 1308, 1123 cm⁻¹.

10.2.5.1 Ester hydrolysis of CCPE **8** to form cross-linked anionic polyelectrolyte (CAPE **9**)

A mixture of **8** (5.07 g, 17.3 mmol) and sodium hydroxide (40 mmol, 1.6 g) in water (150 ml) was stirred for 24 h, after which it was poured onto excess methanol. The Resin (CAPE **9**) was filtered and dried under vacuum at 45 °C to a constant weight (3.4 g, 77%). TGA analysis show initial decomposition around 200°C. The surface area, pore size diameter, and total pore volume were found to be 9.9 m² g⁻¹, 10.7 nm, and 0.026 cm³ g⁻¹, respectively.

10.2.6 Sample characterizations

FT-IR spectra were recorded on a Perkin Elmer 16F PC FTIR spectrometer in the region of 4000-400 cm⁻¹. Thermal gravimetric analysis (TGA) was conducted to measure the thermal stability of the CAPE **6** and CAPE **9** and examine the modes of

decomposition. SEM and EDX images show the morphology and the existence of copper adsorbed on both the cross-linked polymers.

10.2.7 Adsorption experiments

The procedure for the adsorption experiments of the cross-linked polymer CAPE **6** for Cu²⁺ ions can be described briefly as follows: a mixture of CAPE **6** (50 mg) in an aqueous Cu(NO₃)₂ solution (20 mL) having 1 mg L⁻¹ of Cu²⁺ ions was stirred using a magnetic stir-bar at different pH for 24 h. The resin was filtered and carefully washed with deionized water. The combined filtrate was analyzed by ICP-MS to determine the amount of Cu²⁺ remained. The adsorption capacity ($q_{Cu^{2+}}$) in mg g⁻¹ can be calculated using Eq. (1):

$$q_{Cu^{2+}} = \frac{(C_0 - C_f)V}{W} \quad (1)$$

Where C_0 and C_f are the initial and final concentration of Cu²⁺ ions in mg/L, respectively, W is the weight of the polymer in g, and V is the volume of the solution in L. Data presented are average of triplicate runs and varied by less than 4% in all the cases studied.

For adsorption kinetic studies, the resin sample was stirred in a 1 mg L⁻¹ Cu(NO₃)₂ solution for different adsorption times at a preferred pH of 4 (*vide infra*). The adsorption isotherm was constructed by changing the concentration of Cu(NO₃)₂ solution from 200 µg L⁻¹ (i.e., ppb) to 1000 µg L⁻¹ (i.e. 1 ppm) at 25 °C for 24 h. Based on the adsorption data from experiments carried out at different temperatures, the activation energy for the adsorption process and thermodynamic parameters ΔG , ΔH and ΔS for Cu²⁺ removal

were calculated. Real samples of wastewater treatment plants were tested to examine the ability of the cross-linked polymers to adsorb heavy metals^[67, 175].

10.2.8 Desorption experiment

Desorption experiment was conducted by stirring 50 mg resin in aqueous $\text{Cu}(\text{NO}_3)_2$ (1 mg L^{-1}) solution (20 mL) for 24 h. The loaded resin was then filtered, dried and immersed in 0.1 M HNO_3 for 24 h. After filtration, the amount of Cu^{2+} ions desorbed in the filtrate was determined; the efficiency of the desorption process was calculated by the ratio of desorbed amount of Cu^{2+} ions to the amount of adsorbed Cu^{2+} ions in the resin CAPE **6** and CAPE **9**. The results indicated that the percentage efficiency of the desorption process to be 88 and 93% for CAPE **6** and CAPE **9**, respectively.

10.2.9 QA/QC

Quality control for METAL analyses included repeated injections and periodic (two in every 2-h operation of the equipment) analysis of STANDARD SOLUTION (Instrumental parameters are found in Table 10.1). A prior set of samples was rerun if the analyzed value differed from the STANDARD SOLUTION value by $>10\%$. The relative standard deviation among replicate determinations was typically $\leq 5\%$.

Table 10. 1 ICP-MS instrumental operating parameters ICP-MS XSERIES-II Thermo Scientific

RF power (W)	1403.92
Plasma gas flow (L/min)	13.02
Nebulizer gas flow (L/min)	0.95
Auxiliary gas flow (L/min)	0.7
Nebulizer	Quartz pneumatic nebulizer
Spray chamber	Glass with peltier cooling
Number of replicates	3
Acquisition mode	Pulse counting
Dwell time (ms)	10
Sweeps/Reading	100

10.3 Results and discussion

10.3.1 Synthesis of cross-linked polymer 6 and 9

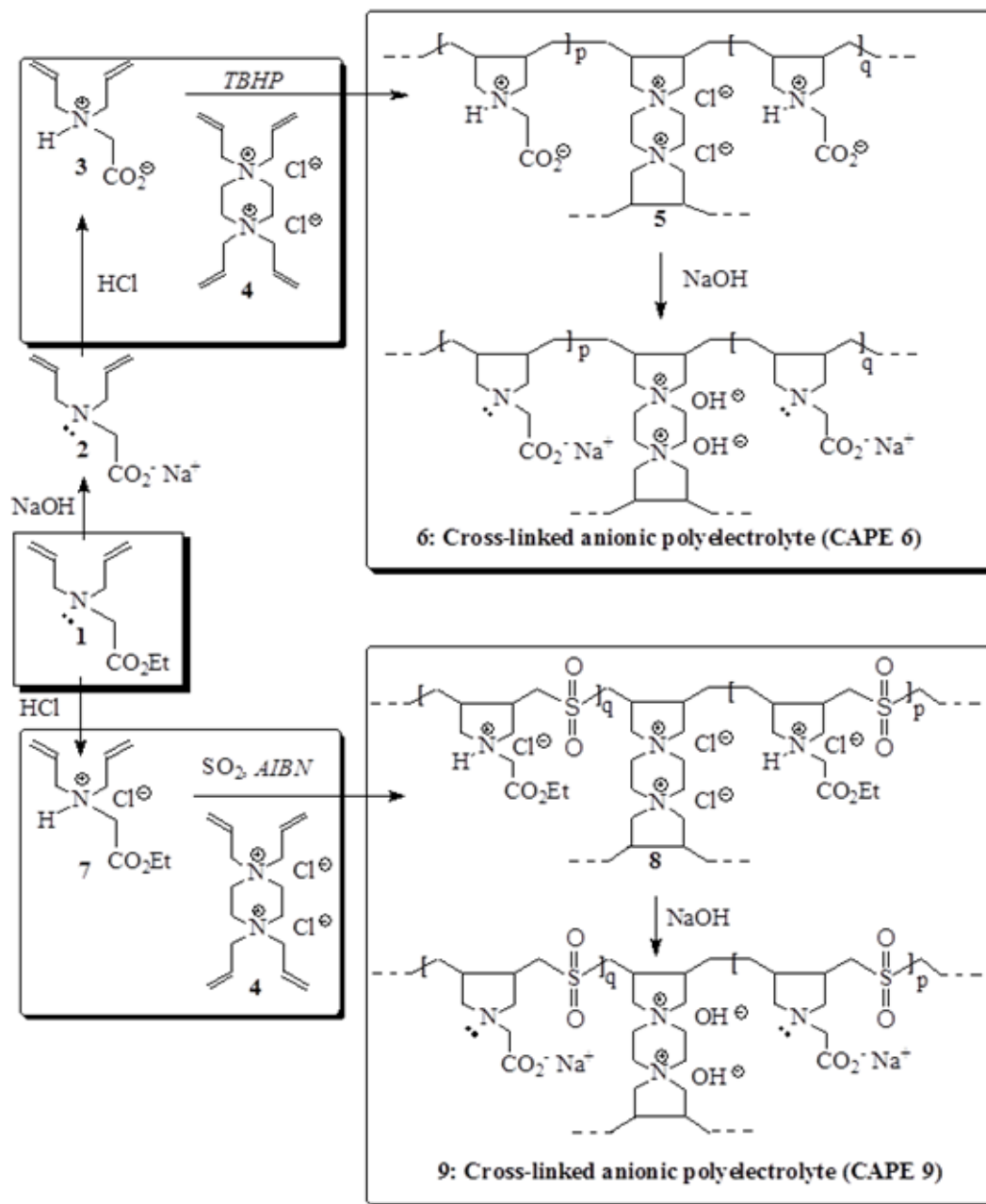
Butler's cyclopolymerization protocol has been utilized to synthesize the current resins **6** and **9** (Scheme 1). Butler's pioneering discovery of the cyclopolymerization involving a variety of *N,N*-diallylammonium salts has led to the synthesis of an array of scientifically and technologically important water-soluble cationic polyelectrolytes^[20, 130, 158]. The polymer-architecture, having the five-membered cyclic units embedded in the backbone, has been recognized as the eighth major structural type of synthetic polymers^[130]. Over 33 million pounds of poly(diallyldimethylammonium chloride) alone are sold annually for water treatment and another 2 million pounds are used for personal care formulation^[20].

Zwitterionic monomer **3** (90 mol%) and cross-linker **4** (10 mol%) underwent cyclopolymerization in the presence of initiator TBHP to give the novel cross-linked polyzwitterion (CPZ) **5** (Scheme 1). Elemental analysis of the CPZ revealed the

incorporation of monomers **3** and **4** in an approximate mol ratio of 90:10 which is the same as the feed ratio. CPZ **5** was found to swell in water while shrank upon soaking in acetone owing to the removal of water. Its basification with excess NaOH led to cross-linked anionic polyelectrolyte (CAPE) **6**.

Cationic monomer **7** (90 mol%), cross-linker **4** (10 mol%), and sulphur dioxide (100 mmol%) in DMSO as a solvent underwent terpolymerization in the presence of initiator AIBN to give the novel cross-linked cationic polyelectrolyte (CCPE) **8** (Scheme 1). Elemental analysis of CCPE **8** revealed the incorporation of monomers **7** and **4** in an approximate mol ratio of 90:10 which is the same as the feed ratio. CCPE **8** was found to swell in water while shrank upon soaking in acetone owing to the removal of water. Treatment with excess NaOH led to the hydrolysis of the ester groups to form CAPE **9**.

Thermogravimetric analysis (TGA) curve of CAPE **6** (Fig. 10.1) showed two major loss in the weight: the first slow weight loss of 24.2% is attributed to the decarboxylation of the pendant carboxylate groups, the second major loss of 70.2% is the result of combustion of nitrogenated organic fraction with the release of CO₂, NO_x and H₂O gases [163]; the residual mass at 800 °C was found to be 5.6%. For CAPE **9**, TGA analysis (Fig. 10.1) showed three major losses in the weight: first sharp loss of 14.4%, second slow loss of 39.0%, and third slow loss of 21.0% are attributed to the loss of SO₂, the decarboxylation of the pendant carboxylate groups, and the decomposition of the nitrogenated organic fraction respectively. The residual mass at 800 °C was found to be 25.6%.



Scheme 1.

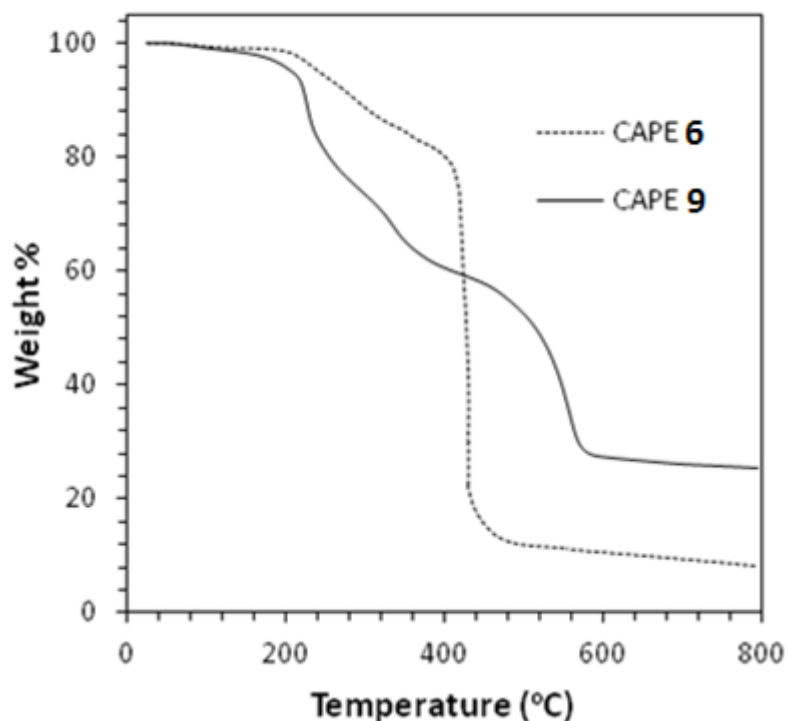


Figure 10.1. TGA analysis for CAPE 6 and CAPE 9.

10.3.2 Adsorption properties of CAPE 6 and CAPE 9

The IR bands in the spectrum (Fig. 10.2a) of CAPE 6 in the region of 1406 and 1590 cm^{-1} are attributed to the stretching vibrations of C-O and C=O of the CO_2^- groups, respectively, and the band at 3421 cm^{-1} is due to the stretching vibration of the -OH group^[175, 201]. The IR spectra of the loaded CAPE 6 (Fig. 10.2b) showed an increase in the broadness and intensity of the C-O band. The shifting of the C=O band to a higher wave number (1629 cm^{-1}) may be attributed to the increase in the covalent character of the copper oxygen bond (C-O-Cu) which in turn increases the double bond character of C=O. The appearances of new strong bands at 1734 and 1386 are attributed to the presence of C=O of the C(=O)OH and the ionic nitrate group, respectively.

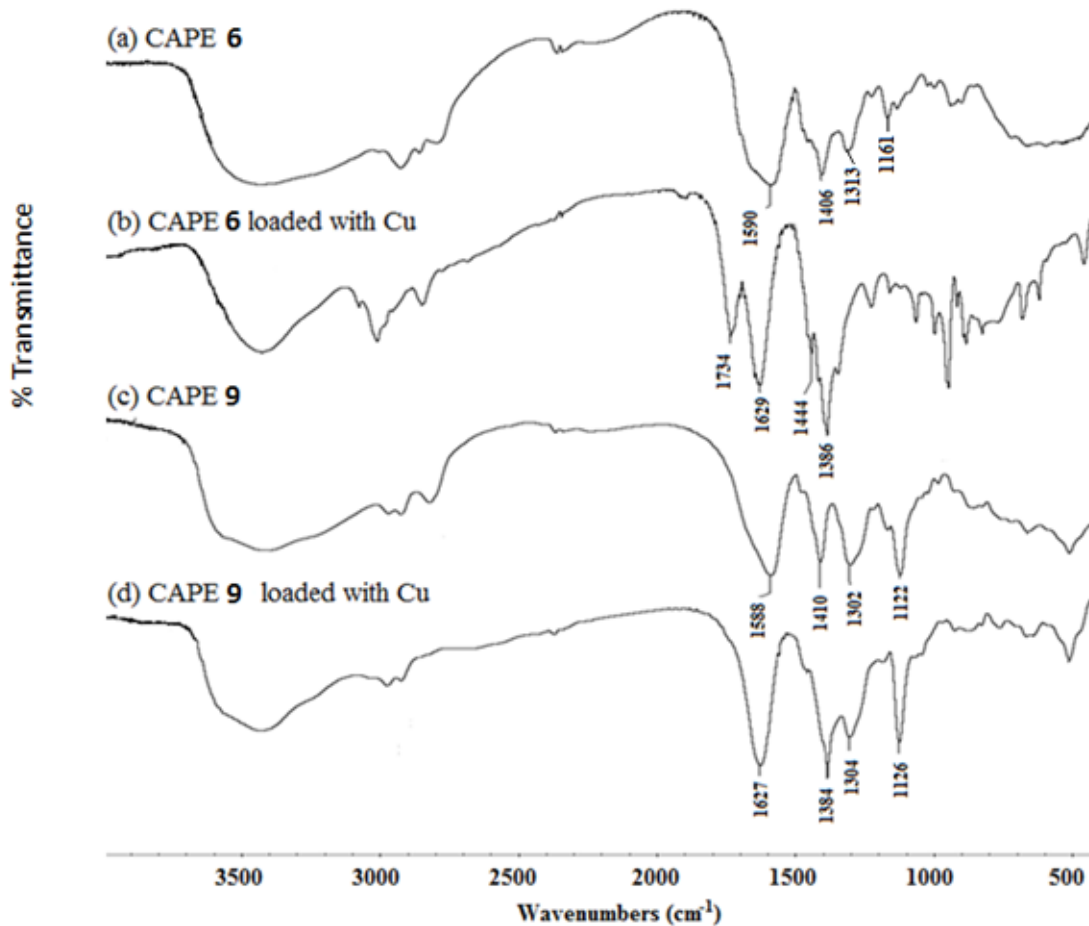
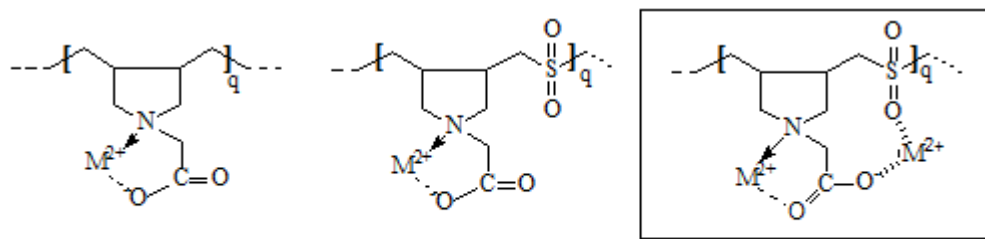


Figure 10.2. IR spectra for unloaded and loaded CAPE 6 and CAPE 9 with Copper.

The later absorption band is possible since the adsorption process was carried out in the presence of copper nitrates.

The bands in the IR spectra of CAPE 9 (Fig. 10.2c) in the region of 1410 and 1588 cm^{-1} are attributed to the stretching vibrations of C-O^- and C=O in the C(=O)O^- groups, respectively^[175, 201] and the bands in the region of 1122 and 1302 cm^{-1} are attributed to the symmetric and asymmetric vibrations of SO_2 unit. IR spectra of CAPE 9 (Fig. 10.2d) loaded with Cu^{2+} revealed the increase in the intensity and broadness of the carboxylate

C–O vibrations and the shifting of the C=O band to 1627 cm^{-1} as a result of the adsorption of the metal ions^[164]. The appearances of new strong bands 1384 cm^{-1} is attributed to the presence of ionic nitrate group since the adsorption process was carried out in the presence copper nitrate^[165]. Interestingly, the presence of the strong nitrate bands implies the ability of the resin **6** and **9** to act also as an anion exchanger. It is interesting to note the increase in the intensity of the SO_2 bands at 1125 and 1304 cm^{-1} which could be attributed to the role of SO_2 in metal adsorption ($\text{S}=\text{O}\cdots\text{Cu}$) as shown in scheme 2.



Scheme 2.

10.3.3 Effect of pH on the adsorption

The effect pH (in the range 3-6) on the uptake Cu^{2+} was investigated at a fixed concentration (1 mg L^{-1}) and time of 24 h. The pH of the solution was controlled by using an acetate buffer ($\text{CH}_3\text{COONa}/\text{CH}_3\text{COOH}$). Results of metal uptake at different pH are shown in Fig. 10.3. Optimum pH was found to be 4; at higher pH values, the hydrolysis of the metal ions occurs by the formation of metal hydroxides, which compete with the metal ion uptake by the resin^[232]. The aminomethylcarboxylate motifs are potentially bidentate ligands, having one coordination site each at the nitrogen and carboxylate motif (Scheme 2). Towards the stronger acid range (< 4), the basic nitrogens are protonated, thus it becomes monodentate ligands with lower adsorption capacities.

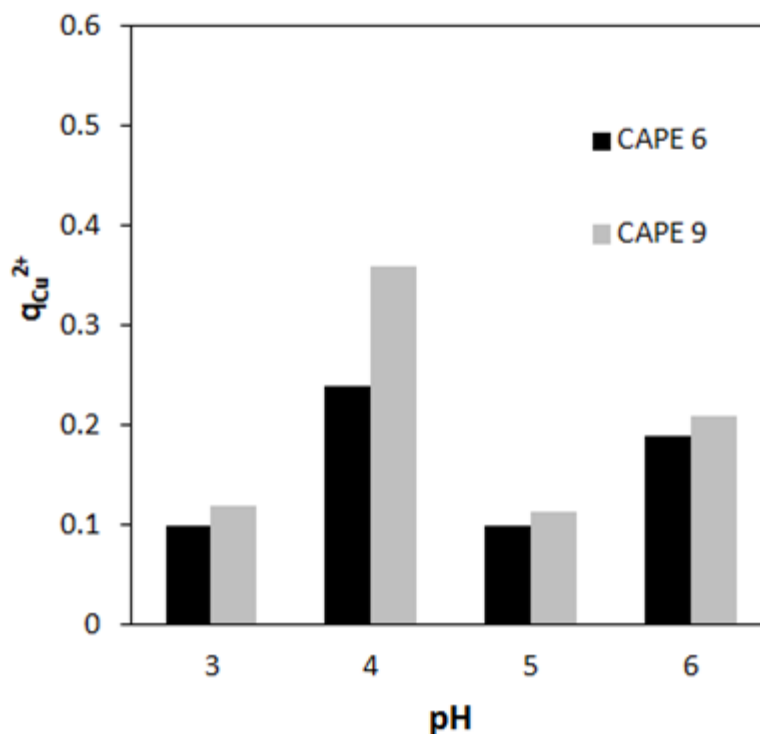


Figure 10.3. Effect of pH on the adsorption capacity.

10.3.4 Effect of contact time on the adsorption

The adsorption kinetics, as described by the relationship between adsorption capacity and adsorption time, are presented in Fig. 10.4a. It was found that the adsorption of Cu^{2+} ions by CAPE 6 and CAPE 9 reached equilibrium within 1 h, indicating the strong ability of these adsorbents to abstract Cu^{2+} ions from aqueous solutions. The higher amount of adsorption by CAPE 9 could be rationalized in terms of the stiffening effect of the sulfur dioxide moieties making the adsorbent more expanded and thus allowing it to have greater access to metal ions and also the ability to complex with Cu ions as shown by the IR spectrum and scheme 2.

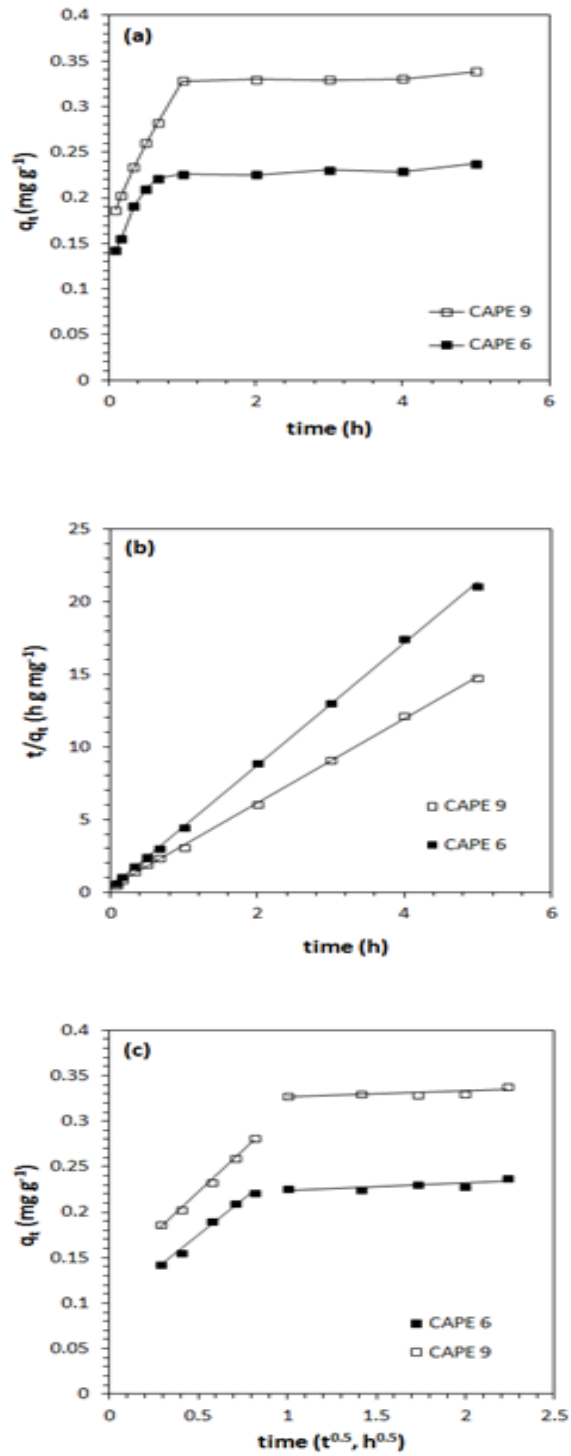


Figure 10.04. (a) Effect of time on the adsorption capacity, (b) Lagergren second order kinetic model; (c) Intraparticle diffusion model

It is reported that Lagergren adsorption kinetic model is a suitable tool to investigate the adsorption properties of a polymer^[67]. The following equations (1) and (2) express the linearly first-order and second-order kinetic equations for the Lagergren model, respectively:

$$\log(q_e - q_t) = \log q_e - \frac{k_1 t}{2.303} \quad (1)$$

$$\frac{t}{q_t} = \frac{1}{k_2 q_e^2} + \frac{t}{q_e} \quad (2)$$

where k_1 and k_2 are the first-order and second-order rate constant, respectively, q_t and q_e are the respective adsorption capacity of the metal ions at a time t and at equilibrium. The adsorption of Cu^{2+} by both the cross-linkers did not fit the first-order Lagergren kinetic model, so the graphs representing the kinetic model have not been displayed. The second-order Lagergren kinetic model (Fig. 10.4b), however, fitted well for the adsorption of Cu^{2+} on CAPE **6** and CAPE **9** indicating that the adsorption process might be a chemical adsorption^[167].

It can be noted in Table 2 that both the second-order rate constant (k_2) and the initial rate of adsorption (h) of Cu^{2+} ions are higher for sorbent CAPE **9** than CAPE **6**, implying the influence of backbone stiffening SO_2 units allowing more open structure of the former resin. Fitted equilibrium capacities ($q_{e, \text{cal}}$) derived from Eq. (2) are in close agreement with those observed ($q_{e, \text{exp}}$) experimentally. The experimental data so far revealed that the resin is an efficient adsorbent for the removal of copper ions from aqueous solutions.

Table 10.2 Lagergren second-order kinetic model parameters for CAPE 6 and CAPE 9 adsorption.

CAPE	Temp (K)	$q_{e, \text{exp}}$ (mg g ⁻¹)	k_2 (h ⁻¹ g mg ⁻¹)	h^a (h ⁻¹ g ⁻¹ mg)	$q_{e, \text{cal}}$ (mg g ⁻¹)	R^2	E_a (kJ mol ⁻¹)
CAPE 6	298	0.234	57.9	3.26	0.237	0.9995	11.8
	306	0.239	64.2	3.78	0.243	0.9995	
	324	0.255	84.6	5.60	0.257	0.9996	
CAPE 9	298	0.364	24.8	2.94	0.344	0.9994	10.6
	306	0.365	27.3	3.25	0.345	0.9993	
	324	0.373	34.9	4.31	0.352	0.9997	

^aInitial adsorption rate $h = k_2 q_e^2$.

The adsorption data may also be described by some adsorption diffusion models which are always constructed on the basis of three consecutive steps: (1) film diffusion (i.e., diffusion across the liquid film surrounding the adsorbent particles); (2) intraparticle diffusion (i.e., diffusion in the liquid contained in the pores and/or along the pore walls); and (3) mass action (i.e., physical adsorption and desorption between the adsorbate and active sites). Since the adsorption step is very rapid, it is assumed that it does not influence the overall kinetics. The overall rate of adsorption process, therefore, will be controlled by either surface diffusion or intraparticle diffusion.

The intraparticle diffusion model assumes that the metal ions are transported from the solution through an interface between the solution and the adsorbent (i.e., film diffusion) followed by a rate-limiting intraparticle diffusion step which bring them into the pores of the particles in the adsorbent. Following equation expresses the relation of the adsorption capacity and time^[200, 201]:

$$q_t = x_i + k_p t^{0.5} \quad (3)$$

where q_t is the adsorption capacity at time t , k_p is the rate constant of intraparticle diffusion, x_i is related to boundary layer thickness^[218]. According to the Weber–Morris model, a straight line fit for the plot of q_t versus $t^{0.5}$ implies the intraparticle diffusion as the rate-limiting step^[218-220]. If the plot passes through the origin then it becomes the sole rate-limiting step^[221]. Since the initial linear plot did not pass through the origin, intraparticle diffusion within the pores of the resins was not the only rate-limiting step. Adsorption kinetics may thus be controlled by film diffusion and intraparticle diffusion simultaneously. Note that the second linear section represents the final equilibrium stage. The value of the intercept x_i in the initial linear plots for CAPE **6** and CAPE **9** were found to be 0.0963 mg g^{-1} and 0.131 mg g^{-1} , respectively with square of regression (R^2) as 0.9886 and 0.9910 (Fig. 10.4c). Larger intercepts (implying larger thickness for the boundary layer) in the case of CAPE **9** suggest that surface diffusion has a larger role in the rate-limiting step than in the case of CAPE **6**. Participation of the SO_2 units in CAPE **9** *via* H-bonding with water presumably helps to have larger boundary layer thickness. The overall larger rate of adsorption of CAPE **9** indicates the greater role of the intraparticle diffusion as it provides a more expanded backbone of CAPE **9** owing to the presence of backbone-stiffening SO_2 motif.

10.3.5 Effect of initial concentration on the adsorption of Cu^{2+} ions

As shown in Fig. 10.5a, the adsorption capacity of CAPE **6** and CAPE **9** increases with the increase in the initial concentration of Cu^{2+} ions.

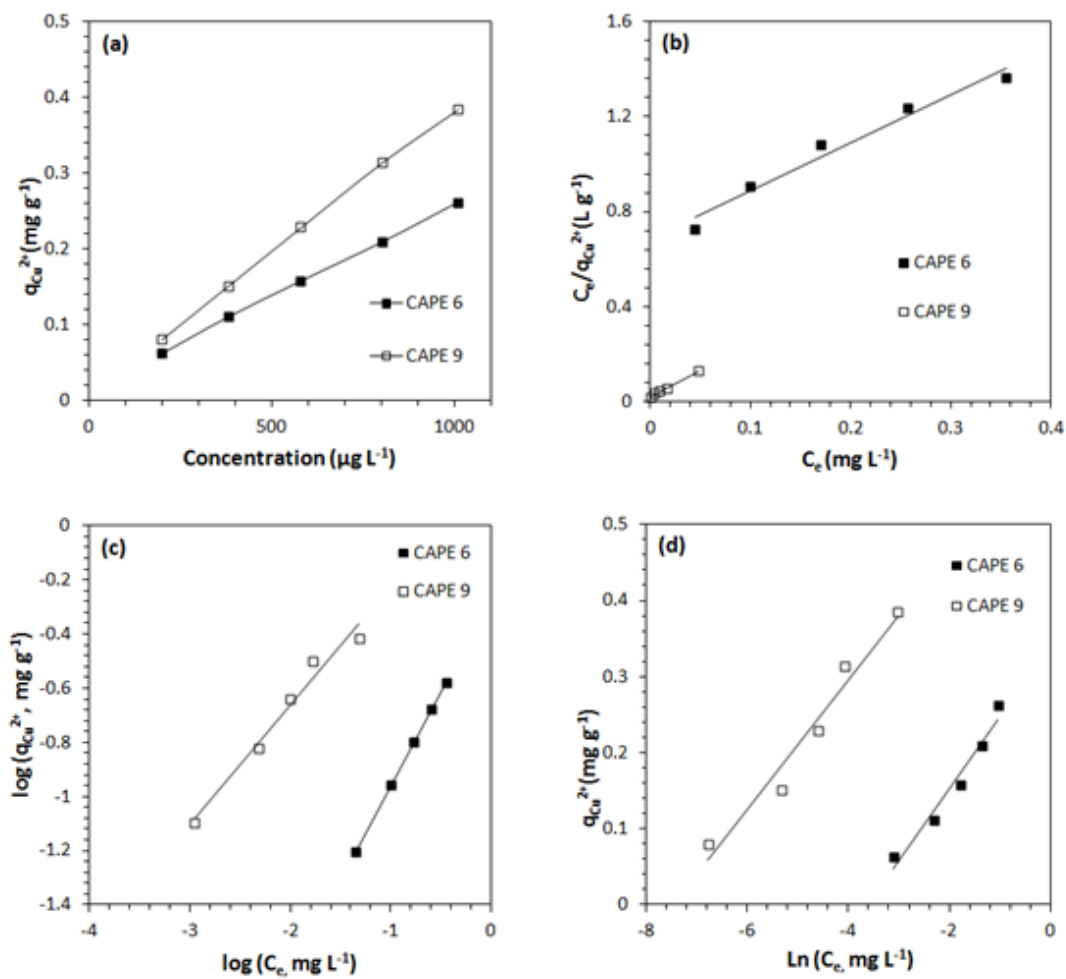


Figure 10.5 (a) Effect of metal concentration on the adsorption capacity (b) Langmuir plot, (c) Freundlich plot, (d) Temkin plot.

To further explore the adsorption mechanism, Langmuir, Freundlich and Temkin isotherm models were used to analyze the adsorption data for the experiments carried out at the preferred pH of 4.

The Langmuir isotherm equation can be expressed by Eq. (4):

$$\frac{C_e}{q_e} = \frac{C_e}{Q_m} + \frac{1}{Q_m b} \quad (4)$$

where C_e and q_e are the concentrations of metal ion in the solution and resin, respectively, Q_m and b are the Langmuir constants. Fig. 10.5b illustrates the Langmuir plot of C_e/q_e versus C_e , enabling the calculation of Langmuir constants from the intercept and slope of the linear plot. Langmuir isotherm model assumes the mechanism of the adsorption process as a monolayer adsorption on completely homogeneous surfaces where interactions between adsorbed molecules are negligible^[233]. This empirical model assumes the adsorbed layer is one molecule in thickness, with adsorption can only occur at a fixed number of definite identical and equivalent localized sites. Once a molecule occupies a site, no further adsorption can take place^[234, 235]. This is described as homogeneous adsorption with uniform energies of ion exchange as all sites possess equal affinity for the adsorbate^[236, 237].

Freundlich isotherm model, on the other hand, describes the non-ideal adsorption occurring on a heterogeneous surface with uniform energy as well as multilayer adsorption; Eqs. (5) and (6) express the model:

$$q_e = k_f C_e^{1/n} \quad (5)$$

$$\log q_e = \log k_f + \frac{1}{n} \log C_e \quad (6)$$

where q_e and C_e are the equilibrium concentrations of metal ion in the adsorbed and liquid phase, respectively, k_f and n represent the Freundlich constants, which can be calculated from the slope and intercept of the linear plot of $\log q_e$ versus $\log C_e$ as presented in Fig. 10.5c. The values of n were determined to be 1.44 and 2.27 for CAPE **6** and **9**, respectively; values lying in the range of 1 to 10 are considered for classification as favorable adsorption^[225, 226]. The slope ($1/n$) range of 0 - 1 is known to be a measure of adsorption intensity or surface heterogeneity, becoming more heterogeneous as its value gets closer to zero. A $1/n$ value below unity (0.693, 0.441 for CAPE **6** and **9**, respectively) is indicative of chemisorption process, whereas $1/n$ above one implies cooperative adsorption^[227]. For CAPE **9**, the higher value of the constant k_f , which is related to adsorption capacity (q), indicates the higher affinity for the metal ion in comparison to CAPE **6**.

The Temkin isotherm equation assumes that the heat of adsorption of all the molecules in layer decreases linearly with coverage due to adsorbent-adsorbate interactions, and that the adsorption is characterized by a uniform distribution of the bonding energies up to some maximum binding energy. The Temkin isotherm^[238, 239] has been used in the following form:

$$q_e = \frac{RT}{b} \ln(aC_e) \quad (7)$$

A linear form of the Temkin isotherm can be expressed as:

$$q_e = \frac{RT}{b} \ln A + \frac{RT}{b} \ln C_e \quad (8)$$

$$q_e = B \ln A + B \ln C_e \quad (9)$$

where R is gas constant ($8.314 \text{ J mol}^{-1} \text{ K}^{-1}$), T is temperature (K), A is the equilibrium binding constant (L/g) corresponding to the maximum binding energy, and constant $B=RT/b$ is related to the heat of adsorption. A plot of q_e versus $\ln C_e$ (Fig. 10.5d) is used to calculate the Temkin isotherm constants A and B . Fig. 10.5(b-d) illustrate that the adsorption of Cu^{2+} ions by both cross-linkers fitted well the Langmuir, Freundlich and Temkin isotherm models, thereby implying that the adsorption may occur as a monolayer as well as a heterogeneous surface adsorption. The Langmuir, Freundlich and Temkin isotherm model constants are given in Table 10.3.

Table 010. 3 Langmuir, Freundlich and Temkin isotherm model constants for Cu^{2+} adsorption.

Langmuir isotherm model			
Cross-linked polyelectrolyte	Q_m (mg g^{-1})	b (L mg^{-1})	R^2
CAPE 6	0.497	2.93	0.9697
CAPE 9	0.443	129	0.9910
Freundlich isotherm model			
Cross-linked polyelectrolyte	k_f ($\text{mg}^{1-1/n} \text{ g}^{-1} \text{ L}^{1/n}$)	n	R^2
CAPE 6	0.537	1.44	0.9998
CAPE 9	1.64	2.27	0.9734
Temkin isotherm model			
Cross-linked polyelectrolyte	A (L g^{-1})	B (J/mol)	R^2
CAPE 6	36.9	0.0944	0.9597
CAPE 9	1753	0.0853	0.9615

For the Langmuir isotherm model^[47, 240], a dimensionless constant (R_L), commonly known as separation factor or equilibrium parameter can be used to describe the favorability of adsorption on the polymer surface by Eq. (10):

$$R_L = \frac{1}{(1+bC_0)} \quad (10)$$

where C_0 is the initial M^{2+} concentration and b is the Langmuir equilibrium constant. The more favourable adsorption is reflected by lower R_L values; the adsorption could be either unfavourable ($R_L > 1$), linear ($R_L = 1$), favourable ($0 < R_L < 1$) or irreversible ($R_L = 0$). The R_L values for the adsorption of both metal ions are given in Table 10.4, which reveals that the values fall in the preferred region (i.e., $0 < R_L < 1$). The lower values of R_L for the CAPE 9 adsorption (approaching 0) point toward irreversible nature of the adsorption.

Table 10.04 The R_L values based on the Langmuir isotherm model and %Cu²⁺ removal at different initial concentration

C_0 (mg L ⁻¹)	CAPE 6		CAPE 9	
	R_L value	%Cu ²⁺ removal	R_L value	%Cu ²⁺ removal
0.200	0.631	77.5	0.0373	99.4
0.400	0.460	73.8	0.0190	98.7
0.600	0.363	70.7	0.0128	98.3
0.800	0.299	67.9	0.00960	97.9
1.000	0.254	64.7	0.00769	95.2

It can be noted in Table 10.4 that the R_L values decrease with the increase in the initial Cu^{2+} concentration indicating that the ion exchange is more favourable at higher initial concentration. For the sorbents CAPE 6 and CAPE 9, the efficiency of Cu^{2+} removal at an initial metal concentration of 200 ppb was found to be 77.5 and 99.4%, respectively (Table 10.4). The favorability of CAPE 9 to follow Langmuir is found to be higher as confirmed by the higher correlation coefficient (0.9910) than in the case of CAPE 6 (0.9697). The fitness order toward the isotherm models for CAPE 6 (Freundlich > Langmuir > Temkin) indicates the favorability of adsorption on a heterogeneous surface, whereas for CAPE 9 (Langmuir > Freundlich > Temkin) the favorable process is a monolayer adsorption. The surface area of CAPE 9 is larger than CAPE 6 ($9.9 \text{ m}^2 \text{ g}^{-1}$ versus $2.15 \text{ m}^2 \text{ g}^{-1}$) which could be due to the stiffening effect of the sulfur dioxide moieties in the former resin making it more expanded. The more expanded surface of CAPE 9 allows it to achieve its adsorption capacity through monolayer formation, while for CAPE 6, adsorption capacity may only be attained *via* adsorption on a heterogeneous surface.

10.3.6 Effect temperature on adsorption

Adsorption experiments were performed at pH 4 to obtain the thermodynamic parameters; the results are illustrated in Fig. 10.6a. As can be seen from the Fig., the adsorption capacity increases with the increase in temperature, suggesting that the adsorption process is endothermic, and this can be explained that at higher temperature swelling of the resin increases which permits greater diffusion of the metal ions^[163].

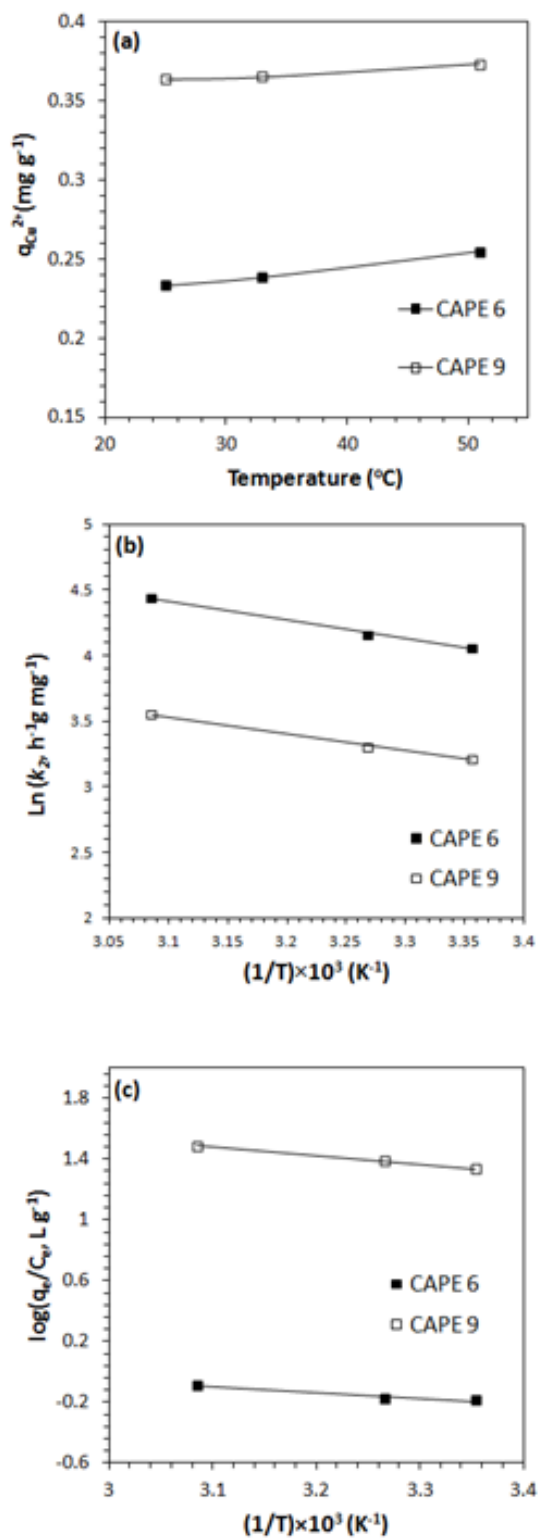


Figure 10.6. (a) Effect of temperature on adsorption capacity, (b) Arrhenius plot, (c) Van't-Hoff plot

The activation energy of the adsorption process can be calculated by plotting $\log q_e$ versus $1/T$ as shown in Fig. 10.6b. Using Arrhenius equation [Eq. (11)], the activation energies were found to be 11.8 and 10.6 kJ/mol for the adsorption by CAPE **6** and CAPE **9**, respectively (Table 10.2). These E_a values are low in comparison to typical chemical reactions with activation energies of 65 – 250 kJ/mol, thereby indicating that the adsorption of the metal ions is relatively easy and a favored process.

$$\ln k_2 = -\frac{E_a}{RT} + \text{constant} \quad (11)$$

A plot of $\log (q_e/C_e)$ versus $1/T$ is displayed in Fig. 10.6c. The thermodynamic parameters ΔG , ΔH and ΔS were calculated using Vant-Hoff equation [Eq. (12)], and are tabulated in Table 10.5^[167]. The negative ΔG values for CAPE **9** ascertain the spontaneity of the adsorption process.

$$\log \left(\frac{q_e}{C_e} \right) = -\frac{\Delta H}{2.303RT} + \frac{\Delta S}{2.303R} \quad (12)$$

Note that for CAPE **6**, the ΔG values were positive; such small positives values are also reported in a recent adsorption study^[201]. As the temperature increases, the ΔG values become smaller (less positive or more negative), thereby indicating that the adsorption is more favorable at the higher temperatures. Favorable adsorption at higher temperatures is attributed to the greater swelling of the resin and increased diffusion of metal ions into the resin. The positive values of ΔH certify that the adsorption is an endothermic process. In addition, it can be found in Table 10.5 that the ΔS values are positive, suggesting that the adsorption is an entropy-driven process as the randomness

increased during the adsorption of metal ions as a result of the release of water molecules from their large hydration shells.

Table 10.05 Thermodynamic Data for Cu²⁺ adsorption.

Cross-linked polyelectrolyte	Temperature (K)	ΔG (kJ/mol)	ΔH (kJ/mol)	ΔS (J/mol K)	R^2
CAPE 6	298	+ 1.13	7.06	19.9	0.9644
	306	+ 0.967			
	324	+ 0.608			
CAPE 9	298	-7.61	10.8	61.9	0.9993
	306	-8.11			
	324	-9.22			

10.3.7 Desorption experiment

The effective usage of adsorbent in industry demands the recycling and reuse of the adsorbent. For this purpose, desorption experiments were carried out as described in the experimental. The results indicated that the percentage efficiency of the desorption process to be 88% and 93% for CAPE 6 and CAPE 9, respectively. The high desorption values, therefore, ascertain the great potential of these new resins for the removal of toxic metal ions.

10.4 SEM and EDX images for CAPE 6 and CAPE 9 unloaded and loaded with Copper ions

Unloaded and loaded resins were investigated by scanning electron microscopy. Unloaded resins were immersed in 0.1 M Cu(NO₃)₂ for 24 h at a pH of 4, filtered, and dried under vacuum until constant weight was achieved. Loaded and unloaded polymers were then sputter-coated for 6 min with a thin film of gold.

SEM and EDX images (Figs. 10.7 and 10.8) show that the morphology has been altered by the adsorption of copper ions (cracked morphology to smooth); the EDX analysis shows that CAPE 6 and CAPE 9 have adsorbed copper ions. The color of the resins has also changed from white to blue after adsorption (Fig. 10.9), giving a positive indication that the adsorption process has occurred. The SEM images showed that the resins adsorbed Cu^{2+} ions, and the adsorption process happened on the surface and throughout the polymer (EDX analysis).

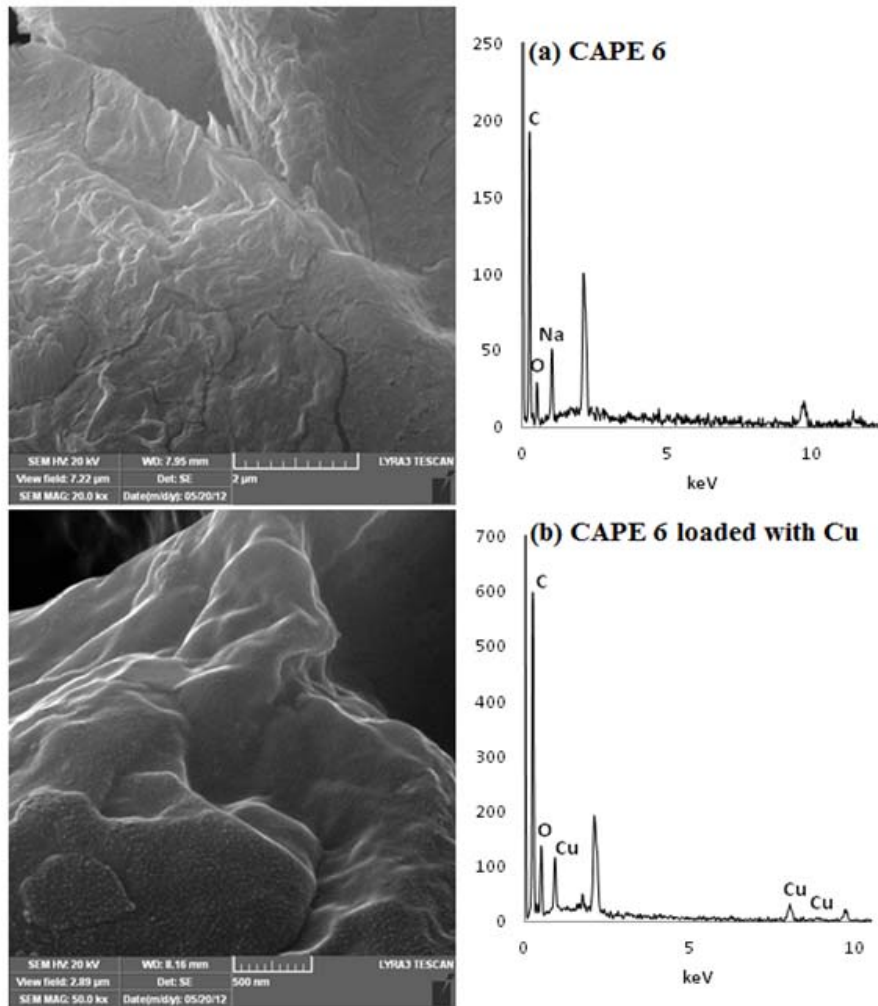


Figure 10.7. SEM and EDX analysis for unloaded and loaded CAPE 6 with Cu.

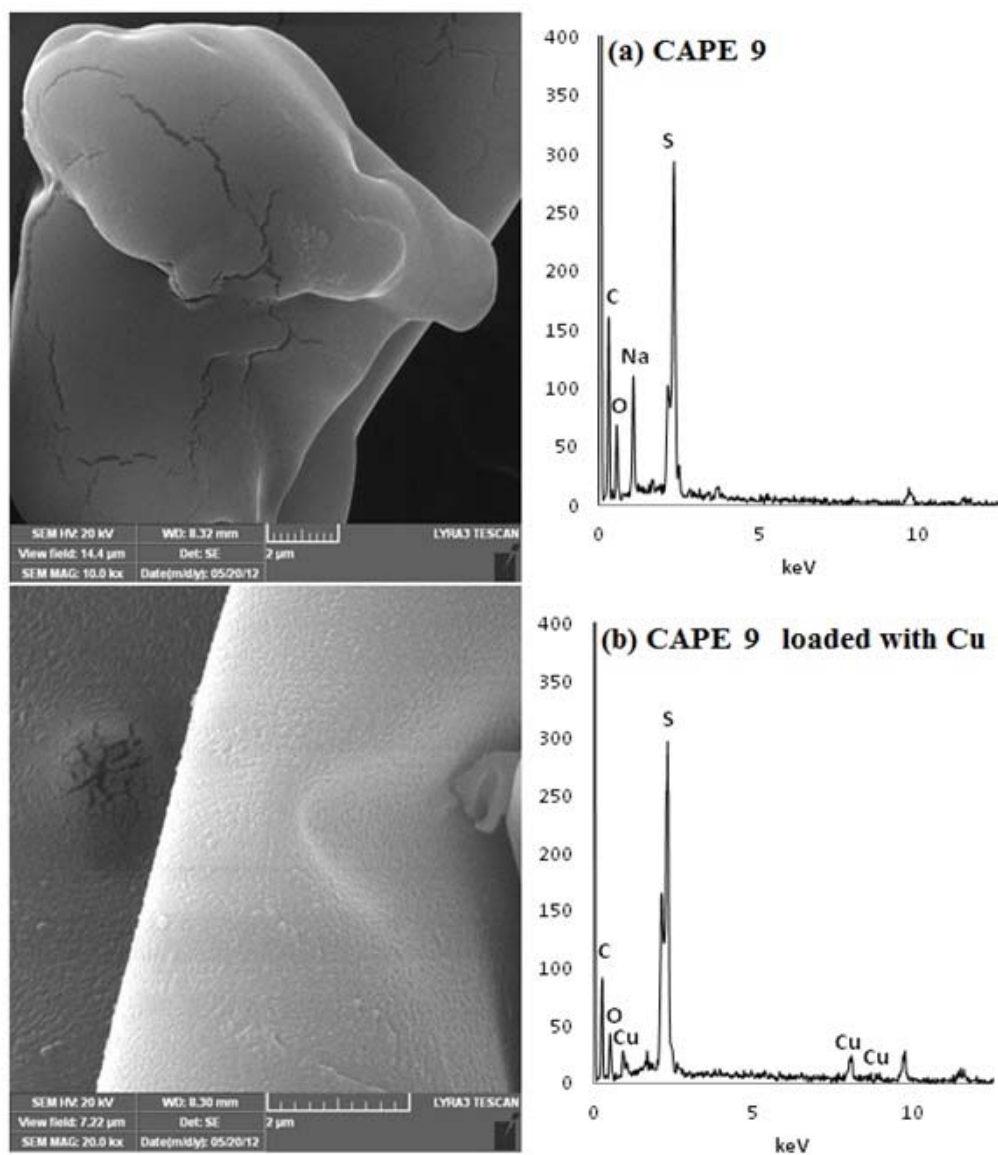


Figure 10.8. SEM and EDX analysis for unloaded and loaded CAPE 9 with Cu.



Figure 10.9. Resins before and after the adsorption of Cu^{2+} ions.

10.5 Treatment of real wastewater samples.

Two wastewater samples were collected from water treatment plant from the Dhahran, Saudi Arabia. The samples were analyzed to measure the concentration of the native copper concentration on the samples. The concentration was found to be below the detection limit of our analytical method. The water samples were spiked with 1 mg L^{-1} copper and the samples were mixed and left to equilibrate for 24 h. Then 20 ml of these samples were loaded with 50 mg of CAPE 6 and CAPE 9 to test the ability of these resins to adsorb heavy metals in real wastewater conditions. The results for the analysis were given in Tables 10.6 and 10.7 which indicate the ability of these resins to adsorb various types of heavy metals from wastewater samples. It is interesting to note that after adsorption the concentration of Cu^{2+} ions were below the detection limit in one case (Table 10.6). The pH of the wastewater samples were found to be 7.8 (Table 10.6) and 8.5 (Table 10.7), whereas experiments involving distilled water were carried out at pH 4. At these high pH values, the resins have more anionic sites which are available for the adsorption of all the Cu^{2+} from the wastewater samples.

Table 10.6 Comparison of metals concentration from Water treatment plant sample (Doha, Saudi Arabia) before and after adding the polymer.

Metal	Original sample #1 ($\mu\text{g L}^{-1}$)	CAPE 6 (After treatment) ($\mu\text{g L}^{-1}$)	CAPE 9 (after treatment) ($\mu\text{g L}^{-1}$)
Co	0.34 ± 0.09	< MDL	0.12 ± 0.09
Cu (spiked)	1180 ± 0.063	< MDL	109 ± 0.063
Zn	75.05 ± 0.024	< MDL	56.52 ± 0.024
As	6.388 ± 0.024	0.555 ± 0.024	< MDL
Sr	6526 ± 0.099	3651 ± 0.099	3774 ± 0.099
Mo	14.14 ± 0.018	10.58 ± 0.018	9.081 ± 0.018
Cd	< 0.015	< 0.015	< 0.015
Sb	< 0.012	< 0.012	< 0.012
Pb	< 0.018	< 0.018	< 0.018

Mean and standard deviation of three replicates (n = 3).

\pm values are the method detection limit (MDL), 3σ of the blank sample.

Table 010.7 Comparison of metals concentration from Petrochemical plant sample (Dhahran, Saudi Arabia) before and after adding the polymer.

Metal	Original sample #2 ($\mu\text{g L}^{-1}$)	CAPE 6 (after treatment) ($\mu\text{g L}^{-1}$)	CAPE 9 (after treatment) ($\mu\text{g L}^{-1}$)
Co	0.162 ± 0.009	0.002 ± 0.009	0.08 ± 0.009
Cu (spiked)	870 ± 0.063	< MDL	< MDL
Zn	10.04 ± 0.024	< MDL	7.7 ± 0.024
As	2.795 ± 0.024	< MDL	0.464 ± 0.024
Sr	5346 ± 0.099	3581 ± 0.099	4084 ± 0.099
Mo	7.546 ± 0.018	6.315 ± 0.018	6.673 ± 0.018
Cd	< 0.015	< 0.015	< 0.015
Sb	0.097 ± 0.012	0.06 ± 0.012	0.061 ± 0.012
Pb	< 0.018	< 0.018	< 0.018

Mean and standard deviation of three replicates (n = 3).

\pm values are the method detection limit (MDL), 3σ of the blank sample.

10.6 Conclusion

Two novel pH-responsive cross-linked polyaminocarboxylates CAPE **6** and CAPE **9** were prepared using Butler's cyclopolymerization protocol. For the sorbents **6** and **9**, the efficiency of Cu^{2+} removal at an initial metal concentration of 200 ppb was found to be 77.5 and 99.4%, respectively. The adsorption followed Lagergren second-order kinetic model and Langmuir as well as Freundlich isotherm models. The adsorption kinetics was found to be controlled by both film diffusion and intraparticle diffusion simultaneously. The negative ΔG s and positive ΔH s ensured the spontaneity and the endothermic nature of the adsorption process. The good adsorption and desorption efficiencies implied the efficacy of the resin in removing Cu^{2+} ions from aqueous solution at low concentrations.

CHAPTER 11: A novel cross-linked polyaminodiphosphonate for the removal of copper and cadmium ions from aqueous solution at low concentrations

Taken from **Othman Charles S. Al-Hamouz**, Shaikh A. Ali, Novel cross-linked polyaminodiphosphonate for the removal of copper and cadmium metal ions from aqueous solutions, Reactive and Functional Polymers, submitted.

ABSTRACT

Butler's cyclocopolymerization protocol has been utilized in the synthesis of a novel pH-responsive cross-linked polyzwitterionic acid (CPZA) containing aminomethyldiphosphonate motif. CPZA was converted into a cross-linked anionic polyelectrolyte (CAPE) by treatment with NaOH. The adsorption kinetics, isotherm, and thermodynamic parameters for the removal of Cu^{2+} and Cd^{2+} at low concentrations (200–1000 ppb) from aqueous solution by CAPE were examined. The experiments showed that the adsorption fitted Lagergren second-order kinetic model and Langmuir as well as Freundlich isotherm models. The adsorption process was spontaneous and endothermic in nature with negative and positive values for ΔG and ΔH , respectively. The adsorption capacity and rate of adsorption of Cu^{2+} was higher than that of Cd^{2+} . The efficiency of Cu^{2+} and Cd^{2+} removal at an initial metal concentration of 200 ppb was found to be 96.8 and 93.8%, respectively. For Cu^{2+} ions, initial adsorption factor (R_i) of 0.28 indicated rapid initial adsorption of 72%; while the other 28% of adsorption is governed by

intraparticle diffusion. The efficacy and selectivity of the resin to adsorb copper and cadmium ions from two waste water samples have been demonstrated.

Key words: adsorption, cross-linked polyaminodiphosphonate, toxic metal ions.

11.1 Introduction

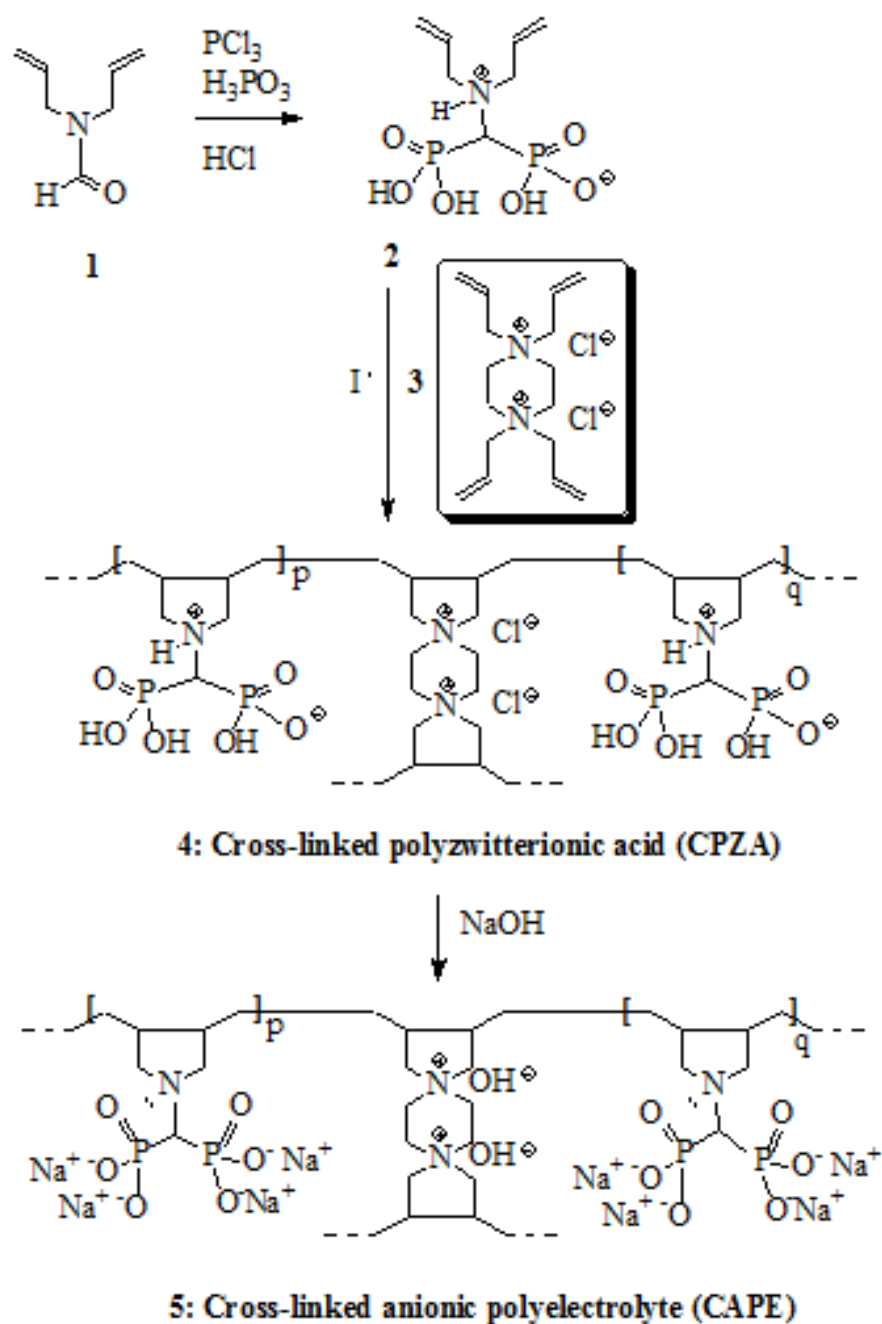
Pollution caused by toxic metal ions has been found to have a large negative impact on the environment. Metal ions like Cu^{2+} and Cd^{2+} metal ions cause various diseases and disorders; for example, copper poisoning can cause liver and kidney damage, irritation of the respiratory system, whereas cadmium can cause nervous system damage, bone damage as well as other serious illnesses^[66-68, 208, 241-243].

According to World Health Organization (WHO) standards, the maximum allowable concentration of copper in drinking water is 0.2 mg/L^[230], while it is 0.2 and less than 2 ppm for agriculture irrigation and ponds fish farming, respectively^[231]. In order to protect humans and the environment, it is of utmost importance to remove copper ions from environments. For Cd, the drinking water guideline value recommended by WHO is 0.003 mg Cd/L^[222]. It is difficult for chemical precipitation methodologies to treat economically low concentration (less than 5 mg/L) of cadmium. Ion exchange and reverse osmosis have been effective in achieving the metal concentration limits but have high operation and maintenance costs^[223].

Cross-linked polymeric materials containing chelating functional groups of amine, carboxylate, phosphonate, etc, motifs have attracted considerable attention in the separation and removal of toxic metals. Functional groups having

aminomethylphosphonate motifs have shown extraordinary chelating properties in the removal of toxic metals from aqueous solutions^[65, 194].

Recently, we have reported the synthesis of a novel cross-linked polymer containing aminomethylphosphonate motifs, and examined its excellent efficacy as an adsorbent for the removal of toxic metal ions like Pb^{2+} and Cu^{2+} ions from aqueous solutions^[181]. In continuation of the preparation of novel cross-linked polymers for the removal of heavy metals from aqueous solution, we report herein the synthesis of a new cross-linked anionic polyelectrolyte (CAPE) **5** containing polydentate aminomethyldiphosphonate motifs using Butler's cyclopolymerization protocol (Scheme 1) and its efficiency in the removal of Cu^{2+} and Cd^{2+} ions from aqueous solutions at low concentrations.



Scheme 1. Synthesis of monomer and cross-linked polymers.

11.2 Experimental

11.2.1 Apparatus

Elemental analysis was carried out on a Perkin Elmer Elemental Analyzer Series II Model 2400. IR spectra were recorded on a Perkin Elmer 16F PC FTIR spectrometer. ^1H and ^{13}C spectra were measured on a JEOL LA 500 MHz spectrometer using HOD signal at δ 4.65 and dioxane signal at 67.4 ppm as internal standards, respectively. Scanning electron microscopy images were taken by TESCAN LYRA 3 (*Czech Republic*) equipped with Oxford, energy-dispersive X-ray spectroscopy (EDX) detector model X-Max. Inductively coupled plasma analysis was performed on ICP-MS XSERIES-II (Thermo Scientific). Thermogravimetric analysis (TGA) was performed using a thermal analyzer (STA 429) manufactured by Netzsch (Germany). The polymer sample to be tested (usually \sim 5 mg) was placed in a platinum crucible. Aluminum oxide (Al_2O_3 ; \sim 4 mg) was placed in an identical platinum crucible as a reference sample. With the sample carrier system, which had two sets of 10% Pt–Pt/Rh thermocouples, the sample carrier was placed in the middle of the vertical furnace, which was programmed and controlled by a microprocessor temperature controller. The temperature was raised at a uniform rate of 10 $^\circ\text{C}/\text{min}$. The analyses were made over a temperature range of 20–800 $^\circ\text{C}$ in an air atmosphere flowing at a rate of 100 mL/min.

11.2.2 Materials

Tertiary butylhydroperoxide (TBHP) (70% in water), paraformaldehyde, phosphorous acid from Fluka Chemie AG (Buchs, Switzerland) and phosphorous trichloride from BDH laboratory reagents (England) were used as received. All solvents used were of analytical grade.

11.2.3 Synthesis of monomers

11.2.3.1 Diallylformamide (1)

Diallylformamide has been synthesized as described in the literature^[244].

11.2.3.2 Diallylaminomethyldiphosphonic acid (2)

Diallylaminomethyldiphosphonic acid **2** has been synthesized as described in the literature^[65], with some modification in the isolation method. Thus diallylformamide (**1**) (0.5 mol) and phosphorous acid (0.5 mol) were mixed in a round bottom flask (1 L). Under ice-cooling, phosphorous trichloride (0.5 mol) was added dropwise to the mixture. After completion of the addition, the temperature was increased to 70 °C until no further HCl gas was liberated. The reaction mixture was left at room temperature for 24 h during which the product became glassy solid. The product was hydrolyzed with water (100 mL) and freeze-dried. The residual glassy material was crystallized using acetone-methanol mixture to give **2** as a white solid whose purity was confirmed by ¹H NMR spectroscopy^[65].

11.2.3.3 1,1,4,4-tetraallylpiperazinium dichloride 3

Cross-linker **3** have been synthesized as described in the literature^[64].

11.2.4 General procedure for the copolymerization of the diallylaminomethylphosphonic acid **2** and 1,1,4,4-tetraallylpiperazinium dichloride **3**

To a solution of monomer **2** (14.6 g, 54 mmol i.e.) and cross-linker **3** (1.920 g, 6 mmol) in deionized water (8.92 g) under N₂ was added the initiator TBHP (320 mg). The reaction mixture in the closed flask was stirred using a magnetic stir-bar at 85 °C for 24 h. Within 3-4 h the stir-bar stopped moving and the mixture became white solid. At the end of the elapsed time, the cross-linked polyzwitterionic acid (CPZA) **4** was allowed to soak in water (48 h) with replacement of water several times. The white solid was filtered and

dried under vacuum at 70°C to a constant weight (57% yield). (Found: C, 33.7; H, 6.1; N, 5.4%. A copolymer from monomer **2** (C₇H₁₅NO₆P₂) (90 mol%) and monomer **3** (C₁₆H₂₈Cl₂N₂) (10 mol%) requires C, 33.93; H, 5.91; N, 5.53%); ν_{\max} (KBr) 3428, 2935, 1652, 1469, 1188, 1075, 912, 805, 708, 568 and 534 cm⁻¹.

11.2.5 Basification of CPZA **4** to cross-linked anionic polyelectrolyte (CAPE) **5**

A mixture of CPZA **4** (5.0 g, ~ 18 mmol) in a solution of NaOH (4.4 g, 110 mmol) in water (150 cm³) was stirred at room temperature for 24 h. The polymer was then poured into methanol (300 mL), filtered, and dried under vacuum at 65 °C to a constant weight to obtain the cross-linked polyanion CAPE **5** (4.8 g).

11.2.6 Sample characterization

FT-IR spectra have been recorded on a Perkin Elmer 16F PC FTIR spectrometer in the region of 4000-400 cm⁻¹. Ion exchange capacity (IEC) was determined by titrimetric analysis method (Eq. 1). The dried and weighed polymer (50 mg) was immersed in 50 mL of 0.1 M hydrochloric acid solution for 24 h. The ion exchange capacity was determined from the decrease in acidity by titration with 0.1 M NaOH solution.

$$IEC = \frac{(mmol_i - mmol_f)}{W} \quad (1)$$

where mmol_i and mmol_f are the initial and final amount of HCl in mmol, respectively, *W* is the weight of the polymer in g^[156].

11.2.7 Adsorption experiments

The procedure for the adsorption experiments of the cross-linked polymer CAPE **5** for Cu²⁺ ions can be described as follow: a mixture of CAPE **5** (30 mg) in a 1 mg L⁻¹ of Cu²⁺ (20 mL) prepared from Cu(NO₃)₂ standard solution was stirred using a magnetic

stir-bar at different pH for 24 h. Then the mixture was filtered and the filtrate was analysed by AAS to determine the amount of Cu^{2+} remained. The adsorption capacity ($q_{\text{Cu}^{2+}}$) in mg g^{-1} can be calculated using Eq. (2):

$$q_{\text{Cu}^{2+}} = \frac{(C_0 - C_f)V}{W} \quad (2)$$

where C_0 and C_f are the initial and final concentration of Cu^{2+} ions in mg/L , respectively, W is the weight of the polymer in g , and V is the volume of the solution in L . Data presented are average of triplicate runs and varied by less than 4% in all the cases studied.

For adsorption kinetic studies, the resin sample was stirred in a $1 \text{ mg L}^{-1} \text{ Cu}^{2+}$ solution for different adsorption times at a preferred pH of 5 (*vide infra*). Adsorption isotherms were constructed by changing the concentration of Cu^{2+} solution from $200 \mu\text{g L}^{-1}$ (i.e., ppb) to $1000 \mu\text{g L}^{-1}$ at $25 \text{ }^\circ\text{C}$ for 24 h. Based on the adsorption data from experiments carried out at different temperatures, the activation energy for the adsorption process and thermodynamic parameters ΔG , ΔH and ΔS for Cu^{2+} removal were calculated. Similar experiments were conducted for the removal of Cd^{2+} ions^[175].

11.2.8 QA/QC

Quality control for METAL analyses included repeated injections and periodic (two in every 2-h operation of the equipment) analysis of STANDARD SOLUTION (Instrumental parameters are found in Table 1). A prior set of samples was rerun if the analyzed value differed from the STANDARD SOLUTION value by $>10\%$. The relative standard deviation among replicate determinations was typically $\leq 5\%$.

Table 11.01 ICP-MS instrumental operating parameters ICP-MS XSERIES-II Thermo Scientific.

RF power (W)	1403.92
Plasma gas flow (L/min)	13.02
Nebulizer gas flow (L/min)	0.95
Auxiliary gas flow (L/min)	0.7
Nebulizer	Quartz pneumatic nebulizer
Spray chamber	Glass with peltier cooling
Number of replicates	3
Acquisition mode	Pulse counting
Dwell time (ms)	10
Sweeps/reading	100

11.3 Results and discussion

11.3.1 Synthesis of cross-linked polyanion (CAPE 5)

Butler's cyclopolymerization protocol has been utilized to synthesize the current resin **5** (Scheme 1). Butler's pioneering discovery of the cyclopolymerization involving a variety of *N,N*-diallylammonium monomers has led to the synthesis of an array of scientifically and technologically important water-soluble cationic polyelectrolytes^[20, 130, 158]. The polymer-architecture, having the five-membered cyclic units embedded in the backbone, has been recognized as the eighth major structural type of synthetic polymers^[130]. Over 33 million pounds of poly(diallyldimethylammonium chloride) alone are sold annually for water treatment and another 2 million pounds are used for personal care formulation^[20].

Diallylaminodiphosphonic acid **2**, a zwitterionic acid (ZA) monomer used for the current cyclopolymerization, was prepared using a modified procedure^[65]. An aqueous solution of monomer **2** (90 mol%) and cross-linker **3** (10 mol%) underwent

cyclocopolymerization in the presence of initiator TBHP to give cross-linked polyzwitterionic acid (CPZA **4**) (scheme 1) as a white solid. To the best of our knowledge this is the first cross-linked polymer containing aminomethyldiphosphonic acid motif obtained *via* Butler's cyclopolymerization protocol. CPZA **4** was found to be in a powder form, which upon treatment with excess NaOH led to the formation of CAPE **5**. Elemental analysis of CPZA **4** confirmed the incorporation of monomer **2** and cross-linker **3** to CPZA **4** in an approximate mol ratio of 90:10, which is similar to the feed ratio. Thermogravimetric analysis (TGA) curve of CAPE **5** (Fig. 11.1) showed two major loss in weight: first slow weight loss of 14.0 % is attributed to loss of water imbedded inside the cross-linked polymer, the second major loss of 85% is the result of combustion of nitrogenated organic fraction with the release of CO₂, NO_x and H₂O gases^[163], mixed with the loss of H₂O and P₂O₅ formed by the condensation reaction between the pendent phosphonate groups^[245]. The residual mass at 800 °C was found to be 1.0 %.

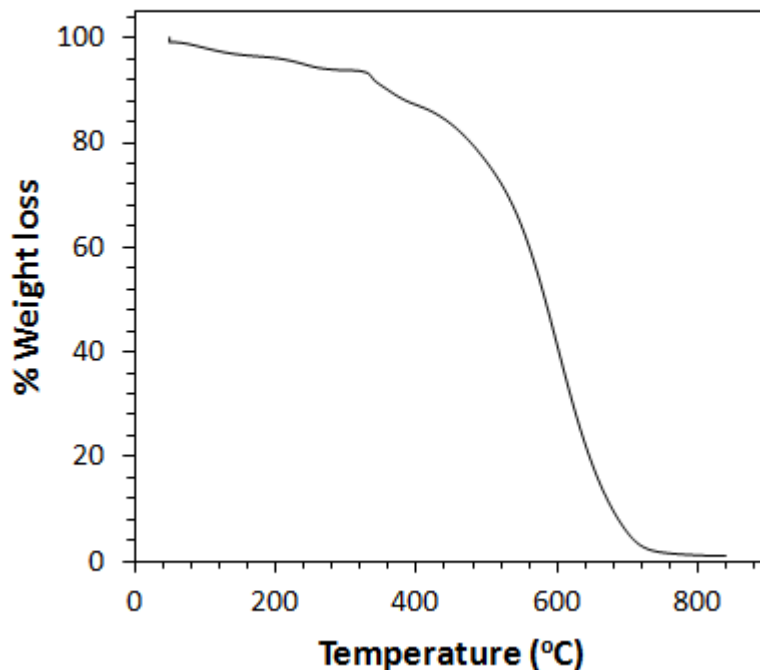


Figure 11.1. TGA analysis of CAPE 5.

11.3.2 Adsorption properties of CAPE 5

The ion exchange capacity (IEC) of CAPE 5 was found to be 5.98 mmol/g which indicated the excellent ability of the copolymer to adsorb metal ions (M^{+2}) as a result of the presence of chelating ligands of $-N^{\cdot}$ and diphosphonate motifs $-[P(=O)(O^-)_2]_2$ (Scheme 2). The bands in the IR spectrum (Fig. 11.2A) of the resin 5 in the region of $900-1050\text{ cm}^{-1}$ are attributed to the phosphonate P-O vibrations^[161, 245]. The IR spectra of the resin loaded with Cu^{2+} and Cd^{2+} (Figures 11.2B and 11.2C) revealed the increase in the intensity and broadness of the phosphonate P-O vibrations as a result of the adsorption of the metal ions^[164]. The C-N absorption was found in near $\sim 1460\text{ cm}^{-1}$. The peaks found around 1650 cm^{-1} were ascribed to the H-O-H bending vibration. The

appearances of a new strong band at 1384 cm^{-1} (Figs. 11.2B and C) was attributed to the presence of ionic nitrate group since the adsorption process was carried out in the presence of copper and cadmium nitrates^[167]. Interestingly, the presence of these strong bands implies the ability of the resin to act also as an anion exchanger. Note that the absorption band attributed to the nitrate ion is absent in the IR spectrum of the unloaded resin **5** (Fig. 11.2A).

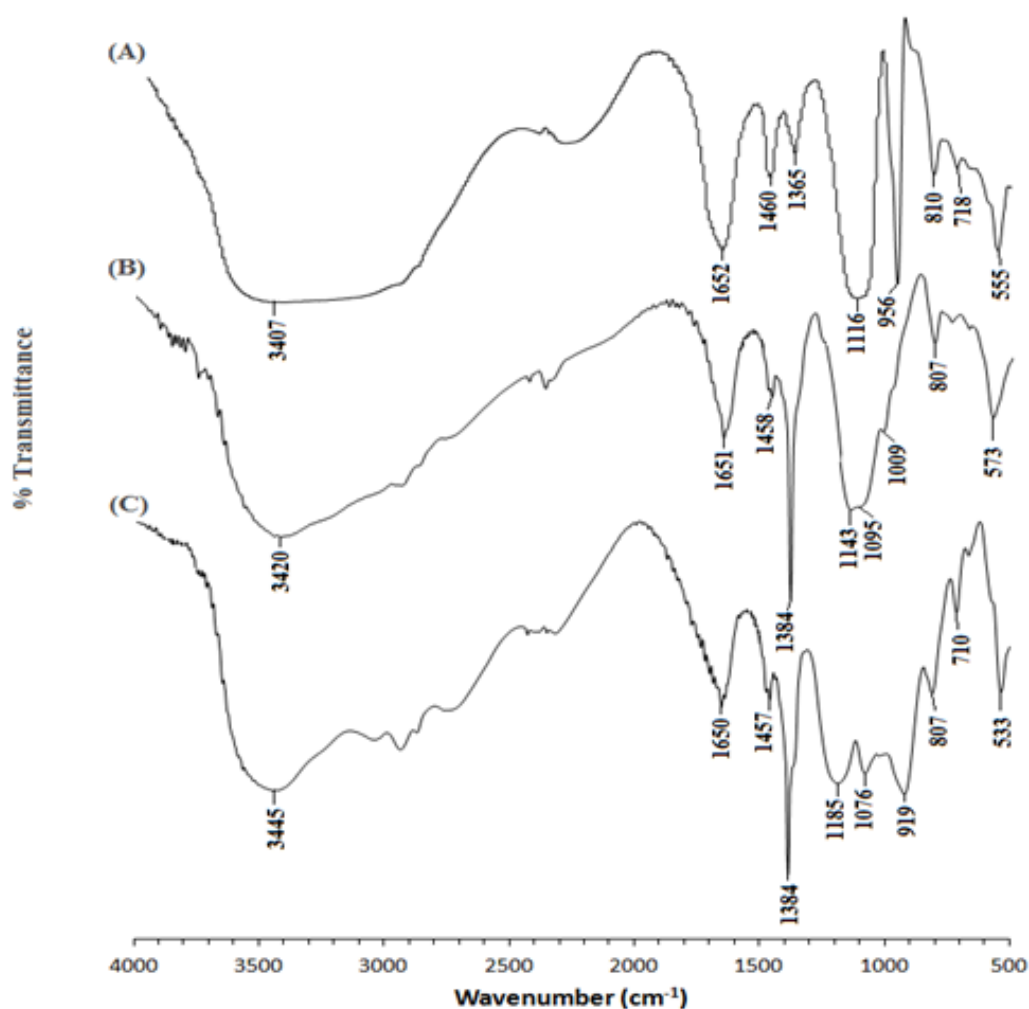
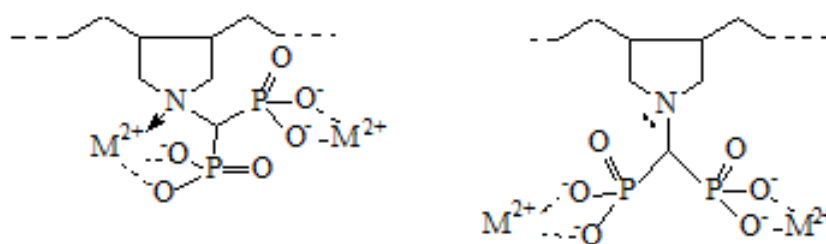


Figure 11.2. FT-IR for: (a) Unloaded CAPE 5; (b) CAPE 5 loaded with Cu^{2+} ; (c) CAPE 5 loaded with Cd^{2+} .



Scheme 2. Metal complex: aminomethyldiphosphonate as tridentate and bidentate ligand

11.3.3 Adsorption kinetics

The adsorption kinetics, which describes the relationship between adsorption capacity and adsorption time at different temperatures, is presented in Figs. 11.3a and 11.4a. The adsorption process was found to be fast and it reached equilibrium within 2 h indicating the strong ability of the resin to remove Cu^{2+} and Cd^{2+} ions from aqueous solutions. At higher temperatures, the adsorption capacities increased indicating larger swelling allowing more ions to be diffused and adsorbed on CAPE 5.

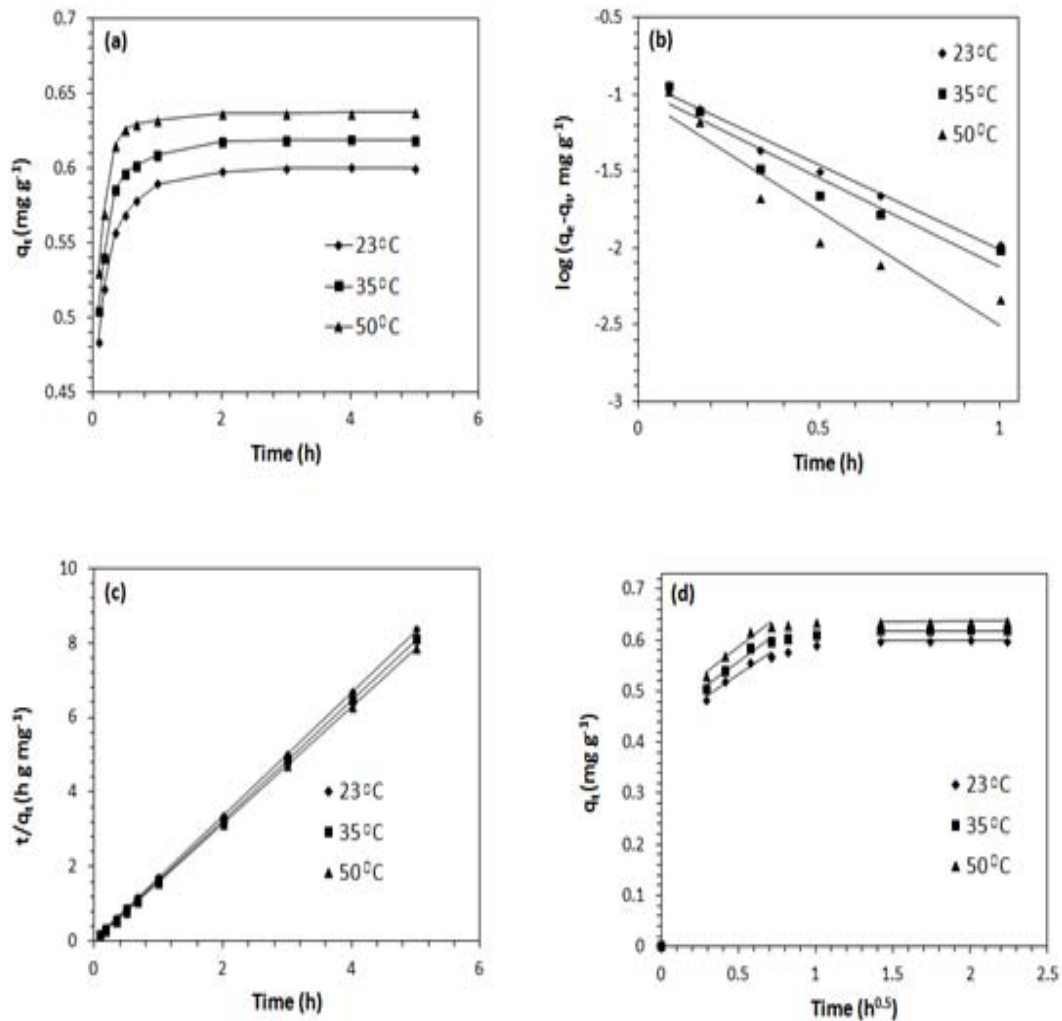


Figure 11.03. (a) Effect of time on the adsorption capacity of Copper. (b) Lagergren First- order kinetic model. (c) Lagergren second-order kinetic model (d) Intraparticle diffusion model.

11.3.3.1 Lagergren first-order kinetics

Lagergren first-order kinetics describes the adsorption process in a solid–liquid system based on the adsorption capacity of the solid, where it assumes that one metal ion is adsorbed onto one adsorption site on the surface of the adsorbent. The linear form of the model can be described in the following equation (Eq. 3):

$$\log (q_e - q_t) = \log q_e - \frac{k_1 t}{2.303} \quad (3)$$

where q_e and q_t (mg g^{-1}) are the adsorption capacities at equilibrium and at time t (h), respectively, and k_1 is the first-order rate constant. The k_1 and q_e at different temperatures were evaluated experimentally using the slope and intercept of the plots of $\log(q_e - q_t)$ versus t (Table 11.2, Figs. 11.3b and 11.4b). The fitness of the data were found to be relatively good, but not as good as the fitness with Lagergren second order kinetics (*vide infra*). The first order kinetic data showed that the calculated values of $q_{e, cal}$ are not in agreement with the experimental values $q_{e, exp}$ indicating that the adsorption process didn't fit with Lagergren first-order kinetic model (Table 11.2) ^[167].

11.3.3.2 Lagergren second-order kinetics

The linear Lagergren second-order kinetic model can be expressed by the following equation (Eq. 4):

$$\frac{t}{q_t} = \frac{1}{k_2 q_e^2} + \frac{t}{q_e} \quad (4)$$

where k_2 is second-order rate constant, q_t and q_e are the respective adsorption capacity of the metal ions at a time t and at equilibrium.

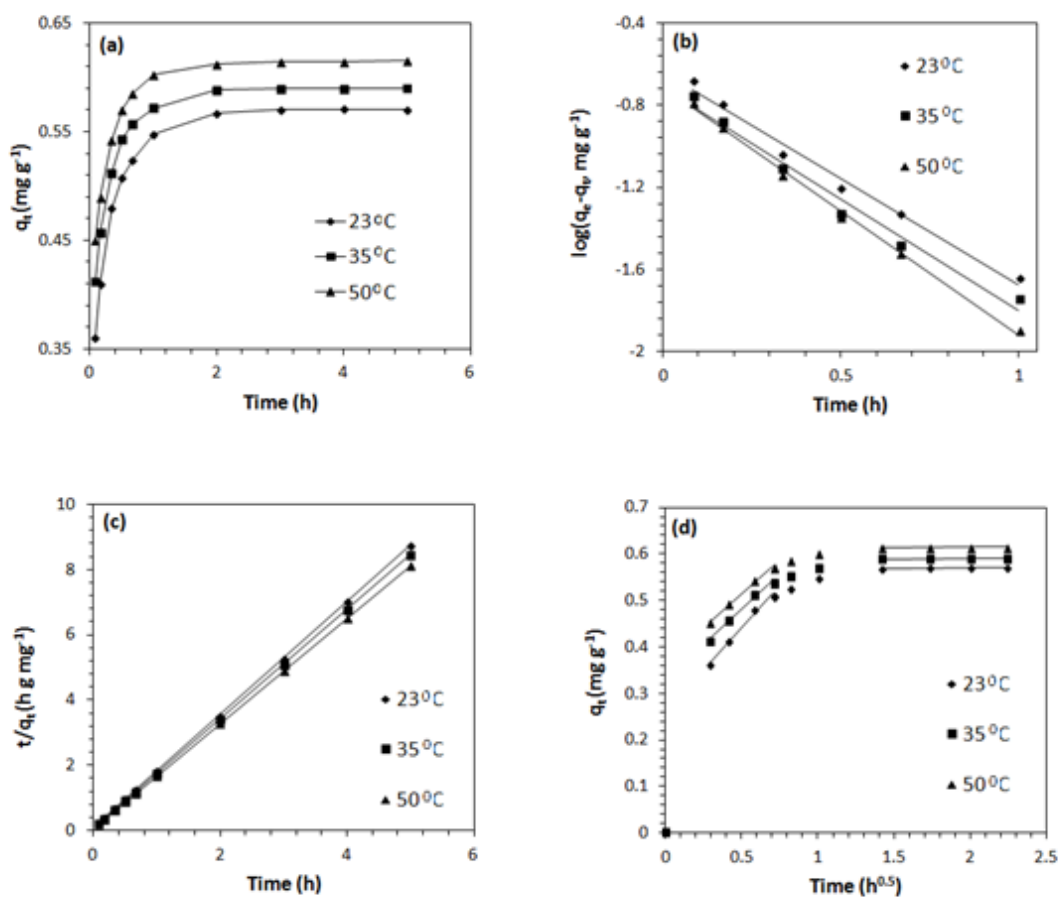


Figure 11.4 (a) Effect of time on the adsorption capacity of Cadmium. (b) Lagergren First-order kinetic model. (c) Lagergren second-order kinetic model (d) Intraparticle diffusion model.

It is evident from Figs. 11.3c and 11.4c and Table 11.2 that the second-order Lagergren kinetic model fitted well the adsorption of Cu^{2+} and Cd^{2+} ions indicating that the adsorption process might be a chemical adsorption^[246]. Also the equilibrium adsorption capacities ($q_{e, \text{cal}}$) derived from Eq. (4) are in close agreement with those observed experimentally ($q_{e, \text{exp}}$). It can be noted in Table 11.2 that the higher rate (k_2) and adsorption capacities ($q_{e, \text{cal}}$) in the case of copper ions than cadmium ions can be explained in terms of ionic radius, electronegativity, hardness index, and the hydration energy (Table 11.3).

Table 11.02 Lagergren First and Second-Order Kinetic Model Parameters for the adsorption of Cu²⁺ and Cd²⁺ ions^a on CAPE 5

Metal ion	Temp (K)	$q_{e, \text{exp}}$ (mg g ⁻¹)	Lagergren first-order			Lagergren second-order				
			k_1 (h ⁻¹)	$q_{e, \text{cal}}$ (mg g ⁻¹)	R^2	k_2 (h ⁻¹ g mg ⁻¹)	h^b (h ⁻¹ g ⁻¹ mg)	$q_{e, \text{cal}}$ (mg g ⁻¹)	R^2	E_a (kJ mol ⁻¹)
Cu ²⁺	296	0.600	2.53	0.122	0.9792	64.2	23.4	0.604	1	18.3
	308	0.618	2.66	0.108	0.9302	78.7	30.4	0.622	1	
	323	0.637	3.43	0.097	0.9039	118.9	48.5	0.639	1	
Cd ²⁺	296	0.570	2.38	0.230	0.9860	28.1	9.43	0.580	1	11.6
	308	0.590	2.51	0.193	0.9794	37.4	13.3	0.597	1	
	323	0.615	2.79	0.195	0.9965	41.8	16.1	0.621	1	

^aInitial metal ion concentration 1 mg/L. ^bInitial adsorption rate $h = k_2 q_e^2$.

Table 11.3 Ionic radius, effective hydrated ionic radius, hydration energy, electronegativity, and hardness Index of Cu²⁺ and Cd²⁺ ions

Metal ion	Ionic radius (nm)	Hydrated radius (nm)	Hydration energy (kJ mol ⁻¹)	Electronegativity (Pauling)	Hardness Index
Cu ²⁺	0.087	0.419	-2174	1.90	0.115
Cd ²⁺	0.124	0.426	-1882	1.69	0.081

Some factors may have greater domination than the others in the absorption process. The more electronegative and harder acid Cu²⁺ prefers to coordinate with harder -O⁻¹ in the phosphonate motifs^[246, 247]. The experimental data so far revealed that the resin is an efficient adsorbent for the removal of both copper and cadmium ions from aqueous solutions.

11.3.3.3 Intraparticle diffusion model

The mechanism of adsorption can be understood by determining the rate-limiting step, and this can be determined by using some adsorption diffusion models which are

always constructed on the basis of three consecutive steps: (1) film diffusion (i.e., diffusion across the liquid film surrounding the adsorbent particles); (2) intraparticle diffusion (i.e., diffusion in the liquid contained in the pores and/or along the pore walls); and (3) mass action (i.e., physical adsorption and desorption between the adsorbate and active sites). The intraparticle diffusion model assumes that the metal ions are transported from the solution through an interface between the solution and the adsorbent (i.e., film diffusion) followed by a rate-limiting intraparticle diffusion step which bring them into the pores of the particles in the adsorbent. Following equation expresses the relation of the adsorption capacity and time^[200, 201, 220, 248].

$$q_t = x_i + k_p t^{0.5} \quad (5)$$

where q_t is the adsorption capacity at time t , k_p is the rate constant of intraparticle diffusion, x_i is related to boundary layer thickness. According to the Weber–Morris model^[234], a straight line fit for the plot of q_t versus $t^{0.5}$ implies the intraparticle diffusion as the rate-limiting step^[218, 219]. If the plot passes through the origin then it becomes the sole rate-limiting step^[221].

The values of the intercept x_i (Table 11.4) in the initial linear plots for Cu were found to be 0.430, 0.445, and 0.470 mg g⁻¹ at 23, 35, and 50°C, respectively, with square of regression (R^2) as 0.9607, 0.9605, and 0.9531 (Fig. 11.3d). The corresponding values of 0.261, 0.329, and 0.370 mg g⁻¹ for Cd with respective R^2 values of 0.9852, 0.9866, and 0.9929 confirms the similar trend of increasing x_i with the increase in temperature (Fig. 11.4d).

Table 11.4 Intraparticle Diffusion coefficients and intercept values for the adsorption of Cu²⁺ and Cd²⁺ ions on CAPE 5 at different temperatures.

Metal ion	Temp (K)	k_p (mg g ⁻¹ h ^{0.5})	Intercept values (x_i)	R^2
Cu ²⁺	296	0.205	0.430	0.9607
	308	0.225	0.445	0.9605
	323	0.233	0.470	0.9531
Cd ²⁺	296	0.361	0.261	0.9852
	308	0.304	0.329	0.9866
	323	0.290	0.370	0.9929

Since the initial linear plot did not pass through the origin, that is, there is an intercept which indicates that rapid adsorption occurs within a short period of time. The intercept x_i of the linearized line was used to define the initial adsorption factor (R_i)^[220] as:

$$R_i = 1 - \frac{x_i}{q_e} \quad (6)$$

where x_i is the initial adsorption amount and q_e the final adsorption amount at the longer time. For Cu²⁺ ions, the x_i and q_e values of 0.430 (Fig. 11.3d) and 0.600 mg g⁻¹, respectively, at 23 °C gave an R_i value of 0.28 which means that the relatively strong rapid initial adsorption has already reached 72% before the first adsorption data was collected at a time of 5 min. The other 28% of adsorption is governed by intraparticle diffusion as indicated by the linear relation (Fig. 11.3d). In this case, the intraparticle diffusion within the pores of the resins was the rate-limiting step. Note that the last linear section represents the final equilibrium stage. For Cd²⁺ ions, the respective x_i and q_e values of 0.261 (Fig. 11.4d) and 0.570 mg g⁻¹ at 23 °C gave an R_i value of 0.46 which

reveals that within 5 min rapid initial adsorption has already reached 54% and the adsorption of the remainder 46% is governed by intraparticle diffusion.

11.3.3.4 Adsorption activation energy

The adsorption activation energy can be deduced from the rate constants (k_2) obtained from the Lagergren second-order kinetic model using the Arrhenius equation (Eq. 7) expressed as:

$$\ln k_2 = -\frac{E_a}{2.303RT} + \text{constant} \quad (7)$$

where k_2 is the second order rate constant ($\text{g mg}^{-1} \text{h}^{-1}$), E_a the activation energy (kJ mol^{-1}), R is the universal gas constant ($8.314 \text{ J mol}^{-1} \text{ K}$) and T is the solution temperature (K). A plot of $\ln k_2$ versus $1/T$ gives a linear plot, with slope $-E_a/R$ (Fig. 11.5, Table 11.2). The low activation energy values obtained (18.3 and 11.6 kJ mol^{-1}) is an indication for the favourability of the adsorption process^[167, 179].

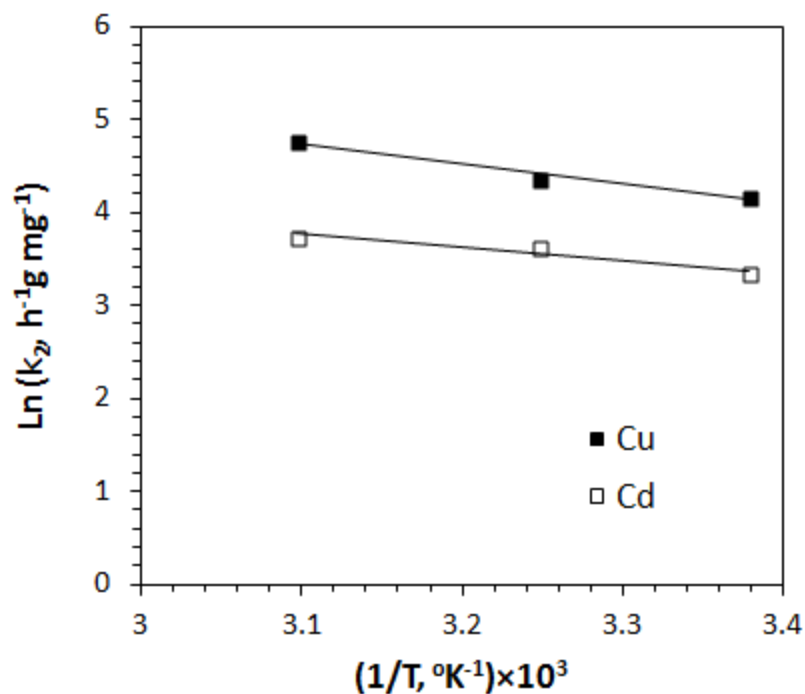


Figure 11.05. Arrhenius plot.

11.3.4 Adsorption isotherms

As shown in Figs 11.6a and 11.7a, the adsorption capacity of CAPE 5 increases with the increase in the initial concentration of Cu²⁺ and Cd²⁺ ions. To further explore the adsorption mechanism, Langmuir and Freundlich models were used to analyze the adsorption data. The Langmuir isotherm equation can be expressed by Eq. (8):

$$\frac{C_e}{q_e} = \frac{C_e}{Q_m} + \frac{1}{Q_m b} \quad (8)$$

where C_e and q_e are the concentrations of metal ion in the solution and resin, respectively, Q_m and b are the Langmuir constants. Figs. 11.6b and 11.7b illustrate the Langmuir plot of C_e/q_e versus C_e , enabling the calculation of Langmuir constants from the intercept and slope of the linear plot (Table 11.5). Langmuir isotherm model assumes the mechanism

of the adsorption process as a monolayer adsorption on completely homogeneous surfaces where interactions between adsorbed molecules are negligible^[233]. This empirical model assumes the adsorbed layer is one molecule in thickness, with adsorption can only occur at a fixed number of definite identical and equivalent localized sites. Once a molecule occupies a site, no further adsorption can take place^[234, 235]. This is described as homogeneous adsorption with uniform energies of ion exchange as all sites possess equal affinity for the adsorbate^[236, 237].

Table 11.05 Langmuir and Freundlich isotherm model constants for Cu²⁺ and Cd²⁺ adsorption at different temperatures.

Metal ion	Temperature (K)	Langmuir isotherm model			Freundlich isotherm model			
		Q _m (mg g ⁻¹)	b (L mg ⁻¹)	R ²	k _f	n	1/n	R ²
Cu ²⁺	296	0.79	29.3	0.9946	2.26	1.82	0.55	0.9817
	308	0.85	39.3	0.9934	3.39	1.69	0.59	0.9507
	323	0.94	47.4	0.9945	4.97	1.60	0.63	0.9709
Cd ²⁺	296	0.87	12.8	0.9976	2.06	1.60	0.63	0.9909
	308	0.93	14.6	0.9914	2.48	1.57	0.64	0.9936
	323	0.96	23.0	0.9967	3.42	1.56	0.64	0.9881

Freundlich isotherm model, on the other hand, describes the non-ideal adsorption occurring on a heterogeneous surface with uniform energy as well as multilayer adsorption; Eqs. (9) and (10) express the model:

$$q_e = k_f C_e^{1/n} \quad (9)$$

$$\log q_e = \log k_f + \frac{1}{n} \log C_e \quad (10)$$

where q_e and C_e are the equilibrium concentrations of metal ion in the adsorbed and liquid phase, respectively, k_f and n represent the Freundlich constants (Table 11.5), which can be calculated from the slope and intercept of the linear plot of $\log q_e$ versus $\log C_e$ as presented in Figs. 11.6c and 11.7c. The values of n were determined to be higher than 1; values lying in the range of 1 to 10 are considered for classification as favorable adsorption^[225, 226]. The slope ($1/n$) range of 0 - 1 is known to be a measure of adsorption intensity or surface heterogeneity, becoming more heterogeneous as its value gets closer to zero. A $1/n$ value below unity (all values at different temperatures fall within the range of (0-1) is indicative of chemisorption process, whereas $1/n$ above one implies cooperative adsorption (Table 11.5)^[227]. For the adsorption of Cu^{2+} ions, the higher values of the constant k_f , which is related to adsorption capacity (q), indicates higher affinity of the ions to the adsorbent in comparison to Cd^{2+} adsorption.

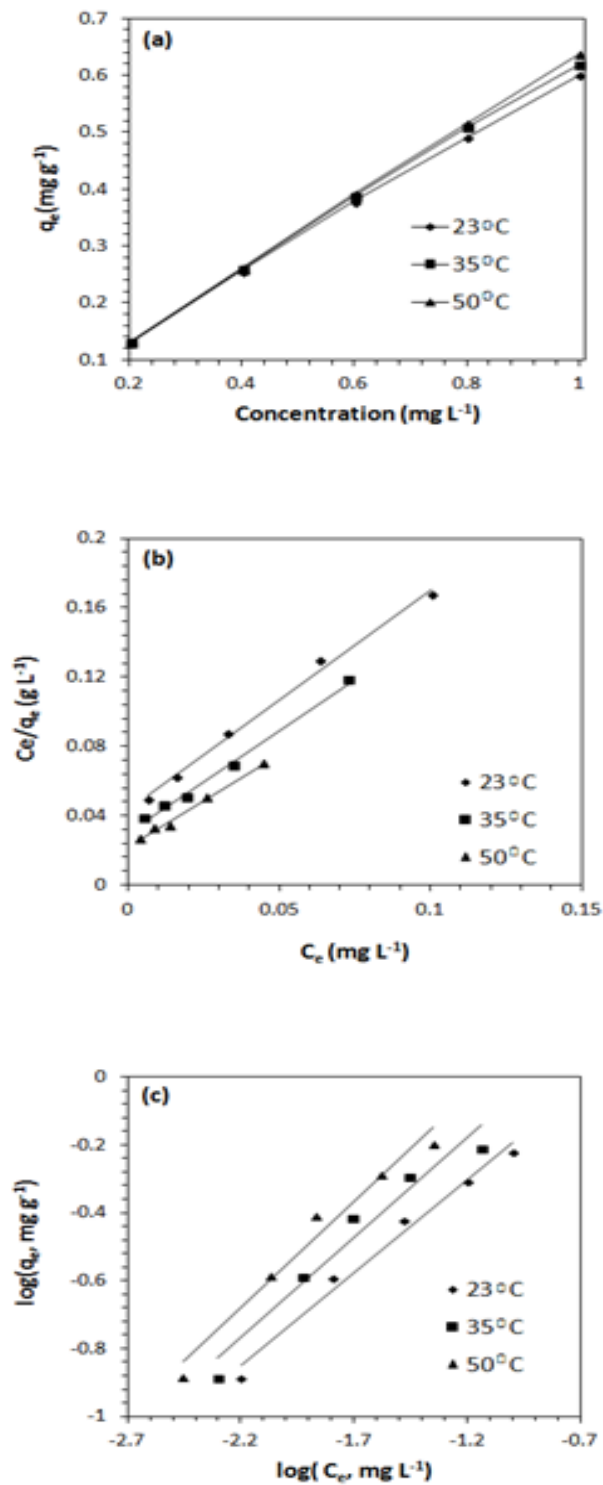


Figure 11.06. (a) Effect of copper initial concentration on the adsorption capacity at different temperatures. (b) Langmuir isotherm model. (c) Freundlich isotherm model.

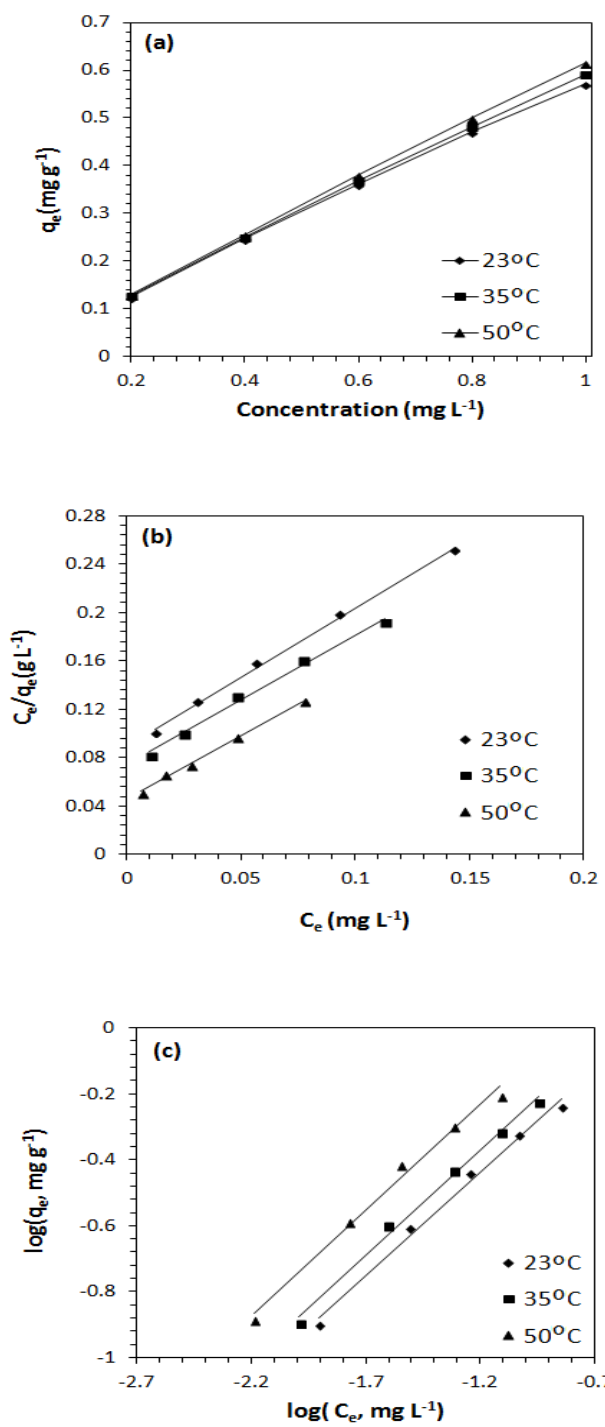


Figure 11.07. (a) Effect of Cadmium initial concentration on the adsorption capacity at different temperatures. (b) Langmuir isotherm model. (c) Freundlich isotherm model.

For the Langmuir isotherm model^[47, 240], a dimensionless constant (R_L), commonly known as separation factor or equilibrium parameter can be used to describe the favorability of adsorption on the polymer surface by Eq. (11):

$$R_L = \frac{1}{(1+bC_0)} \quad (11)$$

where C_0 is the initial M^{2+} concentration and b is the Langmuir equilibrium constant. The more favourable adsorption is reflected by lower R_L values; the adsorption could be either unfavourable ($R_L > 1$), linear ($R_L = 1$), favourable ($0 < R_L < 1$) or irreversible ($R_L = 0$). The R_L values for the adsorption of both metal ions are given in Table 11.6, which reveals that the values fall in the preferred region (i.e., $0 < R_L < 1$). The lower values of R_L for the metal adsorption (approaching 0) point toward the irreversible nature of the adsorption. It can be noted in Table 11.6 that the R_L values decrease with the increase in the initial Cu^{2+} and Cd^{2+} concentration indicating that the ion exchange is more favourable at higher initial concentration. Another factor affecting the adsorptions is the temperature: as shown in Table 11.6, the decreasing R_L values with increasing temperatures imply more favorable adsorption at higher temperatures. The greater percentage removal of metal ions at higher temperatures could be attributed to the greater swelling of the cross-linked polymer allowing the larger amount of metal ions to diffuse through the polymer to reach the active adsorption sites. It is highly gratifying to note that at a 200 ppb initial concentration of Cu^{2+} and Cd^{2+} at 23 °C, percentage metal removal by CAPE **5** was found to be 97% and 94%, respectively (Table 11.6).

Table 11.6 The R_L values based on the Langmuir isotherm model and % Removal at different initial concentration at different temperatures

C_o (mg L ⁻¹)	Cu ²⁺					
	23°C		35°C		50°C	
	R_L value	% Removal	R_L value	% Removal	R_L value	% Removal
0.200	0.1457	96.8	0.1129	97.5	0.0954	98.3
0.400	0.0786	96.0	0.0598	97.1	0.0501	97.9
0.600	0.0538	94.5	0.0407	96.8	0.0340	97.8
0.800	0.0409	92.1	0.0308	95.6	0.0257	96.8
1.000	0.0330	90.0	0.0248	92.7	0.0207	95.6

C_o (mg L ⁻¹)	Cd ²⁺					
	23°C		35°C		50°C	
	R_L value	% Removal	R_L value	% Removal	R_L value	% Removal
0.200	0.2808	93.8	0.2551	94.9	0.1786	96.8
0.400	0.1633	92.3	0.1462	93.8	0.0980	95.8
0.600	0.1152	90.5	0.1025	92.0	0.0676	95.3
0.800	0.0890	88.3	0.0789	90.4	0.0516	94.0
1.000	0.0725	85.7	0.0641	88.7	0.0417	92.3

11.3.5 Effect of pH

The effect pH (in the range 3-6) on the uptake of Cu²⁺ and Cd²⁺ was investigated at a fixed concentration (1 mg L⁻¹) and time of 24 h. The pH of the solution was controlled by using an acetate buffer (CH₃COONa/CH₃COOH). Results of metal uptake at different pH are shown in Fig. 11.8. Optimum pH was found to be 5; at higher pH values, the hydrolysis of the metal ions occurs by the formation of metal hydroxides, which compete with the metal ion uptake by the resin^[227].

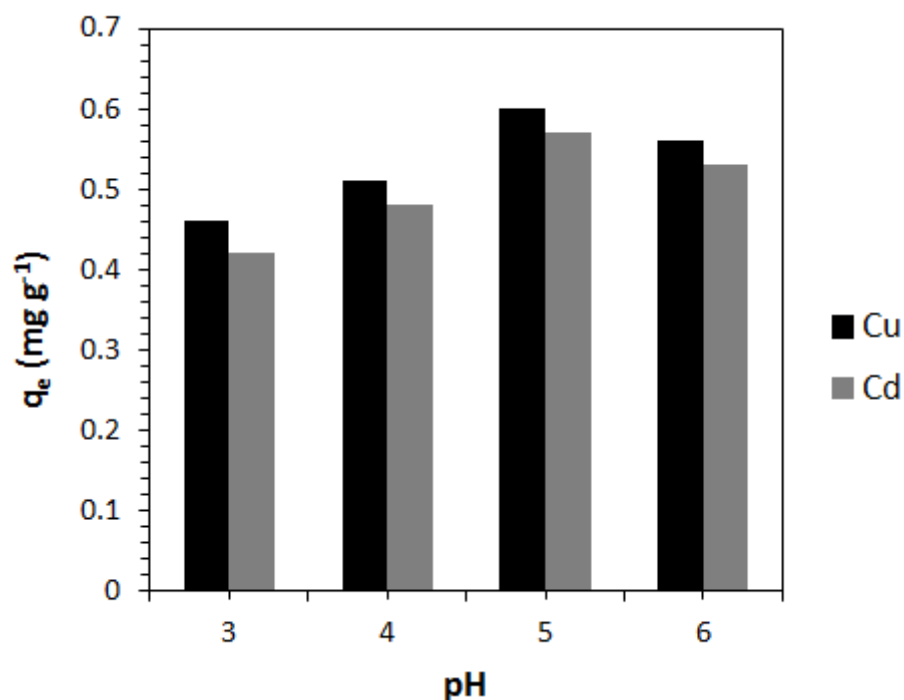


Figure 11.08 Effect of pH on the adsorption capacity of CAPE 5.

11.3.6 Adsorption thermodynamics

Adsorption experiments were also performed to obtain the thermodynamic parameters; the results are illustrated in Fig. 11.9a. The adsorption capacity increases with the increase of temperature thus suggesting the endothermic nature of the adsorption process. A plot of $\log (q_e/C_e)$ versus $1/T$ is displayed in Fig. 11.9b. The thermodynamic parameters ΔG , ΔH and ΔS were calculated using Vant-Hoff equation (Eq.12), and are tabulated in Table 11.7^[167]. The negative ΔG values ascertain the spontaneity of the adsorption process.

$$\log \left(\frac{q_e}{C_e} \right) = -\frac{\Delta H}{2.303RT} + \frac{\Delta S}{2.303R} \quad (12)$$

As the temperature increases, the ΔG values become more negative, indicating that the adsorption process is more favorable at the higher temperatures.

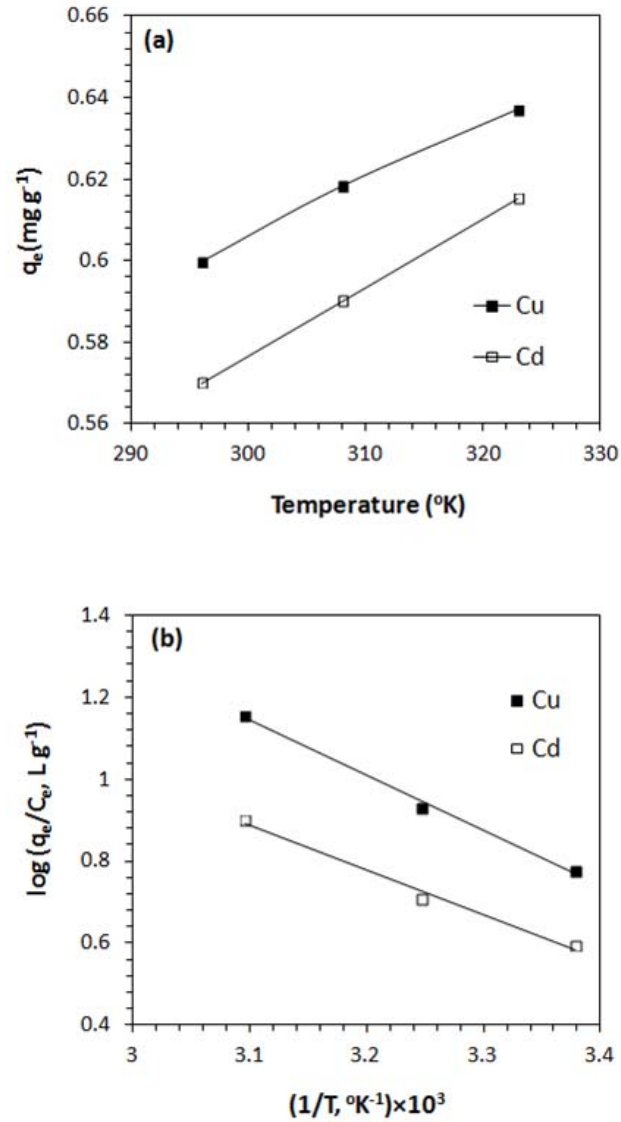


Figure 11.09 (a) Effect of temperature on the adsorption capacity of CAPE 5; (b) Vant-Hoff plot.

Favorable adsorption at higher temperatures is attributed to the greater swelling of the resin and increased diffusion of metal ions into the resin. The positive values of ΔH certify that the adsorption is an endothermic process. In addition, it can be found in Table 11.7 that the ΔS values are positive, suggesting that the adsorption is an entropy-driven process as the randomness increased during the adsorption of metal ions as a result of the release of water molecules from their large hydration shells.

Table 11.7 Thermodynamic Data for Cu^{2+} and Cd^{2+} adsorption on CAPE 5.

Metal ion	Temperature (K)	ΔG (kJ/mol)	ΔH (kJ/mol)	ΔS (J/mol K)	R^2
Cu^{2+}	296	-4.36			
	308	-5.58	25.8	102	0.9952
	323	-7.10			
Cd^{2+}	296	-3.31			
	308	-4.29	20.8	81.6	0.9899
	323	-5.52			

11.3.7 SEM and EDX images for CAPE 5 unloaded and loaded with Copper and Cadmium ions

Unloaded and loaded resins were investigated by scanning electron microscopy (SEM). Unloaded resins were immersed in 0.1 M $\text{Cu}(\text{NO}_3)_2$ for 24 h at a pH of 5, filtered, and dried under vacuum until constant weight was achieved. Loaded and unloaded polymers were then sputter-coated for 1 min with a thin film of gold.

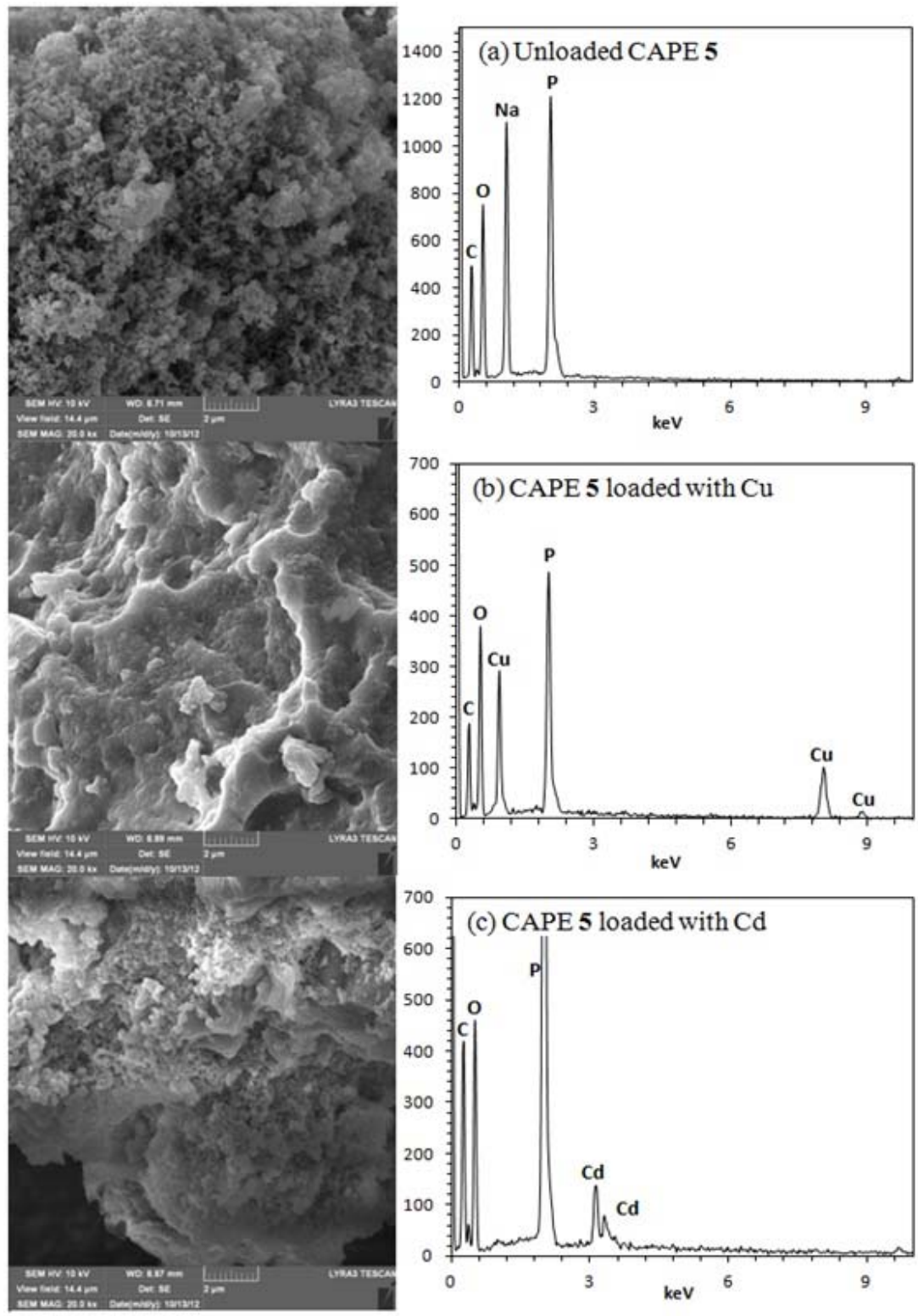


Figure 11.10. (a) Unloaded CAPE 5; (b) CAPE 5 loaded with Cu^{2+} ions; (c) CAPE 5 loaded with Cd^{2+} ions.

SEM and EDX images (Fig. 11.10) show that the morphology has been altered by the adsorption of copper and cadmium ions (cracked morphology to smooth); the EDX analysis (Fig. 11.10a) shows that unloaded CAPE 5 composition was similar to the proposed in scheme 1. Also, Figs 11.10b and c showed that the copper and cadmium ions displaced the sodium ions in CAPE 5 confirming the adsorption of the metal ions. The color of the resins also changed from white to blue after adsorbing copper ions thus giving a positive indication that the adsorption process has occurred. The SEM and EDX confirmed that CAPE 5 could be used as an efficient adsorbent of Cu^{2+} and Cd^{2+} in aqueous solutions at low concentrations.

11.4 Treatment of real wastewater samples.

Two wastewater samples were collected from water treatment plant from the Dhahran, Saudi Arabia. The samples were analyzed to measure the concentration of the native copper and cadmium concentration on the samples. 20 mL of these samples were loaded with 30 mg of CAPE 5 to test the ability of this resin to adsorb heavy metals in real wastewater conditions. The results for the analysis were given in Tables 8 and 9 which indicate the ability of these resins to adsorb various types of heavy metals from wastewater samples and to be selective for the removal of copper and cadmium metal ions from waste water samples. The pH of the wastewater samples were found to be 7.8 (Table 8) and 8.5 (Table 9), whereas experiments involving distilled water were carried out at pH 5. At these high pH values, the resins have more anionic sites which are available for the adsorption of copper and cadmium metal ions, these results shows the ability of the resin to selectively remove metal ions from wastewater.

Table 011.8 Comparison of metals concentration from Water treatment plant sample (Doha, Saudi Arabia) before and after adding the polymer.

Metal	Original sample #1 ($\mu\text{g L}^{-1}$)	(After treatment) ($\mu\text{g L}^{-1}$)
Cu	190.30 \pm 0.006	24.20 \pm 0.006
Zn	20.73 \pm 0.111	18.97 \pm 0.111
As	16.10 \pm 0.042	14.17 \pm 0.042
Sr	12600 \pm 0.012	11500 \pm 0.012
Mo	49.48 \pm 0.027	29.27 \pm 0.027
Cd	559.90 \pm 0.009	71.12 \pm 0.009

Mean and standard deviation of three replicates (n = 3).

\pm values are the method detection limit (MDL), 3 σ of the blank sample.

Table 11.9 Comparison of metals concentration from Petrochemical plant sample (Dhahran, Saudi Arabia) before and after adding the polymer.

Metal	Original sample #2 ($\mu\text{g L}^{-1}$)	(after treatment) ($\mu\text{g L}^{-1}$)
Cu	245.4 \pm 0.006	9.95 \pm 0.063
Zn	275.4 \pm 0.111	24.05 \pm 0.111
Sr	14360.0 \pm 0.012	14390 \pm 0.012
Cd	631.8 \pm 0.015	53.46 \pm 0.015
Sb	0.424 \pm 0.009	0.269 \pm 0.009
Pb	11.99 \pm 0.012	7.004 \pm 0.012

Mean and standard deviation of three replicates (n = 3).

\pm values are the method detection limit (MDL), 3 σ of the blank sample.

11.5 Conclusion

A novel cross-linked polyaminomethyldiphosphonate was prepared from inexpensive starting materials. The resin was found to have a very good adsorption capacity for Cu^{2+} and Cd^{2+} ions. The adsorption followed Lagergren second-order kinetic model and Langmuir as well as Freundlich isotherm models. The negative ΔG s and

positive ΔH s ensured the spontaneity and the endothermic nature of the adsorption process. The efficiency of Cu^{2+} and Cd^{2+} removal at an initial metal concentration of 200 ppb was found to be 96.8 and 93.8%, respectively. The good adsorption efficiencies implied the efficacy of the resin in removing Cu^{2+} and Cd^{2+} ions from aqueous solution at low concentration. Treatment of two wastewater samples showed the ability of the resin to be used in selective removal of metal ions.

REFERENCES

- [1] Kudaibergenov, S.; Jaeger, W.; Laschewsky, A., Polymeric Betaines: Synthesis, Characterization, and Application, In *Supramolecular Polymers Polymeric Betains Oligomers*, Springer Berlin Heidelberg: (2006); Vol. 201, pp 157.
- [2] Singh, P. K.; Singh, V. K.; Singh, M., *e-Polymers*, (2007) **030**, 1.
- [3] Anton, P.; Laschewsky, A., *Die Makromolekulare Chemie*, (1993) **194**, 601.
- [4] Wielema, T. A.; Engberts, J. B. F. N., *European Polymer Journal*, (1987) **23**, 947.
- [5] Ali, S. A.; Rasheed, A., *Polymer*, (1999) **40**, 6849.
- [6] Al-Muallem, H. A.; Wazeer, M. I. M.; Ali, S. A., *Polymer*, (2002) **43**, 4285.
- [7] Jaeger, W.; Bohrisch, J.; Laschewsky, A., *Progress in Polymer Science*, (2010) **35**, 511.
- [8] Salamone, J. C.; Volksen, W.; Olson, A. P.; Israel, S. C., *Polymer*, (1978) **19**, 1157.
- [9] Skouri, M.; Munch, J. P.; Candau, S. J.; Neyret, S.; Candau, F., *Macromolecules*, (1994) **27**, 69.
- [10] Armitage, B. A.; Bennett, D. E.; Lamparski, H. G.; O'Brien, D. F., *Adv. Polym. Sci.*, (1996) **126**, 53.
- [11] Haruta, M.; Kageno, K.; Soeta, M.; Harada, S., Polymers of phosphonic acid derivatives, JP50072987A, (1975).
- [12] Riedelsberger, K.; Jaeger, W., *Des. Monomers Polym.*, (1998) **1**, 387.

- [13] Ali, S. A.; Abu-Thabit, N. Y.; Al-Muallem, H. A., *Journal of Polymer Science Part A: Polymer Chemistry*, (2010) **48**, 5693.
- [14] Abu-Thabit, N. Y.; Kazi, I. W.; Al-Muallem, H. A.; Ali, S. A., *European Polymer Journal*, (2011) **47**, 1113.
- [15] Akgun, B.; Savci, E.; Avci, D., *Journal of Polymer Science Part A: Polymer Chemistry*, (2012) **50**, 801.
- [16] Bilgici, Z. S.; Ordu, O. D.; Isik, M.; Avci, D., *Journal of Polymer Science Part A: Polymer Chemistry*, (2011) **49**, 5042.
- [17] Rajan, K. S.; Murase, I.; Martell, A. E., *J. Amer. Chem. Soc.*, (1969) **91**, 4408.
- [18] Westerback, S. J.; Martell, A. E., *Nature (London, U. K.)*, (1956) **178**, 321.
- [19] Yamashoji, Y.; Matsushita, T.; Shono, T., *technol. rep. osaka univ.*, (1985) **35**, 331.
- [20] Butler, G. B. Ed. *Cyclopolymerization and Cyclocopolymerization*, Marcel Dekker: New York, (1992).
- [21] Butler, G. B., *Acc. Chem. Res.*, (1982) **15**, 370.
- [22] Lancaster, J. E.; Baccei, L.; Panzer, H. P., *Journal of Polymer Science: Polymer Letters Edition*, (1976) **14**, 549.
- [23] De Vynck, V.; Goethals, E. J., *Macromolecular Rapid Communications*, (1997) **18**, 149.

- [24] Ali, S. A.; Aal e, A., *Polymer*, (2001) **42**, 7961.
- [25] Harada, S.; Katayama, M., *Die Makromolekulare Chemie*, (1966) **90**, 177.
- [26] Al-Muallem, H. A.; Wazeer, M. I. M.; Ali, S. A., *Polymer*, (2002) **43**, 1041.
- [27] Ali, S. A.; Rasheed, A.; Wazeer, M. I. M., *Polymer*, (1999) **40**, 2439.
- [28] Ali, M. M.; Perzanowski, H. P.; Ali, S. A., *Polymer*, (2000) **41**, 5591.
- [29] Al-Muallem, H. A.; Wazeer, M. I. M.; Ali, S. A., *Polymer*, (2002) **43**, 4285.
- [30] Ali, S. A.; Mazumder, M. A. J.; Al-Muallem, H. A., *Journal of Polymer Science Part A: Polymer Chemistry*, (2003) **41**, 172.
- [31] Mazumder, M. A. J.; Umar, Y.; Ali, S. A., *Polymer*, (2004) **45**, 125.
- [32] Salamone, J. C.; Tsai, C. C.; Olson, A. P.; Watterson, A. C., *Adv. Chem. Ser.*, (1980) **187**, 337.
- [33] Schulz, D. N.; Peiffer, D. G.; Agarwal, P. K.; Larabee, J.; Kaladas, J. J.; Soni, L.; Handwerker, B.; Garner, R. T., *Polymer*, (1986) **27**, 1734.
- [34] Volpert, E.; Selb, J.; Candau, F., *Macromolecules*, (1996) **29**, 1452.
- [35] Candau, F.; Ohlemacher, A.; Munch, J. P.; Candau, S. J., *Rev. Inst. Fr. Pet.*, (1997) **52**, 133.
- [36] Patrickios, C. S.; Hertler, W. R.; Hatton, T. A., *Biotechnol. Bioeng.*, (1994) **44**, 1031.

- [37] McCormick, C. L.; Lowe, A. B.; Ayres, N., Water-Soluble Polymers, In *Encyclopedia of Polymer Science and Technology*, John Wiley & Sons, Inc.: (2002).
- [38] Patrickios, C. S.; Jang, C. J.; Hertler, W. R.; Hatton, T. A., *ACS Symp. Ser.*, (1994) **548**, 257.
- [39] Boothe, J. E.; Flock, H. G.; Hoover, M. F., *J. Macromol. Sci., Chem.*, (1970) **4**, 1419.
- [40] Glass, J. E., *Adv. Chem. Ser.*, (1986) **213**, 85.
- [41] Rullens, F.; Deligne, N.; Laschewsky, A.; Devillers, M., *Journal of Materials Chemistry*, (2005) **15**, 1668.
- [42] Ohsugi, A.; Furukawa, H.; Kakugo, A.; Osada, Y.; Gong, J. P., *Macromolecular Rapid Communications*, (2006) **27**, 1242.
- [43] Mary, P.; Bendejacq, D. D., *The Journal of Physical Chemistry B*, (2008) **112**, 2299.
- [44] Kudaibergenov, S. E., *Adv. Polym. Sci.*, (1999) **144**, 115.
- [45] Liaw, D.-J.; Huang, C.-C.; Kang, E.-T., *Curr. Trends Polym. Sci.*, (1999) **4**, 117.
- [46] Kudaibergenov, S.; Jaeger, W.; Laschewsky, A., *Adv. Polym. Sci.*, (2006) **201**, 157.
- [47] Liu, J.; Ma, Y.; Zhang, Y.; Shao, G., *J. Hazard. Mater.*, (2010) **173**, 438.
- [48] Kesenci, K.; Say, R.; Denizli, A., *European Polymer Journal*, (2002) **38**, 1443.

- [49] Güçlü, G.; Gürdağ, G.; Özgümüş, S., *Journal of Applied Polymer Science*, (2003) **90**, 2034.
- [50] Camci-Unal, G.; Pohl, N. L. B., *Journal of Chemical and Engineering Data*, (2010) **55**, 1117.
- [51] Vinodh, R.; Padmavathi, R.; Sangeetha, D., *Desalination*, (2011) **267**, 267.
- [52] Geckeler, K. E., *Pure and Applied Chemistry*, (2001) **73**, 129.
- [53] Shahtaheri, S. J.; Khadem, M.; Golbabaie, F.; Rahimi-Froushan, A.; Ganjali, M. R.; Norouzi, P., *Int. J. Occup. Saf. Ergon.*, (2007) **13**, 137.
- [54] Zhang, Q.; Pan, B.; Zhang, W.; Pan, B.; Zhang, Q.; Ren, H., *Ind. Eng. Chem. Res.*, (2008) **47**, 3957.
- [55] He, Z. Y.; Nie, H. L.; Branford-White, C.; Zhu, L. M.; Zhou, Y. T.; Zheng, Y., *Bioresource Technology*, (2008) **99**, 7954.
- [56] Kumar, M.; Tripathi, B. P.; Shahi, V. K., *Journal of Hazardous Materials*, (2009) **172**, 1041.
- [57] Laatikainen, M.; Sirola, K.; Paatero, E., *Colloids Surf., A*, (2007) **296**, 191.
- [58] Tao, Y.; Ye, L.; Pan, J.; Wang, Y.; Tang, B., *J. Hazard. Mater.*, (2009) **161**, 718.
- [59] Innocenzi, P.; Miorin, E.; Brusatin, G.; Abbotto, A.; Beverina, L.; Pagani, G. A.; Casalboni, M.; Sarcinelli, F.; Pizzoferrato, R., *Chem. Mater.*, (2002) **14**, 3758.
- [60] Liu, J.; Xu, T.; Fu, Y., *J. Membr. Sci.*, (2005) **252**, 165.

- [61] Zhang, X.-J.; Ma, T.-Y.; Yuan, Z.-Y., *J. Mater. Chem.*, (2008) **18**, 2003.
- [62] Liang, W.-J.; Wu, C.-P.; Hsu, C.-Y.; Kuo, P.-L., *J. Polym. Sci., Part A: Polym. Chem.*, (2006) **44**, 3444.
- [63] Ezquerro, J.; Yruretagoyena, B.; Moreno-Manas, M.; Roglans, A., *Synth. Commun.*, (1995) **25**, 191.
- [64] Ali, S. A.; Ahmed, S. Z.; Hamad, E. Z., *J. Appl. Polym. Sci.*, (1996) **61**, 1077.
- [65] Riedelsberger, K.; Jaeger, W., *Designed Monomers and Polymers*, (1998) **1**, 387.
- [66] Kiefer, R.; Höll, W. H., *Industrial & Engineering Chemistry Research*, (2001) **40**, 4570.
- [67] Liu, J.; Ma, Y.; Xu, T.; Shao, G., *Journal of Hazardous Materials*, (2010) **178**, 1021.
- [68] Vinodh, R.; Padmavathi, R.; Sangeetha, D., *Desalination*, (2011) **267**, 267.
- [69] Albertsson, P. Ed. *partition of cell particles and macromolecules*, Wiley: new york, (1986); Vol.
- [70] Albertsson, P. A.; Tjerneld, F., *Methods in Enzymology*, (1994) **228**, 3.
- [71] walter, H.; Brooks, D. E.; Fischer, D. Eds., *partitioning in aqueous two-phase systems*, academic press: new york, (1985); Vol. Eds.
- [72] Bulgariu, L.; Bulgariu, D., *Journal of Chromatography A*, (2008) **1196-1197**, 117.

- [73] Bulgariu, L.; Bulgariu, D., *Separation and Purification Technology*, (2011) **80**, 620.
- [74] Lacerda, V. G.; Mageste, A. B.; Santos, I. J. B.; da Silva, L. H. M.; da Silva, M. d. C. H., *Journal of Power Sources*, (2009) **193**, 908.
- [75] Patrício, P. D. R.; Mesquita, M. C.; da Silva, L. H. M.; Da Silva, M. C. H., *Journal of Hazardous Materials*, (2011) **193**, 311.
- [76] Felty, W. L., *Journal of Chemical Education*, (1978) **55**, 576.
- [77] Asrof Ali, S.; Zaka Ahmed, S.; Wazeer, M. I. M.; Hamad, E. Z., *Polymer*, (1997) **38**, 3385.
- [78] Aguiñaga-Díaz, P. A.; Guzmán, R. Z., *Separation Science and Technology*, (1996) **31**, 1483.
- [79] Butler, G. B.; Angelo, R. T., *Journal of the American Chemical Society*, (1957) **79**, 3128.
- [80] Walsh, D. J.; Cheng, G. L., *Polymer*, (1984) **25**, 499.
- [81] Monroy Soto, V. M.; Galin, J. C., *Polymer*, (1984) **25**, 254.
- [82] Munk, P., *Introduction to macromolecular science / Petr Munk*, Wiley: New York :, (1989).
- [83] Barbucci, R.; Casolaro, M.; Ferruti, P.; Nocentini, M., *Macromolecules*, (1986) **19**, 1856.

- [84] Barbucci, R.; Casolaro, M.; Nocentini, M.; Corezzi, S.; Ferruti, P.; Barone, V., *Macromolecules*, (1986) **19**, 37.
- [85] Waziri, S. M.; Abu-Sharkh, B. F.; Ali, S. A., *Fluid Phase Equilibria*, (2003) **205**, 275.
- [86] Waziri, S. M.; Abu-Sharkh, B. F.; Ali, S. A., *Biotechnology Progress*, (2004) **20**, 526.
- [87] Singh, P. K.; Singh, V. K.; Singh, M., *e-Polymers*, (2007), 1.
- [88] Ali, S. A.; Abu-Thabit, N. Y.; Al-Muallem, H. A., *Journal of Polymer Science, Part A: Polymer Chemistry*, (2010) **48**, 5693.
- [89] Al-Hamouz, O. C. S.; Ali, S. A., *J. Polym. Sci., Part A: Polym. Chem.*, (2012) **50**, 3580.
- [90] Barbucci, R.; Casolaro, M.; Ferruti, P.; Barone, V.; Lelj, F.; Oliva, L., *Macromolecules*, (1981) **14**, 1203.
- [91] Ali, S. A.; Ahmed, S. Z.; Wazeer, M. I. M.; Hamad, E. Z., *Polymer*, (1997) **38**, 3385.
- [92] Pike, R. M.; Cohen, R. A., *Journal of Polymer Science*, (1960) **44**, 531.
- [93] Barbucci, R.; Casolaro, M.; Danzo, N.; Barone, V.; Ferruti, P.; Angeloni, A., *Macromolecules*, (1983) **16**, 456.
- [94] Ali, S. A.; Al-Muallem, H. A.; Mazumder, M. A. J., *Polymer*, (2003) **44**, 1671.

- [95] Albertsson, P. A., *Partition of Cell Particles and Macromolecules*, Wiley: (1986); 346 .
- [96] Bora, M. M.; Borthakur, S.; Rao, P. C.; Dutta, N. N., *Sep. Purif. Technol.*, (2005) **45**, 153.
- [97] Duarte, S. P.; Fortes, A. G.; Prazeres, D. M. F.; Marcos, J. C., *J. Chromatogr., A*, (2007) **1164**, 105.
- [98] Johansson, H.-O.; Magaldi, F. M.; Feitosa, E.; Pessoa, A., *J. Chromatogr., A*, (2008) **1178**, 145.
- [99] Su, C.-K.; Chiang, B. H., *Process Biochem. (Amsterdam, Neth.)*, (2006) **41**, 257.
- [100] Andrews, B. A.; Schmidt, A. S.; Asenjo, J. A., *Biotechnol. Bioeng.*, (2005) **90**, 380.
- [101] Benavides, J.; Aguilar, O.; Lapizco-Encinas, B. H.; Rito-Palomares, M., *Chem. Eng. Technol.*, (2008) **31**, 838.
- [102] Salabat, A.; Abnosi, M. H.; Bahar, A. R., *J. Chromatogr., B: Anal. Technol. Biomed. Life Sci.*, (2007) **858**, 234.
- [103] Walter, H.; Brooks, D. E.; Fisher, D.; Editors, *Partitioning in Aqueous Two-Phase Systems: Theory, Methods, Uses, and Applications to Biotechnology*, Academic Press, Inc.: (1985); p 704.
- [104] Huddleston, J. G.; Willauer, H. D.; Boaz, K. R.; Rogers, R. D., *J. Chromatogr., B: Biomed. Sci. Appl.*, (1998) **711**, 237.

- [105] Hatti-Kaul, R.; Editor, *Aqueous Two-Phase Systems: Methods and Protocols. [In: Methods Biotechnol., 2000; 11]*, Humana: (2000); p 440.
- [106] Rogers, R. D.; Willauer, H. D.; Griffin, S. T.; Huddleston, J. G., *J. Chromatogr., B: Biomed. Sci. Appl.*, (1998) **711**, 255.
- [107] Bergfeldt, K.; Piculell, L.; Tjerneld, F., *Macromolecules*, (1995) **28**, 3360.
- [108] Dissing, U.; Mattiasson, B., *Biotechnol. Appl. Biochem.*, (1993) **17**, 15.
- [109] Svensson, M.; Linse, P.; Tjerneld, F., *Macromolecules*, (1995) **28**, 3597.
- [110] Hughes, P.; Lowe, C. R., *Enzyme Microb. Technol.*, (1988) **10**, 115.
- [111] Ba, X.-g.; Lin, J.-x.; Qiu, Z.-f., *Huaxue Shijie*, (2007) **48**, 240.
- [112] Li, Z.; Pei, Y.; Wang, H.; Fan, J.; Wang, J., *TrAC, Trends Anal. Chem.*, (2010) **29**, 1336.
- [113] Hamad, E. Z.; Ijaz, W.; Ali, S. A.; Hastaoglu, M. A., *Biotechnol Prog*, (1996) **12**, 173.
- [114] Ali, S. A., *Korean J. Chem. Eng.*, (2012) **29**, 1426.
- [115] Ali, S. A.; Al-Hamouz, O. C. S., *Polymer*, (2012) **53**, 3368.
- [116] Candau, F.; Joanny, J. F., Polyampholytes. Properties in Aqueous Solution, In *Polymeric Materials Encyclopedia*, Salamone J, F. Ed. CRC Press: Boca Raton, (1996); pp 5462.
- [117] Everaers, R.; Johner, A.; Joanny, J. F., *Europhys. Lett.*, (1997) **37**, 275.

- [118] Higgs, P. G.; Joanny, J. F., *J. Chem. Phys.*, (1991) **94**, 1543.
- [119] Wittmer, J.; Johner, A.; Joanny, J. F., *Europhys. Lett.*, (1993) **24**, 263.
- [120] Dobrynin, A. V.; Rubinstein, M.; Joanny, J.-F., *Macromolecules*, (1997) **30**, 4332.
- [121] Sukhishvili, S. A.; Granick, S., *J. Chem. Phys.*, (1998) **109**, 6861.
- [122] Van, d. S. H. G. M.; Cohen, S. M. A.; De, K. A.; Bijsterbosch, B. H., *Langmuir*, (1992) **8**, 2538.
- [123] Diamond, A. D., (1991), p 244 pp.
- [124] Diamond, A. D.; Hsu, J. T., *AIChE Symp. Ser.*, (1992) **290**, 105.
- [125] Lowe, A. B.; McCormick, C. L., *Chem. Rev. (Washington, DC, U. S.)*, (2002) **102**, 4177.
- [126] Ali, S. A.; Umar, Y.; Abu-Sharkh, B. F.; Al-Muallem, H. A., *J. Polym. Sci., Part A: Polym. Chem.*, (2006) **44**, 5480.
- [127] Umar, Y.; Abu-Sharkh, B. F.; Asrof, A. S., *Polymer*, (2005) **46**, 10709.
- [128] Abu-Thabit, N. Y.; Al-Muallem, H. A.; Ali, S. A., *J. Appl. Polym. Sci.*, (2011) **120**, 3662.
- [129] Harada, S.; Arai, K., *Makromol. Chem.*, (1967) **107**, 64.
- [130] Butler, G. B., *Journal of Polymer Science, Part A: Polymer Chemistry*, (2000) **38**, 3451.

- [131] McGrew, F. C., *J. Chem. Educ.*, (1958) **35**, 178.
- [132] Corpart, J. M.; Candau, F., *Macromolecules*, (1993) **26**, 1333.
- [133] Salamone, J. C.; Volksen, W.; Israel, S. C.; Olson, A. P.; Raia, D. C., *Polymer*, (1977) **18**, 1058.
- [134] Yoshizawa, M.; Ohno, H., *Chem. Lett.*, (1999), 889.
- [135] Ohno, H.; Ito, K., *Chem. Lett.*, (1998), 751.
- [136] Yoshizawa, M.; Hirao, M.; Ito-Akita, K.; Ohno, H., *J. Mater. Chem.*, (2001) **11**, 1057.
- [137] Kudaibergenov, S. E., *Polyampholytes: Synthesis, Characterization and Application*, Kluwer Academic/Plenum Publishers: (2002); p 220 pp.
- [138] Mumick, P. S.; Welch, P. M.; Salazar, L. C.; McCormick, C. L., *Macromolecules*, (1994) **27**, 323.
- [139] Salamone, J. C.; Rice, W. C., Polyampholytes, In Wiley: (1987); Vol. 11, pp 514.
- [140] Filippini, D.; Aasberg, P.; Nilsson, P.; Inganaes, O.; Lundstroem, I., *Sens. Actuators, B*, (2006) **B113**, 410.
- [141] Kathmann, E. E. L.; White, L. A.; McCormick, C. L., *Macromolecules*, (1997) **30**, 5297.
- [142] Lowe, A. B.; Billingham, N. C.; Armes, S. P., *Chem. Commun. (Cambridge)*, (1996), 1555.

- [143] King, J. F.; Skonieczny, S., *Phosphorus Sulfur*, (1985) **25**, 11.
- [144] Timofeeva, L. M.; Vasilieva, Y. A.; Kleshcheva, N. A.; Topchiev, D. A., *Russ. Chem. Bull.*, (1999) **48**, 856.
- [145] Lloyd, A. W.; Olliff, C. J.; Rutt, K. J., *Int. J. Pharm.*, (1996) **131**, 257.
- [146] Galin, M.; Chapoton, A.; Galin, J. C., *J. Chem. Soc., Perkin Trans. 2*, (1993), 545.
- [147] Ernst, R.; Miller, E., *surfaces-active betaines. in amphoteric surfactants*, marcel dekker: new york, (1982); Vol.
- [148] Lloyd, A. W.; Baker, J. A.; Smith, G.; Olliff, C. J.; Rutt, K. J., *J. Pharm. Pharmacol.*, (1992) **44**, 507.
- [149] Zhang, L. M.; Tan, Y. B.; Li, Z. M., *Carbohydrate Polymers*, (2001) **44**, 255.
- [150] Kiefer, R.; Höll, W. H., *Industrial and Engineering Chemistry Research*, (2001) **40**, 4570.
- [151] Wu, H.; Jin, Y.; Luo, M.; Bi, S., *Anal Sci*, (2007) **23**, 1109.
- [152] Kumar, G. P.; Kumar, P. A.; Chakraborty, S.; Ray, M., *Sep. Purif. Technol.*, (2007) **57**, 47.
- [153] Liang, W. J.; Wu, C. P.; Hsu, C. Y.; Kuo, P. L., *Journal of Polymer Science, Part A: Polymer Chemistry*, (2006) **44**, 3444.
- [154] Popa, A.; Davidescu, C.-M.; Negrea, P.; Ilia, G.; Katsaros, A.; Demadis, K. D., *Ind. Eng. Chem. Res.*, (2008) **47**, 2010.

- [155] Prakash, S.; Kumar, M.; Tripathi, B. P.; Shahi, V. K., *Chem. Eng. J. (Amsterdam, Neth.)*, (2010) **162**, 28.
- [156] Hwang, G.-J.; Ohya, H., *J. Membr. Sci.*, (1998) **140**, 195.
- [157] Stanford Research Institute, chemical economics handbook, In menlo park (CA) 581-5022L, 581-1012D, (1983); pp 581.
- [158] Butler, G. B., *Journal of Polymer Science, Part A: Polymer Chemistry*, (1996) **34**, 913.
- [159] Ottenbrite, R. M.; Ryan, W. S., Jr., *Ind. Eng. Chem. Prod. Res. Dev.*, (1980) **19**, 528.
- [160] Ottenbrite, R. M.; Shillady, D. D., Ring size of cyclopolymerized N,N-dialkyldiallylammonium halides, In Pergamon: (1980); pp 143.
- [161] Cabeza, A.; Ouyang, X.; Sharma, C. V. K.; Aranda, M. A. G.; Bruque, S.; Clearfield, A., *Inorg. Chem.*, (2002) **41**, 2325.
- [162] Demadis, K. D.; Katarachia, S. D., *Phosphorus, Sulfur Silicon Relat. Elem.*, (2004) **179**, 627.
- [163] Martinez-Tapia, H. S.; Cabeza, A.; Bruque, S.; PertierraS.Garcia-Granda, P.; Aranda, M. A. G., *J. Solid State Chem. Synth.*, (2000) **151**, 122.
- [164] Kolodynska, D.; Hubicki, Z.; Pasieczna-Patkowska, S., *Acta Phys. Pol., A*, (2009) **116**, 340.
- [165] Sahni, S. K.; Van, B. R.; Reedijk, J., *Polyhedron*, (1985) **4**, 1643.

- [166] Liu, J.; Ma, Y.; Xu, T.; Shao, G., *J. Hazard. Mater.*, (2010) **178**, 1021.
- [167] Ramesh, A.; Hasegawa, H.; Maki, T.; Ueda, K., *Separation and Purification Technology*, (2007) **56**, 90.
- [168] Liu, J.; Wang, X.; Xu, T.; Shao, G., *Sep. Purif. Technol.*, (2009) **66**, 135.
- [169] Al-Asheh, S.; Duvnjak, Z., *Water, Air, Soil Pollut.*, (1999) **114**, 251.
- [170] Cao, Z.; Ge, H.; Lai, S., *Eur. Polym. J.*, (2001) **37**, 2141.
- [171] Shannon, R. D., *Acta Crystallogr., Sect. A*, (1976) **A32**, 751.
- [172] Hillel, d., *environmental soil physics*, In academic press: san diego, CA, (1998).
- [173] lide, D. R. Ed. *handbook of chemistry and physics*, CRC Press: boca raton, (1998); Vol.
- [174] Veli, S.; Pekey, B., *Fresenius Environ. Bull.*, (2004) **13**, 244.
- [175] Coşkun, R.; Soykan, C.; Saçak, M., *Reactive and Functional Polymers*, (2006) **66**, 599.
- [176] Kertman, S. V.; Kertman, G. M.; Leykin, Y. A., *Thermochim. Acta*, (1995) **256**, 227.
- [177] Chen, A.-H.; Yang, C.-Y.; Chen, C.-Y.; Chen, C.-Y.; Chen, C.-W., *J. Hazard. Mater.*, (2009) **163**, 1068.
- [178] Atia, A. A.; Donia, A. M.; Yousif, A. M., *Sep. Purif. Technol.*, (2008) **61**, 348.

- [179] Lin, Y.; Chen, H.; Lin, K.; Chen, B.; Chyowsan, C., *J. Environ. Sci. (Beijing, China)*, (2011) **23**, 44.
- [180] Wang, J.-W.; Kuo, Y.-M., *J. Appl. Polym. Sci.*, (2007) **105**, 1480.
- [181] Singh, V.; Tiwari, S.; Sharma, A. K.; Sanghi, R., *J. Colloid Interface Sci.*, (2007) **316**, 224.
- [182] Warnana, D. D.; Utama, W., *Asian Transactions on Engineering*, (2011) **1**, 2221.
- [183] Karnit, O., Jr.; Gurgel, L. V. A.; Pereira, d. F. R.; Gil, L. F., *Carbohydr. Polym.*, (2009) **77**, 643.
- [184] Liu, J.; Ma, Y.; Xu, T.; Shao, G., *Journal of Hazardous Materials*, (2010) **178**, 1021.
- [185] Wang, Y.-J.; Zhou, D.-M.; Sun, R.-J.; Jia, D.-A.; Zhu, H.-W.; Wang, S.-Q., *J. Hazard. Mater.*, (2008) **151**, 179.
- [186] Jain, C. K.; Singhal, D. C.; Sharma, M. K., *J. Hazard. Mater.*, (2004) **114**, 231.
- [187] Sgarlata, C.; Arena, G.; Longo, E.; Zhang, D.; Yang, Y.; Bartsch, R. A., *J. Membr. Sci.*, (2008) **323**, 444.
- [188] Shahtaheri, S. J.; Khadem, M.; Golbabaee, F.; Rahimi-Froushan, A.; Ganjali, M. R.; Norouzi, P., *International journal of occupational safety and ergonomics : JOSE*, (2007) **13**, 137.
- [189] Kumar, G. P.; Kumar, P. A.; Chakraborty, S.; Ray, M., *Separation and Purification Technology*, (2007) **57**, 47.

- [190] Laatikainen, M.; Sirola, K.; Paatero, E., *Colloids and Surfaces A: Physicochemical and Engineering Aspects*, (2007) **296**, 191.
- [191] Tao, Y.; Ye, L.; Pan, J.; Wang, Y.; Tang, B., *Journal of Hazardous Materials*, (2009) **161**, 718.
- [192] Zhang, Q.; Pan, B.; Zhang, W.; Ren, H., *Industrial and Engineering Chemistry Research*, (2008) **47**, 3957.
- [193] Liu, J.; Xu, T.; Fu, Y., *J. Non-Cryst. Solids*, (2005) **351**, 3050.
- [194] Al-Hamouz, O. C. S.; Ali, S. A., *Sep. Purif. Technol.*, (2012) **98**, 94.
- [195] Akporhonor, E. E.; Egwaikhide, P. A., *scientific research and essay*, (1996) **2**, 132.
- [196] McCormick, C. L., *J. Polym. Sci., Part A: Polym. Chem.*, (1996) **34**, 911.
- [197] Cooper, T. E.; Carl, D. R.; Oomens, J.; Steill, J. D.; Armentrout, P. B., *J. Phys. Chem. A*, (2011) **115**, 5408.
- [198] Undabeytia, T.; Morillo, E.; Maqueda, C., *Clay Miner.*, (1996) **31**, 485.
- [199] Kinraide, T. B.; Yermiyahu, U., *J. Inorg. Biochem.*, (2007) **101**, 1201.
- [200] Dong, Q.; Liu, J.; Song, L.; Shao, G., *Journal of Hazardous Materials*, (2011) **186**, 1335.
- [201] Liu, J.; Si, J.; Zhang, Q.; Zheng, J.; Han, C.; Shao, G., *Industrial and Engineering Chemistry Research*, (2011) **50**, 8645.

- [202] Abollino, O.; Aceto, M.; Malandrino, M.; Sarzanini, C.; Mentasti, E., *Water Res.*, (2003) **37**, 1619.
- [203] Boonamnuyvitaya, V.; Chaiya, C.; Tanthapanichakoon, W.; Jarudilokkul, S., *Sep. Purif. Technol.*, (2004) **35**, 11.
- [204] Dimitrova, S. V., *Water Res.*, (1996) **30**, 228.
- [205] Sahu, R. C.; Patel, R.; Ray, B. C., *Desalination*, (2011) **266**, 93.
- [206] Mohapatra, M.; Rout, K.; Mohapatra, B. K.; Anand, S., *J Hazard Mater*, (2009) **166**, 1506.
- [207] Leyva-Ramos, R.; Rangel-Mendez, J. R.; Mendoza-Barron, J.; Fuentes-Rubio, L.; Guerrero-Coronado, R. M., *Water Sci. Technol.*, (1997) **35**, 205.
- [208] Camci-Unal, G.; Pohl, N. L. B., *Journal of Chemical & Engineering Data*, (2009) **55**, 1117.
- [209] Güçlü, G.; Gürdağ, G.; Özgümüş, S., *Journal of Applied Polymer Science*, (2003) **90**, 2034.
- [210] He, Z.-Y.; Nie, H.-L.; Branford-White, C.; Zhu, L.-M.; Zhou, Y.-T.; Zheng, Y., *Bioresour. Technol.*, (2008) **99**, 7954.
- [211] Liu, J.; Xu, T.; Fu, Y., *Journal of Membrane Science*, (2005) **252**, 165.
- [212] Kolodynska, D.; Hubicki, Z.; Geca, M., *Ind. Eng. Chem. Res.*, (2008) **47**, 3192.
- [213] Ripperger, K. P.; Alexandratos, S. D., *Stud. Surf. Sci. Catal.*, (1999) **120B**, 473.

- [214] Wang, Z.; Yin, P.; Qu, R.; Xu, Q., *J. Appl. Polym. Sci.*, (2012) **126**, 544.
- [215] Yamabe, K.; Ihara, T.; Jyo, A., *Sep. Sci. Technol.*, (2001) **36**, 3511.
- [216] Sheals, J.; Persson, P.; Hedman, B., *Inorg. Chem.*, (2001) **40**, 4302.
- [217] Dean, J. A. Ed. *Lange's Handbook of Chemistry*, McGraw-Hill: New York, (1998).
- [218] Kavitha, D.; Namasivayam, C., *Bioresource Technology*, (2007) **98**, 14.
- [219] Taqvi, S. I. H.; Hasany, S. M.; Bhangar, M. I., *Journal of Hazardous Materials*, (2007) **141**, 37.
- [220] Wu, F. C.; Tseng, R. L.; Juang, R. S., *Chemical Engineering Journal*, (2009) **153**, 1.
- [221] Ozcan, A.; Ozcan, A. S.; Gok, O., Adsorption kinetics and isotherms of anionic dye of Reactive Blue 19 from aqueous solutions onto DTMA-sepiolite, In Nova Science Publishers, Inc.: (2007); pp 225.
- [222] WHO, Guidelines for Drinking Water Quality: Recommendations, In World Health Organization: Geneva, (2008); Vol. 1.
- [223] Butter, T. J.; Evison, L. M.; Hancock, I. C.; Holland, F. S.; Matis, K. A.; Philipson, A.; Sheikh, A. I.; Zouboulis, A. I., *Water Res.*, (1998) **32**, 400.
- [224] Al-Hamouz, O. C. S.; Ali, S. A., *Ind. Eng. Chem. Res.*, (2012) **51**, 14178.
- [225] Raji, C.; Anirudhan, T. S., *Indian Journal of Chemical Technology*, (1997) **4**, 228.

- [226] Rao, M.; Bhole, A. G., *J Indian Water Works Asso*, (2001), 97.
- [227] Haghseresht, F.; Lu, G. Q., *Energy and Fuels*, (1998) **12**, 1100.
- [228] Pandey, P.; Sambi, S. S.; Sharma, S. K.; Singh, S., *Proceedings of the World Congress on Engineering and Computer Science*, (2009) **1**.
- [229] Teker, M.; Imamoğlu, M.; Saltabaş, O., *Turkish Journal of Chemistry*, (1999) **23**, 185.
- [230] WHO, Copper in Drinking-Water, Guidelines for Drinking-Water Quality, In World Health Organization: Geneva, (2003).
- [231] Netzer, A.; Hughes, D. E., *Water Research*, (1984) **18**, 927.
- [232] Veli, S.; Alyüz, B., *Journal of Hazardous Materials*, (2007) **149**, 226.
- [233] Larous, S.; Meniai, A. H.; Bencheikh Lehocine, M., *Desalination*, (2005) **185**, 483.
- [234] Allen, S. J.; McKay, G.; Porter, J. F., *Journal of Colloid and Interface Science*, (2004) **280**, 322.
- [235] Demirbas, E.; Kobya, M.; Konukman, A. E. S., *Journal of Hazardous Materials*, (2008) **154**, 787.
- [236] Kundu, S.; Gupta, A. K., *Chemical Engineering Journal*, (2006) **122**, 93.
- [237] Vijayaraghavan, K.; Padmesh, T. V. N.; Palanivelu, K.; Velan, M., *Journal of Hazardous Materials*, (2006) **133**, 304.

- [238] Alyüz, B.; Veli, S., *Journal of Hazardous Materials*, (2009) **167**, 482.
- [239] Liu, J.; Song, L.; Shao, G., *Journal of Chemical and Engineering Data*, (2011) **56**, 2119.
- [240] Webber, T. W.; Chakkravorti, R. K., *AIChE J.*, (1974) **20**, 228.
- [241] Boparai, H. K.; Joseph, M.; O'Carroll, D. M., *J. Hazard. Mater.*, (2011) **186**, 458.
- [242] Hasan, S. H.; Talat, M.; Rai, S., *Bioresour. Technol.*, (2006) **98**, 918.
- [243] Ali, S. A.; Al-Hamouz, O. C. S.; Hassan, N. M., *J Hazard Mater*, (2013) **248-249C**, 47.
- [244] Ploeger, W.; Schindler, N.; Wollmann, K.; Worms, K. H., *Z. Anorg. Allg. Chem.*, (1972) **389**, 119.
- [245] Perrin, R.; Elomaa, M.; Jannasch, P., *Macromolecules (Washington, DC, U. S.)*, (2009) **42**, 5146.
- [246] Minceva, M.; Markovska, L.; Meshko, V., *Maced. J. Chem. Chem. Eng.*, (2007) **26**, 125.
- [247] Wang, X. S.; Miao, H. H.; He, W.; Shen, H. L., *J. Chem. Eng. Data*, (2011) **56**, 444.
- [248] Weber, W. J.; Morris, J. C., *J. Sanit. Eng. Div. Am. Soc. Civ. Eng.*, (1963) **89**, 31.

Vitae

Name :Othman Charles Sadeq Othman Al hamouz
Nationality :Jordanian
Date of Birth :8/9/1979
Email :g200901870@kfupm.edu.sa
Address :KFUPM, P.O.Box: 5048, Dhahran, 31261, Saudi Arabia.
Alternative Email :othmancharles@gmail.com

Educational Qualifications:

Assistant Professor, King Fahd University of Petroleum and Minerals, chemistry Department, Joining at Sep 2013.

PhD. Chemistry, 2013, (Thesis title: Synthesis and Applications of Linear and Cross-linked pH- Responsive Polycarbo-, Polyphospho- and PolySulfobetaines).

M.Sc. Chemistry, University of Jordan, 2004 (Thesis title: synthesis and characterization of polycarbonates based on bisalkyl (aryl) carbonates).

B.Sc. applied chemistry, 2001, Jordan University of Science and Technology. |